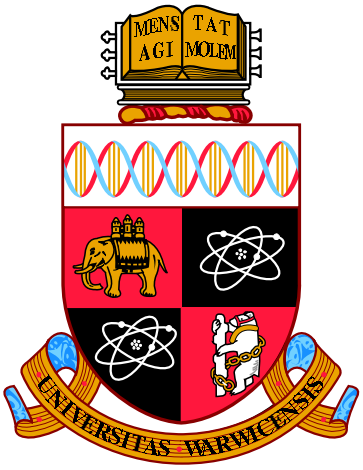

Design and Analysis of DNA Controllers

by

Nuno Miguel Gomes Paulino

Thesis

Submitted to the University of Warwick

for the degree of

Doctor of Philosophy

School of Engineering

August 2021

WARWICK
THE UNIVERSITY OF WARWICK

Contents

List of Figures

List of Tables

Acknowledgements

I am very grateful to Prof. Declan G. Bates for his support and effective guidance, and for creating the conditions that allowed me to develop this work with room for autonomy and exploration.

I also thank Dr. Mathias Foo for his aid and continuous support, and for the discussions and suggestions which elevated my work, manuscripts, and this thesis.

I am grateful for the collaborations with Prof. Jongmin Kim and Prof. Tom de Greef, which provided a realistic experimental ground to the theoretical work, and guided me through the mechanisms of chemistry with nucleic acids.

I must thank the sponsors which funded this work: the University of Warwick, the EPSRC/BBSRC Centre for Doctoral Training in Synthetic Biology via grant EP/L016494/1 and the BBSRC/EPSRC Warwick Integrative Synthetic Biology Centre via grant BB/M017982/1.

I also thank everyone in the welcoming institutions during the different parts of the PhD: the UK's Synthetic Biology CDT, the Warwick Integrative Synthetic Biology Centre, the School of Engineering from the University of Warwick, the Doctoral Training Centre in the University of Oxford, and the BrisSynBio at the University of Bristol.

Finally, I am indebted to all the support and understanding at home.

Declarations

This thesis is submitted to the University of Warwick in support of my application for the degree of Doctor of Philosophy. It has been composed by myself and has not been submitted in any previous application for any degree.

The work presented in this thesis was carried out by the author under the supervision of Prof. Declan G. Bates and co-supervision of Dr. Mathias Foo, with consultancy of Prof. Jongmin Kim on DNA biophysics, and Prof. Tom de Greef on constructing DNA based circuits.

Most of this thesis has been published by the author (see Chapter 1 for how the publications relate to the thesis), and presented in conferences and invited seminars.

Journal papers

1. N. M. G. Paulino, M. Foo, J. Kim, & D. G. Bates (2019). "Robustness analysis of a nucleic acid controller for a dynamic biomolecular process using the structured singular value", Journal of Process Control, 78:34-44.

2. N. M. G. Paulino, M. Foo, J. Kim, & D. G. Bates (2019). "PID and State Feedback Controllers Using DNA Strand Displacement Reactions", IEEE Control Systems Letters, 3(4):805-810. *Presented at the 58th IEEE Conference on Decision and Control, 2019, Nice, France.*

3. N. M. G. Paulino, M. Foo, J. Kim, & D. G. Bates (2020). "On the stability of nucleic acid feedback controllers", Automatica 119, 109103. *A pre-print is available at* arXiv, https://arxiv.org/abs/1812.01481

Conference papers

1. N. M. G. Paulino, M. Foo, J. Kim, & D. G. Bates, "Uncertainty modelling and stability robustness analysis of nucleic acid-based feedback control systems". In Proceedings of the 57th IEEE Conference on Decision and Control (pp. 1077-1082), IEEE, Florida, USA, 2018.

2. N. M. G. Paulino, M. Foo, T. F. A. de Greef, J. Kim, & D. G. Bates, "Minimally complex nucleic acid feedback control systems for first experimental implementations", Proceedings of the 21st IFAC World Congress, Berlin, 2020. *A pre-print is available at* bioRχiv, https://www.biorxiv.org/content/10.1101/867945v1

Presentations

1. Invited seminar at Eindhoven University of Technology, on "Linear feedback control circuits using DNA strand displacement reactions: design and robust analysis", Eindhoven, The Netherlands, May 2019. Invited by the Control Systems Technology group from the Mechanical Engineering Department.

2. Invited seminar at the University of Cambridge, "On nucleic acid feedback control systems", Cambridge, UK, November 28th, 2019. Invitation from the Control Group, in Engineering Department.

3. Poster presentation: N. M. G. Paulino, M. Foo, J. Kim, & D. G. Bates, "Design and analysis of feedback control circuits implemented using DNA strand displacement reactions", International Workshop on Control Engineering and Synthetic Biology, Oxford, UK, September 2019.

Abstract

Reliable biochemical implementations of linear controllers can provide a large set of tools for the design and analysis of control in Synthetic Biology. Theoretical frameworks are now available to represent feedback control systems as chemical reaction networks which can be readily translated into equivalent nucleic acid-based chemistry. However, the development of tools for constructing and analysing such controllers is still in its infancy.

Nucleic acid-based chemistry is a strong candidate framework for the construction of future synthetic biomolecular control circuits. The capacity of strand displacement reactions with Deoxyribonucleic Acid (DNA) to implement analogue signal processing *in vitro* and *in vivo* makes them a promising candidate to embed synthetic feedback control circuitry in biomolecular environments. However, little progress has so far been made in developing the requisite theoretical machinery to inform the systematic design of feedback controllers in this context.

Here, the potential complexity of such controllers is extended significantly by showing how time-delays, numerical differentiation (to allow proportional-integral-derivative control), and state feedback may be implemented via chemical reaction network-based designs.

This work also provides a number of foundational theoretical results on the equilibria, stability, and dynamics of nucleic acid controllers, and the analysis highlights the many interesting and unique characteristics of this important new class of feedback control systems. In particular, that the implementation of feedback controllers using DNA strand displacement reactions introduces additional nonlinear dynamics, even in the case of purely linear control designs, and a robust design of the linear system does not imply the robustness of its chemical implementation.

The robustness of the controllers to experimental uncertainty is analysed with the structured singular value (μ) analysis tool, which is extended with a model of how parametric uncertainty in the system affects the location of its equilibrium. This framework provides more reliable results than sampled based statistical methods, where analysis via Monte Carlo simulation fails to uncover the worst-case uncertainty combination found by μ-analysis.

The implementations of the examples and controllers in nucleic acid-based chemistry are simulated and checked using the Visual DSD simulation package, a bespoke software tool for simulating nucleic acid-based circuits.

Abbreviations

CME Chemical Master Equation.
CRN Chemical Reaction Network.
DNA Deoxyribonucleic Acid.
DSD DNA Strand Displacement.
dsDNA Double Stranded DNA.
FE Fixed Equilibrium.
FOTD First Order and Time Delay.
GAS Globally Asymptotically Stable.
I/O Input-to-Output.
IPR Internal Positive Representation.
LFT Linear Fractional Transformation.
LNA Linear Noise Approximation.
MAK Mass Action Kinetics.
ME Moving Equilibrium.
mRNA Messenger Ribonucleic Acid.
ODE Ordinary Differential Equations.
PDE Partial Differential Equation.
PI Proportional and Integral.
PID Proportional-Integrator-Derivative.
QSS Quasi-Steady State.
RNA Ribonucleic Acid.
RS Robust Stability.
SFI State Feedback and Integral.
SISO Single Input Single Output.
SSA Stochastic Simulation Algorithm.
ssDNA Single Stranded DNA.
SSV Structured Singular Value.

Chapter 1

Introduction

The field of Synthetic Biology has emerged in the last decade with the objective of designing biological parts and systems, and it differentiates itself from pre-existing life sciences due to its approach, where beyond understanding biological systems, it aims at the rational design of new biological processes from scratch [1–3].

The need for process information and control of biomolecular processes led to designs based on protein expression and gene regulation mechanisms for logic circuits [4,5], oscillators [6] and filters [7]. However, such a bottom-up approach faces the hard task of developing well characterised and modular genetic components [8] for a reliable assembly without problems like retroactivity [9]. Moreover, engineered gene networks in living cells suffer from interactions with the host, with effects arising from the cell context, competition for shared resources and loading effects [10].

Cell-free biology and information processing functions with biochemical processes outside of cells have shown several advantages, like a high degree of control, reduced design–build–test cycles which allow streamline design processes and facilitate debugging of complex synthetic circuits [11], flexibility, and relaxed design constraints compared to *in vivo* [12, 13].

Such an alternative paradigm of building embedded information processing with molecular circuits based on non-living components is currently the subject of intense research efforts. With the proposal of computation based on DNA [14], a number of approaches based on dynamic DNA nanotechnology [15] have emerged using DSD reactions and DNA enzymes, with which to wire arbitrary networks and experimentally reproduce the dynamic features of a genetic network *in vitro* [15,16]. The understanding of toehold mediated DNA strand displacement reactions [17, 18] and the use of DNA strands as fuel for autonomous nano-machines [19] led to the development of DNA hybridisation networks for sensing, analogue and digital

computation [20, 21].

The development of processes to assemble oligonucleotides at a low cost provides strands of DNA as building blocks for completely synthetic circuits based on hybridisation and strand displacement reactions. The biomolecular circuitry is based on non-living components that can be decoupled from self-replication and evolution, face fewer regulatory hurdles, and result in predictable and programmable chemistry. Nevertheless, the systems retain their biocompatibility and capacity to interface with biological DNA and RNA, making them very interesting for therapeutics [22], biosensing, bioimaging and biomedicine [23].

The capability of enzyme-free strand displacement reactions to realise sophisticated information processing, computation, and control, resulted in a large growth and interest in dynamic DNA nanotechnology in recent years [24]. DNA circuits have been constructed to implement amplifiers [25], digital logic [26], Boolean neural networks [27], Kalman filters [28], programmed oscillations [29], weighted-sum operations [30], and analogue computation [31, 32].

As one of the most used processes in nucleic acid nanotechnology, there is also interest in using strand displacement reactions in living cells [33], and on top of the aforementioned benefits, we also have also the capacity of nucleic acids to operate *in vivo* and interface with endogenous cellular machinery. Some notable examples demonstrated in mammalian cells include engineered oligonucleotide "AND" gates responding to Messenger Ribonucleic Acid (mRNA) inputs [34], multi-input logic based on DNA circuitry interacting with native mRNA [35], and reliable strand displacement probes triggered by mRNA being transcribed into cells [36].

The programmability, predictability, versatility and biological compatibility of nucleic acids makes them the current molecules of choice for molecular programming and strong candidates for implementing computing and controllers in synthetic biology [37].

1.1 Feedback control in synthetic biology

Synthetic biology requires systematic design and analysis frameworks for biomolecular processes that can regulate concentrations of molecular species inside the cell [38, 39]. Such necessity motivated the urgent development of control tools for biomolecular processes [38, 40, 41] and the development of molecular circuits suitable for analogue computations in different biological contexts [42].

Control theory is an interdisciplinary branch of engineering that studies how the behaviour of dynamical systems is modified by feedback, and recent advances

in synthetic biology incorporate many control engineering design principles into the construction of biomolecular circuits [43–46]. For decades, control and systems theory in other fields of engineering has produced vast bodies of work ensuring performance and robustness of large and complex systems [47, 48]. Now, these concepts need to be precisely defined and investigated in the biological context [49, 50], and there are expectations that control systems engineering can contribute in order to improve metabolic product and chemical network robustness [43, 51, 52].

There is an extensive list of autoregulation and feedback network motifs in biology [53], and mechanisms for gene regulation such as promoter occupancy, rate of activated transcription, repressible transcription, regulation with multiple transcription factors, and cooperative factor binding [54], all result in nonlinear expressions for the reaction rates. Moreover, either by simplification methods or empirical fitting, in biological systems we typically arrive at a set of nonlinear differential equations.

Of interest are also systems with *monostable steady state step response* (where the dynamics have a single global attractor) which provide well-behaved building blocks for arbitrary systems [55], because we can map a static input–state *characteristic curve*, where for each constant input value there exists a globally asymptotically stable equilibrium [56]. However, these *characteristics* are usually nonlinear. For example, the Michaelis-Menten dynamics for enzymatic reactions (derived from mass action laws assuming timescale separation to get rate laws in enzymatic reactions [54]), Hill functions and cooperativity [57], and ultrasensitivity [58] have hyperbolic and sigmoidal *characteristic* curves.

It can be argued then, that new control approaches must come from regulating living systems [55], and the resulting controllers may not resemble a direct counter part from the usual linear operators. For example, the functioning of the control structure introduced in [59] applies integral control to a network using an annihilation/sequestration reaction as comparator, and the results are analysed and proved in a stochastic framework, where the proof of ergodicity substitutes stability. A control based on the same type of comparison with annihilation or sequestration and using covalent modification cycles for gain implementation [60] also differs from the classical error feedback controller. Additionally, like the analysis and characterisation of biological systems, there is usually a focus on the steady state outcome and the *characteristic curve*.

1.2 Biochemical networks for linear negative feedback

Even if the processes suffer from positive and nonlinear dynamics, with the recent increase in the scope and industrial potential of synthetic control systems, it is appealing to exploit the long-established tools and techniques of *linear control theory* for the synthesis and analysis of biomolecular controllers. The application of linear negative feedback to synthetic biology is desired and foreseen [38], including classical control and design in the frequency domain [61, 62]. Such a view departs from the emphasis on the characteristic curves and steady state conditions, and recovers more traditional control requirements and objectives.

A promising direction is to integrate control theory with CRN theory within the overall context of deterministic Mass Action Kinetics (MAK) [63], which have traditionally been used to model biochemical processes [11,42,64]. CRN theory is an area of applied mathematics that analyses the behaviour of chemical systems, with applications in biochemistry and chemical engineering. Computations using MAK implementations of polynomial Ordinary Differential Equations (ODE) make CRNs Turing universal [65,66] and suitable for use as an abstract programming language, with which to perform biomolecular computations and design synthetic circuits [67]. System representations and models can be built from system theoretic operators using CRNs, such as algebraic [68], polynomial [69], and rational functions [62], using direct or dual-rail computation [70].

Recent work has shown how CRN theory may be used to design dynamical systems and operators, which can be implemented biologically with nucleic acids [31, 59, 71] where the CRN programs can be translated into enzyme-free, entropy-driven DSD reactions in a systematic manner [21,72,73]. Predictable mechanistic models for DNA hybridisation and the law of mass action provide nucleic acid nanocontrollers with kinetics equivalent to the regimes of the CRN [72,74], and a systematic pipeline for engineering dynamical systems with DSD cascades [29].

Theoretical frameworks and software tools are now available that allow a CRN to be translated directly into nucleic acid-based chemistry [75–77], but gaps remain in the synthesis and analysis when representing linear feedback control systems.

One challenge is the positivity of the CRNs, where the subtraction modules which compare concentrations are usually one sided and compute only the positive control error [68, 78]. With the adoption of dual-rail representation [20, 70] and idealised versions of catalysis, annihilation, and degradation reactions, we can represent linear systems and negative feedback controllers [62, 79] with a CRN, which in turn

can be systematically translated to DSD reactions with equivalent dynamics for implementation. However, to date, linear feedback control system designs attempted within this framework have been restricted to extremely simple Proportional and Integral (PI) controller architectures [76, 79], and a linear framework, to be useful, needs to allow for frequency and state space design using classical control.

Moreover, when considering uncertainty due to unknown dynamics and parametric variability (for example due to spurious dynamics and variability in reaction rates [29,74]), concepts of robustness and performance must be defined and assessed to retrieve information about the system's sensitivity and capacity to perform under uncertainty. Little progress has so far been made in developing the requisite theoretical machinery to inform the systematic design of feedback controllers in this context and the development of tools for analysing the robustness of such controllers is still in its infancy. The application of control engineering tools and concepts from nonlinear and positive systems can aid the advance towards a comprehensive theory of feedback control for biochemical reaction networks.

1.3 Aims and objectives of this thesis

This work is at the intersection of Control Engineering and Synthetic Biology, and addresses several gaps with the aim to

- develop methodologies for both design and robust analysis of linear feedback control systems implemented with nucleic acids;
- provide a development cycle for design and analysis, with the same formality and rigour as in other less recent engineering disciplines.

The particular objectives for *design* are:

1. the use of the current framework of dual-rail representation to propose the chemical computation of more complex components or linear control strategies missing in literature such as higher order transfer functions, time delays, derivative control and linear state feedback;
2. the collaboration with biochemists to identify the main bottlenecks that have hindered the experimental testing of linear negative feedback using DNA based circuits;
3. the testing of the designs beyond the dynamics of the chemical representation, by simulating the constructions with DNA based reactions with suitable tools that account for the DNA biophysics and stochastic nature of the reactions;

4. the proposal to the synthetic biology community of candidate chemical reaction networks that represent classical linear negative feedback control systems, which are simultaneously feasible with the current capabilities in experimental research laboratories.

The particular objectives for *analysis* are:

1. the understanding of the properties of the positive dynamics involved in the representation of linear negative feedback with chemical reactions;
2. the characterisation of the role and impact of nonlinear dynamics present in the chemical reaction network which are used to represent linear systems;
3. the investigation of possible conditions that guarantee performance and/or stability of the designed chemical network using positive control theory;
4. the investigation of the impact of experimental conditions in the designed chemical representation, in particular, parametric variability due to inexact reaction rates;
5. the rigorous quantification of the robustness of the chemical representation to variability in the reaction rates, using established or modified tools from robust control theory which account for the nonlinearity, positivity and multiple equilibria of the dynamics of the chemical reaction network.

1.4 Contributions and organisation of this thesis

The contributions are identified in Figure 1.1, and the manuscript is organised as follows:

Chapter 2 recaps control and feedback concepts necessary to understand the subsequent chapters. It provides background on CRN theory and modelling, the methods and DSD technology considered in this work, nomenclature, and results from the literature used to support the work presented.

Chapter 3 significantly extends the potential complexity of pre-existing controllers by proposing novel CRN representations for plants with time-delays and for two important classes of linear feedback controllers - PID and SFI control.

The structure of the PID controller uses a novel filtered approximation of the derivative, with a fundamental tradeoff in the parameterisation between the

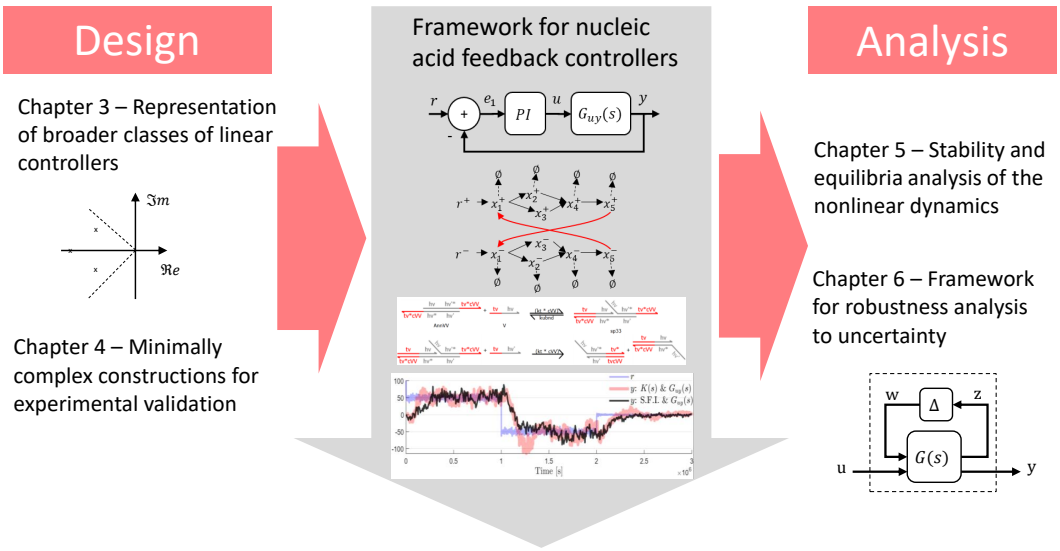

Figure 1.1: Contributions from the thesis to the design and analysis of feedback nucleic acid controllers. Chapter 3 broadens the classes of linear feedback controllers represented with nucleic acids, and Chapter 4 proposes constructions feasible for experimental validation. Chapters 5 and 6 provide results and tools for stability and robustness analysis lacking in the current building frameworks.

accuracy of differentiation and the feasibility of DNA binding reaction rates. The SFI structure takes advantage of the ready access of the controller to the chemical species, and it is posed as a regulation problem with a simpler CRN and fewer DNA strand species. The controllers are implemented and tested using VisualDSD [80], via both deterministic and stochastic simulations of the DSD reactions.

This chapter has been peer reviewed and published in N.M.G. Paulino, M. Foo, J. Kim, & D.G. Bates, "*PID and State Feedback Controllers Using DNA Strand Displacement Reactions*", IEEE Control Systems Letters, 2019, 3(4):805-810.

Chapter 4 proposes designs representing reference tracking control circuits (integral and state-feedback control), for which the complexity of the chemical reactions required for implementation has been minimised.

Experimental construction, validation and scale-up of nucleic acid control systems is still significantly lagging theoretical developments, due to several technical challenges, such as leakage, crosstalk, and toehold sequence design.

The designs proposed in this chapter use fewer reactions and species to alleviate spurious effects, to simplify the design of the DNA strands and the construction of the DSD circuits, and to encourage the progress towards experimental implementation while still capturing important features of relevant linear negative feedback

control systems.

This work has been peer reviewed and presented in N.M.G. Paulino, M. Foo, J. Kim, T.F.A. de Greef & D.G. Bates, "*Minimally complex nucleic acid feedback control systems for first experimental implementations*", Proceedings of the 21st IFAC World Congress, Berlin, 2020.

Chapter 5 presents a number of foundational theoretical results on the equilibria, stability, and dynamics of nucleic acid controllers.

Several recent works have applied dual-rail representation to obtain linear I/O models of synthetic feedback control systems without explicitly considering the potential impact of the internal nonlinear positive dynamics of the representation. The implementation of feedback controllers using dual-rail representation with DSD reactions relies on bimolecular reactions which introduce nonlinear dynamics, even in the case of purely linear designs, e.g. PI controllers. By decomposing the effects of these non-observable nonlinear dynamics, this chapter highlights the many interesting and unique characteristics of this important new class of feedback control systems.

One of the main results is that under the unavoidable experimental variability of the reaction rates, the stability of the represented I/O linear system does not necessarily guarantee the stability of the underlying chemical network. Although the dual-rail construction is very useful to design CRNs that represent linear negative feedback I/O systems, the experimental realisation of the chemical reactions will violate the assumption of nominal conditions with exact parameterisation of the reaction rates. The representation of the I/O dynamics assumes exact parameters, and does not consider the additional feedback interconnections introduced by variability in the parameters.

We show that in practice, we need to perform an analysis to the complete nonlinear dynamics, to assess their robustness to the inevitable parametric variability introduced by the experimental implementation. An example illustrates how the robustness of the represented linear system does not guarantee robustness of the CRN representation, justifying the need for robust analysis of the positive nonlinear MAK, and motivates the development of the techniques in the following chapter.

This work (except Section 5.4.2) has been peer reviewed in N.M.G. Paulino, M. Foo, J. Kim, & D.G. Bates, (2020) "*On the stability of nucleic acid feedback controllers*", Automatica 119, 109103.

Chapter 6 covers how the Structured Singular Value (SSV) analysis framework can be extended to rigorously analyse the robustness of the class of systems in the previous chapters, overcoming how the parametric uncertainty in the system affects the location of its equilibrium. The methodology is applied to an example of a linear system represented by the Input/Output of nonlinear mass action kinetics. The SSV (or μ) framework, which tells us how much the uncertain parameters can vary before losing closed-loop stability, is applied to obtain a stability margin more reliably than sample based methods like Monte Carlo simulations. It is also shown how the parameterisation of the system can be scaled for experimental feasibility with nucleic acid-based chemistry without affecting its robustness properties.

This work has been peer reviewed and published in N.M.G. Paulino, M. Foo, J. Kim, & D.G. Bates, "*Robustness analysis of a nucleic acid controller for a dynamic biomolecular process using the structured singular value*", Journal of Process Control, 2019, 78:34-44.

Chapter 7 concludes the thesis with a summary of the main results of this work and suggests future research.

Chapter 2

Background

What follows is a summary and aggregation of some fundamental concepts necessary to understand the contributions presented in the following chapters.

2.1 Linear control theory and negative feedback

For decades, control and systems theory has produced in other fields of engineering vast bodies of work ensuring performance and robustness of large and complex systems. Established references exist for the different topics in control such as classical multivariable control in the frequency domain [81–83], uncertainty, robust and optimal control [82, 84, 85], application of of convex optimisation tools (Linear Matrix Inequalities and Integral Quadratic Constraints) [86, 87], and nonlinear dynamics analysis and control [88–92].

The most extensive body of work in control relates to *linear systems*, and classical control relies extensively on analysis and design in the frequency-domain. For this class of systems, given an input signal $i(t) = I_0 \sin(\omega t)$ oscillating in time t, with gain I_0 and frequency ω, the linear process modifies the output gain O_o and phase ϕ to the output signal $o(t) = O_o \sin(\omega t + \phi)$, Figure 2.1a. Applying the Laplace transform [83] we can express the linear sets of differential equations in the frequency domain, with a transfer function that maps the gains and phase modifications for each frequency of the input (for the complex variable $s = j\omega$), Figure 2.1b.

In linear feedback, the output of a linear plant $P(s)$ is used as input to a linear controller $K(s)$, to modify the response of the closed loop, Figure 2.2, and nullify the error signal $E(s)$. In a *regulation problem*, the objective is to reject the effect of a disturbance $D(s)$ on the output of the plant, while in a *reference tracking*

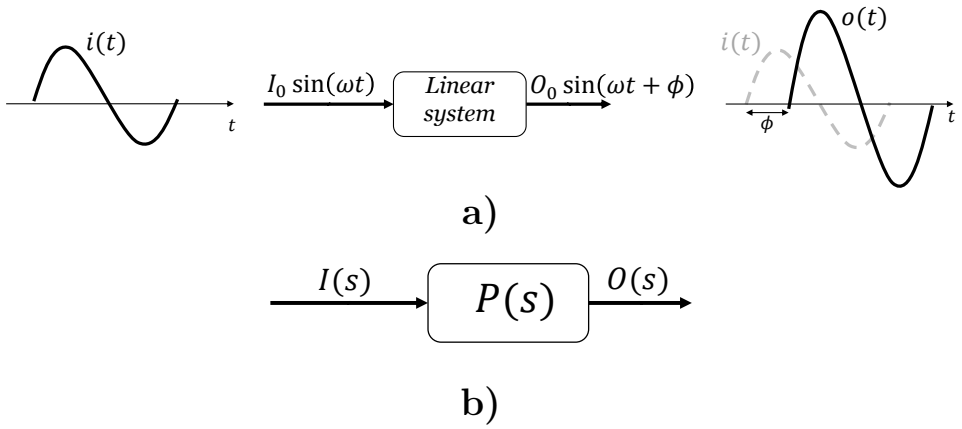

Figure 2.1: Representation of linear systems: a) for each sinusoidal input $i(t)$ at a frequency ω, the output of a linear system results only in modifications in amplitude (or gain) and delay (or phase); b) how the linear system affects the gain and phase at each frequency can be mapped by a transfer function, dependent on the complex variable $s = j\omega$ (frequency).

problem, the objective is to have the output of the plant track the reference signal $R(s)$. In classical linear negative feedback, the reference and output are compared with a subtraction where the error is given by the algebraic difference between the reference and the output, Figure 2.2a, such that a null error entails reference tracking and disturbance rejection.

Given a linear plant and linear controller, we can take the Laplace transforms of the ODEs modelling $P(s)$ and $K(s)$ to express in the frequency-domain the loop transfer of the system, where

$$Y(s) = L(s)R(s) = K(s)G(s)R(s) \tag{2.1}$$

represents the open loop response (without feedback). Once the negative feedback is in place, Figure 2.2b, we can derive the closed loop response from the reference to the output with

$$\begin{aligned} Y(s) &= L(s)\left(R(s) - Y(s)\right) && \text{(2.2a)} \\ \Rightarrow Y(s) &= \left[I + K(s)G(s)\right]^{-1} K(s)G(s)R(s) && \text{(2.2b)} \\ &= \left[I + L(s)\right]^{-1} L(s)R(s)\ . && \text{(2.2c)} \end{aligned}$$

In classical frequency-domain designs, given the transfer function of the plant, the controller $K(s)$ is designed to shape the loop gain transfer function $L(s)$ and fulfil the control requirements (e.g. stability margins, response time, damping, and settling

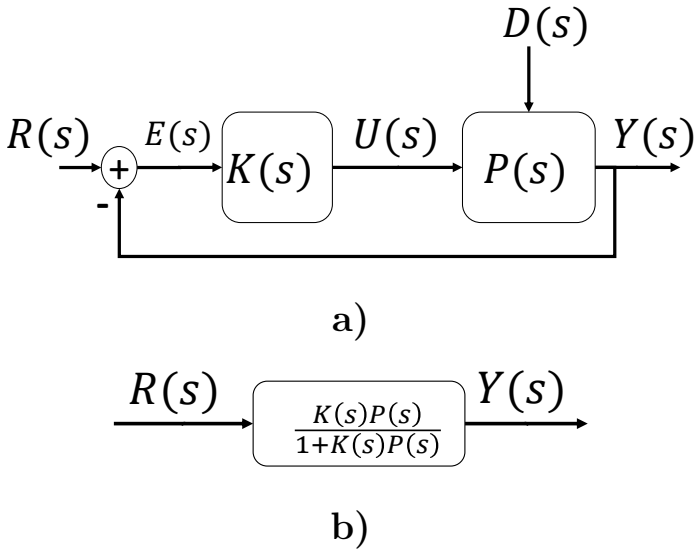

Figure 2.2: Linear negative feedback structure: a) a controller $K(s)$ us be used to reject a disturbance $D(s)$ in the output $Y(s)$ of the plant $G(s)$, or to drive $Y(s)$ towards a reference $R(s)$; b) transfer function of the closed loop system from the reference to the output.

time). The controller is used not only to set the steady state conditions, but also to modulate the dynamical response of the closed loop system.

For systems with multiple inputs and outputs, a convenient way to write the differential equations is through a *state space representation*, using matrix and vectorial algebra. Let us represent the elements of column vectors $\mathbf{v}$ and multiplication of matrices to a vector $\mathbf{x} = \mathbf{M}\mathbf{v}$ with $x_j = [\mathbf{M}\mathbf{v}]_j = \sum_i m_{ji} v_i$. Define also the constants $\mathbf{1}$ as a vector with elements 1, and $\mathbf{I}$ as the identity matrix.

If the vector $\mathbf{x} = [x_1, x_2, \ldots, x_N]^T$ is a vector collecting the states of a linear system, we can write the differential equations of the linear system with the state space representation given by

$$\dot{\mathbf{x}} = \mathbf{A}\mathbf{x} + \mathbf{B}\mathbf{u} \tag{2.3a}$$

$$\mathbf{y} = \mathbf{C}\mathbf{x} + \mathbf{D}\mathbf{u} \tag{2.3b}$$

where $\mathbf{u}$ and $\mathbf{y}$ are vectors with the respective input and output signals. For brevity, time dependency in state variables is implicit, i.e. $x_j \equiv x_j(t)$, and $\dot{x}_j$ represents the derivative with respect to time. The Laplace transform of a signal x_j is represented by $X_j(s)$, and the steady state conditions are represented in the time-domain with $x_j^* = \lim_{t\to\infty} x_j(t)$, or $X_j(0) = \lim_{s\to 0} X_j(s)$ in the frequency-domain. The transfer func-

tions between the different inputs and outputs can be recovered with

$$\mathbf{Y}(s) = \left(\mathbf{C}\left(s\mathbf{I} - \mathbf{A}\right)^{-1}\mathbf{B} + \mathbf{D}\right)\mathbf{U}(s)\ . \tag{2.4}$$

The state space representation of the system is not unique, and can be expressed in different state space coordinates. For example, taking the similarity transformation $\mathbf{z} = \mathbf{T}\mathbf{x}$ given by the non-singular matrix $\mathbf{T}$ [86], the dynamics in the new coordinates are given by

$$\dot{\mathbf{z}} = \mathbf{T}\mathbf{A}\mathbf{T}^{-1}\mathbf{z} + \mathbf{T}\mathbf{B}\mathbf{u} \tag{2.5a}$$

$$\mathbf{y} = \mathbf{C}\mathbf{T}^{-1}\mathbf{z} + \mathbf{D}\mathbf{u}. \tag{2.5b}$$

A change of coordinates is useful to express the dynamics in more convenient variables, or to decompose the system into its natural modes.

2.1.1 Stability

Among the conveniences of linear systems are the state space dependence on linear algebra and that the stability properties are determined by the spectral properties of the matrix $\mathbf{A}$ in (2.3) [86].

Definition 2.1. *Given a square matrix $\mathbf{A}$, for a scalar λ and a non-zero vector $\mathbf{v}$ that fulfil the equation $\mathbf{A}\mathbf{v} = \lambda\mathbf{v}$, λ is an eigenvalue of $\mathbf{A}$ and $\mathbf{v}$ is the corresponding eigenvector associated to λ.*

Definition 2.2. *The spectrum $\rho\{\mathbf{A}\}$ is the set of the eigenvalues λ_i of a matrix $\mathbf{A}$, and the spectral abscissa is represented as $\alpha\{\mathbf{A}\} = \max_i \Re\{\lambda_i\}$.*

For a linear system, we have from literature a direct result for stability, based on the spectral abscissa and eigenvalues.

Lemma 2.1 (see for example [88])**.** *For the linear system $\dot{\mathbf{x}} = \mathbf{A}\mathbf{x}$, the origin is Globally Asymptotically Stable (GAS) if and only if all eigenvalues of $\mathbf{A}$ satisfy $\Re\{\lambda_i\} < 0$.*

Definition 2.3. *Represent the set of Hurwitz (stable) matrices with $\mathcal{H}$, such that $\mathbf{A} \in \mathcal{H} \Leftrightarrow \alpha\{\mathbf{A}\} < 0$.*

It suffices to check the eigenvalues of the state matrix to determine the global stability of the system, and $\mathbf{A} \in \mathcal{H}$ entails GAS. Moreover, the similarity transformation in (2.5) does not change the stability of the system, since $\rho\{\mathbf{A}\} = \rho\left\{\mathbf{T}\mathbf{A}\mathbf{T}^{-1}\right\}$ and $\mathbf{A} \in \mathcal{H} \Leftrightarrow \mathbf{T}\mathbf{A}\mathbf{T}^{-1} \in \mathcal{H}$ [86].

In the presence of non-linearities, the ODEs no longer result in the linear representation in (2.3). Nevertheless, some of the linear tools can still be applied to study stability.

Definition 2.4. *Consider the system*

$$\dot{\mathbf{x}} = \mathbf{f}\left\{\mathbf{x}, \mathbf{u}\right\} \tag{2.6}$$

where $\mathbf{f}$ *is a continuously differentiable function in* $\mathbf{x}$ *and* $\mathbf{u}$*. Define the state* $\mathbf{x}^0$ *and input* $\mathbf{u}^0$ *the equilibrium (or trim) conditions such that* $\mathbf{f}\left\{\mathbf{x}^0, \mathbf{u}^0\right\} = 0$ *with* $\mathbf{f}$ *continuously differentiable around* $\mathbf{x}^0$ *and* $\mathbf{u}^0$*.*

For a linear system we have a closed form to determine the equilibrium with

$$\mathbf{x}^0 = \mathbf{A}^{-1}\mathbf{B}\mathbf{u}^0 \ . \tag{2.7}$$

For a nonlinear system, we must first determine the possibly multiple equilibrium solutions of (2.6), either analytically or numerically, depending on the complexity of the system. Then, taking the Jacobian matrices of $\mathbf{f}(\mathbf{x}, \mathbf{u})$ evaluated at the trim values, we obtain a linear local approximation of the dynamics around the equilibrium conditions, given by

$$\frac{\partial\left(\mathbf{x} - \mathbf{x}^0\right)}{\partial t} = \frac{\partial \mathbf{f}}{\partial \mathbf{x}}\left\{\mathbf{x}, \mathbf{u}\right\}\Big|_{\mathbf{x}=\mathbf{x}^0, \mathbf{u}=\mathbf{u}^0}\left(\mathbf{x} - \mathbf{x}^0\right) + \frac{\partial \mathbf{f}}{\partial \mathbf{u}}\left\{\mathbf{x}, \mathbf{u}\right\}\Big|_{\mathbf{x}=\mathbf{x}^0, \mathbf{u}=\mathbf{u}^0}\left(\mathbf{u} - \mathbf{u}^0\right) \tag{2.8}$$

Such a linearised system can provide information about the local stability around the equilibrium.

Theorem 2.1 (Lyapunov's indirect method [88])**.** *Let* $\mathbf{x}^0$ *be an equilibrium point for the system* $\dot{\mathbf{x}} = \mathbf{f}\left\{\mathbf{x}\right\}$*, where* $\mathbf{f}$ *is continuously differentiable in the neighbourhood of* $\mathbf{x}^0$*. Given*

$$\mathbf{A} = \frac{\partial \mathbf{f}}{\partial \mathbf{x}}\left(\mathbf{x}\right)\Big|_{\mathbf{x}=\mathbf{x}^0} \tag{2.9}$$

then

1. $\mathbf{x}^0$ *is exponentially stable if and only if* $\alpha\left\{\mathbf{A}\right\} < 0$
2. $\mathbf{x}^0$ *is unstable if* $\alpha\left\{\mathbf{A}\right\} > 0$

Theorem 2.1 provides a simple test to determine local stability a nonlinear system around its equilibrium, based on eigenvalues of the linearised system. The

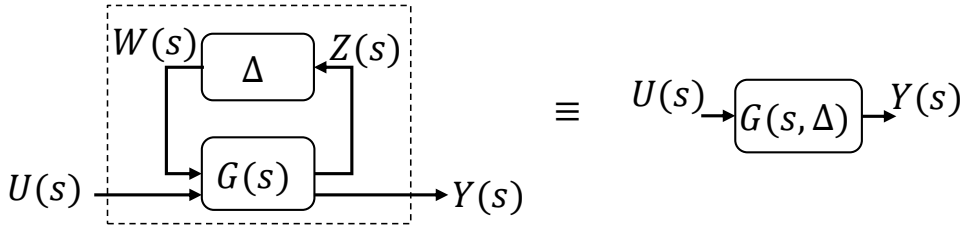

Figure 2.3: $\mathbf{M}-\Delta$ and LFT representation of the uncertainty system for μ-analysis.

limitation is that if $\alpha\{\mathbf{A}\} = 0$, then the linearisation cannot inform on the stability of the equilibrium point. This is the case if $\mathbf{A}$ has eigenvalues at the origin or pairs of purely complex poles.

2.1.2 Robustness analysis with the Structured Singular Value

In biology it is common to have parametric sloppiness [93] in the parameters of the system, motivating the search for a structural stability as viewed in CRN theory. Nevertheless, relating stability and performance with individual uncertainties in the system is of value, especially when the parameters are designed such as in the DNA strand displacement framework used in this work.

Uncertainty in the model may result from simplifications, approximated knowledge of the parameters, and unknown dynamics in the plant. For synthetic CRNs the most common approach for testing robustness is the probabilistic Monte Carlo method [60, 94, 95], relying on sampling possible values of the reaction rates. However, this method does not provide a certification of robustness, and may not correlate properly the robustness with specific parameters or parametric ranges.

Definition 2.5. *Take a parameter p_i decomposed into*

$$p_i \quad = \quad \bar{p_i}\,(1 + \delta_i) \tag{2.10}$$

where $\bar{p_i}$ is the nominal *value of the parameter, and δ_i represents the* multiplicative uncertainty *associated with such parameter.*

The design is based on the *nominal* values of the parameters, which are assumed to be perfectly known and exact. In practice, manufacturing tolerances, unmodelled dynamics and random variability in the implementation deviate the parameterisation from the nominal values used for design. For analysis and validation, we define instead a possible continuous range for the parameters, and treat the parameterisation as an uncertainty interval around the nominal value.

While the nominal parameterisation represents the ideal and perfectly known conditions used in design, for analysis we need to include in the system description a representation of their realistic uncertainty. If the parameters are within characterised uncertainty, linear analysis like the structured singular value analysis [82], combined with a linear representation of the system, opens the way for robust analysis and robust control in biological systems. This type of analysis has been carried in the context of systems biology [49, 50, 57, 96, 97]. The input for the SSV analysis is a Linear Fractional Transformation (LFT) representing the linear system in the presence of uncertainties, Figure 2.3. A transfer function which depends on the collection of parameters p_i, can be decomposed into the $\mathbf{M} - \Delta$ interconnection in Figure 2.3, where the uncertainties δ_i are lumped into the uncertainty matrix Δ.

From the interconnection between the two systems in Figure 2.3 we have

$$\begin{bmatrix} \mathbf{Z}(s) \\ \mathbf{Y}(s) \end{bmatrix} = \begin{bmatrix} \mathbf{M}_{11}(s) & \mathbf{M}_{12}(s) \\ \mathbf{M}_{21}(s) & \mathbf{M}_{22}(s) \end{bmatrix} \begin{bmatrix} \mathbf{W}(s) \\ \mathbf{U}(s) \end{bmatrix} \tag{2.11a}$$

$$\mathbf{W}(s) = \Delta(s)\mathbf{Z}(s) \tag{2.11b}$$

and the uncertain system

$$\mathbf{Y}(s) = \mathbf{G}\left(s, \Delta\right)\mathbf{U}(s) \tag{2.12}$$

is modelled by the LFT given by

$$\mathbf{G}\left(s, \Delta\right) = \mathbf{M}_{21}(s)\left(\mathbf{I} - \Delta(s)\mathbf{M}_{11}(s)\right)^{-1}\Delta(s)\mathbf{M}_{12}(s) + \mathbf{M}_{22}(s)\ . \tag{2.13}$$

The response of the system without uncertainty ($\Delta = 0$) is given by $\mathbf{M}_{22}(s)$ and defines the *nominal* performance of the system. However, from (2.13) we can see the presence of uncertainty can destabilise the system if $(\mathbf{I} - \Delta(s)\mathbf{M}_{11}(s)) = 0$. In this framework, Robust Stability (RS) is defined as the system remaining stable for all possible combinations of the parameters within the limits of their continuous ranges. If the system in (2.13) is robust, then (2.13) remains stable for any possible combination of δ_i.

The condition for robust stability is defined in terms of the maximum singular value $\bar{\sigma}\left(\Delta\right)$. In our case, we have parametric uncertainty given by the variability of reaction rates and other physical parameters, which results in a diagonal $\Delta \in \mathbb{R}$ with real diagonal elements. The SSV, or μ is a generalisation which takes into account the structure of Δ for a less conservative result. The real non-negative function μ

is then defined [82] for a structured Δ, as

$$\frac{1}{\mu(\mathbf{M})} = \min\{k_m | \det(\mathbf{I} - k_m \mathbf{M}\Delta) = 0\} \tag{2.14}$$

where a larger μ entails that a smaller uncertainty level $\bar{\sigma}(\Delta)$ exists which destabilises the system. The value of μ is not computed directly, but is instead taken from upper ($\bar{\mu}$) and lower ($\underline{\mu}$) bound values, which may be computationally expensive, especially in the case of a real μ problem, like the one above with strictly real uncertainties $\delta_i \in \mathbb{R}$. Given normalised uncertainties $|\delta_i| \leq 1$, we can make two interpretations from the bounds [82, 98, 99]:

- if for the lower bound we have $1/\underline{\mu} < 1$, then the system is robustly stable.
- the parameterisation corresponding to $1/\bar{\mu}$ has the minimum $\bar{\sigma}(\Delta)$ which results in an unstable system.

The former provides a powerful validation criterion for stability of the system for the entire possible range of uncertainties, which cannot be obtained by sampling and testing the system. The latter can be used to compute the smallest parameterisation vector that destabilises the system.

Definition 2.6. *The* worst case *parameterisation (or worst case Δ) is the vector of parameters p_i (or associated δ_i) corresponding to the smallest $\bar{\sigma}(\Delta)$ that destabilises the system in* (2.12).

It is noteworthy how this method differs from sampled based systems like Monte Carlo methods, where the system is simulated with possible combinations of the values of the parameters, and the results rely on large numbers of samples to fulfil a prescribed level of confidence. Sample based methods cannot completely cover the continuous range of the parameters, while the bounds provided by the SSV analysis do apply to the complete infinite family of systems in (2.13) covering the entire range of the parameters. On the other hand, sampled based methods can be applied to complex and nonlinear systems, while the results from the SSV depend on the description of uncertainty and validity of the linear or linearised model. The bounds or worst case identified by the μ bounds must be checked with the nonlinear process.

2.2 Chemical reaction networks

The theory behind CRNs is inherited from chemistry [63] and we apply the same principles to model and analyse biochemical reaction networks. With their exten-

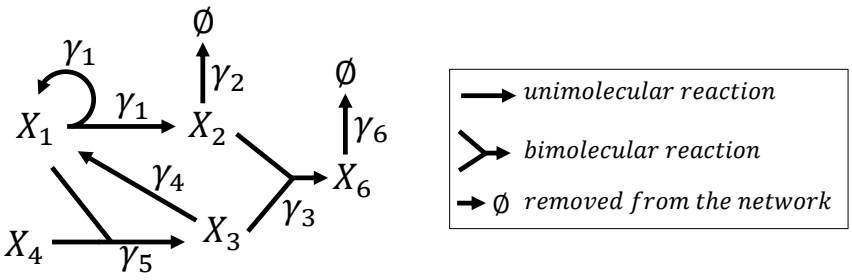

Figure 2.4: Example of a graph description of a chemical network, involving unimolecular and bimolecular reactions. When a species is removed from the network the resulting product is indicated as $\emptyset$.

sive computational capabilities [66, 100], CRNs provide a convenient representation for implementing elementary arithmetic operations [68] or the computation of polynomials [69], using any chemical system with mass action kinetics (MAK). They also provide an appropriate level of abstraction for designing complex circuits [67], and integrating the different elements necessary to build linear feedback control systems [76, 79]. Definitions of models and properties for CRNs are widely available: in connection with Petri nets and monotone systems [101, 102]; deficiency theorems and structural analysis work from [103–106] and applied to biochemical networks in [107].

Definition 2.7. *We define a CRN as a set of M reactions between N chemical species X_j, represented by*

$$\sum_{j=1}^{N} a_{jm} X_j \xrightarrow{\gamma_m} \sum_{j=1}^{N} b_{jm} X_j, \ (m = 1, \ldots, M) \tag{2.15}$$

where for each reaction m, the reactants on the left are converted into the products on the right, at a rate γ_m, according to the stoichiometric coefficients a_{jm} and b_{jm}.

The use of the same species in different reactions creates an interconnection between the different species, leading to a *graph* description of the network, Figure 2.4. Where the product is inactive (either due to degradation or sequestration) and no longer participates in the reactions, it is replaced by the symbol $\emptyset$.

2.2.1 Modelling chemical reaction networks

The time evolution of the species concentrations can be modelled assuming different principles. Here we focus on deterministic models based on MAK [63] traditionally used in biochemical applications [11, 42, 64]. Assuming a large number of available

molecules, MAK describe the time progression of the average concentrations of the species with a deterministic model expressed as a set of ODE [54,57,108], which are suitable for control systems theory, even if these are usually nonlinear.

Definition 2.8. *For a deterministic model based on MAK [63], we have that for each species X_j in (2.15), the dynamics of its concentration x_j is given by*

$$\dot{x}_j = \sum_{m=1}^{M} \left(\gamma_m \left(b_{jm} - a_{jm} \right) \prod_{i=1}^{N} x_i^{a_{im}} \right) . \tag{2.16}$$

Example 2.1. *Take the reaction between the reactant species X_1 and X_2 which produces species X_3, represented by*

$$a_1 X_1 + a_2 X_2 \xrightarrow{\gamma} b X_3 \tag{2.17}$$

where the reactants on the left are converted into the product on the right at a rate γ, according to the stoichiometric coefficients a_1, a_2 and b. The MAK model results in the ODEs

$$\dot{x}_1 = -a_1 \gamma x_1^{a_1} x_2^{a_2}, \quad x_1(0) \text{ given} \tag{2.18a}$$

$$\dot{x}_2 = -a_2 \gamma x_1^{a_1} x_2^{a_2}, \quad x_2(0) \text{ given} \tag{2.18b}$$

$$\dot{x}_3 = +b \gamma x_1^{a_1} x_2^{a_2}, \quad x_3(0) \text{ given} \tag{2.18c}$$

where the stoichiometric coefficients a_1, a_2 and b indicate, respectively, the relative number of molecules consumed and produced during the reaction.

Representing the positive orthant with $\mathbb{R}_0^+$, where all the coordinates of a vector $\mathbf{v}$ are non-negative, $v_j \geq 0$, we have that expressing the dynamics of (2.18) in their natural coordinates, the concentrations, results in a non-negative state vector $\mathbf{x} \in \mathbb{R}_0^+$. If the sets of reactions are properly modelled with realistic non-negative initial conditions, the system is non-negative ($\mathbf{x}(0) \geq 0 \Rightarrow \mathbf{x}(t) \geq 0$), where the concentrations are always non-negative.

Quasi-steady state and singular perturbation analysis

The presence of nonlinear terms is the general case in biological systems, and it is usual to aim for simplifications of the model by reducing the ODE system through singular perturbation analysis, timescale separation, and quasi-equilibrium approximation (e.g. [54, 108–110]). Take two sets of state variables $\mathbf{x} \in \mathbb{R}^N$ and $\mathbf{z} \in \mathbb{R}^M$,

and the dynamics

$$\dot{\mathbf{x}} = \mathbf{f}(\mathbf{x}, \mathbf{z}, \epsilon, t), \quad \mathbf{x}(0) \; given \tag{2.19a}$$

$$\epsilon\dot{\mathbf{z}} = \mathbf{g}(\mathbf{x}, \mathbf{z}, \epsilon, t), \quad \mathbf{z}(0) \; given. \tag{2.19b}$$

The model is in *standard-form* where it is explicit which states have the derivatives multiplied by a "small" scalar $\epsilon > 0$ [109]. To reduce the model, we consider a singular perturbation parameter and consider the limit when $\epsilon \to 0$. In that case, part of the dynamics turns into an algebraic equation

$$0 = \mathbf{g}(\mathbf{x}, \mathbf{z}^*, 0, t) \tag{2.20}$$

and the model is reduced from $N + M$ states to N with

$$\dot{\mathbf{x}} \approx \mathbf{f}(\mathbf{x}, \mathbf{z}^*(\mathbf{x}), 0, t), \quad \mathbf{x}(0) \; given. \tag{2.21}$$

The states $\mathbf{z}$ may be referred as at Quasi-Steady State (QSS) assuming that for a small ϵ, $\dot{\mathbf{z}}$ is very large and $\mathbf{z}$ rapidly converges to a root of the equation in (2.20) [109].

Although trimolecular reactions are unlikely and an overall chain of bimolecular reactions is more plausible [111] (see also [63] on stoichiometric coefficients), it is common to assume timescale separation between different reactions to remove state variables at the cost of replacing chains of reactions with higher order nonlinear rate functions. However, in the case of the synthetic biochemical networks considered in this work, timescale separation can be exploited by design without necessarily resulting in additional complexity, and the QSS assumption proves useful.

Stochastic analysis

Other modelling approaches use stochastic descriptions, such as a Markov process leading to the Chemical Master Equation (CME), which has simple principles but are hard to integrate [101]. Instead of concentrations, we have random variables to describe the number of molecules at a given time, and their time evolution is modelled by a differential equation for the probability function of the state.

Under some assumptions we can derive stochastic differential equations, such as the chemical Langevin equation [112], or the Linear Noise Approximation (LNA) where the process is the sum of the solutions for deterministic ODE and a zero mean solution to a linear stochastic differential equation [113]. The LNA is particularly useful for analysis since it scales better for large number of species and reactions [114]. For accuracy the LNA requires a large enough volume and number

of molecules, whereas the CME can be used in certain cases such as affine propensities to express closed systems of differential equations for the dynamics of the moments and covariances [115].

When dealing with low numbers of molecules, a stochastic approach is the most representative, but the CME is limited by the lack of analytical solutions. For stochastic analysis and validation, this work uses simulations with Gillespie's Stochastic Simulation Algorithm (SSA) [116, 117], which models exactly the probability distribution and species concentrations to update the propensity of a specific reaction. Gillespie's SSA is available in tools like Visual DSD [80].

2.2.2 CRN theory and positive systems analysis

The network structure and non-negative property of CRNs give way to the use of specific theoretical results for these kinds of systems. Two approaches lead to somewhat complementary results. CRN theory is specific for MAK, but relies only on the topology of the network. Positive and monotone systems can deal with other types of kinetics but need a signed incidence graph [57].

The CRN theory from [103–105] arranges the reactions guided by mass action laws as a network of complexes (groups of reagents) without arrow directionality, and aggregates them into linkage classes. From the number of linkage classes, number of complexes, and rank of the network it defines the deficiency of the network. The deficiency theorems allow conclusions about the existence of steady state or cyclic trajectories in networks with zero and one deficiency, just based on the structure and stoichiometry. The existence of structural motifs which increase robustness independent of the reaction rates and parameterisation lead to the definition of absolute concentration robustness [118, 119], and network based criteria to find species which always have the same value for all admissible steady states.

Non-linear analysis uses phase plane and direction fields, bifurcation analysis, nullclines, and eigenvalue analysis [54, 57], although they can suffer from some limitations. Bifurcation analysis for variations of three parameters or more are difficult and not well understood [57]. Most results for nonlinear dynamics take a local analysis around operating equilibria (usually the regulated set point), and try to use linear approximations, to enable the use of the extensive toolkit for linear systems [54].

Another approach is to bring in the results from positive systems [92]. This characteristic of CRNs actually helps since some counterparts to control results simplify, and provides new ways of analysis. Most of them rely on Lyapunov direct and indirect theorems.

Definition 2.9. *Define the notation where* $\mathbf{x} = \mathbf{v} \circ \mathbf{u} \Rightarrow x_j = v_j u_j$ *represents the element-wise (or Hadamard) product.*

We can use the element-wise product to write linear and quadratic Lyapunov functions based on norms, since for positive vectors $\mathbf{v} \geq 0$ it results

$$V\{\mathbf{v}\} = \mathbf{1}^T\mathbf{v} = \sum v_j = \|\mathbf{v}\|_1 \geq 0 \tag{2.22a}$$

$$V\{\mathbf{v}\} = \mathbf{v}^T\mathbf{I}\mathbf{v} = \mathbf{1}^T(\mathbf{v} \circ \mathbf{v}) = \sum v_j^2 = \|\mathbf{v}\|_2^2 \geq 0\ . \tag{2.22b}$$

The framework from [40] shows how the use of quadratic Lyapunov functions may not be suitable for stability assessment in monotonic systems, with linear Lyapunov functions being sufficient and in some cases being better than quadratic. The work in [111] provides over 44 motifs of biochemical networks with monotone reaction rates, for which stability was tested, and which can be used to show the stability of interconnected motifs. In [120] it is shown how a joint linear Lyapunov function can be used to show stability of a polytope of positve systems (see also [121] for co-positive linear Lyapunov functions). These can be combined with integral and quadratic Lyapunov functions, if the structure of the system demands it [92].

For the specific case of positive *linear* systems there is a long list of properties such as irreducibility, excitability and transparency, that can be inferred just from the influence matrix which captures the graph structure of the network [122]. It happens that, for the state space realisation of a *positive linear* system given by

$$\dot{\mathbf{x}} = \mathbf{M}\mathbf{x} + \mathbf{B}\mathbf{u}, \quad \textit{given } \mathbf{x}(0) \geq 0 \tag{2.23}$$

the state matrix $\mathbf{M}$ is a Metzler matrix [122], where the interconnections (off-diagonal elements) between states are always given by positive gains. For convenience of representation, take the following definitions.

Definition 2.10. *In this work, the inequality* $\mathbf{M} \geq 0$ *means all elements of the matrix* $\mathbf{M}$ *are positive,* $m_{ji} \geq 0$*, and* $\mathbf{M} \in \mathbb{R}_0^+$ *(unrelated to positive definite matrices).*

Definition 2.11. *For a vector* $\mathbf{v}$*, define the operator* $\mathbf{D}\{\mathbf{v}\}$*, which represents a square matrix with* $\mathbf{v}$ *on its diagonal:* $d_{jj} = v_j$ *and* $\forall_{j\neq i}, d_{ji} = 0$*.*

Definition 2.12. *If* $\mathbf{m}$ *is the diagonal of* $\mathbf{M}$*, the matrix* $\mathbf{M}^{\diagdown\!\!\diagdown}$ *containing the off-diagonal elements of* $\mathbf{M}$ *and zeros in the diagonal is defined as* $\mathbf{M}^{\diagdown\!\!\diagdown} = \mathbf{M} - \mathbf{D}\{\mathbf{m}\}$*.*

We can then write a definition for the group of Metzler matrices.

Definition 2.13. *The group of Metzler matrices* $\mathcal{M}$ *is defined such that if* $\mathbf{M} \in \mathcal{M}$*, then* $m_{ji} \geq 0$*,* $\forall_{i\neq j}$*. Or more compactly* $\mathbf{M} \in \mathcal{M} \Leftrightarrow \mathbf{M}^{\diagdown\!\!\diagdown} \geq 0$

Further discussion on minimality and realisability of positive systems is done in [123]. Despite the non-negative constraints of Metzler matrices, some results simplify for linear positive systems, such as the condition for stability.

Theorem 2.2 (Lyapunov theorem for positive systems from [122])**.** *A continuous-time positive system is asymptotically stable if and only if there exists a strictly positive diagonal matrix* $\mathbf{D}\{\mathbf{d}\}$ *(*$\mathbf{d} > 0$*) such that* $\mathbf{M}^T\mathbf{D}\{\mathbf{d}\} + \mathbf{D}\{\mathbf{d}\}\mathbf{M}$ *is negative definite.*

Proof. Omitted. See [122]. □

Further properties result from the structure of the positive network and the Metzler dynamics matrix $\mathbf{M}$. For example, a stable positive system is automatically $D - stable$ [92, 122]. Also, we have $\mathbf{M} \in \mathcal{M}, \mathcal{H} \Rightarrow \mathbf{m} < 0$, which means that for any chance of stable dynamics and $\alpha\{\mathbf{M}\} < 0$ it is necessary to have a negative diagonal (but not sufficient, since $\mathbf{M} \in \mathcal{M}, \mathbf{m} < 0 \nRightarrow \alpha\{\mathbf{M}\} < 0$).

Also very useful is the Perron-Frobenius theorem and the definition of a dominant eigenvalue [92]. Consider the following definitions.

Definition 2.14. *Define the set of lower triangular matrices* $\mathcal{L}$*, such that if* $\mathbf{M} \in \mathcal{L}$ *then* $m_{ji} = 0, i > j$*.*

Dynamics where $\mathbf{M} \in \mathcal{L}$, the derivative of an element in the state vector depends only on the preceding state variables. For spectral information, we have the trivial result for triangular matrices that $\mathbf{M} \in \mathcal{L} \Rightarrow \lambda_i\{\mathbf{M}\} = m_{ii}$.

Definition 2.15. *Defining the set* $\mathcal{I}$ *of irreducible matrices [122], if* $\mathbf{M} \in \mathcal{I}$*, then there is no permutation matrix* $\mathbf{P}$ *such that* $\mathbf{PMP}^T \in \mathcal{L}$*. Conversely, if* $\mathbf{M} \in \mathcal{L}$ *then* $\mathbf{M} \notin \mathcal{I}$*.*

If $\mathbf{M} \in \mathcal{I}$, a lower triangular form is not achievable by reordering the state vector, and the derivative of a state variable depends at least on one other state. For spectral information in the case $\mathbf{M} \in \mathcal{M}, \mathcal{I}$, we use the following results.

Theorem 2.3 (Dominant Frobenius eigenvalue and eigenvector [122])**.** *Define the* Frobenius eigenvalue λ_F *as the dominant eigenvalue of a continuous positive system. Then* λ_F *is real and unique. The positive eigenvectors* $\mathbf{w}_F$ *associated with* λ_F *are defined as* Frobenius eigenvectors*.*

Proof. Omitted. See [122]. □

Theorem 2.4 (Frobenius eigenvalue and eigenvector of irreducible systems [122])**.** *The Frobenious eigenvector* $\mathbf{w}_F$ *of an irreducible system (*$\mathbf{M} \in \mathcal{I}, \mathcal{M}$*) is unique and strictly positive,* $\mathbf{w}_F > 0$*, and the Frobenius eigenvalue* λ_F *has an algebraic multiplicity equal to 1. There are no positive eigenvectors other than* $\mathbf{w}_F$*.*

Proof. Omitted. See [122]. □

Additionally, exploiting the Perron-Frobenius theorem, we can put bounds on the stability radius for non-positive systems using properties of Metzler matrices [124, 125]. While in general systems the analysis of robustness in the presence of uncertainty (μ-analysis) can numerically be a hard problem [126], in positive systems for some structures of uncertainty a closed solution is available from the state matrices [127]. An extension on the stability conditions for monotone norms, and how bounds on the stability radius of a non-positive system can be obtained from a Metzler type version of the system, are found in [120].

2.3 Representing negative feedback with chemical reactions

The positivity of the biological models hinders the direct implementation of classical control feedback. Problems that appear suitable for available control theory can have fundamental differences that call for new tools [55], and many counterpart results for control theory of positive systems have been proposed and solved.

This includes conditions for stability [128] and methods for state and output stabilisation [128–131]. Specifically [128] also discusses and shows observer-based stabilisation using the separation principle. For the design of nonlinear control, there is the approach of making the system dissipative using Lyapunov storage functions (for example, based on entropy [101, 107]) to ensure asymptotic convergence (see for example [90] on passivity by feedback). The fact that static gain determines the induced norms of positive systems [132] invites the use of norm-based operators to establish control problems, such as for L_1-induced [133–136], and L_∞-induced gains [137], H_∞ feedback design is possible [138, 139], with some recent work attempts at H_2 state feedback on positive switched systems [140]. The sub-class of monotone systems has further interesting properties since conclusions can be drawn about the interconnection of this type of system [102]. Properties like stability carry over from individual parts to the integrated system, which is relevant when designing and decomposing a larger system into monotone sub-components [55].

In terms of feedback it is an important result that for an interconnection of positive systems to be stable, all the sub-systems need to be stable [122]. This is not true for non-positive systems, and this has fundamental consequences in terms of feedback since it implies that an unstable positive system cannot be stabilised by interconnecting it with another positive system [129].

2.3.1 Dual-rail representation

The application of negative feedback, with the implementation of linear operators common in control, like gain and integration, need careful attention in the context of CRNs. The operation of subtraction, critical for the computation of the error in negative feedback, is a challenge when the states are concentrations that are always non-negative, and the output must be a non-negative concentration [68].

The so-called *dual-rail* representation [20, 71, 79] overcomes the limitation of the positivity of CRNs, and allows the representation of both positive and negative signals (crucial for the generation of error signals in feedback control) using molecular concentrations.

Definition 2.16. *Consider two chemical species X_j^+ and X_j^-, and respective concentrations $x_j^+ \geq 0$ and $x_j^- \geq 0$. A dual-rail signal $p_j \in \mathbb{R}$ is represented by $p_j = x_j^+ - x_j^-$, with dynamics given by $\dot{p}_j = \dot{x}_j^+ - \dot{x}_j^-$.*

We then have signals given by the difference between two positive quantities, allowing the subtraction between signals (instead of concentrations) to result in positive or negative signals. Linear negative feedback systems with simple proportional and PI controllers have been designed with this now standard practice [76, 79], resorting to only three types of elementary reactions

$$\textit{catalysis} \quad : \quad X_i \xrightarrow{\gamma} X_i + X_j \tag{2.24a}$$

$$\textit{degradation} \quad : \quad X_j \xrightarrow{\gamma} \emptyset \tag{2.24b}$$

$$\textit{annihilation} \quad : \quad X_i + X_j \xrightarrow{\eta} \emptyset \ . \tag{2.24c}$$

The MAK of (2.24) in their natural coordinates result in non-negative state variables, the concentrations, not suitable for circuits involving negative gains and negative control error for linear feedback. However, defining instead dual-rail signals we can compute positive and negative control errors, using positive concentrations.

Example 2.2 (Representation of subtraction)**.** *Let $p_1 = (r - y)$, with positive or negative outcomes $p_1, r, y \in \mathbb{R}$. With the chemical species $\left\{X_1^+, X_1^-, R^+, R^-, Y^+, Y^-\right\}$*

and respective concentrations $\left\{x_1^+, x_1^-, r^+, r^-, y^+, y^-\right\}$ *(M), define* $r = r^+ - r^-$, $y = y^+ - y^-$, *and* $p_1 = x_1^+ - x_1^-$. *From the following CRNs*

$$R^+ \xrightarrow{\gamma} R^+ + X_1^+,\ R^- \xrightarrow{\gamma} R^- + X_1^- \tag{2.25a}$$

$$Y^+ \xrightarrow{\gamma} Y^+ + \boldsymbol{X_1^-},\ Y^- \xrightarrow{\gamma} Y^- + \boldsymbol{X_1^+} \tag{2.25b}$$

$$X_1^+ \xrightarrow{\gamma} \emptyset,\ X_1^- \xrightarrow{\gamma} \emptyset \tag{2.25c}$$

$$X_1^+ + X_1^- \xrightarrow{\eta} \emptyset \tag{2.25d}$$

we obtain the nonlinear MAK

$$\dot{x}_1^+ = -\gamma x_1^+ + \gamma r^+ + \gamma \boldsymbol{y^-} - \eta x_1^+ x_1^-, \quad x_1^+(0) = 0 \tag{2.26a}$$

$$\dot{x}_1^- = -\gamma x_1^- + \gamma r^- + \gamma \boldsymbol{y^+} - \eta x_1^+ x_1^-, \quad x_1^-(0) = 0 \tag{2.26b}$$

where the notations in bold highlight the crossed contributions from the components of y *to the result* p_1. *Expressing the dynamics from the inputs* r *and* y *to the output* p_1, *under steady state conditions, we obtain the linear operation of subtraction*

$$\gamma^{-1}\left(\dot{x}_1^+ - \dot{x}_1^-\right) = -x_1^+ + x_1^- + r^+ - r^- - y^+ + y^- \tag{2.27a}$$

$$\Rightarrow \left(x_1^{+*} - x_1^{-*}\right) = \left(r^{+*} - r^{-*}\right) - \left(y^{+*} - y^{-*}\right) \tag{2.27b}$$

$$\Rightarrow p_1^* = r^* - y^* \ . \tag{2.27c}$$

Crossing the contributions in (2.25b) *results in a negative gain when expressing the subtraction in terms of differences of concentrations in* (2.27b).

Since the dual representation admits infinite combinations of the pair of concentrations x_1^+ and x_1^- for the same difference $p_1 = x_1^+ - x_1^-$, in practice, the annihilation reaction in (2.25d) is used to keep the concentrations of all molecular species low (that is, experimentally feasible) even in the presence of peak transients.

The cost to pay for this representation is the duplication of the required number catalysis and degradation reactions, which can be problematic in practice. The implementation of a larger network is more challenging since it needs more species and leads to more reaction rates and parameters to be tuned. A larger network is more complex overall, with increased risk of leakage and unforeseen interactions.

Remark 2.1. *Following [79], we compact the notation so that* $X_1^\pm$ *represents simultaneously both species* X_1^+ *and* X_1^-, *and* $x_1^\pm$ *the respective concentrations* x_1^+ *and*

x_1^-. *We also abbreviate the pair of duplicated reactions and ODEs with*

$$Y^{\pm} \xrightarrow{\gamma^{\pm}} Y^{\pm} + X^{\mp} \Leftrightarrow \begin{cases} Y^{+} \xrightarrow{\gamma^{+}} Y^{+} + X_1^{-} \\ Y^{-} \xrightarrow{\gamma^{-}} Y^{-} + X_1^{+} \end{cases} \tag{2.28a}$$

$$\dot{x}_1^{\pm} = -\gamma^{\pm} x_1^{\pm} + \gamma^{\mp} \boldsymbol{y}^{\mp} - \eta x_1^{+} x_1^{-} \Leftrightarrow \begin{cases} \dot{x}_1^{+} = -\gamma^{+} x_1^{+} + \gamma^{-} \boldsymbol{y}^{-} - \eta x_1^{+} x_1^{-} \\ \dot{x}_1^{-} = -\gamma^{-} x_1^{-} + \gamma^{+} \boldsymbol{y}^{+} - \eta x_1^{+} x_1^{-} \end{cases} . \tag{2.28b}$$

Assumption 2.1. *The nominal parameterisation and nominal implementation assume perfectly designed reaction rates in the absence of variability, and a symmetrical parameterisation where the reaction rates are the same for each pair of duplicated reactions with* $\gamma^+ = \gamma^- = \gamma$.

Assumption 2.1 is used in the duplicated reactions to represent linear systems (for example, the derivation of (2.27b) from (2.26)), and it is implicit in the methodology that the ideal CRNs have perfect or closely matched reaction rates, or mechanisms for fine tuning of the reaction rates [62, 79].

We see also in Example 2.2 how the representation of the first order system is the dynamics from the dual signal input to the dual signal output, which leads to the definition of input to output systems in [79].

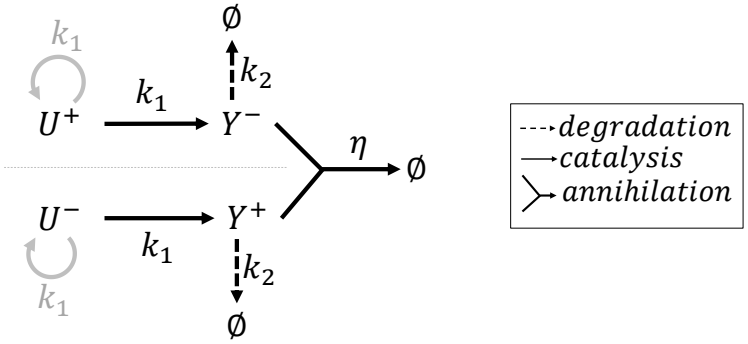

Figure 2.5: Network for dual-rail representation of the first order transfer function in Example 2.3. The unimolecular reactions of catalysis and degradation are duplicated (the representation of the autocatalysis *in grey* will be omitted in the CRN representations throughout the thesis). The two components of the output signal $y = y^+ - y^-$ annihilate each other through a bimolecular reaction.

Definition 2.17. *The Input-Output (I/O) dynamics of the positive real system is the response* $Y(s) = G(s)U(s)$, *from an input* $u = (u^+ - u^-)$ *to an output* $y = (y^+ - y^-)$. *The states are also dual-rail* $p_j = x_j^+ - x_j^-$, *where* $u, y, p_j \in \mathbb{R}$ *and* $u^{\pm}, y^{\pm}, x_j^{\pm} \in \mathbb{R}_0^+$.

Example 2.3 (First order system)**.** *To chemically represent the first order system with a negative gain given by the transfer function*

$$Y(s) = -\frac{k_1}{s + k_2} U(s) \tag{2.29}$$

with $u, y \in \mathbb{R}$, we take the pairs of chemical species $\{U^{\pm}, Y^{\pm}\}$ and the CRN from Figure 2.5 with

$$U^{\pm} \xrightarrow{k_1} U^{\pm} + Y^{\mp} \tag{2.30a}$$

$$Y^{\pm} \xrightarrow{k_2} \emptyset \tag{2.30b}$$

$$Y^{+} + Y^{-} \xrightarrow{\eta} \emptyset \ . \tag{2.30c}$$

From the MAK we derive the ODEs for the concentrations

$$\dot{y}^{+} = -k_2 y^{+} + k_1 u^{-} - \eta y^{+} y^{-}, \quad y^{+}(0) = 0 \tag{2.31a}$$

$$\dot{y}^{-} = -k_2 y^{-} + k_1 u^{+} - \eta y^{+} y^{-}, \quad y^{-}(0) = 0 \tag{2.31b}$$

and from Definition 2.17, the linear I/O system results

$$\dot{y}^{+} - \dot{y}^{-} = -k_2 \left(y^{+} - y^{-}\right) - k_1 \left(u^{+} - u^{-}\right) \tag{2.32a}$$

$$\Leftrightarrow \dot{y} = -k_2 y - k_1 u, \quad y(0) = 0 \ . \tag{2.32b}$$

Following a systematic construction using the elementary reactions in (2.24), we can perform computations with the steady state solutions, represent linear dynamics and transfer functions, and represent negative gains [62,76,79]. The linearity of the I/O system in Definition 2.17 results from how the nonlinear terms in the MAK in (2.31) cancel out in the ODEs of the I/O dynamics in (2.32).

Albeit the linearity of the I/O dynamics, even in ideal design conditions (with perfect implementation and parameterisation), the representation of the I/O linear system relies on a realisation with internal unobservable nonlinear dynamics and unidentifiable parameters.

The constructed MAK is an augmented system to address the problem of designing a realisation of a non-positive I/O system using a combination of positive realisations. This problem is relevant in practical applications, when a positive realisation design is the implementable choice [141]. In this case, the goal is a positive realisation with concentrations of biochemical species, even if the realisation with dual rail networks results in a duplication of most of the dynamics, with additional parameters. Moreover, we have nonlinearities since the annihilation reactions are

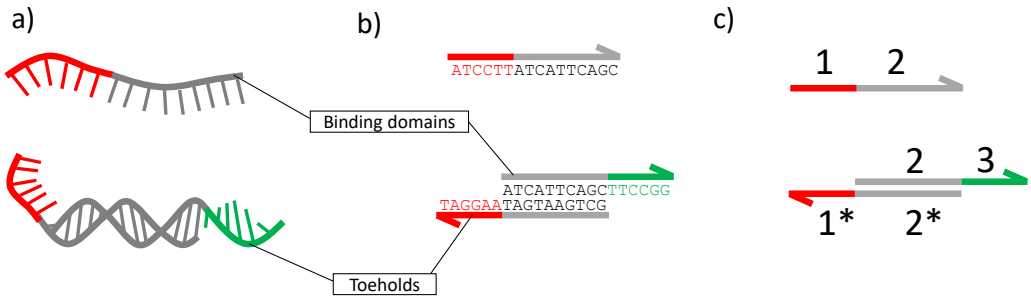

Figure 2.6: Three different representations of single and double stranded DNA: (a) as sugar-phosphate backbones with either exposed sugar bases, or forming an helicoidal double structure; (b) as sequences of bound pairs of complementary sequences of nucleotides; (c) with numbered domains, where 2^* is the complementary sequence to the domain 2.

essential in order to ensure that species concentrations remain within the bounds of experimental feasibility.

Even if the dimension of the linear I/O system is half of the nonlinear MAK, and there are nonlinearities unobservable between the selected inputs and outputs, the realisation of the representation is always the larger augmented and nonlinear Internal Positive Representation (IPR) [142]. We also note that analysing the linear I/O system overlooks dynamics and parameters present in the realised system, and the impact and consequences of the annihilation reactions in the properties of this class of IPR are the topic of Chapter 5.

2.4 Chemical circuits with nucleic acids

Nucleic acids are chains of nucleotides connected by phosphodiester linkages. Each nucleotide is composed by a purine or pyrimidine base, one or more phosphoryl groups, and a five-carbon sugar: ribose (in Ribonucleic Acid (RNA)) or deoxyribose (in DNA) [143]. A Single Stranded DNA (ssDNA) is composed of a sequence of four types of nucleotides, Adenine (A), Guanine (G), Cytosine (C) and Thymine (T), forming a chain connected by phosphodiester links.

Hydrogen bonds between pairs of nucleotides, A-T and C-G, result in helicoidal shaped Double Stranded DNA (dsDNA) formed by two antiparallel strands of DNA, Figure 2.6a, where the sugar-phosphate backbones of each strand have opposing directions [143]. The hydrophilic backbone together with the hydrophobic nature of the bases stabilise the bonding between the complementary pairs A-T and C-G, leading to an enzyme free hybridisation reaction between two antiparallel

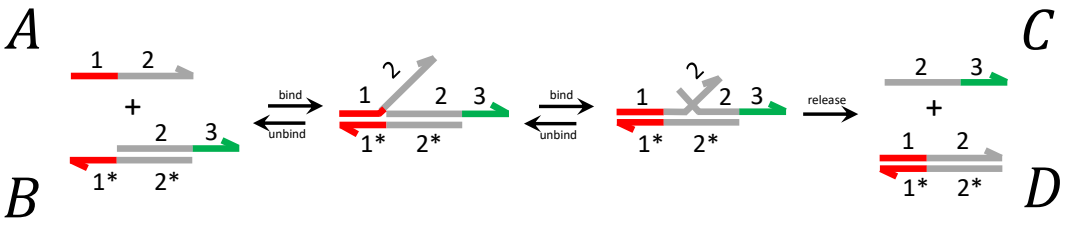

Figure 2.7: Illustration of a bimolecular DNA strand displacement reaction $A + B \rightarrow C + D$ involving single and double strands. The displacement is initiated by hybridisation between overhanging complementary toeholds 1 and 1^*, and the incoming strand A competes with the incumbent strand for the domain 2^*. The hybridisation continues until the incumbent is completely displaced resulting in new "species" C and D. The single strand C has an exposed toehold that can trigger other hybridisation reactions. Species D is considered unreactive waste, due to the absence of exposed toeholds.

complementary ssDNA to form a dsDNA, Figure 2.6b.

The development of processes to assemble oligonucleotides at a low cost enables the use of synthetic ssDNA as building blocks for circuits based on hybridisation reactions and networks of DSD reactions. Systematic ways to program and compose circuits have been proposed [75], which translate CRN programs into reactions using nucleic acids, where the reaction rates and binding affinities can, to some degree, be defined. Simple chemical reactions like catalysis, degradation and annihilation can be readily mapped into reactions based on nucleic acids with equivalent dynamics [21, 72], resulting in an implementation technology for circuits on CRNs, where the nucleotide sequences of the DNA strands effectively program the biochemical circuitry to compute digital and analogue functions [74, 75].

2.4.1 DNA strand displacement reactions

Looking at the domains (sequences of nucleotides) in Figure 2.6b, we have the domain 2 bound to its complementary sequence 2^*, Figure 2.6c, and two overhanging single stranded sequences 1^* and 3. If the illustrated ssDNA is also present, its domain 1 will hybridise with 1^*, and its domain 2 will compete with the existing double strand for the domain 2^*. This process may start a DSD reaction, where a strand of DNA displaces another strand from its binding to a complementary strand.

In Figure 2.7 we represent a bimolecular $A + B \rightarrow C + D$ reaction using DNA strands, where the hybridisation of the toehold 1 in the incoming strand A with a complementary toehold 1^* in strand B starts branch migration, displacing the domain 2 and releasing the output strands C and D. The displacement of the in-

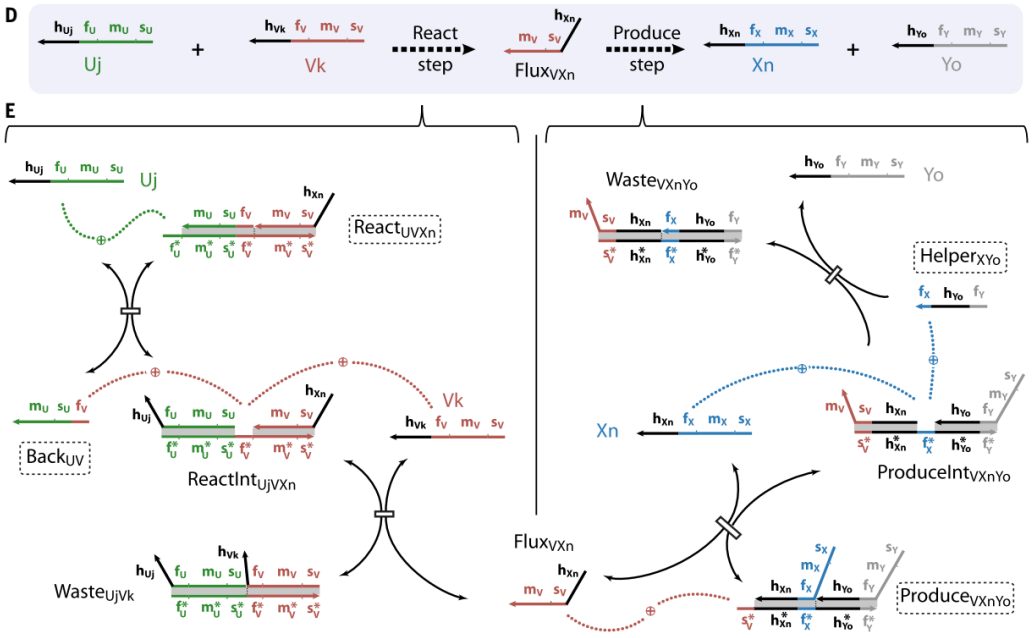

Figure 2.8: Cascade of strand displacement reactions to implement with DNA the dynamics of a bimolecular reaction $U + V \rightarrow X + Y$ (figure taken from [29]).

cumbent domain 2 is thermodynamically favoured over the unbinding of the toehold 1, leading to the complete displacement of C. Due to the absence of overhanging complementary toeholds in the output strands C and D the displacement is irreversible. Given its irreversibility, and that the output strand C can participate in other reactions, this enables a cascade of multiple reactions.

The single-stranded overhangs, toeholds, provide initial binding sites for incoming strands to initiate toehold-mediated branch migration process that can result in strand displacement [74, 75]. An accurate description on the hybridisation reaction is challenging, however some predictive models provide an estimation of the reaction rate based on the nucleotide sequences [74]. We then have that, in a DSD reaction, the signal species are DNA molecules composed of binding domains, and the hybridisations between strands are bimolecular reactions with unitary stoichiometric coefficients. The mediating complementary toeholds code in their sequences which strands can initially hybridise to trigger strand displacement, and define the propensities of the reactions.

2.4.2 Implementation of chemical reaction networks

Several frameworks assign formal species in the CRN to sets of DNA species, allowing the construction of circuits supported by a high level of automation using available

Table 2.1: Scheme in [21] to translate elementary reactions of catalysis, degradation and annihilation into DSD reactions with equivalent dynamics. Considering large concentrations of auxiliary strands at a value C_{max} nM, the bimolecular reactions are approximated by unimolecular reactions.

Catalysis

$$\underbrace{Z_i \xrightarrow{k_i} Z_i + Z_j}_{\text{CRN}} \quad \Rightarrow \quad \underbrace{\begin{cases} Z_j + G_i \xrightarrow{c_i} & O_i \\ O_i + T_i \xrightarrow{c_M} & Z_j + Z_j \end{cases}}_{\text{DSD reactions}} \quad \approx \quad \underbrace{\begin{cases} Z_i \xrightarrow{C_{max}c_i} & O_i \\ O_i \xrightarrow{C_{max}c_M} & Z_i + Z_j \end{cases}}_{\text{Approximation}}$$

Degradation

$$\underbrace{Z_i \xrightarrow{k_i} \emptyset}_{\text{CRN}} \quad \Rightarrow \quad \underbrace{Z_i + G_i \xrightarrow{c_i} \emptyset}_{\text{DSD reactions}} \quad \approx \quad \underbrace{Z_i \xrightarrow{c_i C_{max}} \emptyset}_{\text{Approximation}}$$

Annihilation

$$\underbrace{Z_i + Z_j \xrightarrow{k_i} \emptyset}_{\text{CRN}} \quad \Rightarrow \quad \underbrace{\begin{cases} Z_i + L_i \underset{c_M}{\overset{c_i}{\rightleftharpoons}} & H_i + B_i \\ Z_j + LS_i \underset{c_M}{\overset{c_M}{\rightleftharpoons}} & HS_i + BS_i, \\ Z_j + H_i \xrightarrow{c_M} & \emptyset \end{cases}}_{\text{DSD reactions}} \quad \approx \quad \underbrace{\begin{cases} Z_i \underset{c_M C_{max}}{\overset{c_i C_{max}}{\rightleftharpoons}} & H_i \\ Z_j + H_i \xrightarrow{c_M} & \emptyset \end{cases}}_{\text{Approximation}}$$

syntax and software tools [75, 76, 80].

For example, the DSD reactions in Figure 2.8 were used in [29] to implement a CRN with programmed oscillations, based on bimolecular reactions of the form $U + V \to X + Y$. The signal strands have four domains: a *first toehold* ($< f >$), the *branch-migration* domain ($< m >$), the *second toehold* ($< s >$), and an *history* domain ($< h >$). Besides the input signal strands U and V, the reactions need auxiliary molecules *React*, *Back*, *Produce* and *Helper* available in large concentrations. The intermediary species like *Flux* and the output strands X and Y are released from the auxiliary strands due to strand displacement. The competition for the branch strands $< m >$ and their eventual displacement, are mediated by the affinities between the toeholds $< f >$ and $< s >$ and the toeholds with complementary nucleotide sequences $< f^* >$ and $< s^* >$. To implement dual-rail circuits, the influential work from [21] supplies a framework to translate the three types of reactions of interest in (2.24) into bimolecular reactions using DSD reactions, Table 2.1. In the catalysis circuit, the intermediate species O_i serve as a map of identifiers between

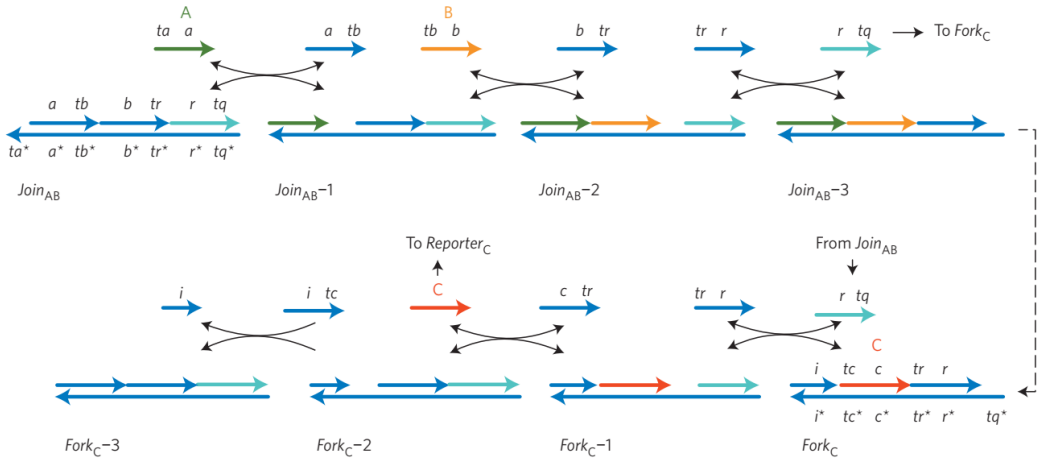

Figure 2.9: Implementation of $A + B \rightarrow C$ with a cascade of strand displacement reactions where the presence of species A and B lead to the release of a signal strand $< r\ tq >$ from the *Join* template (top), which in turn triggers the release of a strand C from the *Fork* strand (bottom) (figure adapted from [72]).

the reactant and the two products. The *gate* G_i and *translator* T_i species serve as translators of O_i, thus decoupling the identifying sequences between different Z_i (further details in [21]). In the degradation circuit, G_i sequesters Z_i into a waste complex, removing it from the reaction network. For the annihilation reaction, the *backward* strand B_i minimizes the use of Z_i when Z_j is absent. The reversibility of the first reaction keeps H_i and Z_i at equilibrium, allowing the conversion of unused H_i back to Z_i. When both Z_i and Z_j are present, H_i is irreversibly consumed, affecting the equilibrium and causing Z_i to be used.

The reactions produce *waste* in the form of inactivated double stranded molecules which cannot participate in any reaction. As a consequence, the gate G_i and translator T_i are consumed irreversibly as *fuel*, and the reactions stop if these are not replenished. In practice, the auxiliary species are initialised at high concentrations, to prevent their consumption from significantly impacting the dynamics.

In Table 2.1, the rate c_M $(\text{nMs})^{-1}$ is the maximum strand displacement rate for full toehold binding and the *bimolecular* reaction rate c_i $(\text{nMs})^{-1}$ can be tuned by the sequence of nucleotides of the complementary toeholds which initiate the strand displacement reactions, together with partial mismatches which weaken their propensity to hybridise [74]. Considering that we have limiting reactions ($c_i \ll c_M$), we end up with approximating unimolecular catalysis reactions (where O_i is only an intermediary). Assuming high concentrations of the fuel species and that these

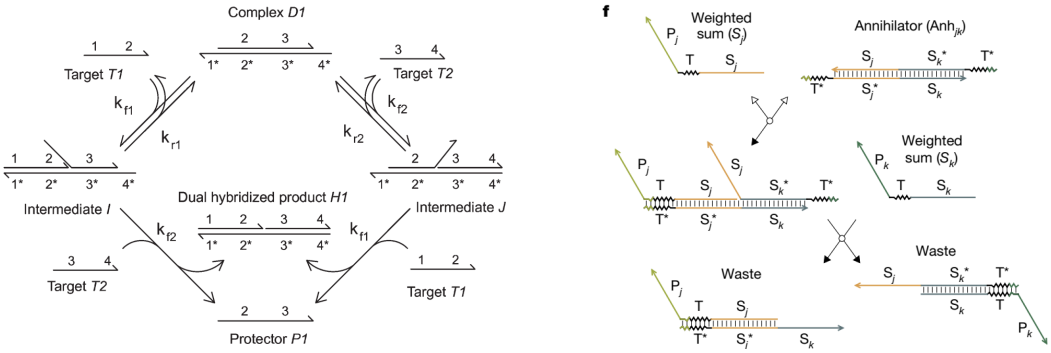

Figure 2.10: Left: cooperative hybridisation with a net reaction of the system $T1 + T2 + D1 \rightarrow H1 + P1$ as proposed in [144]. Right: cooperative hybridisation used in [145] where $S_j + S_k + Ann_{jk} \rightarrow \emptyset$ (figures adapted from [144, 145]).

remain (approximately) constant around an initial value C_{max}, or that they can be replenished, we can write the simplifying reactions in Table 2.1 [21], and we can map the rates between the CRN representation and the DSD rates.

Other schemes provide different architectures to represent the elementary reactions, also based on toehold mediation and auxiliary strands supplied in abundance. Chapter 4 proposes and describes in further detail an architecture for the DSD networks using Join-Fork templates and cooperative hybridisation. The implementations for catalysis and degradation are based on the Join-Fork templates from [72] in Figure 2.9. The $Join$ complex interacts with one or several input strands to release a signal strand ($< r\ tq >$), which will start a cascade of DSD reactions in the $Fork$ template, to release one or more output strands. The $Join$ and $Fork$ templates and the auxiliary two-domain strands (for example, $< tr\ r >$) must be present in large concentrations.

The implementation of the annihilation reactions use the cooperative hybridisation in Figure 2.10 (left) from [144], in which a single auxiliary species $D1$ hybridises with both input signals $T1$ and $T2$ to produce waste species. Both input species must be present for the cascade to become irreversible with a net reaction of the system of $T1 + T2 + D1 \rightarrow H1 + P1$. The same cooperative hybridisation was used in [145] to remove the weighted sum species S_j and S_k using a single complex $Annihilator(Ann_{jk})$ to produce two waste species, Figure 2.10 (right). Again, the removal of the species is only irreversible if both inputs are present.

Chapters 3 and 5 use a different architecture, based on the primitives explored in [76]. The implementation of all elementary reactions can be related in terms of Join-Fork templates, including the replacement of cooperative hybridisation with

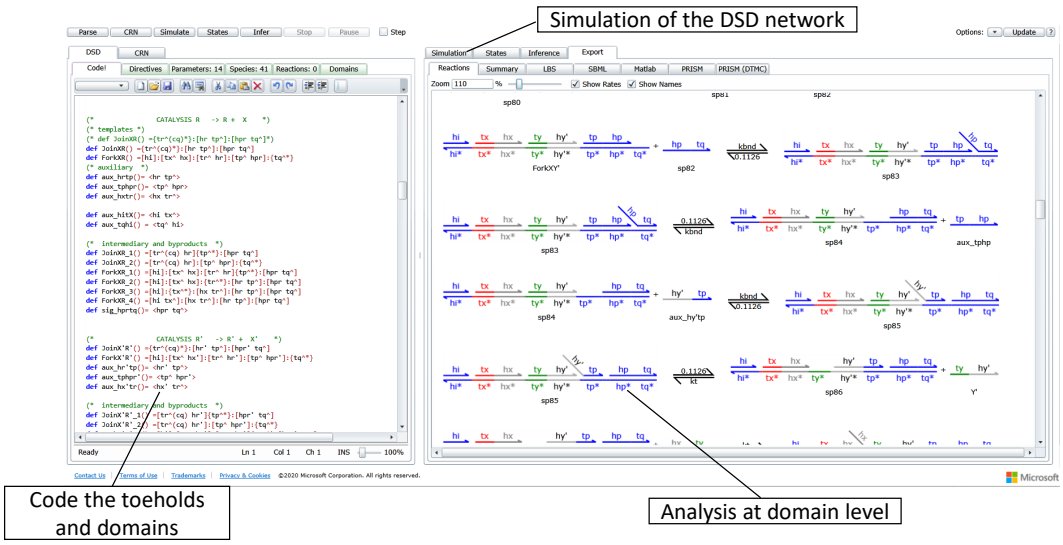

Figure 2.11: User interface for Visual DSD [80, 147], with a panel to express the domain structure of the DNA strands (left) and resulting domain level analysis of the domain interactions (right).

two auxiliary Join templates. A detailed description of the used reactions can be found in Section 3.5.

We then have several ways to map the reactions and reaction rates of the CRN into sets of DNA strands with tuned affinities of the toeholds, based on the base-pair complementarities and the nucleotide sequences [74,146]. These frameworks provide a direct translation from CRNs into an experimental set of biomolecules for design testing and validation.

2.5 Simulation and analysis software

Control design and analysis is carried out in Matlab™ using the Robust Control Toolbox™ [148] and optimisation toolboxes, which allow for the representation of uncertain systems, LFTs and to carry SSV analysis. The simulation of the mass action kinetics of the developed CRNs is carried out in Matlab™, using solvers with methods intended for stiff problems that may arise from timescale separation (for example, *ode15s* and *ode23s*).

Considering the MAK to model the DSD reactions, it results in much larger systems of ODEs. Fortunately, modelling of DNA systems is supported by existing tools, with domain level analysis and simulation of interacting strands. The software Visual DSD [80,147] uses a domain-level description language for formally describing

DSD systems [75] and to model and analyse their behaviour. It provides extensive analysis capabilities, enumerating all possible reactions between domain-level DNA complexes, stochastic simulations (SSA [149], CME and its LNA [114]), tiles with tethered species, and spatio-temporal dynamics for CRNs described by reaction-diffusion equations [150]. Throughout this work, Visual DSD is used to program the rates and domain interactions in the DSD networks, Figure 2.11, and verify and analyse their performance via both deterministic and stochastic simulations of the DSD reactions.

Other available tools include the analysis at base-pair sequence level, which must account for additional non-ideal interactions between domains such as binding due to partial domain sequence matches. The NUPACK package [146] calculates free energies and equilibrium concentrations of ordered complexes [151], providing sequence-level thermodynamic analysis to reaction rate constants and secondary structure formation. The Piperine compiler [29] automates the translation of a CRN into DNA at domain and sequence level, with toehold candidates based on NUPACK analysis, albeit for a fixed DSD scheme. The more recent Nuskell CRN-to-DNA compiler [77] promises a growing library of translation schemes (e.g. from [21, 29, 72, 73]), and can be used to compare DSD implementations in terms of molecule size, network size, or simulation behaviour (in this case using the domain-level reaction enumerator Peppercorn [152]).

Chapter 3

Linear feedback controllers using DNA strand displacement reactions

In classical linear negative feedback control, the controller is driven by comparing the output of the system with a reference signal, usually through a *two sided subtraction* where the result can be positive or negative. A key challenge when using CRNs to realise negative feedback system, is the inability to represent negative outcomes with "negative" concentrations. A CRN generally can only compute a positive difference between two positive inputs, resulting in *one-sided* subtractions [68]. Concentrations can only be non-negative, whereas signals in arbitrary linear systems take on positive and negative values [79]. The use of chemical concentrations as state variables is therefore not suitable for circuits involving negative signals necessary in negative feedback control, since the representation of a subtraction must always result positive.

The dual-rail methodology from [20,79] facilitates the implementation of embedded synthetic controllers due to the fact that linear operations (e.g., integration, sum, gain, etc.) can be implemented with networks of elementary chemical reactions, i.e. catalysis, degradation and annihilation. In this methodology, instead of representing a signal directly with the concentration of a species, each signal in the system is given by the *difference* between two species' concentrations. Despite the positivity of the concentrations, dual-rail computations can yield a two-sided subtraction, where a negative outcome is still represented by the difference of two positive concentrations.

For implementation, the elementary chemical reactions can be mapped into

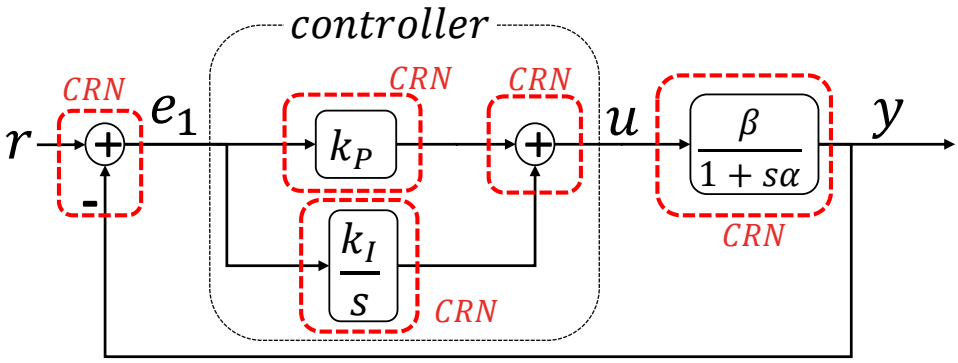

Figure 3.1: PI control of a first order system, where individual algebraic and dynamic modules are represented by a CRN.

chemistry based on DNA strands, through programmable DSD reactions [21, 29]. The sequence design of DNA species provides a mechanism to tag species and program the affinities in each reaction [72, 76]. It preserves modularity and can be scaled up to a very large number of chemical species [153].

The available mapping between transfer functions, CRNs and DSD reactions makes straightforward the use of classical control theory in the synthesis and implementation of biomolecular control systems, [76, 79, 95, 154]. This approach was exploited in [62] to define configurable primitives, that can be combined to realise any strictly proper transfer function. So far, however, the examples in the literature for linear negative controllers have been limited to very simple plants like static gains or first order systems [76, 79], and are also limited to PI control action as in Figure 3.1.

Three fundamental limitations of recent efforts to develop a comprehensive theory of feedback control for nucleic acids have been the lack of:

1. methods for computing the derivative of a signal, necessary for the implementation of PID controllers,

2. a convenient way to represent time delays, and

3. the ability to implement state feedback controller architectures.

This chapter proposes novel designs based on CRNs that address each of these open questions. It provides a representation for a linear system common in industry, and illustrates how to apply two fundamental classes of linear controllers: PID and state feedback control. The correct functioning of the circuits is checked via deterministic and stochastic simulations of the DNA strand displacement network using the Visual DSD rapid prototyping tool [80].

3.1 Representation of linear systems with CRNs

Considering a linear negative feedback system such as the one in Figure 3.1, the objective of a linear controller is to cancel the difference between a reference r and an output y. Since concentrations are non-negative, they are ill-suited to represent a subtraction $e_1 = r - y$, since we need e_1 to be a real number. We apply, instead, the *dual-rail* representation of [79], with sets of reactions for each operation in the feedback loop, Figure 3.1.

3.1.1 Dual-rail representation of a plant with delay approximation with a CRN

Here we consider for the plant a first order system with a pure time-delay.

Definition 3.1. *A FOTD system, with gain β, a pole at $s = -\alpha^{-1}$, and a phase delay θ, can be expressed in the frequency domain as*

$$F(s) = \frac{\beta}{1 + s\alpha} e^{-\theta s} \ . \tag{3.1}$$

The FOTD plant is commonly used to approximate more complex systems into a simpler form suitable for the tuning rules of PID controllers [155], while remaining complex enough to represent the bandwidth, gain and phase of a system, all of which are critical metrics for linear feedback design. In the case of biomolecular systems, the pole can model the effects of degradation and dilution, while the phase can capture signalling delays due to diffusion. For the latter, we introduce a novel method for representing time-delays using the dual-rail CRN formulism.

Definition 3.2 (Plant)**.** *Modelling the delay θ with the first order Padé approximation, decomposed into a subtraction and a first order system, we have*

$$e^{-\theta s} \approx \frac{2 - \theta s}{2 + \theta s} = \frac{4}{s\theta + 2} - 1 \tag{3.2}$$

and the FOTD system in (3.1) *can be approximated by the transfer function*

$$G_{uy}(s) = \frac{\beta}{1+s\alpha}\frac{2-\theta s}{2+\theta s} = \frac{g_1}{s+g_2}\left(\frac{g_3}{s+g_4} - 1\right) = \underbrace{\frac{g_1}{s+g_2}}_{G_{u1}(s)}\left(\underbrace{\overbrace{\frac{g_3}{s+g_4}}^{G_{1y}(s)} - 1}_{G_{12}(s)}\right) \tag{3.3}$$

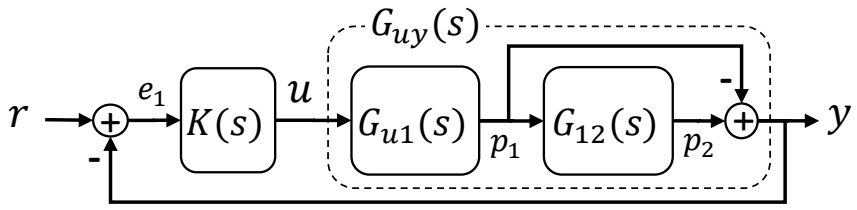

Figure 3.2: Linear negative feedback for reference tracking, with a linear plant $G_{uy}(s)$ decomposed into two first order systems $G_{u1}(s)$ and $G_{12}(s)$. Two side subtractions are necessary to compute the control error e_1 and the output y from the states p_1 and p_2.

where

$$g_1 = \beta\alpha^{-1} \tag{3.4a}$$
$$g_2 = \alpha^{-1} \tag{3.4b}$$
$$g_3 = 4\theta^{-1} \tag{3.4c}$$
$$g_4 = 2\theta^{-1}\ . \tag{3.4d}$$

The plant (3.3) is decomposed as shown in Figure 3.2, into two first order systems G_{u1} and G_{12}, with intermediary states p_1 and p_2. The approximation of the delay introduces a non-minimum phase zero at $s = 2\theta^{-1}$ and an additional two-sided subtraction

Result 3.1. *Using the* dual-rail *representation, we assign species to each signal according to the methods in Section 2.3.1, to arrive at the CRN representation of a plant with a time-delay*

$$U^{\pm} \xrightarrow{g_1} U^{\pm} + P_1^{\pm}, \qquad P_1^{\pm} \xrightarrow{g_2} \emptyset, \quad P_1^{+} + P_1^{-} \xrightarrow{\eta} \emptyset \tag{3.5a}$$
$$P_1^{\pm} \xrightarrow{g_3} P_1^{\pm} + P_2^{\pm}, \qquad P_2^{\pm} \xrightarrow{g_4} \emptyset, \quad P_2^{+} + P_2^{-} \xrightarrow{\eta} \emptyset \tag{3.5b}$$
$$P_1^{\pm} \xrightarrow{\gamma} P_1^{\pm} + \boldsymbol{Y}^{\mp}, \qquad P_2^{\pm} \xrightarrow{\gamma} P_2^{\pm} + Y^{\pm}, \quad Y^{\pm} \xrightarrow{\gamma} \emptyset \tag{3.5c}$$
$$U^{+} + U^{-} \xrightarrow{\eta} \emptyset, \qquad Y^{+} + Y^{-} \xrightarrow{\eta} \emptyset\ . \tag{3.5d}$$

The first order system $G_{u1}(s)$ is represented in (3.5a), and (3.5b) is the representation for $G_{12}(s)$. The subtraction results from the steady state conditions of (3.5c), and the annihilation reactions in (3.5d) are introduced to limit the con-

centrations. Writing the MAK, the ODEs for (3.5) are given by

$$\dot{p}_1^{\pm} = -g_2 p_1^{\pm} + g_1 u^{\pm} - \eta p_1^{+} p_1^{-}, \quad p_1^{\pm}(0) = 0 \tag{3.6a}$$
$$\dot{p}_2^{\pm} = -g_4 p_2^{\pm} + g_3 p_1^{\pm} - \eta p_2^{+} p_2^{-}, \quad p_2^{\pm}(0) = 0 \tag{3.6b}$$
$$\dot{y}^{\pm} = -\gamma y^{\pm} + \gamma \boldsymbol{p_1^{\mp}} + \gamma p_2^{\pm} - \eta y^{+} y^{-}, \quad y^{\pm}(0) = 0\ . \tag{3.6c}$$

The choice of reactions for the representation might not be unique. For example, the *catalytic degradation* scheme from [76] replaces the use of the degradation reactions with catalysis and annihilation reactions. An example is also discussed in Chapter 4 (see Figure 4.9), where we have two possible CRNs to represent the same I/O system.

The use of dual-rail representation can lead to a considerable increase in the number of reactions in (3.5). The degradation and catalysis reactions are duplicated, with additional annihilation reactions. Moreover, number of reactions is aggravated by the representation of the subtraction, which introduces the six reactions in (3.5c). Although the method is very convenient to represent non-positive linear dynamics, such an increase in the number of reactions and species makes the realisation more difficult.

In some cases, it might be possible to combine representations of operations in the same reactions, to decrease the complexity of the CRN. These possibilities are the topic of Chapter 4.

3.1.2 I/O dynamics of the CRN representation

To derive the linear representation we use the I/O systems from Definition 2.17.

Definition 3.3. *Define the I/O dynamics of the plant* (3.3) *as the response of the CRN dynamics in* (3.6)*, from the input* $u = u^{+} - u^{-}$ *to the outputs* $p_j = p_j^{+} - p_j^{-}$ *and* $y = y^{+} - y^{-}$*.*

The dynamics for $\dot{p}_j = \dot{p}_j^{+} - \dot{p}_j^{-}$ and $\dot{y} = \dot{y}^{+} - \dot{y}^{-}$ are linear because the bimolecular terms cancel out (see details in [79]), and the I/O dynamics do not depend on η. From (3.6), we have

$$\dot{p}_1 = -g_2 p_1 + g_1 u, \quad p_1(0) = 0 \tag{3.7a}$$
$$\dot{p}_2 = -g_4 p_2 + g_3 p_1, \quad p_2(0) = 0 \tag{3.7b}$$
$$\gamma^{-1}\dot{y} = -y + \boldsymbol{p_1} + p_2, \quad y(0) = 0\ . \tag{3.7c}$$

Although we recover $G_{u1}(s)$ from (3.6a) and $G_{12}(s)$ from (3.6b), the I/O dynamics are an approximation of $G_{uy}(s)$ in (3.3). The additional dynamics in (3.6c) that

Table 3.1: Parameterisation for the CRN representation of the plant

Parameter	Value	Units	Rates	Value	Units
θ	10^5	s	g_1	5×10^{-6}	s^{-1}
α	2×10^5	s	g_2	5×10^{-6}	s^{-1}
β	1	-	g_3	4×10^{-5}	s^{-1}
			g_4	2×10^{-5}	s^{-1}
			γ	2.5×10^{-4}	s^{-1}

result from the crossed contributions P_1^+ to Y^- and P_1^- to Y^+, provide an exact subtraction only at steady state, when $\dot{y} = 0$ and

$$y^* \quad = \quad y^{+*} - y^{-*} = p_2^{+*} - p_2^{-*} - p_1^{+*} + p_1^{-*} = p_2^* - p_1^* \; . \tag{3.8}$$

From the standard-form in (3.7), it is straightforward that under singular perturbation analysis [109], we are considering a QSS approximation, or timescale separation, for $\gamma \gg g_i, \; i = 1, ..., 4$, so that (3.7c) degenerates into an algebraic equation.

The parameterisation of the plant and the resulting reaction rates in the CRN are provided in Table 3.1. The values for the pole, gain and delay (α, β and θ) are prescribed as an arbitrary example of a plant that we wish to represent with a CRN, although there was some care to ensure the feasibilty of the reaction rates.

Since the bimolecular reactions for implementation with DSD reactions are limited by the maximum feasible hybridisation rate and concentrations of DNA strands, the timescale and rates of the plant were chosen to ensure the reaction rates $g_i, \; i = 1, 2, 3, 4$ of the CRN (from (3.4)) result in a realistic and feasible parameterisation suitable for realisation with DSD reactions.

The value of γ was set to be faster than the remaining reaction rates to allow timescale separation, but without introducing stiffness issues. Theoretically, γ should be as fast as possible but in practice it is also limited by the maximum hybridisation rate in the DSD reactions, and the dynamics of (3.7c) will impact the representation of the I/O system.

3.2 CRN representation of PID and state feedback controllers

We now introduce novel CRN representations for two important classes of reference tracking controllers in linear control theory.

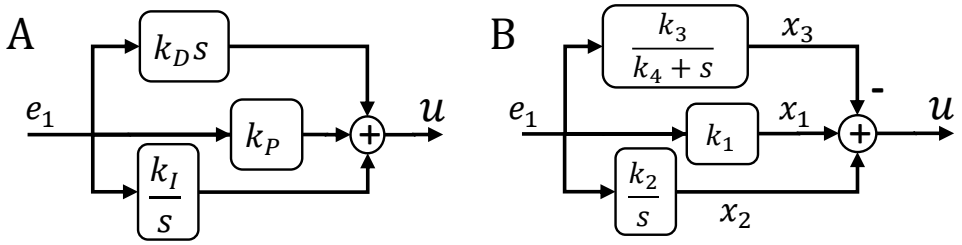

Figure 3.3: PID control structures: A) with a pure derivative; B) using the approximation $\mathcal{D}(s)$ in (3.12) that results in the controller $K(s)$ in (3.13).

3.2.1 Proportional-integral-derivative control

Definition 3.4. *Define the classical PID as the control law depicted in Figure 3.3 A), with the actuation $U(s)$ given by*

$$U(s) \quad = \left(k_P + \tfrac{k_I}{s} + k_D s\right) E_1(s) \ . \tag{3.9}$$

The challenge here is how to represent the derivative using a proper transfer function which can be represented with a CRN.

Approximation of the derivative

We approximate the limit for the differentiation of a signal v with the difference between the signal without and with a delay of τ seconds, so that we have

$$\dot{v}(t) \quad \approx \quad \frac{v(t) - v(t-\tau)}{\tau} \Leftrightarrow sV(s) \approx \frac{1}{\tau}\left(1 - e^{-\tau s}\right) V(s) \ . \tag{3.10}$$

Replacing the delay with its Padé approximation results in a transfer function with zero relative degree

$$\frac{1}{\tau}\left(1 - e^{-\tau s}\right) \approx \frac{1}{\tau}\left(1 - \frac{2 - \tau s}{2 + \tau s}\right) = \frac{2s}{2 + \tau s} \ . \tag{3.11}$$

Definition 3.5. *Define the proper transfer function of zero relative degree*

$$\mathcal{D}(s) \quad \coloneqq \quad \frac{2s}{2+\tau s} = \frac{2}{\tau}\left(1 - \frac{2}{2+\tau s}\right) = \frac{2}{\tau} - \frac{4}{2\tau + \tau^2 s} \tag{3.12a}$$

$$\mathcal{D}(s) \quad \approx \quad s, \, |s| \ll \frac{2}{\tau} \tag{3.12b}$$

which is equivalent to a subtraction with a first order system, that closely approximates the derivative over a frequency domain satisfying $|s| \ll 2\tau^{-1}$.

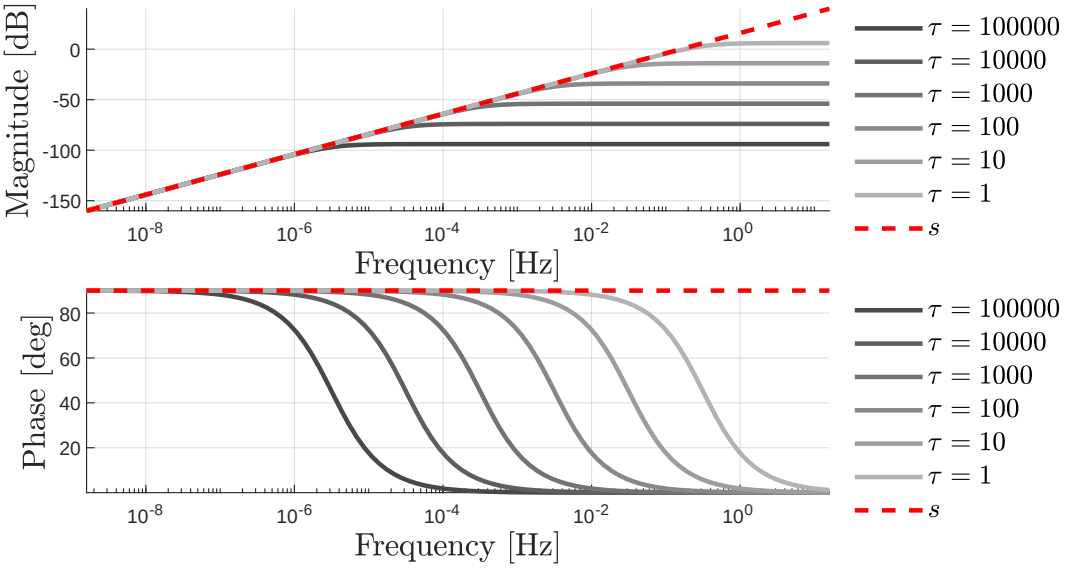

Figure 3.4: Comparison of the Bode plots for the derivative s, and the approximation in (3.12) as function of the delay τ. A lower value of τ increases the bandwidth where $\mathcal{D}(s) \approx s$.

Remark 3.1. *The frequency domain where the approximation* (3.12) *is valid depends on a single parameter τ, where a smaller τ results in a larger bandwidth (Figure 3.4). Its parameterisation can be naturally related with the frequency description of the plant and specifications of the controller.*

Remark 3.2. *With the CRNs for the dual-rail representation of subtraction, we can represent the transfer function with a zero relative degree* (3.12) *as the difference between a static and a dynamic system [155]. This avoids the need for approximations based on* strictly *proper transfer functions, and removes assumptions on saturated regimes or constraints in the parameterisation to disregard higher-order terms (as in [156, 157]).*

We can now construct a new controller that replaces the derivative with the defined approximation $\mathcal{D}(s)$. Its decomposition into a subtraction and first order system can be represented using the dual-rail methods.

Definition 3.6. *Define the modified PID control law in Figure 3.3B, which uses* (3.12) *instead of differentiation, to arrive at the control law given by*

$$K(s) \quad = k_P + \frac{k_I}{s} + k_D \left(\frac{2}{\tau} - \frac{4}{2\tau + \tau^2 s} \right) = k_1 + \frac{k_2}{s} - \frac{k_3}{k_4 + s} \tag{3.13}$$

where $k_2 = k_I$, $k_1 = k_P + \frac{2k_D}{\tau}$, $k_3 = \frac{4k_D}{\tau^2}$, and $k_4 = \frac{2}{\tau}$.

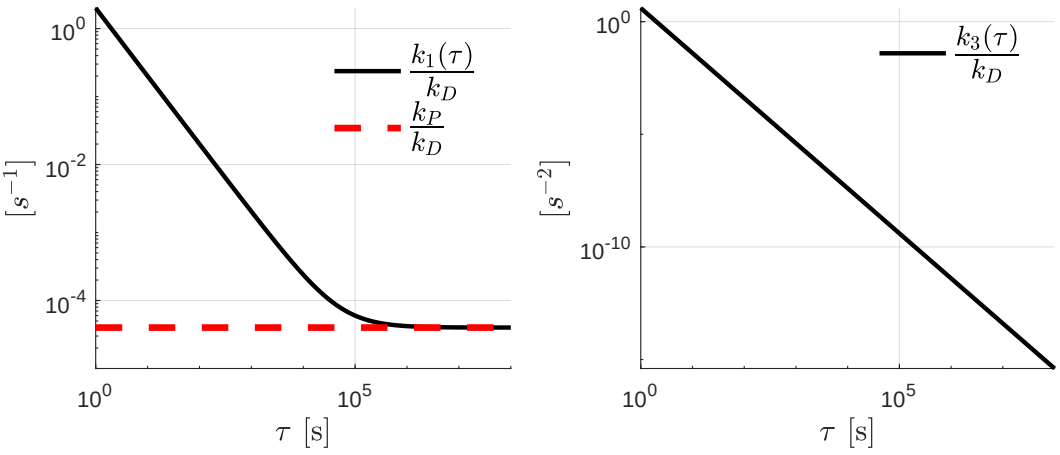

Figure 3.5: Dependency of the parameters k_1 and k_3 on the delay τ, used in the control law $K(s)$ in (3.13).

A smaller τ results in a wider bandwidth and a faster pole $s = -k_4$. However, a larger τ can also be beneficial to filter peaks introduced by the derivative, acting as low pass filter on the delayed signal (similar to the filtered PID controller [155]).

Remark 3.3. *While k_2 depends only on the integral gain k_I, the remaining parameters k_1, k_3 and k_4 depend also on τ. Both k_1 and k_3 depend on the inverse of τ, and quickly increase for a very small delay τ (Figure 3.5). We then have that the physical limits of the reaction rates lead to a trade-off, between having a τ which is large enough for feasible reaction rates and a τ that is small enough to ensure the bandwidth and accuracy of $\mathcal{D}(s)$.*

In practice, the parameterisation of the control gains and bandwidth of the differentiation are limited by the reaction rates achievable in the experimental realisation of the system. The design of the control law in (3.13)*, and the choice for the gains and tuning of the differentiation need to be checked against the feasibility space of the implementable reaction rates.*

CRN representation of PID controller

A CRN is derived, following the formalism of [79] and Section 2.3.1, where species are assigned to each signal in Figure 3.3B, so that $e_1 = e_1^+ - e_1^-$, $x_1 = x_1^+ - x_1^-$, $x_2 = x_2^+ - x_2^-$, and $x_3 = x_3^+ - x_3^-$.

Result 3.2. *The PID controller of* (3.13) *is represented by*

$$R^{\pm} \xrightarrow{\gamma} R^{\pm} + E_1^{\pm},\ Y^{\pm} \xrightarrow{\gamma} Y^{\pm} + \boldsymbol{E_1^{\mp}},\ E_1^{\pm} \xrightarrow{\gamma} \emptyset \tag{3.14a}$$

$$R^{+} + R^{-} \xrightarrow{\eta} \emptyset,\ Y^{+} + Y^{-} \xrightarrow{\eta} \emptyset,\ E_1^{+} + E_1^{-} \xrightarrow{\eta} \emptyset \tag{3.14b}$$

$$E_1^{\pm} \xrightarrow{\gamma k_1} E_1^{\pm} + X_1^{\pm},\ X_1^{\pm} \xrightarrow{\gamma} \emptyset,\ X_1^{+} + X_1^{-} \xrightarrow{\eta} \emptyset \tag{3.14c}$$

$$E_1^{\pm} \xrightarrow{k_2} E_1^{\pm} + X_2^{\pm}, \quad X_2^{+} + X_2^{-} \xrightarrow{\eta} \emptyset \tag{3.14d}$$

$$E_1^{\pm} \xrightarrow{k_3} E_1^{\pm} + X_3^{\pm},\ X_3^{\pm} \xrightarrow{k_4} \emptyset,\ X_3^{+} + X_3^{-} \xrightarrow{\eta} \emptyset \tag{3.14e}$$

$$X_1^{\pm} \xrightarrow{\gamma} X_1^{\pm} + U^{\pm},\ X_2^{\pm} \xrightarrow{\gamma} X_2^{\pm} + U^{\pm},\ U^{\pm} \xrightarrow{\gamma} \emptyset \tag{3.14f}$$

$$X_3^{\pm} \xrightarrow{\gamma} X_3^{\pm} + \boldsymbol{U^{\mp}},\ U^{+} + U^{-} \xrightarrow{\eta} \emptyset\ . \tag{3.14g}$$

The error $e_1 = r - y$ is represented in (3.14a-3.14b), using the same steady state computation and assumption of timescale separation as in (3.8).

From constructions in literature for PI controllers [76,79], we have the CRNs for the gain $x_1 = k_1 e_1$ in (3.14c) and integration $\dot{x}_2 = k_2 e_1$ in (3.14d). The first order system $\dot{x}_3 = -k_4 x_3 + k_3 e_1$ is represented by the reactions in (3.14e) in the same way as we did for the plant in (3.5). The summing junction results from (3.14f-3.14g), where the crossed contributions to represent the subtraction are highlighted in bold in (3.14g).

Remark 3.4. *In the case of negative gains, the constraint of positive reaction rates* $k_i > 0$*,* $(i = 1, \ldots, 4)$ *can be fulfilled by applying the negative signs in the computation of* u*. For example, if* $k_I < 0$*, we keep* $k_2 = |k_I| > 0$ *and reverse the contributions in* (3.14f) *with* $X_2^{\pm} \xrightarrow{\gamma} X_2^{\pm} + \boldsymbol{U^{\mp}}$*, to obtain the negative gain in the I/O dynamics.*

3.2.2 State feedback with integral control

Since we are not dealing with compartmentalised modules, the plant species are in the same solution as the controller species, and the control law can have access to the species involved in the representation of states of the plant. This direct measurement is exploited to show for the first time how to design linear state feedback biomolecular controllers, where measurements upstream of the output are used for damping purposes, as an alternative to the derivative gain in the PID controller.

To design the controller, we first define an error vector, which we wish to cancel. The problem is then solved as a disturbance rejection with state feedback control, and after it is translated to a reference tracking problem with state feedback and feed-forward control.

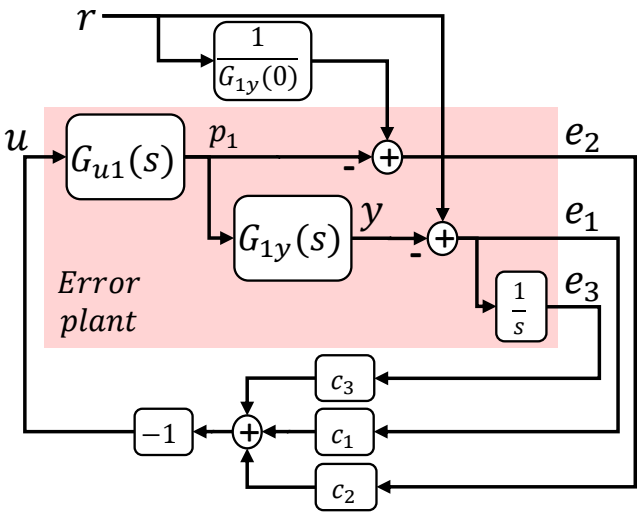

Figure 3.6: Structure of static state feedback for regulation control defined in the error space coordinates. The controlled plant contains an additional integrator and subtractions to compute the error signals.

Definition 3.7. *Given the plant in Figure 3.2, let us define the error coordinates as*

$$\mathbf{e} = \begin{bmatrix} e_1 \\ e_2 \\ e_3 \end{bmatrix} = \begin{bmatrix} r - y \\ G_{1y}^{-1}(0)\, r - p_1 \\ \int e_1 \end{bmatrix} \tag{3.15}$$

where e_1 is the output tracking error. The second component e_2 is the error between the state p_1 and its steady state condition p_1^*, when $r = y^* = G_{1y}(0)p_1^*$. For the purposes of integral control, we augment the state vector with the integral $e_3 = \int e_1 dt = \int (r - y)dt$.

Regulation problem for controller design

For the error defined in (3.15), we have that $\mathbf{e}^* = 0 \Rightarrow y^* = r$. Hence, we restate the controller as the regulation solution, which cancels the error vector $\mathbf{e}$ from Definition 3.15 when the plant is subjected to a static disturbance r. With $\dot{r} = 0$, the error dynamics are $\dot{e}_1 = -\dot{y}$ and $\dot{e}_2 = -\dot{p}_1$, and therefore, the error plant used

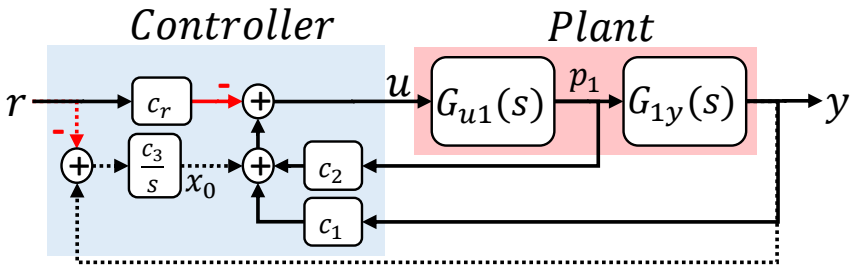

Figure 3.7: Structure of static state feedback (gains c_1 and c_2) and feed-forward gain control (c_r), extended with integral control $c_3 s^{-1}$ (dashed). The constants gains are the solution of a regulator with negative static state feedback.

for control design is given by

$$E(s) = \begin{bmatrix} -G_{uy}(s) \\ -G_{u1}(s) \\ \frac{1}{s}\left(-G_{uy}(s)\right) \end{bmatrix} U(s) \tag{3.16}$$

as depicted in Figure 3.6. The control law is chosen as the static negative state feedback law

$$U(s) = -\begin{bmatrix} c_1 & c_2 & c_3 \end{bmatrix} E(s) \tag{3.17}$$

with scalar static gains $c_i \in \mathbb{R}$, $i = 1, 2, 3$, such that the closed loop dynamics (3.16-3.17) have zero steady state error $\mathbf{e}^* = 0$. Assuming all of the states of (3.16) are available for the controller, the gains c_i can be designed using linear control methods like pole placement or through optimisation (for example as a linear quadratic regulator) [81, 83].

Controller structure

Once the gains c_i are solved for the problem (3.16-3.17), we can use (3.15) to express the actuation u as a functions of p_1, y, and r, and recover the reference tracking control structure with the original plant.

Definition 3.8. *Defining the feed-forward gain $c_r = c_2 G_{1y}^{-1}(0) + c_1$, we have from (3.15) that the static reference tracking control law can be written in the original coordinates as*

$$u = -\sum c_i e_i = c_1 y + c_2 p_1 - c_3 \int (r - y) - c_r r \ . \tag{3.18}$$

With the control written in function of the states of the plant, we can apply the control law (3.18) to the original plant, resulting in the control architecture in Figure 3.7.

We can also derive the closed loop transfer function. Recalling from (3.3) and Figure 3.7 that

$$G_{uy}(s)P_1(s) = G_{u1}(s)G_{1y}(s)P_1(s) = G_{u1}(s)Y(s) \tag{3.19}$$

we can take (3.18) and solve for $Y(s) = G_{uy}(s)U(s)$ to obtain the closed loop transfer function as

$$\begin{aligned} Y(s) &= G_{uy}(s)\left(c_1Y(s) + c_3s^{-1}Y(s) + c_2P_1(s) - c_3s^{-1}R(s) - c_rR(s)\right) \\ &= G_{uy}(s)Y(s)\left(c_1 + c_3s^{-1}\right) + c_2G_{uy}(s)P_1(s) - \left(c_3s^{-1} + c_r\right)G_{uy}(s)R(s) \\ &= \left(G_{uy}(s)\left(c_1 + c_3s^{-1}\right) + c_2G_{u1}(s)\right)Y(s) - \left(c_3s^{-1} + c_r\right)G_{uy}(s)R(s) \\ \Rightarrow Y(s) &= \frac{-\left(c_3s^{-1} + c_r\right)G_{uy}(s)}{1 - G_{uy}(s)\left(c_1 + c_3s^{-1}\right) - c_2G_{u1}(s)}R(s)\ . \end{aligned} \tag{3.20}$$

Remark 3.5. *We then confirm that with integral control we achieve steady state reference tracking, since it follows that*

$$\lim_{s\to 0}\frac{Y(s)}{R(s)} = \lim_{s\to 0}\frac{-G_{uy}(s)\left(c_r + \frac{c_3}{s}\right)}{1 - G_{uy}(s)\left(c_1 + \frac{c_3}{s}\right) - c_2G_{u1}(s)} = \lim_{s\to 0}\frac{G_{uy}(s)\frac{c_3}{s}}{G_{uy}(s)\frac{c_3}{s}} = 1\ . \tag{3.21}$$

CRN representation

The CRN for the state feedback control law (3.18) is then given as follows.

Result 3.3. *Assuming negative gains $c_i < 0$ $(i = 1, 2, 3)$ (hence $c_r < 0$), the state feedback in* (3.18) *can be written as*

$$u = -\left|c_1\right| y - \left|c_2\right| p_1 + \left|c_3\right| \int r - \left|c_3\right| \int y + \left|c_r\right| r \tag{3.22}$$

and represented by the CRN

$$Y^{\pm} \xrightarrow{\gamma|c_1|} Y^{\pm} + \boldsymbol{U^{\mp}}, \qquad P_1^{\pm} \xrightarrow{\gamma|c_2|} P_1^{\pm} + \boldsymbol{U^{\mp}}, \tag{3.23a}$$

$$R^{\pm} \xrightarrow{\gamma|c_r|} R^{\pm} + U^{\pm}, \qquad U^{\pm} \xrightarrow{\gamma} \emptyset, \quad R^{+} + R^{-} \xrightarrow{\eta} \emptyset \tag{3.23b}$$

$$R^{\pm} \xrightarrow{|c_3|} R^{\pm} + X_0^{\pm}, \qquad Y^{\pm} \xrightarrow{|c_3|} Y^{\pm} + \boldsymbol{X_0^{\mp}} \tag{3.23c}$$

$$X_0^{\pm} \xrightarrow{\gamma} X_0^{\pm} + U^{\pm}, \qquad X_0^{+} + X_0^{-} \xrightarrow{\eta} \emptyset\ . \tag{3.23d}$$

We ensure positive reaction rates in the CRN, by setting them as the absolute values

of the controller gains, and addressing the signs of the gains in the catalysis reactions in the summing junctions.

The annihilation reactions for $Y^{\pm}$, $U^{\pm}$ and $P_1^{\pm}$ are included in the CRN of the plant in (3.5a) and (3.5d). Both (3.23a-3.23b) apply the feedback and feed-forward gains at steady state, where γ should be on a faster timescale for a QSS approximation. The reactions (3.23a) apply the subtractions in (3.18) by inverting the contributions to U (in bold). The negativity of c_r cancels the minus sign in (3.18) and results in the catalysis in (3.23b). The gain and integral of the tracking error are applied in (3.23c-3.23d).

Remark 3.6. *Comparing* (3.23) *to the CRN for the PID controller (3.14), the state feedback scheme needs fewer reactions and fewer additional species, making it highly attractive for the experimental implementation of feedback with DSD reactions. The CRN simplifies even further without integral control, since removing $X_0^{\pm}$ and (3.23c-3.23d) reduces the controller to a summing junction. However, this results in a non-zero steady state error.*

For example, without integral gain ($c_3 = 0$ in (3.20)) we get

$$Y(s) = \frac{-G_{uy}(s)(c_r)}{1-G_{uy}(s)(c_1)-c_2G_{u1}(s)}R(s) \ . \tag{3.24}$$

From Table 3.1 we have that $G_{uy}(0) = G_{u1}(0) = G_{1y}(0) = 1$, hence the steady state results

$$y^* = -\frac{c_1 + c_2}{1 - c_1 - c_2}r \ . \tag{3.25}$$

The steady state error can be reduced with the use of high gain feedback, but not entirely eliminated.

3.3 CRN dynamics for the closed loop systems

The full dynamics of the CRNs representing each of the closed-loop systems are now derived from the mass action law in (2.16). The crossed contributions are highlighted in bold, which ultimately result in subtractions and negative gains in the I/O systems.

For the PID controller $K(s)$ from (3.13), we combine the CRNs of the plant (3.5) and the controller (3.14). The dynamics are given by the dynamics

of the plant (3.6) together with

$$\begin{aligned}
\dot{e}_1^{\pm} &= -\gamma e_1^{\pm} + \gamma \boldsymbol{y}^{\mp} + \gamma r^{\pm} - \eta e_1^{+} e_1^{-}, \quad e_1^{\pm}(0) = 0 && \text{(3.26a)}\\
\dot{x}_1^{\pm} &= -\gamma x_1^{\pm} + \gamma k_1 e_1^{\pm} - \eta x_1^{+} x_1^{-}, \quad x_1^{\pm}(0) = 0 && \text{(3.26b)}\\
\dot{x}_2^{\pm} &= k_2 e_1^{\pm} - \eta x_2^{+} x_2^{-}, \quad x_2^{\pm}(0) = 0 && \text{(3.26c)}\\
\dot{x}_3^{\pm} &= -k_4 x_3^{\pm} + k_3 e_1^{\pm} - \eta x_3^{+} x_3^{-}, \quad x_3^{\pm}(0) = 0 && \text{(3.26d)}\\
\dot{u}^{\pm} &= -\gamma u^{\pm} + \gamma x_1^{\pm} + \gamma x_2^{\pm} + \gamma \boldsymbol{x_3}^{\mp} - \eta u^{+} u^{-}, \quad u^{\pm}(0) = 0\ . && \text{(3.26e)}
\end{aligned}$$

Similar to Definition 3.3, the I/O dynamics of the closed loop systems are given by the response from $r = r^+ - r^-$ to the output $y = y^+ - y^-$ and actuation $u = u^+ - u^-$. The I/O system for the closed loop results then in the linear ODEs

$$\begin{aligned}
\gamma^{-1}\dot{e}_1 &= -e_1 - \boldsymbol{y} + r, \quad e_1(0) = 0 && \text{(3.27a)}\\
\gamma^{-1}\dot{x}_1 &= -x_1 + k_1 e_1, \quad x_1(0) = 0 && \text{(3.27b)}\\
\dot{x}_2 &= k_2 e_1, \quad x_2(0) = 0 && \text{(3.27c)}\\
\dot{x}_3 &= -k_4 x_3 + k_3 e_1, \quad x_3(0) = 0 && \text{(3.27d)}\\
\gamma^{-1}\dot{u} &= -u + x_1 + x_2 - \boldsymbol{x_3}, \quad u(0) = 0 && \text{(3.27e)}\\
\dot{p}_1 &= -g_2 p_1 + g_1 u, \quad p_1(0) = 0 && \text{(3.27f)}\\
\dot{p}_2 &= -g_4 p_2 + g_3 p_1, \quad p_2(0) = 0 && \text{(3.27g)}\\
\gamma^{-1}\dot{y} &= -y - \boldsymbol{p_1} + p_2, \quad y(0) = 0\ . && \text{(3.27h)}
\end{aligned}$$

A QSS approximation with a faster γ is assumed for the subtractions that compute the control error e_1, control actuation u and the output of the plant y, and also to compute the proportional gain in (3.27b).

For the state feedback controller in (3.18), combining the CRN of the plant (3.5) with the CRN from (3.23), we get the dynamics of the plant (3.6) together with

$$\begin{aligned}
\dot{x}_0^{\pm} &= |c_3|\boldsymbol{y}^{\mp} + |c_3| r^{\pm} - \eta x_0^{+} x_0^{-}, \quad x_0^{\pm}(0) = 0 && \text{(3.28a)}\\
\dot{u}^{\pm} &= -\gamma u^{\pm} - \eta u^{+} u^{-} + \gamma x_0^{\pm} + \gamma |c_2| \boldsymbol{p_1}^{\mp} + \gamma |c_1| \boldsymbol{y}^{\mp}\\
&\quad + \gamma |c_r| r^{\pm},\ u^{\pm}(0) = 0 && \text{(3.28b)}
\end{aligned}$$

Table 3.2: Parameterisation of the controllers and CRNs

Control designed parameters	Reaction rates in CRN
$k_P = 2$	$k_1 = 4$
$k_I = 9.5 \times 10^{-6}$ s^{-1}	$k_2 = 9.5 \times 10^{-6}$ s^{-1}
$k_D = 5 \times 10^{5}$ s	$k_3 = 8 \times 10^{-5}$ s^{-1}
$\tau = 5 \times 10^{5}$ s	$k_4 = 4 \times 10^{-5}$ s^{-1}
$c_1 = -0.4064$	$\lvert c_1 \rvert = 0.4064$ s^{-1}
$c_2 = -3.7264$	$\lvert c_2 \rvert = 3.7264$
$c_3 = -6.656 \times 10^{-6}$ s^{-1}	$\lvert c_3 \rvert = 6.656 \times 10^{-6}$ s^{-1}
$c_r = -4.1328$	$\lvert c_r \rvert = 4.1328$
	$\gamma = 2.5 \times 10^{-4}$ s^{-1}

resulting in the linear I/O system given by

$$\dot{x}_0 = |c_3|r - |c_3|\boldsymbol{y}, \quad x_0(0) = 0 \tag{3.29a}$$

$$\gamma^{-1}\dot{u} = -u + x_0 - |c_2|\boldsymbol{p_1} - |c_1|\boldsymbol{y} + |c_r|r, \quad u(0) = 0 \tag{3.29b}$$

$$\dot{p}_1 = -g_2 p_1 + g_1 u, \quad p_1(0) = 0 \tag{3.29c}$$

$$\dot{p}_2 = -g_4 p_2 + g_3 p_1, \quad p_2(0) = 0 \tag{3.29d}$$

$$\gamma^{-1}\dot{y} = -y - \boldsymbol{p_1} + p_2, \quad y(0) = 0\ . \tag{3.29e}$$

The closed loop system has fewer states than the PID control system, and the controller has a single operation dependent on the QSS approximation and a fast reaction rate γ.

3.4 Closed-loop performance of the controllers

To simulate the closed loop systems with the proposed representations, we create two examples for the two types of control. The controller $K(s)$ in (3.13) was tuned with the PID block available in the toolboxes of Matlab/Simulink® to achieve steady state reference tracking, and response times than the plant, while avoiding tracking overshoot. A similar response was obtained for the state feedback control setting the closed loop poles of (3.16-3.17) at $(-2 \pm j0.4) \times 10^{-5}$ and -1.6×10^{-6} rad/s.

The tuned controllers result in the parameters in the left column of Table 3.2, and are examples of prescribed designs that we can represent with CRNs. From (3.13) and the construction in (3.23) we derive the reaction rates for the CRN representations in the right column of Table 3.2, which are within the limitations of the hybridisation rates of DSD reactions.

The MAK for both control systems were simulated in Matlab/Simulink® to

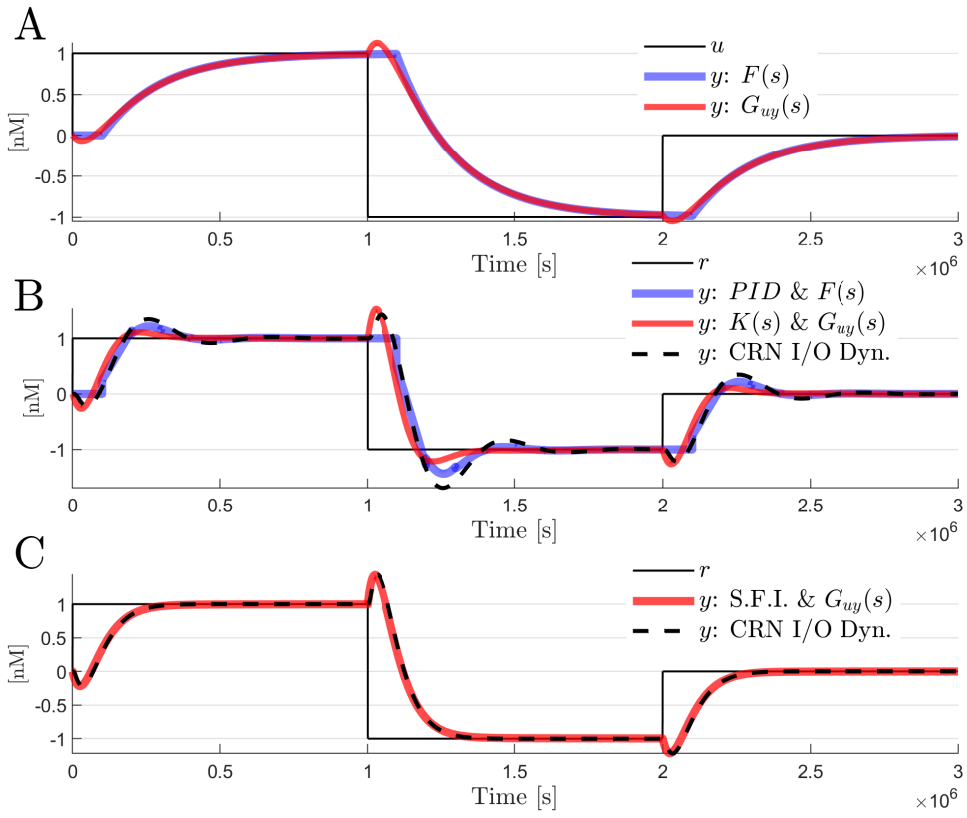

Figure 3.8: Simulation in Matlab of the feedback systems and CRN representations: A) step responses of the FOTD $F(s)$ and its approximating transfer function $G_{uy}(s)$. B) comparison of the reference tracking with ideal PID control of $F(s)$, the control system using both approximations $K(s)$ and $G_{uy}(s)$, and the output signal using the MAK from (3.6) together with (3.26). C) comparison of the designed reference tracking of $G_{uy}(s)$ with SFI control, and the I/O dynamics of (3.6) and (3.28).

compare the closed-loop transfer functions with the I/O dynamics of the CRNs in Section 3.3. Since we have the controller parameters positive $k_P > 0$, $k_I > 0$ and $k_D > 0$, we did not have to change the connections in the CRN (3.14) to introduce additional negative gains (as discussed in Remark 3.4).

The step response of the FOTD plant $F(s)$ with pure delay from (3.1) is compared in Figure 3.8A with the plant $G_{uy}(s)$ from (3.3) with the approximation of the delay, where the output of the approximating transfer function shows the characteristic initial reversed action introduced by its non-minimum phase zero.

The FOTD system $F(s)$ controlled with the classical PID from (3.9) is compared in Figure 3.8B to the control of $G_{uy}(s)$ using $K(s)$ from (3.13). The main difference is the non-minimum phase response due to the delay approximating model.

The trajectories of the I/O dynamics of the CRN are different from the closed loop response with $G_{uy}(s)$ and $K(s)$ due to the additional dynamics introduced by the implementation of subtractions and sums in (3.26a) and (3.26e).

Figure 3.8C shows the closed loop response of $G_{uy}(s)$ with the designed state feedback control from (3.18). The controller provides reference tracking with zero steady-state error, for both the transfer function (3.20) and the I/O dynamics of the CRN composed of (3.6) and (3.28). The non-minimum phase behaviour is introduced by the approximation of the plant delay in (3.3).

3.5 Verification with DSD reaction networks

We validate the experimental feasibility of our designs for implementation with DSD reactions, by demonstrating their correct functioning with the dedicated simulation package Visual DSD [80]. Each reaction of the elementary reactions in (2.24) are translated to the DSD networks according to [76] and detailed in Figures 3.9, 3.10 and 3.11.

For the catalysis reactions of the form $U \rightarrow U + Y$, the cascade of reactions are in Figure 3.9 (see also Figure 8 in [76]). The set of reactions is given by:

$$\boldsymbol{JoinU} + U \underset{k_s}{\overset{c\times k_s}{\rightleftharpoons}} JoinU^{-1} + sig_{sut2} \tag{3.30a}$$

$$JoinU^{-1} + \boldsymbol{aux_{t2sy}} \underset{k_s}{\overset{k_s}{\rightleftharpoons}} JoinU^{-2} + sig_{syt2} \tag{3.30b}$$

$$sig_{sut2} + \boldsymbol{ForkU} \underset{k_s}{\overset{k_s}{\rightleftharpoons}} ForkU^{-1} + U \tag{3.30c}$$

$$sig_{syt2} + \boldsymbol{ForkY} \underset{k_s}{\overset{k_s}{\rightleftharpoons}} ForkY^{-1} + Y \tag{3.30d}$$

$$JoinU^{-2} + \boldsymbol{aux_{t2si}} \xrightarrow{k_s} \emptyset \tag{3.30e}$$

$$ForkU^{-1} + \boldsymbol{aux_{sit1}} \xrightarrow{k_s} \emptyset \tag{3.30f}$$

$$ForkY^{-1} + \boldsymbol{aux_{sit1}} \xrightarrow{k_s} \emptyset \tag{3.30g}$$

where the auxiliary species in bold are supplied in high concentrations. In the first reaction, k_s is maximum toehold hybridisation rate k_s and $0 < c < 1$ is a scalar parameter that reflects a degree of complementary between the toeholds $< t1 >$ and $< t1^* >$ in U and $JoinU$, respectively.

For example, mismatches in $< t1^* >$ in $JoinU$ decrease the hybridisation rate and slowdown the propensity of (3.30a) Since the first reaction has the slowest reaction rate ($c \times k_s < k_s$), the production of $JoinU^{-1}$ is the limiting reaction and

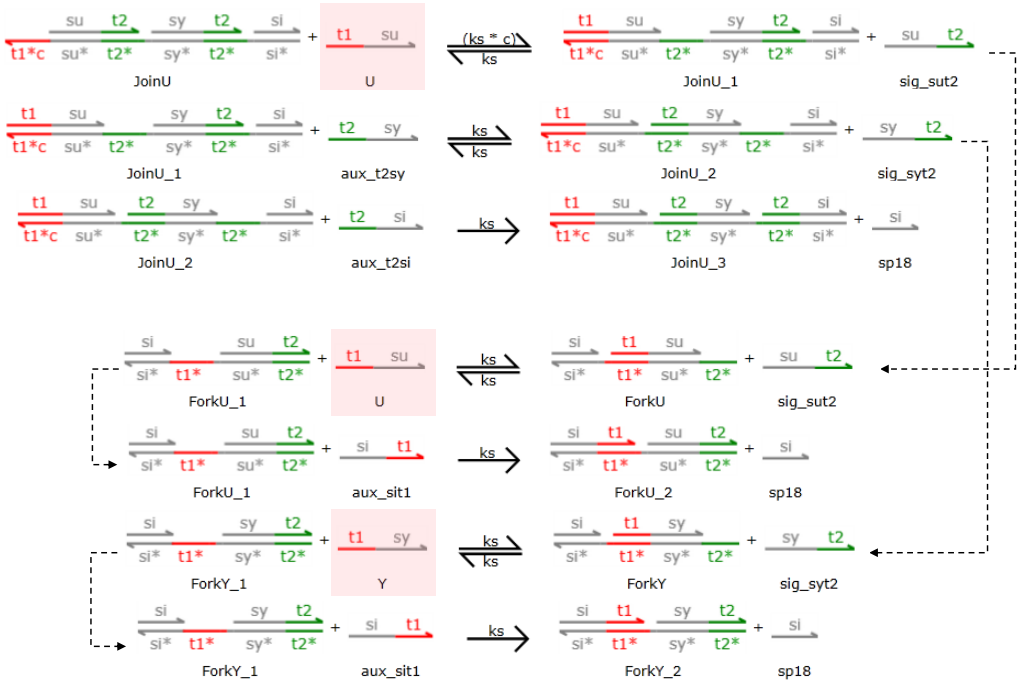

Figure 3.9: Cascade of strand displacement reactions to implement a catalysis reaction of the form $U \to U + Y$, based on the primitives of [76]. The presence of the input strand U triggers strand displacements in the template $JoinU$ which leads to the release of signal strands sig_{sut2}, sig_{syt2}. In turn, these strand displacements in $ForkU^{-1}$ and $ForkY^{-1}$ to release the outputs U and Y.

sets the overall production of the output strands. The reactions removing $JoinU^{-2}$, $ForkU^{-1}$ and $ForkY^{-1}$ in (3.30e-3.30g) ensure that the overall catalysis of U and Y is irreversible, and the overall conversion rate is defined by the reaction rate $c \times k_s \ll k_s$ of the limiting reaction (3.30a).

For an annihilation reaction between two species $Y + Y' \to \emptyset$, the scheme in [76] uses only one toehold (the same in the definition of the species Y and Y'), as illustrated in Figure 3.10. The scheme uses two templates $JoinYY'$ and $JoinY'Y$ and two auxiliary strands $< hy\ ty >$ and $< hy'\ ty >$ which need to be initialised at high concentrations. The reactions are

$$\boldsymbol{JoinYY'} + Y \underset{k_s}{\overset{k_s}{\rightleftharpoons}} JoinYY'^{-1} + \boldsymbol{aux_{hyty}} \tag{3.31a}$$

$$JoinYY'^{-1} + Y' \xrightarrow{k_s} \emptyset \tag{3.31b}$$

$$\boldsymbol{JoinY'Y} + Y' \underset{k_s}{\overset{k_s}{\rightleftharpoons}} JoinY'Y^{-1} + \boldsymbol{aux_{hy'ty}} \tag{3.31c}$$

$$JoinY'Y^{-1} + Y \xrightarrow{k_s} \emptyset\ . \tag{3.31d}$$

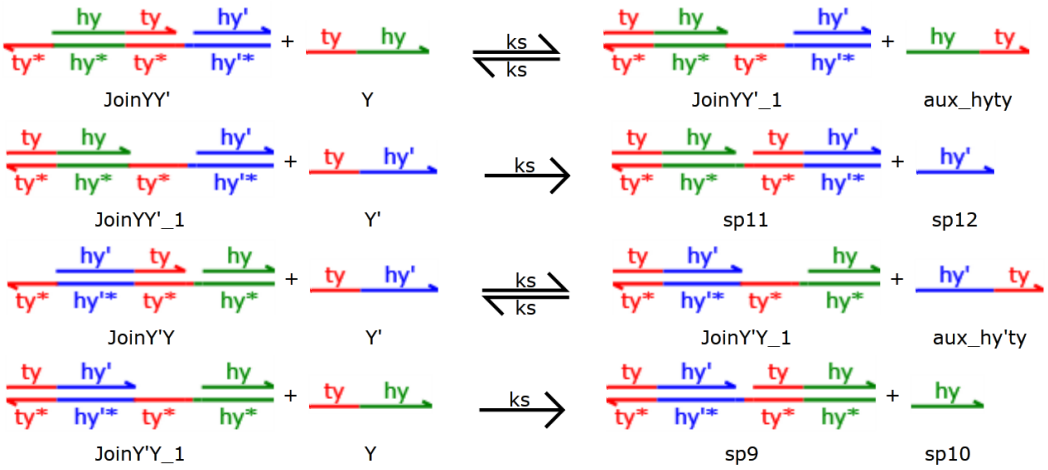

Figure 3.10: Cascade of strand displacement reactions to implement an annihilation reaction $Y + Y' \to \emptyset$ based on the primitives of [76]. The sequestration of Y by the template strand $JoinYY'$ is reversible, unless with the simultaneous presence of Y'. And *vice-versa* for Y' and $JoinY'Y$.

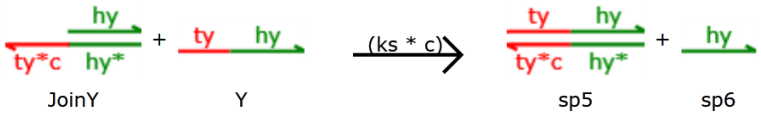

Figure 3.11: Strand displacement reactions to implement the degradation reaction $Y \to \emptyset$ based on the primitives of [76], where a template $JoinY$ sequesters the input Y irreversibly into a dsDNA without exposed toeholds.

The auxiliary species (in bold) are initialised at high concentrations, and k_s is the maximum hybridisation rate between the toeholds $< ty >$ and $< ty^* >$. This scheme differs from the cooperative hybridisation schemes in Figure 2.10 in that it uses more auxiliary species.

Finally, to implement the degradation reaction we only need an auxiliary Join template at large concentrations, so that

$$\boldsymbol{JoinY} + Y \xrightarrow{c \times k_s} \emptyset \tag{3.32}$$

and Y is removed from the reaction by being sequestered into unreactive dsDNA.

As pointed out in Section 2.4, the implementation of the DSD reactions depends on auxiliary species which are consumed irreversibly. The auxiliary species highlighted in bold in (3.30), (3.31), and (3.32), are all initialised at a large con-

centration C_{max}. This prevents their consumption from impacting the dynamics significantly and allows an approximation of the bimolecular reactions with unimolecular reactions (see for example Table 2.1 with the scheme from [21]).

With feasible values of a large initial concentration of $C_{max} = 10^4\,\text{nM}$ [21] and maximum toehold hybridisation $k_s = 10^{-3}\,(\text{nMs})^{-1}$ (from [74]), the unimolecular reaction rates in the CRNs are translated into toehold affinities assuming the concentrations of the auxiliary species remains almost constant at C_{max} nM.

Considering the buffering cancellation discussed in [21,79], the DSD reaction rates for simulation in Visual DSD are computed from Table 3.1 and Table 3.2 with

$$q_{gi} = 2g_i/C_{max}\,(\text{nMs})^{-1},\ i = 1,2,3,4 \tag{3.33a}$$
$$q_{\gamma} = 2\gamma/C_{max}\,(\text{nMs})^{-1} \tag{3.33b}$$
$$q_{ki} = 2k_i/C_{max}\,(\text{nMs})^{-1},\ i = 1,2,3,4 \tag{3.33c}$$
$$q_{|ci|} = 2|c_i|/C_{max}\,(\text{nMs})^{-1},\ i = 1,2,3 \tag{3.33d}$$
$$q_{|cr|} = 2|c_r|/C_{max}\,(\text{nMs})^{-1},\ i = 1,2,3\ . \tag{3.33e}$$

The annihilation reaction is defined by the maximum hybridisation reaction rate, set from the literature at $k_s = 2\eta = 10^6\ (\text{Ms})^{-1}$ [74].

The programming of DSD reactions uses the capacity of Visual DSD to define and re-use primitive functions to code the complete system (the code for both implementations is listed in Chapter A). Instead of manually assigning toeholds and specific domains for every strand in the system, each reaction is coded by the respective primitive function and the software automatically defines and initialises the necessary auxiliary species and their domains for the full system. The tool returns a realisation of the complete feedback systems with 128 initial DNA strands for the PID feedback system, and 88 strands with state feedback, confirming the expectations of Remark 3.6 of a simpler implementation for static state feedback.

Remark 3.7. *The total number of initial strands is lower than expected just by looking at the size of the CRN and the choice of DSD networks to implement each type of reactions in the CRN. The representation of the plant in* (3.5) *uses eight catalysis reactions, six degradation reactions, and four annihilation reactions.*

The representation of the PID controller from (3.14) *requires the implementation of sixteen catalysis reactions, eight degradation reactions and seven annihilation reactions. In the case of the state feedback, the implementation requires twelve catalysis reactions, a pair of degradation reactions and two annihilation reactions. For*

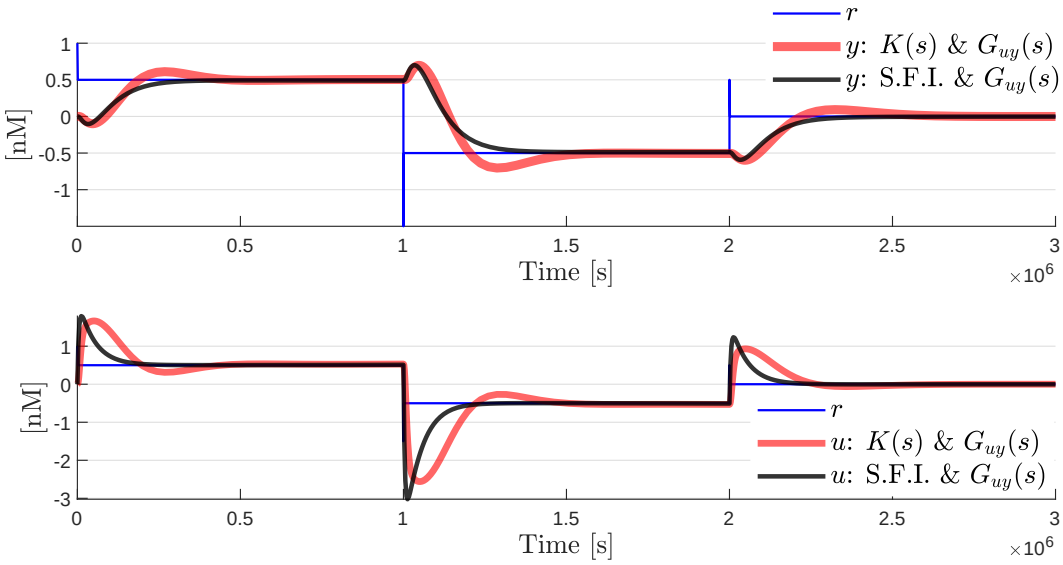

Figure 3.12: Time histories of the output $y = y^+ - y^-$ and the control signal $u = u^+ - u^-$ for deterministic simulations with Visual DSD of the DSD networks implementing the PID and SFI control systems.

the architectures presented above we have that the implementation of each catalysis in (3.30) *uses six auxiliary strands, the implementation of the annihilation reaction in* (3.31) *uses two, while for the degradation reaction in* (3.32) *needs only one auxiliary strand. By direct multiplication, we would expect 178 auxiliary strands for the feedback system with the PID controller and 138 strands for the state feedback system.*

However, when Visual DSD automatically defines and generates the domains for the strands, it reuses auxiliary species in the implementations of more than one reaction, and the total number of auxiliary strands in the generated realisation is not necessarily proportional to the total number reactions in the CRN.

The time histories of the concentrations with deterministic simulations using Visual DSD are presented in Figure 3.12, and show a successful steady state tracking of the reference signal, and an agreement with the transfer functions of the CRN I/O dynamics.

The described constructions using dual rail methodology and representations with I/O systems fall within assumptions of deterministic models and MAK (large number of molecules in an homogeneous mix). Nevertheless, stochastic simulations were used as an additional step of verification, to test if such constructions could work with lower numbers of molecules, outside the assumptions of MAK. The simulations in Figure 3.13 were carried using the same constructions, using the Gillespie's

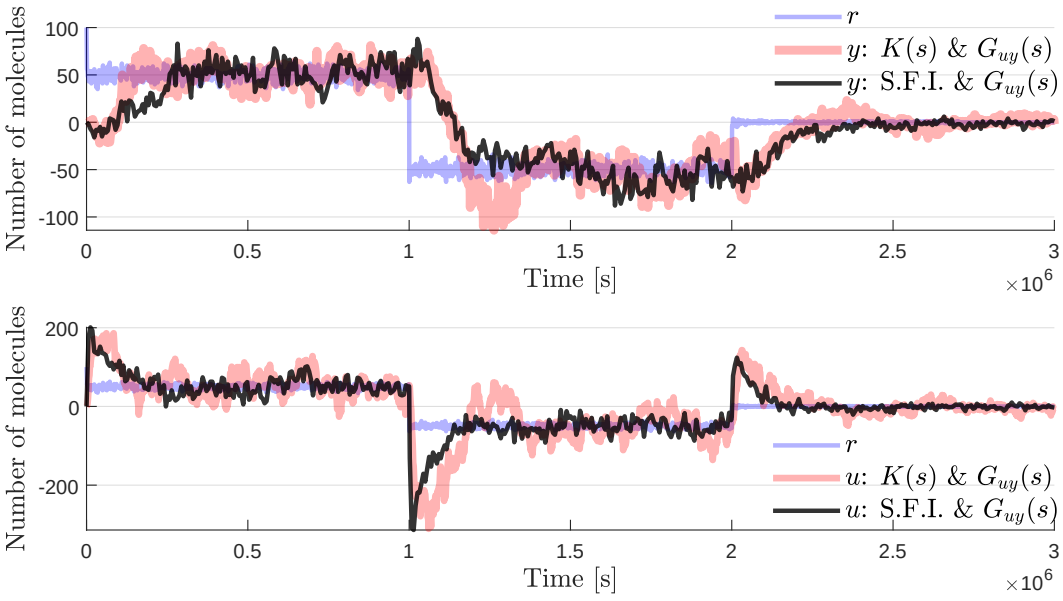

Figure 3.13: Time histories of the difference in number of molecules between Y^+ and Y^-, and between U^+ and U^-, for stochastic simulations in Visual DSD of the PID and SFI control systems.

SSA engine available in Visual DSD. Although a stochastic interpretation of the models and results are beyond the scope of this work, the trajectories show some of the designed behaviours (reference tracking and response times) even with the added complexity of a stochastic environment.

3.6 Conclusion

This chapter proposes novel CRN representations for plants with time-delays and for two important classes of linear feedback controllers, PID and state feedback with integral action. The representations rely on a dual-rail representation to construct a CRN which is realisable using strand displacement of nucleic acids. Existing applications of such approaches to linear negative feedback systems have been limited to the representation of PI control of static or first order plants.

This work starts by increasing the complexity of the plant to include the modelling of time-delay. The representation of the delay uses the first order Padé approximation decomposed into a subtraction and a first order system, which can be represented by modules of chemical reactions.

Previous attempts at representing PID controllers with chemical reactions were in the context of positive systems with complicated assumptions. The new

CRNs for time-delay and differentiation representations proposed in this work have simpler assumptions and parameterisation, and the dual rail approach allows the representation of differentiation for non-positive systems. Such constructions allow for the first time a chemical representation of linear negative feedback systems with PID control, realisable with DSD reactions.

The proposed module for differentiation exploits the same decomposition of time-delay to derive a transfer function that approximates the derivative of a signal, depending only on the sampling interval time. The parameterisation of the interval time must be traded off between accuracy and feasibility of the reaction rates of its CRN representation. The structure of the PID controller results in a filtered approximation of the derivative, with a fundamental trade-off in the parameterisation between the accuracy of differentiation and the feasibility of chemical reaction binding rates.

Furthermore, this work also addresses for the first time how a linear static state feedback system could be represented using the dual-rail methodology for realisation with DSD reactions. The state feedback takes advantage of the ready access of the controller to the chemical species, and it is posed as a regulation problem with zero steady-states. It results in a simpler CRN and requires fewer DNA strand species since it relies mostly on summing junctions.

The realisations using DSD reaction networks were verified in Visual DSD using deterministic simulations with similar performance, suggesting the viability of realising the proposed CRNs with DSD reactions.

Stochastic simulations seem to suggest that the CRN constructions may work outside the assumptions of inherent to MAK models used for the representation with I/O systems. However, further investigation with stochastic analysis tools and simulation campaigns are necessary to properly quantify and assess the validity of the constructions in a stochastic framework.

Nevertheless, the realisations of such feedback systems still result in large DSD networks that are challenging for experimental implementation, demanding the design and tuning of a considerable amount of strands and toeholds. Such difficulties are addressed in the next chapter.

Chapter 4

Minimally Complex Nucleic Acid Feedback Control Systems

4.1 Introduction

The previous chapters cover how chemical reaction networks based on catalysis, degradation, and annihilation may be used as building blocks to construct a variety of dynamical and feedback control systems, and why DNA hybridisation programmed using Watson-Crick base pairing is an effective primitive to implement such reactions experimentally. However, experimental construction, validation and scale-up of nucleic acid control systems is still significantly lagging theoretical developments, due to several technical challenges, such as leakage, crosstalk, and toehold sequence design [29, 74]. Experimental implementations of even the simplest types of feedback controllers (for example PI controllers) using DNA circuitry have still not been reported as far as I am aware.

To help the progress towards experimental implementation, we provide here designs representing two fundamental classes of reference tracking control circuits (integral and state-feedback control), for which the complexity of the chemical reactions required for implementation has been minimised. The supplied 'minimally complex' control circuits should be ideal candidates for first experimental validations of nucleic acid controllers.

4.1.1 Experimental challenges

Examples of successful experimental implementations of nucleic-acid feedback control circuits have yet to emerge. DSD networks implementing open-loop cascades for logical or analogue computation have been reported [158], but there is a signifi-

cant theory-experiment gap for dynamical circuits implementing negative feedback, where the transient dynamics impact system stability and performance. This is due to a variety of reasons.

Starting with the kinetics, the reaction rate constants are altered by unwanted bindings, modifying the dynamics (see, for example, the oscillating circuits in [29] or the seesaw gate reported in [153]). Although it is possible to predict the toehold affinities from their nucleotide sequence [74], there is always variability and granularity in the resulting binding propensities.

The stochastic mechanism of the chemical reactions, especially in a biological noisy environment, means that any experimental implementation abandons a noise-free and deterministic context, and makes difficult the interpretation and analysis of control concepts as fundamental as integral feedback [159].

The triggering of undesired reactions is another key experimental challenge, which leads to leakage of outputs in the absence of input. Potential methods of mitigation include *clamps* (as in [29] and [160]), which impede the spurious hybridisations, or compartmentalisation and localisation strategies as proposed in [161–163], which keep apart strand complexes that may trigger leak reactions. Furthermore, leakage is aggravated at high concentrations, and therefore the reacting species are typically kept at low concentrations [164], which together with limits on hybridisation rates [74], places upper bounds on the speed of these circuits. Localisation can also help here, by placing adjacent gates, which can interact without diffusion at faster rates, as discussed in [153].

Finally, even if spurious reactions are avoided, it may still be necessary to manage the sequence of reactions, which compete for common reactants, either through compartmentalisation, or with timescale separation (as adopted in [145]).

4.1.2 Reducing complexity

Some of the experimental challenges can be mitigated by designs that reduce the number of reactions in the circuit. Fewer reactions decrease the number of designs for the template strands, which demands less work to characterise and tune the kinetics. Fewer species also decreases the chance of unwanted interactions and leakage. The issue is particularly relevant in feedback systems employing the dual-rail representation of negative signals, which requires a duplication of most of the reactions (as discussed in [154]).

A key challenge for theorists is therefore to design the least complex circuits, with the fewest number of chemical reactions, in order to maximise the likelihood of successful experimental implementation with currently available technical capabili-

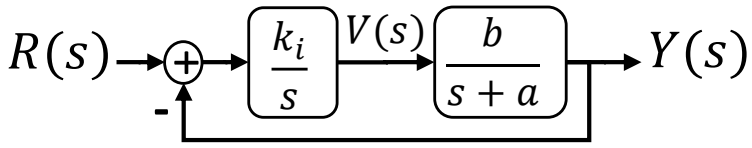

Figure 4.1: Block diagram for a reference tracking problem with integral control of a stable first order plant.

ties, which still accurately represent a given negative feedback control problem. To this end, minimally complex representations of two fundamental classes of feedback control systems are proposed here. The first applies integral control for reference tracking, with a single tuning parameter, to a stable first order system. The second example accomplishes reference tracking and stabilisation of the classic double integrator plant through static state feedback of the two integrated states. The controller has two design parameters, and the open-loop system is marginally stable with two poles at the origin.

Both circuits operate within the dual-rail framework, and parameterise control requirements like steady state tracking and transient dynamics. The constructions with DSD reactions are detailed, and verified with Visual DSD [80] to increase the confidence on their experimental viability.

4.2 A minimally complex integral feedback control system

We now propose a representation of an integral feedback control system, using the fewest number of chemical reactions possible, followed by an implementation in Visual DSD using strand displacement reactions.

4.2.1 Integral control of a stable first order system

For this example we consider the following first order system

$$Y(s) = \frac{b}{s+a}V(s) \Rightarrow sY(s) = bV(s) - aY(s) \tag{4.1}$$

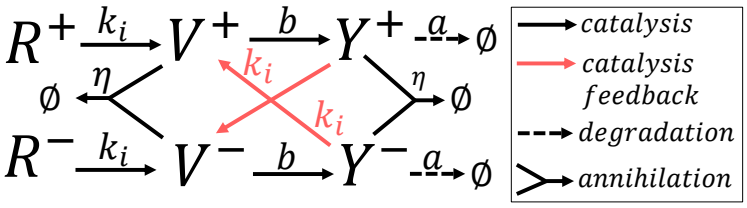

Figure 4.2: Representation of the integral control problem, with a chemical network of catalysis, degradation and annihilation reactions.

where $V(s)$ is the integral control action to have the output $Y(s)$ track a reference $R(s)$, according to Figure 4.1. The closed-loop dynamics are then

$$Y(s) = \frac{bk_i}{s^2 + as + bk_i} R(s) \tag{4.2}$$

where the integral control ensures steady state tracking with $Y(0) = R(0)$.

The transient dynamics are defined by the roots of the characteristic polynomial given by

$$\lambda = \frac{1}{2}\left(-a \pm \sqrt{a^2 - 4bk_i}\right) \tag{4.3}$$

with a natural frequency $\omega = \sqrt{bk_i}$ and damping coefficient $\xi = \frac{a}{2\sqrt{bk_i}}$.

4.2.2 Representation with chemical reactions

Figure 4.2 shows a network of catalysis, degradation and annihilation reactions used to represent the closed-loop response, where

$$V^+ \xrightarrow{b} V^+ + Y^+ \quad , \quad V^- \xrightarrow{b} V^- + Y^- \tag{4.4a}$$

$$Y^+ \xrightarrow{a} \emptyset \quad , \quad Y^- \xrightarrow{a} \emptyset \tag{4.4b}$$

$$R^+ \xrightarrow{k_i} R^+ + V^+ \quad , \quad R^- \xrightarrow{k_i} R^- + V^- \tag{4.4c}$$

$$Y^+ \xrightarrow{k_i} Y^+ + V^- \quad , \quad Y^- \xrightarrow{k_i} Y^- + V^+ \tag{4.4d}$$

$$Y^+ + Y^- \xrightarrow{\eta} \emptyset \quad , \quad V^+ + V^- \xrightarrow{\eta} \emptyset \; . \tag{4.4e}$$

The reactions (4.4a-4.4b) represent the plant, where the reaction rate b sets the gain and the reaction rate a sets a stable pole at $s = -a$.

Instead of using separate CRNs for subtraction and integration, both operations are combined to reduce the number of reactions. The additional dynamics used to compute the error in Chapter 3 are removed, and the contributions of the

reference and output to the integral are subtracted in (4.4c-4.4d) by crossing the contributions from $Y^{\pm}$ to $V^{\mp}$. The same reactions apply the control gain corresponding to the reaction rate k_i. The annihilation reactions in (4.4e) ensure low concentrations of the chemical species [79].

Writing the respective mass action kinetics guiding the concentrations of the species, we have

$$\begin{aligned}
\dot{v}^+ &= k_i r^+ + k_i y^- - \eta v^+ v^- && \text{(4.5a)}\\
\dot{v}^- &= k_i r^- + k_i y^+ - \eta v^+ v^- && \text{(4.5b)}\\
\dot{y}^+ &= b v^+ - a y^+ - \eta y^+ y^- && \text{(4.5c)}\\
\dot{y}^- &= b v^- - a y^- - \eta y^+ y^- && \text{(4.5d)}\\
& v^{\pm}(0) = 0, y^{\pm}(0) = 0 \ . && \text{(4.5e)}
\end{aligned}$$

We have then for the dual-rail quantities $y = y^+ - y^-$, $v = v^+ - v^-$, $r = r^+ - r^-$, that the I/O dynamics are $\dot{v} = \dot{v}^+ - \dot{v}^-$, $\dot{y} = \dot{y}^+ - \dot{y}^-$, and

$$\begin{aligned}
\dot{v} &= k_i \left(r - y\right) && \text{(4.6a)}\\
\dot{y} &= b v - a y && \text{(4.6b)}\\
& v(0) = 0, y(0) = 0 \ . && \text{(4.6c)}
\end{aligned}$$

The I/O dynamics in (4.6) are linear and we recover the dynamics of the closed-loop system in (4.2). For simplification, any annihilation reaction between the reference species $R^+ + R^- \xrightarrow{\eta} \emptyset$ is disregarded, assuming the input concentrations are low and constant throughout the operation of the circuit, and the dynamics in (4.6) depend only on the difference r and not the concentration levels of R^+ and R^-.

4.2.3 Representation with strand displacement reactions

To translate the CRNs into nucleic acid chemistry we need sets of DSD reactions with dynamics equivalent to each of the three types of reactions, and a mechanism to tune the reaction rates. The catalysis and degradation reactions are set based on Join-Fork templates from [72] and cooperative hybridisation [144], mentioned in Section 2.4.2.

The programmability of the DSD reactions results from the nucleotide sequences in the toeholds, which initiate strand hybridisation. As investigated in [74], the affinities between the base pairs define somewhat predictably the hybridisation kinetics, although, as described in [29], other factors can also influence the effective

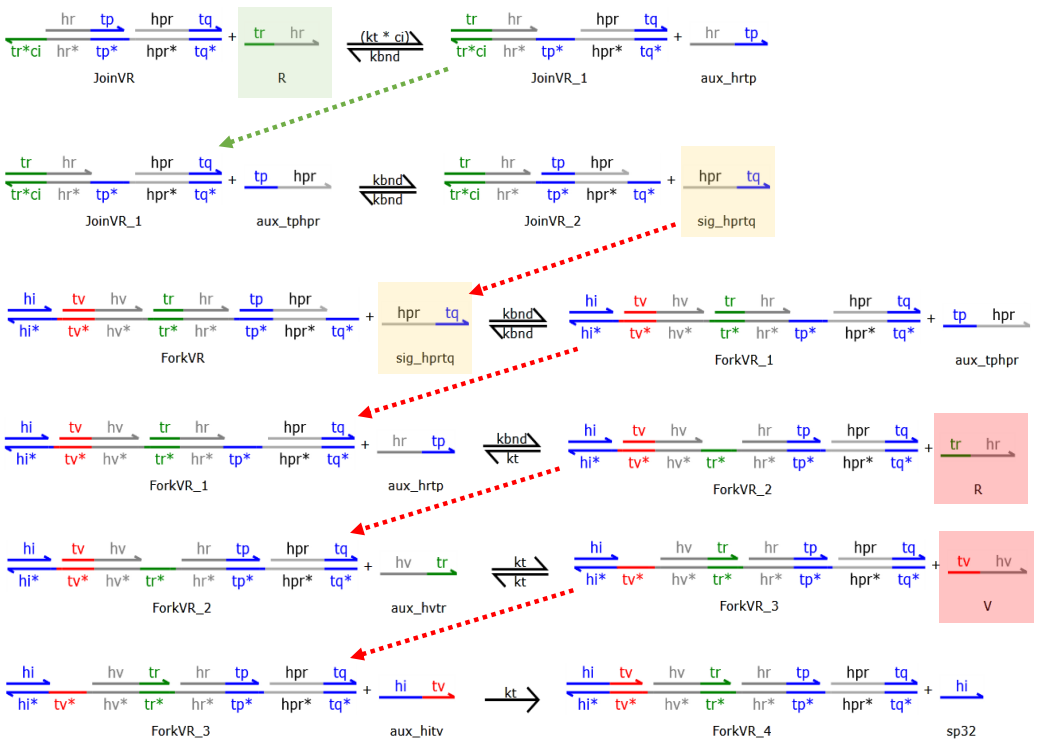

Figure 4.3: Example generated in Visual DSD, of the DSD sets of reactions with dynamics equivalent to catalysis reaction $R \rightarrow R + V$, using Join-Fork templates as in [72]. The first cascade is triggered by R and leads to the release of sig_hprtq, which in turn triggers the cascade reaction involving $ForkVR$ leading to the release of R and V strands.

reaction rate constants.

For the purpose of our analysis, the rates of the DSD reactions are tuned by assigning *degrees of complementarity* between toeholds as in [76] (see also [147]), where mismatches in the nucleotide sequences weaken the binding affinities [18] and decrease the binding rate. For example, the toehold $< tr^*ci >$ in the complex $Join_{VR}$ in Figure 4.3 has a degree of complementarity to the signal toehold $< tr >$ of $0 < c_i \leq 1$. If k_t is the maximum binding rate between complementary toeholds $< tr >$ and $< tr* >$, then the reaction mediated by $< tr >$ and $< tr*ci >$ is slowed down to $k_t \times c_i$.

As an example, the cascade of DSD reactions used to implement the unimolecular reaction of catalysis $R \rightarrow R + V$ is shown in Figure 4.3, using toeholds to mediate the interactions with the auxiliary templates and intermediary strands. Each signal species, such as R in Figure 4.3, is a single strand DNA containing toehold ($< tr >$) and binding ($< hr >$) domains. The toehold domain initiates hy-

bridisation to the multi-stranded complex $Join_{VR}$, triggering a cascaded process to release an intermediary strand sig_{hprtq}. The exposed toehold in $Join_{VR}$ is designed to have a complementary degree c_i to decrease the affinity of the hibridisation and slow down the binding rate to $c_i \times k_t$ [18].

The availability of the released strand sig_{hprtq} triggers a cascade of strand displacements involving the $Fork_{VR}$ complex, which releases the signal species V and returns a strand of R (according to the stoichiometry of $R \to R + V$). The sets of reactions to implement the catalysis are then

$$R + \boldsymbol{Join_{VR}} \underset{k_{bnd}}{\overset{c_i \times k_t}{\rightleftharpoons}} Join_{VR}^{-1} + \boldsymbol{aux_{hrtp}} \tag{4.7a}$$

$$Join_{VR}^{-1} + \boldsymbol{aux_{tphpr}} \underset{k_{bnd}}{\overset{k_{bnd}}{\rightleftharpoons}} Join_{VR}^{-2} + sig_{hprtq} \tag{4.7b}$$

$$sig_{hprtq} + \boldsymbol{Fork_{VR}} \underset{k_{bnd}}{\overset{k_{bnd}}{\rightleftharpoons}} Fork_{VR}^{-1} + \boldsymbol{aux_{tphpr}} \tag{4.7c}$$

$$Fork_{VR}^{-1} + \boldsymbol{aux_{hrtp}} \underset{k_t}{\overset{k_{bnd}}{\rightleftharpoons}} Fork_{VR}^{-2} + R \tag{4.7d}$$

$$Fork_{VR}^{-2} + \boldsymbol{aux_{hvtr}} \underset{k_t}{\overset{k_t}{\rightleftharpoons}} Fork_{VR}^{-3} + V \tag{4.7e}$$

$$Fork_{VR}^{-3} + \boldsymbol{aux_{hitv}} \xrightarrow{k_t} \emptyset \tag{4.7f}$$

and the overall rate of production of the outputs is limited by the hybridisation rate of the first reaction with $c_i \times k_t < k_t$ and $c_i \times k_t < k_{bnd}$.

The annihilation reactions are set with a single template per signal, following the cooperative hybridisation approach from [144] and [145], where

$$V + V' + Anh_{VV} \xrightarrow{c_{VV} \times k_t} \emptyset \ . \tag{4.8}$$

In the example shown in Figure 4.4, we have the DSD reactions with the intermediary complexes and reversible displacement reactions, resulting the CRN

$$\boldsymbol{Ann_{VV}} + V \underset{k_{ubnd}}{\overset{c_{VV} \times k_t}{\rightleftharpoons}} I_V \tag{4.9a}$$

$$I_V + V' \xrightarrow{c_{VV} \times k_t} W_V + W_{V'} \tag{4.9b}$$

$$\boldsymbol{Ann_{VV}} + V \underset{k_{ubnd}}{\overset{c_{VV} \times k_t}{\rightleftharpoons}} I_{V'} \tag{4.9c}$$

$$I_{V'} + V \xrightarrow{c_{VV} \times k_t} W_V + W_{V'} \ . \tag{4.9d}$$

The irreversible capture of simultaneously present V and V' is mediated by the

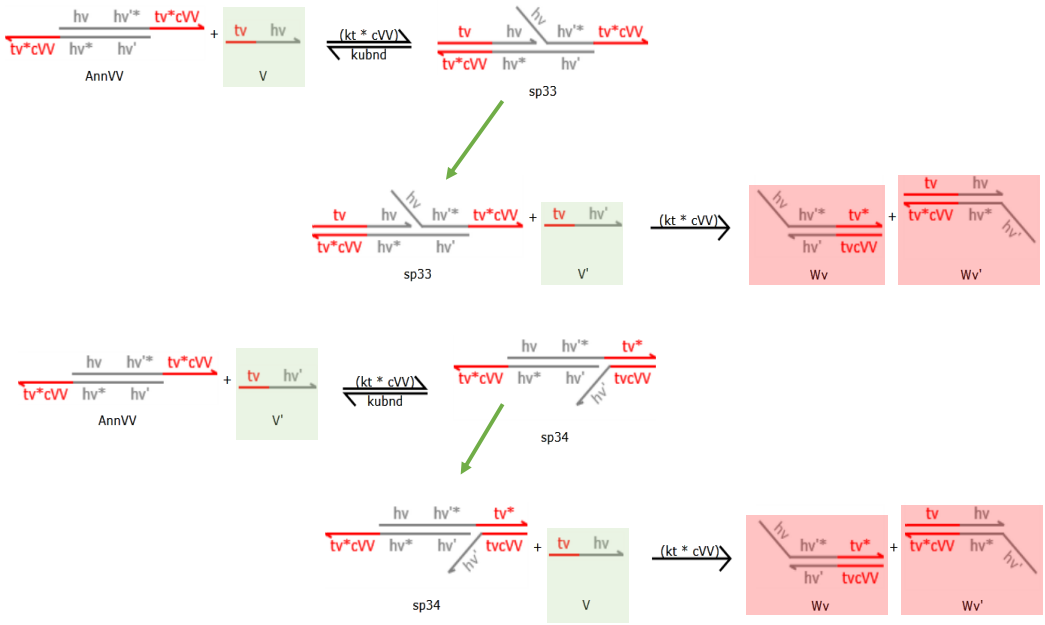

Figure 4.4: Example generated in Visual DSD, of the DSD sets of reactions with dynamics equivalent to an annihilation reaction $V + V' \rightarrow \emptyset$, using the cooperative hybridisation approach from [144] and [145]. There are two possible pathways depending on which strand binds first to $AnnVV$, and the initial binding is temporary. Only the simultaneous binding of V and V' leads to the production of waste products.

presence of the template Ann_{VV}. The presence of both V and V' enables the second irreversible reaction into two waste double stranded complexes W_V and $W_{V'}$.

The DSD reactions for the degradation in Figure 4.5 are simpler, since the $Join_Y$ complex only needs to irreversibly capture the signal species Y, with

$$Y + \boldsymbol{Join_Y} \xrightarrow{c_a \times k_t} Join_Y^{-1} + d_Y \ . \tag{4.10}$$

Since the double stranded product does not have exposed toeholds, it becomes inert and no longer participates in the reactions. The rate of removal of Y is determined by the hybridisation rate $c_a \times k_t$ and the concentration of $Join_{VR}$.

The template complexes and auxiliary single stranded species (highlighted in bold in (4.7), (4.10) and (4.9)) are made available at an initial high concentration C_{max} to avoid their irreversible consumption from significantly impacting the dynamics.

Assumption 4.1. *The auxiliary species are considered to remain close to their*

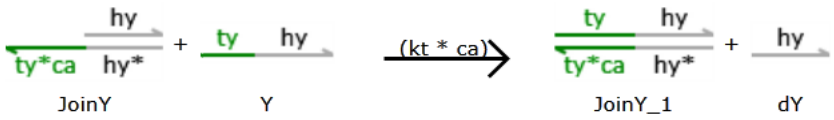

Figure 4.5: Example generated in Visual DSD, of the DSD sets of reactions with dynamics equivalent to a degradation reaction $Y \to \emptyset$, using Join templates as in [72]. The resulting strands do not have exposed toeholds, and are considered unreactive waste.

initial value C_{max}, either due to replenishment, or due to slow consumption during the duration of the operation of the circuit.

Such assumption provides a simplified mapping between the MAK of the DSD reactions and the conceptual CRN of catalysis, degradation and annihilation reactions, as the one found in [21] and Table 2.1). For example, if we consider in (4.10) that the concentration of $Join_Y$ remains around C_{max} during the duration of the circuit, then the removal rate of Y can be written as

$$Y \xrightarrow{C_{max} \times c_a \times k_t} \emptyset \ . \tag{4.11}$$

The DSD reactions for the implementation of each type of reaction are set using the templates from Figures 4.3, 4.5 and 4.4. The architectures adopted here differ slightly from the choice in Chapter 3, due to experimental considerations, such as the use of fewer auxiliary strands. For catalysis, we use a single $Fork$ template for both outputs of catalysis, and with cooperative hybridisation, the two annihilated species share the same sequestering template.

The implementation of the DSD reactions follows the six catalysis and two degradations from the CRN in (4.4), but with only one annihilation reaction. From the analysis with Visual DSD, we can remove the reaction $Y^+ + Y^- \to \emptyset$ to simplify further the implementation, since the concentrations of Y^+ and Y^- remain sufficiently low.

The simulation with Visual DSD is set with the parameters in Table 4.1, where the maximum binding rate k_{bnd}, unbinding rate k_{ubnd} and binding rate k_t are taken from studies in biophysics of DSD reactions [21,29,74], to ensure experimental feasibility.

The circuit is initialised with fifteen double stranded DNA templates and twenty single stranded auxiliary species Figure 4.6 set at an initial concentration of C_{max}. The initial concentration for the auxiliary species is set at $C_{max} = 10^4$ nM so that we can assume that the consumption of the auxiliary species does not

Table 4.1: Parameterisation for the Visual DSD simulation of the integral control circuit

	Description	Values	Units
C_{max}	Initial concentrations of template and auxiliary species	10^4	nM
k_{bnd}	Toehold maximum binding rate for auxiliary strands ($< tp >$,$< tq >$)	10^{-3}	$(\text{nMs})^{-1}$
k_{ubnd}	Unbinding rate	0.1	$(\text{s})^{-1}$
k_t	Toehold maximum binding rate for signal species ($< tr >$,$< ty >$,$< tv >$)	10^{-4}	$(\text{nMs})^{-1}$
c_a	Toehold degree of complementarity for the degradation of $Y^{\pm}$	2.5×10^{-3}	–
c_b	Toehold degree of complementarity for catalysis reaction in the plant	10^{-3}	–
c_i	Toehold degree of complementarity for feedback catalysis implementing integral control	5×10^{-2}	–
c_{VV}	Toehold degree of complementarity for the annihilation reaction	0.25	–

impact significantly the dynamics [21]. We can then approximate the network with unimolecular reactions with rates amplified by C_{max} using the same rationale behind Table 2.1). Nevertheless, in the simulations, the auxiliary strands are consumed irreversibly and not replenished.

The degrees of toehold complementarity c_a, c_i, c_b and c_{VV} are chosen to achieve hybridisation rates which equivalent to the reaction rates in the CRN. The impact of buffering [21, 76, 79], a finite unbinding rate, and interactions between the realisations resulted in some necessary tuning effort to map the reaction rates of the CRN to these coefficients (see in appendix Section B.3).

By definition, the coefficients are smaller than 1 and do not result in reaction rates exceeding the biophysics of DSD reactions. However, there is still the challenge of the predictability, granularity and wide range of reaction rates resulting from toehold design [18, 74].

The input for the I/O system is defined as two steps according to:

$$r(t) = \begin{cases} 0.1\text{nM} & 0\,\text{s} \leq t < 1200\,\text{s} \\ -0.1\text{nM} & 1200\,\text{s} \leq t \leq 2400\,\text{s} \end{cases} . \tag{4.12}$$

To realise the input we use two strands R^+ and R^- such that $r = [R^+] - [R^-]$.

Figure 4.6: Strands used to initialise the DSD network that represents the integral feedback control system: signal strands R, R', V, V', Y, Y', and auxiliary strands initialised at high concentrations. Due to the syntax in Visual DSD, the notation is slightly different, where instead of the superscripts $\pm$ we have the correspondence $R = R^+$, $R' = R^-$, $V = V^+$, $V' = V^-$, $Y = Y^+$, $Y' = Y^-$.

However, when they are introduced, there are very fast dynamics that sequester fractions of R^+ and R^- in the reversible reactions of the realisation of the catalysis reactions (further details in appendix Section B.3.3 and Definition B.2). For the chosen parameterisation, it results in Figure 4.7b that half of the species R^+ and R^- are buffered in the realisation of the reactions (4.4c), and the initialisation of the concentrations are adjust accordingly: the concentration of the species R^+ is initialised at $[R^+](0) = 0.2\,\text{nM}$, and R^- is added to the system at $1200\,\text{s}$ so that $[R^-](1200) = 0.4\,\text{nM}$.

Since the annihilation reaction $R^+ + R^- \to \emptyset$ is not included, once equilibrium is achieved in the DSD reactions, both species remain at a steady state value. Disregarding the very fast buffering dynamics, the realisation of the input signal

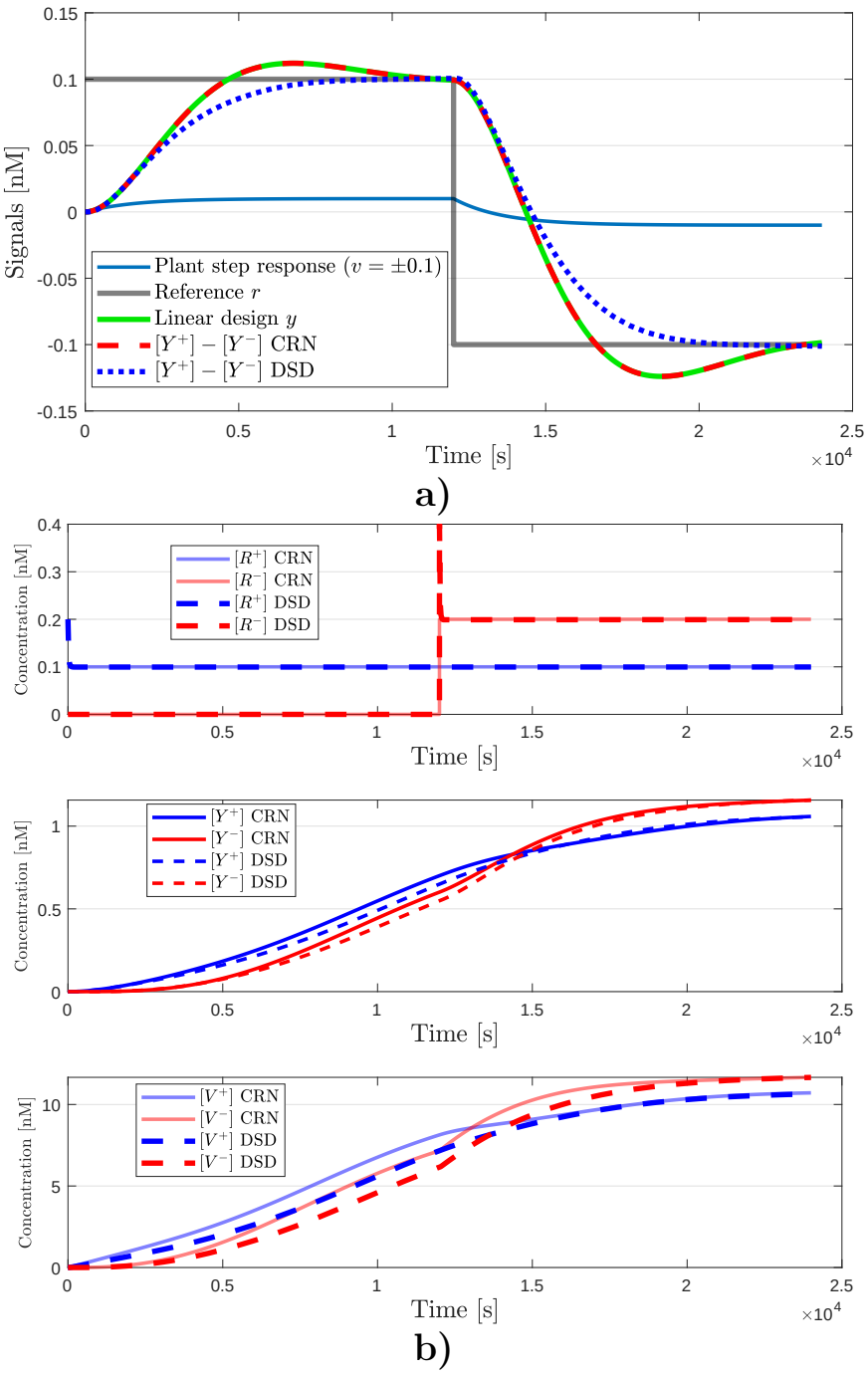

Figure 4.7: Simulations for the integral control example: a) comparison of the output y for the plant open-loop step response, closed-loop dynamics, CRN mass action kinetics and DSD reactions; b) comparison of the concentrations in the CRN and DSD representations.

in (4.12) results approximately in:

$$\left[R^+\right](t) \approx 0.1\,\text{nM}, \quad 0\,\text{s} \leq t \leq 2400\,\text{s} \tag{4.13a}$$

$$\left[R^-\right](t) \approx \begin{cases} 0\,\text{nM} & 0\,\text{s} \leq t < 1200\,\text{s} \\ 0.2\,\text{nM} & 1200\,\text{s} \leq t \leq 2400\,\text{s} \end{cases}. \tag{4.13b}$$

The simulations in Figure 4.7 show the reference tracking behaviour of the output $y = y^+ - y^-$ and evolution of the concentrations in the DSD reactions, and compares it with the output and concentrations of the CRN in (4.5) obtained by mass-action kinetics. The I/O dynamics from the DSD reactions do show tracking behaviour with unitary gain and a settling time similar to the prescribed linear design of integral feedback system.

Although we can see that the CRN representation matches the designed I/O system, for the output of the DSD circuit the transient dynamics are more damped. This is probably due to the additional dynamics of the auxiliary species and bimolecular reactions. For example, we are considering in the simulation a finite unbinding rate, which results in many reversible DSD reactions, buffering effects, and effectively changes the mapping unimolecular reaction rates of the CRN to the bimolecular reactions of the DSD. The example in Appendix B discusses some of these effects in Section B.3.

Moreover, the use of the same species as input to different reactions also impacts the reaction rates [21, 79]. For example, the buffering of V^+ or V^- in the realisation of the annihilation reaction $V^+ + V^- \to \emptyset$ decreases the concentration and available amount of V^+ or V^- for other reactions, and effectively slows down the catalysis where V^+ and V^- are input species. The interaction and loading effects between the realisation of reactions with common input species need more investigation to clarify the tuning of the DSD reactions, when additional effects are modelled (like a finite unbinding rate).

Nevertheless, the simulations suggest that further tuning can result in a better match between the realisation with DSD reactions and the CRN. The concentrations are in the same magnitude, and remain at levels low enough that prevent a fast consumption of the auxiliary species. The simulations do not include the realisation of $Y^+ + Y^- \to \emptyset$, and the resulting levels of the concentrations suggest that the circuit may work without the annihilation reaction, simplifying further an experimental implementation.

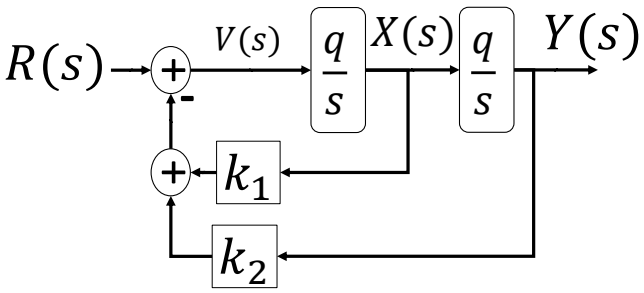

Figure 4.8: Block diagram representation of a double integrator plant stabilised by static state feedback.

4.3 A minimally complex state feedback control system

In static state feedback, the controller modifies the closed-loop dynamics using only gains on the state of the plant and does not add dynamics to the open-loop system. For the plant, we use the simplest second order system, a double integrator. Besides output feedback, we thus have an extra state for feedback. The plant is more challenging than in the previous example, since it is marginally stable, with two poles at the origin, and thus besides the reference tracking requirement, the closed-loop system also needs to stabilise the open-loop system.

4.3.1 State feedback control of a double integrator

The process to be controlled is the classic double integrator where each integration has a gain q (Figure 4.8). The state space representation of the plant is given by

$$\begin{bmatrix} \dot{x} \\ \dot{y} \end{bmatrix} = \begin{bmatrix} 0 & 0 \\ q & 0 \end{bmatrix} \begin{bmatrix} x \\ y \end{bmatrix} + \begin{bmatrix} q \\ 0 \end{bmatrix} v, \quad \begin{bmatrix} x(0) \\ y(0) \end{bmatrix} = \begin{bmatrix} 0 \\ 0 \end{bmatrix} . \tag{4.14}$$

We apply static state feedback control using the output and the intermediate state. With the negative state feedback control law $v = r - k_1 x - k_2 y$, we have two parameters to tune the dynamics of the closed-loop state space given by

$$\begin{bmatrix} \dot{x} \\ \dot{y} \end{bmatrix} = \begin{bmatrix} -qk_1 & -qk_2 \\ q & 0 \end{bmatrix} \begin{bmatrix} x \\ y \end{bmatrix} + \begin{bmatrix} q \\ 0 \end{bmatrix} r, \quad \begin{bmatrix} x(0) \\ y(0) \end{bmatrix} = \begin{bmatrix} 0 \\ 0 \end{bmatrix} . \tag{4.15}$$

The closed-loop frequency response results in a second order system with the transfer function

$$Y(s) = \frac{q^2}{s^2 + qk_1 s + q^2 k_2} R(s) \tag{4.16}$$

where the transient response is defined by the poles

$$\lambda = \frac{q}{2}\left(-k_1 \pm \sqrt{k_1^2 - 4k_2}\right) \ . \tag{4.17}$$

The closed-loop system has only three parameters: one for the plant and two gains for the controller. From (4.16), we have q which sets the timescale of the system, a static gain $1/k_2$, a natural frequency $\omega = q\sqrt{k_2}$, and the damping coefficient $\xi = \frac{k_1}{2\sqrt{k_2}}$. We can set steady state reference tracking with $k_2 = 1$, which means that any error or deviation in this parameter introduced by implementation will impact the steady state error. We also have that for an overdamped response $\xi > 1 \Rightarrow k_1 > 2$.

4.3.2 Representation with chemical reactions

As in the previous example, the CRN representation is further simplified by combining the sum of the feedback contributions and reference with the integration of the first state. In this way, we avoid the additional dynamics of representing the sum with the steady state solution of additional reactions, as proposed in Chapter 3.

Accounting for the dual-rail representation, the CRN results in eight catalysis and two annihilation reactions, given by

$$R^+ \xrightarrow{q} R^+ + X^+ \quad , \quad R^- \xrightarrow{q} R^- + X^- \tag{4.18a}$$

$$X^+ \xrightarrow{q} X^+ + Y^+ \quad , \quad X^- \xrightarrow{q} X^- + Y^- \tag{4.18b}$$

$$X^+ \xrightarrow{qk_1} X^+ + X^- \quad , \quad X^- \xrightarrow{qk_1} X^- + X^+ \tag{4.18c}$$

$$Y^+ \xrightarrow{qk_2} Y^+ + X^- \quad , \quad Y^- \xrightarrow{qk_2} Y^- + X^+ \tag{4.18d}$$

$$X^+ + X^- \xrightarrow{\eta} \emptyset \quad , \quad Y^+ + Y^- \xrightarrow{\eta} \emptyset \ . \tag{4.18e}$$

The chain of two catalysis reactions (4.18a-4.18b) represents the double integrator in the plant. The marginal stability of the integration can be related with the marginal stability of the stoichiometry in the catalysis reactions, where the produced species need to be bound for stability. The reactions in (4.18c-4.18d) implement the negative gains, by crossing the contributions between the dual-rail species (Figure 4.9a). Finally, the annihilation reactions are put in place in (4.18e), to ensure the concentrations are kept at feasible levels.

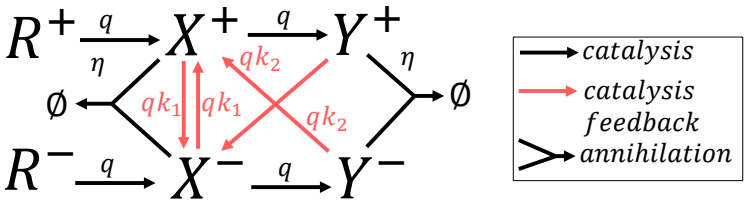

a)

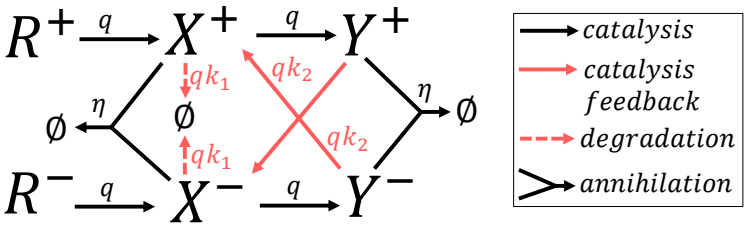

b)

Figure 4.9: Network of chemical reactions with dual-rail representation, using a) *catalytic degradation* [76] or b) degradation reactions.

The mass action kinetics for the chemical network results in

$$\begin{aligned}
\dot{x}^+ &= q\left(r^+ + k_2 y^- + k_1 x^-\right) - \eta x^+ x^- && \text{(4.19a)}\\
\dot{x}^- &= q\left(r^- + k_2 y^+ + k_1 x^+\right) - \eta x^+ x^- && \text{(4.19b)}\\
\dot{y}^+ &= q x^+ - \eta y^+ y^- && \text{(4.19c)}\\
\dot{y}^- &= q x^- - \eta y^+ y^- && \text{(4.19d)}\\
x^\pm(0) &= y^\pm(0) = 0\ . && \text{(4.19e)}
\end{aligned}$$

From the reversed contributions in (4.19a-4.19b), the negative gains in the I/O dynamics of $\dot{x} = \dot{x}^+ - \dot{x}^-$ and $\dot{y} = \dot{y}^+ - \dot{y}^-$ are given by

$$\begin{aligned}
\dot{x} &= qr - qk_2 y - qk_1 x && \text{(4.20a)}\\
\dot{y} &= qx && \text{(4.20b)}\\
x(0) &= y(0) = 0\ . && \text{(4.20c)}
\end{aligned}$$

In (4.20) we recover the linear closed-loop dynamics, and the representation of the negative gains.

The combined effect of crossed catalysis reactions $X^\pm \xrightarrow{qk_1} X^\pm + X^\mp$ and the fast annihilation $X^+ + X^- \xrightarrow{\eta} \emptyset$ results in the *catalytic degradation* proposed in [76]. Hence, the auto repressing gain is the same as $X^\pm \xrightarrow{qk_1} \emptyset$ (for $\eta \gg qk_1$),

and alternatively we can replace the catalysis in (4.18c) with degradation reactions. This results in the CRN from Figure 4.9b with six catalysis, two degradations, and two annihilation reactions given by

$$R^+ \xrightarrow{q} R^+ + X^+ \quad , \quad R^- \xrightarrow{q} R^- + X^- \tag{4.21a}$$
$$X^+ \xrightarrow{q} X^+ + Y^+ \quad , \quad X^- \xrightarrow{q} X^- + Y^- \tag{4.21b}$$
$$X^+ \xrightarrow{qk_1} \emptyset \quad , \quad X^- \xrightarrow{qk_1} \emptyset \tag{4.21c}$$
$$Y^+ \xrightarrow{qk_2} Y^+ + X^- \quad , \quad Y^- \xrightarrow{qk_2} Y^- + X^+ \tag{4.21d}$$
$$X^+ + X^- \xrightarrow{\eta} \emptyset \quad , \quad Y^+ + Y^- \xrightarrow{\eta} \emptyset \; . \tag{4.21e}$$

The mass action kinetics are now different, with

$$\dot{x}^+ = q\left(r^+ + k_2 y^- - k_1 x^+\right) - \eta x^+ x^- \tag{4.22a}$$
$$\dot{x}^- = q\left(r^- + k_2 y^+ - k_1 x^-\right) - \eta x^+ x^- \tag{4.22b}$$

but the I/O dynamics of $\dot{x}$ are the same as in (4.20), where the negative gain in the state x results from direct degradation instead of the dual-rail representation.

The time histories of the CRN representation are compared with the linear design in Figure 4.10, with the input signal

$$r(t) = \begin{cases} 0.1\text{nM} & 0\,\text{s} \leq t < 125000\,\text{s} \\ -0.1\text{nM} & 125000\,\text{s} \leq t \leq 250000\,\text{s} \end{cases} \; . \tag{4.23}$$

As in the previous example, for simulation of the MAK, the input signal is split into two input concentrations

$$\left[R^+\right](t) = 0.1\,\text{nM},\; 0\,\text{s} \leq t \leq 250000\,\text{s} \tag{4.24a}$$
$$\left[R^-\right](t) = \begin{cases} 0\,\text{nM} & 0\,\text{s} \leq t < 125000\,\text{s} \\ 0.2\,\text{nM} & 125000\,\text{s} \leq t \leq 250000\,\text{s} \end{cases} \tag{4.24b}$$

such that $r = [R^+] - [R^-]$. The species are introduced at $t = 0$ s and $t = 125000$ s, and since they are not consumed, they remain at their introduced values.

The trajectories show the prescribed reference tracking behaviour, and the matching between the linear control design and the trajectories of the dual-rail signals resulting from I/O dynamics of the CRN.

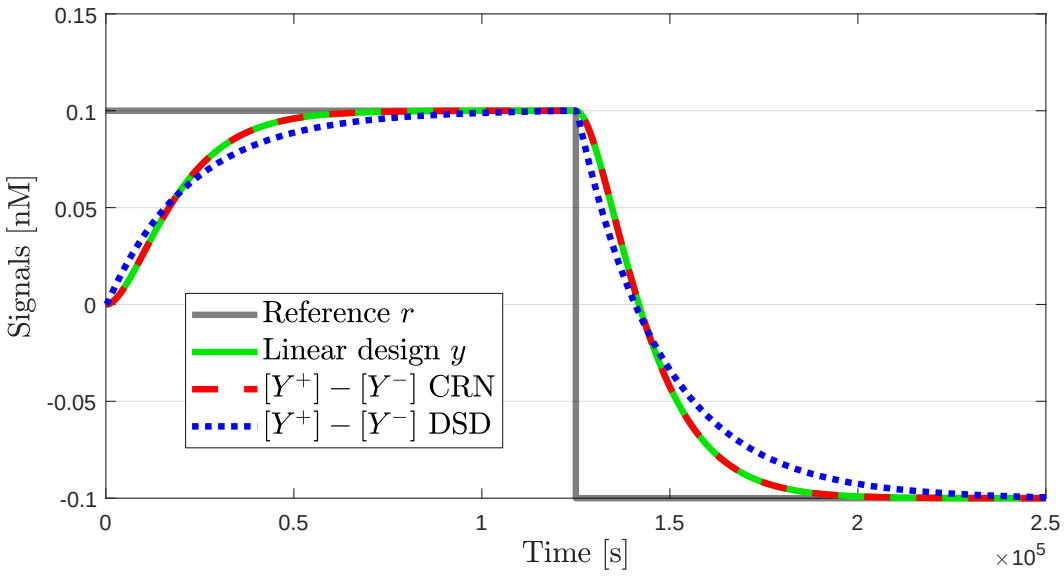

Figure 4.10: Steady state tracking response of the state feedback design and the I/O dynamics of the representations with chemical reactions and DSD reactions.

4.3.3 Representation with strand displacement reactions

The architectures from Figures 4.3-4.5 are applied to obtain DSD reactions equivalent to the CRN in (4.21), where the crossed feedback between X^+ and X^- is replaced by degradation reactions. Furthermore, with the use of degradation for $X^\pm$ the circuit can operate without the annihilation reaction $X^+ + X^- \xrightarrow{\eta} \emptyset$, since from the analysis with Visual DSD these concentrations remain low. Depending on the experimental set-up, this is yet another possible simplification.

Remark 4.1. *Adopting the construction in* (4.21)*, where catalysis reactions responsible for the state feedback are replaced with the degradation reactions in* (4.21c)*, use the simpler template complexes in Figure 4.5 and fewer species. However, there may be advantages in building the circuit relying only on catalysis reactions (and annihilation). When introducing the catalytic degradation scheme in [76] the authors argue that spatial localisation of the catalysis reactions could allow faster degradation rates.*

With these simplifications, although we have state feedback of a more complex marginally stable second order system and more degrees of freedom, the implementation has the same level of complexity as the previous integral control problem, with six catalysis reactions, two degradation reactions, and one annihilation reaction. The simulation in Visual DSD has fifteen double stranded complexes and twenty auxiliary single stranded species initialised at $C_{max} = 10^4$ nM (irreversibly consumed without replenishment), with a maximum toehold binding rate

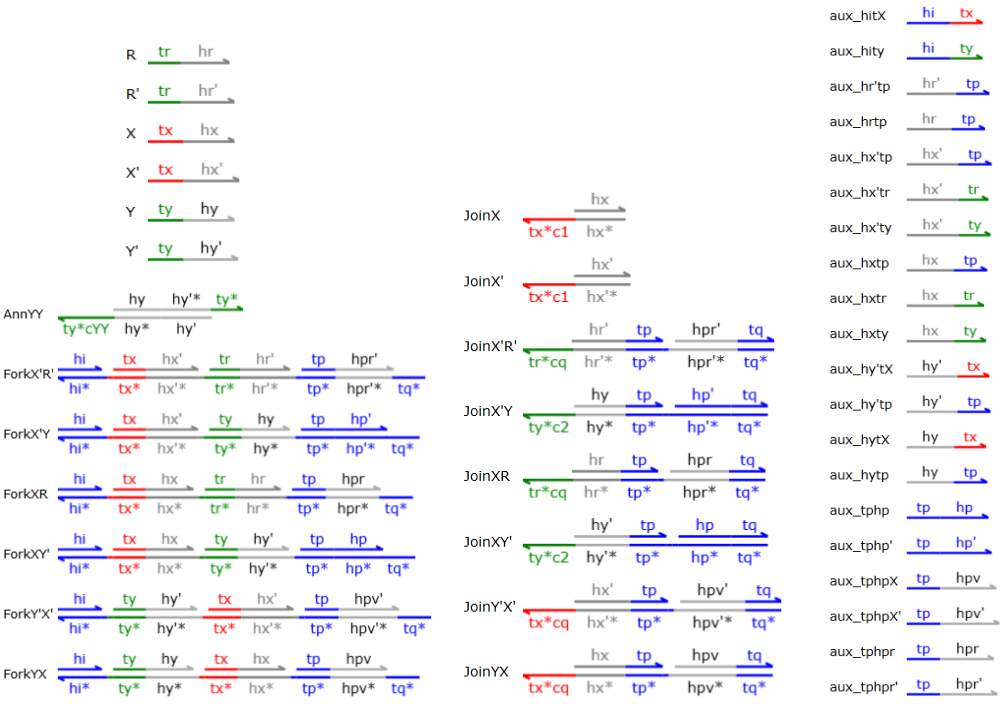

Figure 4.11: Strands used to initialise the DSD network that represents the state feedback control of the double integrator: signal strands R, R', X, X', Y, Y', and auxiliary strands initialised at high concentrations. Due to the syntax in Visual DSD, the notation is slightly different, where instead of the superscripts $\pm$ we have the correspondence $R = R^+$, $R' = R^-$, $X = X^+$, $X' = X^-$, $Y = Y^+$, $Y' = Y^-$.

$10^{-3}\,(\mathrm{nMs})^{-1}$, and unbinding rate $0.1\,\mathrm{s}^{-1}$. See all the parameters in Table 4.2 and the supplied auxiliary strands in Figure 4.11. The parameterisation for C_{max}, the unbinding rate k_{ubnd} and the maximum toehold rates k_{bnd} and k_t are the same as in the realisation of the integral feedback controller. The differences in the design are the degrees of complementarity, set to map the reaction rates of the CRN representing the design of the state feedback controller to binding rates in the realisation with DSD reactions.

For the simulation with Visual DSD, the input signal defined in (4.23) is realised in the same fashion as (4.13). The introduced concentrations of R^+ and R^- were adjusted in the code of Visual DSD to account for initial buffering, resulting in:

$$\left[R^+\right](t) \approx 0.1\,\mathrm{nM} \tag{4.25a}$$

$$\left[R^-\right](t) \approx \begin{cases} 0\,\mathrm{nM} & 0\,\mathrm{s} \le t < 125000\,\mathrm{s} \\ 0.2\,\mathrm{nM} & 125000\,\mathrm{s} \le t \le 250000\,\mathrm{s} \end{cases}. \tag{4.25b}$$

Table 4.2: Parameterisation for the Visual DSD simulation of the state feedback circuit

	Description	Vales	Units
C_{max}	Initial concentrations of template and auxiliary species	10^4	nM
$kbnd$	Toehold maximum binding rate for auxiliary strands ($< tp >$,$< tq >$)	10^{-3}	$(\text{nMs})^{-1}$
$kubnd$	Unbinding rate	0.1	$(\text{s})^{-1}$
kt	Toehold maximum binding rate for signal species ($< tr >$,$< ty >$,$< tx >$)	10^{-4}	$(\text{nMs})^{-1}$
cq	Toehold degree of complementarity for reactions in the plant	8×10^{-3}	–
$c1$	Toehold degree of complementarity for the degradation of $X^{\pm}$	8×10^{-3}	–
$c2$	Toehold degree of complementarity for feedback catalysis of $Y^{\pm}$	8×10^{-3}	–
cYY	Toehold degree of complementarity for the annihilation reaction	1	–

The initially buffered fractions of the species R and R' in Figure 4.12 are smaller than in Figure 4.7b because of a different parameterisation and the slower timescale of the represented system (see Remark B.2 in Appendix in Section B.3.3).

The concentrations from the simulation of the DSD circuit shows reference tracking behaviour (in Figure 4.10), and while the I/O dynamics of the CRN matches the linear design well, the transient dynamics with the DSD reactions are slower. Comparing in Figure 4.12 the concentrations of the CRN with the concentrations in the Visual DSD simulation, we also see slower dynamics for $Y^{\pm}$ and lower equilibrium levels for $X^{\pm}$, indicating a higher damping of the state x. Although further tuning is necessary, the dynamics are close to the desired state feedback design, and also suggest that the annihilation reaction for $X^{\pm}$ may not be necessary due to the limiting degradation.

4.4 Conclusions

There currently exist mature theoretical frameworks for the design of linear feedback controllers with chemical reaction networks. Systematic procedures and software tools provide a translation to equivalent reactions based on nucleic acid chemistry, which should be amenable to experimental implementation. However, the readiness

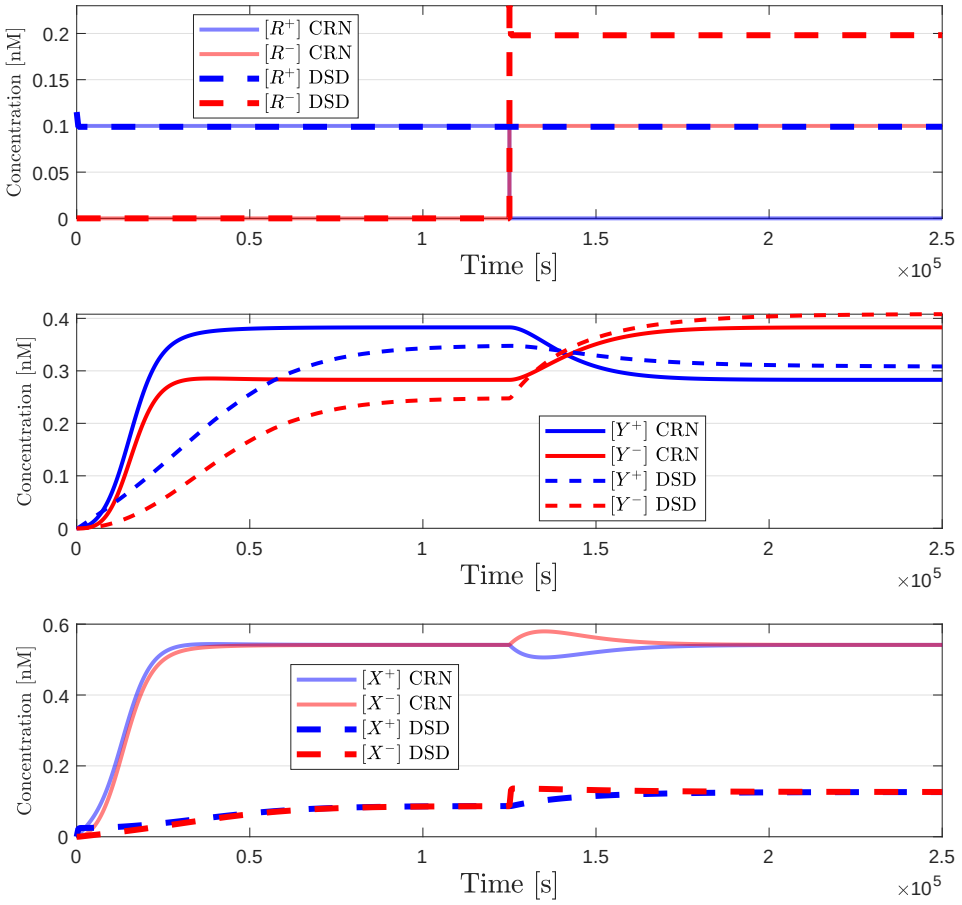

Figure 4.12: Comparison of the concentrations for the abstract CRN, and the DSD implementation. The steady state conditions for the output species $Y^{\pm}$ are similar in the CRN and DSD representations, although smaller for $X^{\pm}$ in the DSD circuit.

level of this technology has not followed the theoretical developments, and we are lacking experimental validation of such systems. The two control problems proposed here can be represented with very few CRN and DSD reactions, and are minimally complex candidates for immediate experimental validation of feedback circuits using strand displacement reaction networks.

The complexity is reduced with a careful choice of plant and by combining gain, integration and subtraction in the same chemical reactions, eliminating the need for additional dynamics and QSS approximations. The result is the removal of two catalysis reactions, two degradation reactions, and one annihilation reaction in the integral control problem, with respect to the approach of Chapter 3.

In Chapter 3 we saw that the state feedback controller can already be simplified with respect to a classical PID controller, just by combining the gains with the

subtractions in the same CRNs. The minimal complex example is further simplified, with the removal of four catalysis and one annihilation reactions, by combining the subtraction with the integration of the first state, and by selecting a plant that does not need degradation reactions for its representation.

Both problems can be implemented using similar low numbers of chemical reactions - six catalysis, two degradations and one or two annihilation reactions, and the reduced number of reactions puts these DSD networks within the current capabilities for experimental investigation.

Although simple, the examples are representative of standard control designs capturing important features of general linear feedback control systems, and the circuits are interesting for future experimental investigation of the dependence of closed-loop dynamics on toehold design, and integration of the annihilation reactions.

Chapter 5

Dynamics and stability of nucleic acid feedback controllers

For representation of linear negative feedback we cannot be limited to a positive difference between two positive inputs with a "one-sided" subtraction [31]. The previous chapters shows how the dual-rail representation [20] circumvents this problem by representing each signal as the difference of concentrations of two different species.

Although it increases the number of required reactions, as exemplified in previous chapters, the dual-rail representation enables the computation of a two-sided subtraction with the steady state of a CRN [71]. Moreover, dynamic and computation systems can be represented with CRNs assembled from elementary reactions of catalysis, degradation, and annihilation with corresponding sets of DSD reactions with equivalent dynamics. We then have a systematic process to translate control theory to implementable biochemistry with synthetic DNA oligonucleotides, where DSD networks can be assembled to represent transfer functions [62], linear feedback systems [76, 79], and nonlinear controllers [95].

The MAK that results from the dual-rail representation using the three elementary reactions in (2.24) can be classified as an IPR [142] of the I/O system in Definition 2.17. An IPR is a positive system, which together with input, state and output transformations, can realise arbitrary non positive input-to-output dynamics, Figure 5.1. In the case of linear positive systems, the system is internally positive if the state space matrices B, C and D are non-negative, and A is Metzler (Definition 2.13) [142].

We have from practical experimentation that in the constructed dual-rail CRNs, the annihilation reactions are essentially in order to ensure that species concentrations remain within the bounds of experimental feasibility. Since these

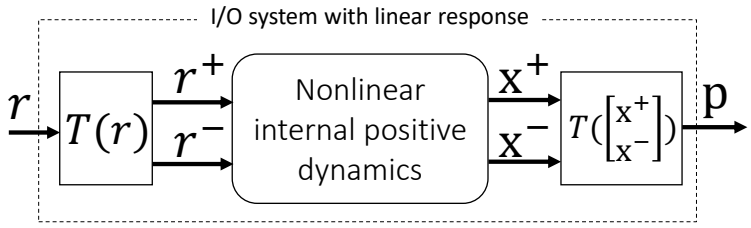

Figure 5.1: A linear system can be represented as the dynamics from the inputs to the outputs of an nonlinear internal positive representation.

bimolecular reactions introduce nonlinear dynamics, the MAK result in an IPR of a linear system based on nonlinear internal positive dynamics which are not observable in the represented I/O linear dynamics. This is very much in contrast to IPRs based on linear positive dynamics [142].

This chapter considers and formally characterises the effects of the nonlinear internal dynamics on the equilibria and the stability of the representation of linear negative feedback systems. The dynamics of the representation are analysed in the light of positive control theory from Section 2.2.2, applying stability and structural results for positive systems, to show how the annihilation reactions can relax some of the restrictions from linear IPR, and how they are important in the presence of inevitable experimental variability. These results provide many useful insights that can guide the design and construction of these circuits, and also highlight some of the associated technical challenges and limitations.

We have seen how using the dual-rail CRNs to compute gains, sums, subtractions, or any proper transfer-function [62, 79], we can take a prescribed frequency-domain description of a control system, which we wish to represent chemically, and assemble a CRN representation using only the elementary reactions (2.24). We now illustrate the construction of a simple example feedback system (for more complex examples see Chapter 3), which will be used throughout the chapter.

Example 5.1 (Simple feedback control system)**.** *Consider the feedback control system in Figure 5.2,*

$$\dot{y} = -k_2 y + k_1 u, \quad y(0) = 0 \tag{5.1a}$$

$$u = k_P (r - y) + k_0 \int (r - y) \tag{5.1b}$$

which we wish to represent chemically. According to [62, 79], we define the dual-rail signals $p_j = x_j^+ - x_j^-$ as the output of linear operators in the loop, each represented

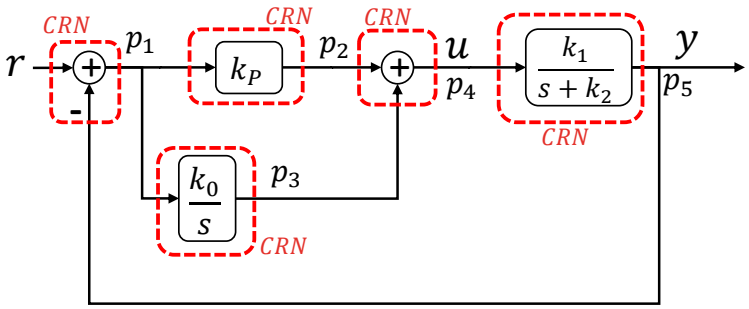

Figure 5.2: Frequency-domain representation of controller and plant of Example 5.1.

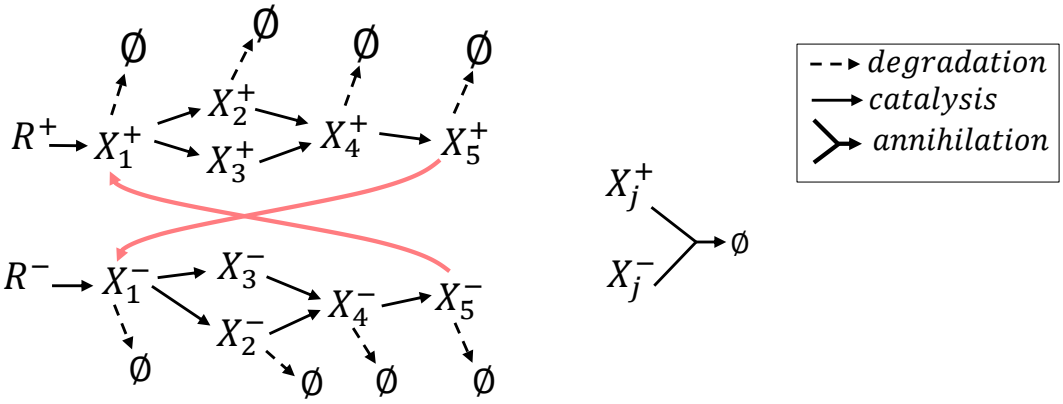

Figure 5.3: Chemical network to represent Example 5.1: each signal $p_j = x_j^+ - x_j^-$ results from representing a linear operator with chemical reactions, using unimolecular catalysis and degradation reactions, and annihilation reactions between the pairs $X_j^\pm$ (arrows from autocatalysis are omitted). The representation of the negative feedback is introduced by the catalysis from $X_5^\pm$ to $X_1^\mp$ (in red).

with reactions of the types in (2.24). The complete CRN in Figure 5.3 gives

$$R^\pm \xrightarrow{\gamma_1^\pm} R^\pm + X_1^\pm, \quad X_5^\mp \xrightarrow{\gamma_2^\mp} X_5^\mp + \boldsymbol{X_1^\pm}, \tag{5.2a}$$

$$X_1^\pm \xrightarrow{\gamma_3^\pm} \emptyset, \quad X_1^+ + X_1^- \xrightarrow{\eta} \emptyset \tag{5.2b}$$

$$X_1^\pm \xrightarrow{k_0^\pm} X_1^\pm + X_3^\pm, \quad X_3^+ + X_3^- \xrightarrow{\eta} \emptyset \tag{5.2c}$$

$$X_1^\pm \xrightarrow{\gamma_4^\pm} X_1^\pm + X_2^\pm, \quad X_2^\pm \xrightarrow{\gamma_5^\pm} \emptyset,\ X_2^+ + X_2^- \xrightarrow{\eta} \emptyset \tag{5.2d}$$

$$X_2^\pm \xrightarrow{\gamma_6^\pm} X_2^\pm + X_4^\pm, \quad X_3^\pm \xrightarrow{\gamma_7^\pm} X_3^\pm + X_4^\pm, \tag{5.2e}$$

$$X_4^\pm \xrightarrow{\gamma_8^\pm} \emptyset, \quad X_4^+ + X_4^- \xrightarrow{\eta} \emptyset \tag{5.2f}$$

$$X_4^\pm \xrightarrow{k_1^\pm} X_4^\pm + X_5^\pm, \quad X_5^\pm \xrightarrow{k_2^\pm} \emptyset,\ X_5^+ + X_5^- \xrightarrow{\eta} \emptyset\ . \tag{5.2g}$$

The control error is computed in (5.2a) and (5.2b), and the integral gain is represented in (5.2c). The gain k_P results from the steady state conditions of (5.2d), where $k_P^{\pm} = \gamma_4^{\pm}/\gamma_5^{\pm}$, and (5.2e-5.2f) sum the contributions of the control inputs to the plant represented in (5.2g). The resulting ODEs using MAK are given by:

$$\begin{aligned}
\dot{x}_1^{\pm} &= -\gamma_3^{\pm} x_1^{\pm} + \gamma_2^{\mp} x_5^{\mp} + \gamma_1^{\pm} r^{\pm} - \eta x_1^{+} x_1^{-} && \text{(5.3a)}\\
\dot{x}_2^{\pm} &= \gamma_4^{\pm} x_1^{\pm} - \gamma_5^{\pm} x_2^{\pm} - \eta x_2^{+} x_2^{-} && \text{(5.3b)}\\
\dot{x}_3^{\pm} &= k_0^{\pm} x_1^{\pm} - \eta x_3^{+} x_3^{-} && \text{(5.3c)}\\
\dot{x}_4^{\pm} &= \gamma_6^{\pm} x_2^{\pm} + \gamma_7^{\pm} x_3^{\pm} - \gamma_8^{\pm} x_4^{\pm} - \eta x_4^{+} x_4^{-} && \text{(5.3d)}\\
\dot{x}_5^{\pm} &= k_1^{\pm} x_4^{\pm} - k_2^{\pm} x_5^{\pm} - \eta x_5^{+} x_5^{-} && \text{(5.3e)}\\
x_i^{\pm}(0) &= 0, \quad i = 1,2,3,4,5\ . && \text{(5.3f)}
\end{aligned}$$

Recalling Assumption 2.1 of nominal and symmetrical parameterisation, and assuming additionally that $\gamma_5^{\pm} = \epsilon_2$, $\gamma_1^{\pm} = \gamma_2^{\pm} = \gamma_3^{\pm} = \epsilon_1$ and $\gamma_6^{\pm} = \gamma_7^{\pm} = \gamma_8^{\pm} = \epsilon_4$, we obtain the linear I/O dynamics $\dot{p}_j = \dot{x}_j^{+} - \dot{x}_j^{-}$, where

$$\begin{aligned}
\begin{bmatrix} \epsilon_1^{-1}\dot{p}_1 \\ \epsilon_2^{-1}\dot{p}_2 \\ \dot{p}_3 \\ \epsilon_4^{-1}\dot{p}_4 \\ \dot{p}_5 \end{bmatrix} &= \begin{bmatrix} -1 & 0 & 0 & 0 & -1 \\ k_P & -1 & 0 & 0 & 0 \\ k_0 & 0 & 0 & 0 & 0 \\ 0 & 1 & 1 & -1 & 0 \\ 0 & 0 & 0 & k_1 & -k_2 \end{bmatrix} \begin{bmatrix} p_1 \\ p_2 \\ p_3 \\ p_4 \\ p_5 \end{bmatrix} + \begin{bmatrix} r \\ 0 \\ 0 \\ 0 \\ 0 \end{bmatrix} && \text{(5.4a)}\\
p_i(0) &= 0, \quad i = 1,2,3,4,5\ . && \text{(5.4b)}
\end{aligned}$$

Remark 5.1. *It is important to notice that the CRNs constructions to compute the subtraction, sum and gain are exact only at steady state. The representation of these algebraic operators in the CRN add dynamics to the I/O system and increase the dimension of the state vector [79].*

Nevertheless, the impact of the additional transient dynamics for subtraction, gain and summation can be mitigated by setting the reaction rates γ_i faster than the dynamics of the controller and plant. To see how, we expressed (5.4) as a singular perturbation model [109], where by increasing ϵ_i we get timescale separation. With

Table 5.1: Nominal parameters for Example 5.1

Rates for plant	$k_1^{\pm} = 0.0008/\text{s},\ k_2^{\pm} = 0.001/\text{s}$
Rates for integrator	$k_0^{\pm} = 0.001/\text{s}$
Rates for steady state computations	$\gamma_4^{\pm} = 0.0025/\text{s},\ \gamma_{j\neq 4}^{\pm} = 0.005/\text{s}$
Annihilation rate	$\eta = 5 \times 10^5/\text{M/s}$

a QSS approximation for the fast variables, we have

$$
\begin{aligned}
p_1 &\approx r - p_5 && \text{(5.5a)}\\
p_2 &\approx k_P p_1 && \text{(5.5b)}\\
p_4 &\approx p_2 + p_3 && \text{(5.5c)}\\
\dot{p}_3 &= k_0 p_1 && \text{(5.5d)}\\
\dot{p}_5 &= k_1 p_4 - k_2 p_5 && \text{(5.5e)}\\
p_3(0) &= p_5(0) = 0 && \text{(5.5f)}
\end{aligned}
$$

and we recover the feedback control system from 5.1 and the algebraic relationships.

In practice, the reactions rates γ_i are limited by the physical limits of implementation, and albeit faster, the respective reactions can still influence the dynamics of the I/O system . Consequently, the additional dynamics for the representation of the sum, subtraction, and gain are kept in the MAK.

To demonstrate how the CRN in (5.3) is able to represent a prescribed I/O dynamics with the structure of Figure 5.2, we define an example of a possible parameterisation for Example 5.2. The reaction rates $k_1^{\pm}$, $k_2^{\pm}$ result directly in the gain and pole of the plant and $k_0^{\pm}$ from the integral control gain we wish to represent.

The computation of the controller gain $k_P^{\pm}$, the sum and subtraction depend on the reaction rates the rates γ_i, $i = 1 \dots 8$, which for purposes of timescale separation (Remark 5.1), are set faster than the dynamics of the controller and plant. Despite the timescale separation, the QSS assumption is not used for model reduction, and the simulation includes the complete set of the ODEs in (5.3).

The chosen parameters are given in Table 5.1, to ensure that the represented I/O feedback system is stable and able to track a step reference input. An additional consideration was that the dynamics the plant and the controller are slow enough so that the reaction rates result in a feasible DSD realisation with realistic strand displacement reaction rates.

For simulation, we also define a reference signal given by a sequence of posi-

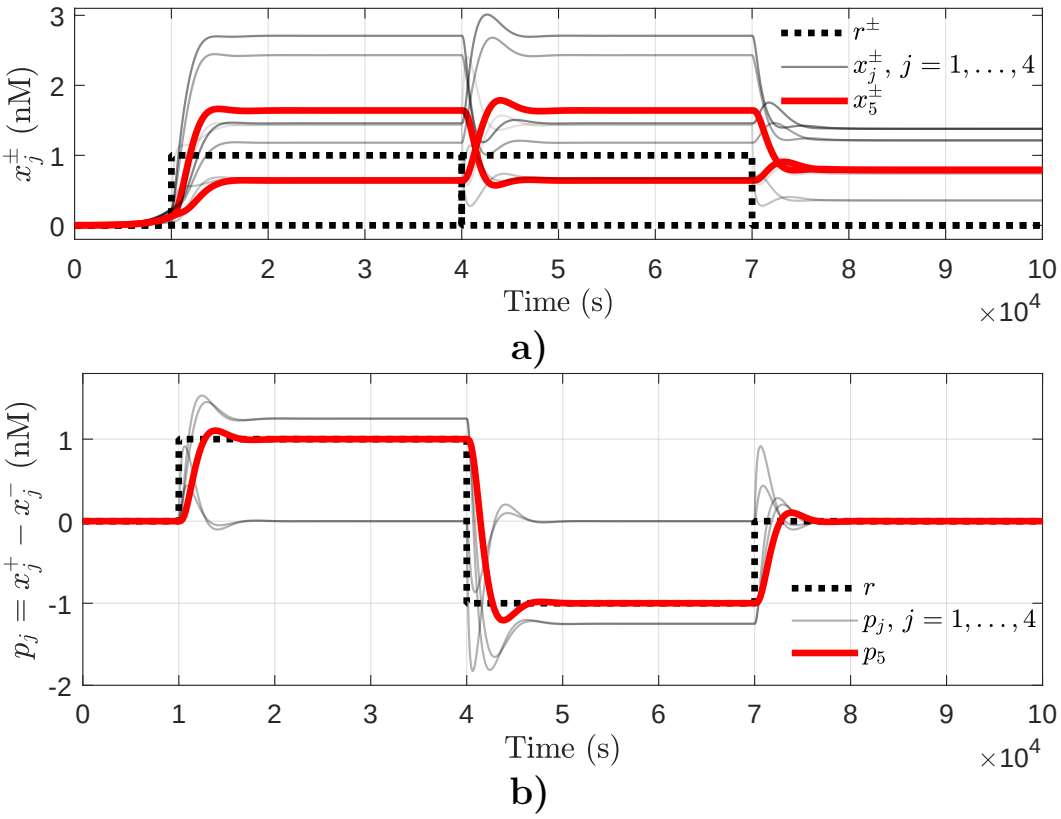

Figure 5.4: Simulation of the chemical representation of Example 5.1, to a sequence of steps on the reference concentrations $r^{\pm}$, where $x_j^{\pm} \geq 0$: A) the mass action kinetics of the concentrations; B) respective dual-rail signals, showing the reference tracking response of the output signal $y = p_5 = x_5^+ - x_5^-$ to the reference $r = r^+ - r^-$.

tive and negative steps given by

$$r(t) \quad = \quad \begin{cases} 0\,\text{nM} & 0\,\text{s} \leq t < 10000\,\text{s} \\ 1\,\text{nM} & 10000\,\text{s} \leq t < 40000\,\text{s} \\ -1\,\text{nM} & 40000\,\text{s} \leq t < 70000\,\text{s} \\ 0\,\text{nM} & 70000\,\text{s} \leq t \end{cases} . \tag{5.6}$$

However, for simulation of the MAK, we need the reference signal to be a dual-rail input to the internal positive representation (Figure 5.1). The reference signal is split into two concentrations $r^+ > 0$ or $r^- > 0$, where only one of them are positive

at any given time. The inputs to the MAK are given by

$$r^+(t) = \begin{cases} 0\,\text{nM} & 0\,\text{s} \leq t < 10000\,\text{s} \\ 1\,\text{nM} & 10000\,\text{s} \leq t < 40000\,\text{s} \\ 0\,\text{nM} & 40000\,\text{s} \leq t \end{cases} \tag{5.7a}$$

$$r^-(t) = \begin{cases} 0\,\text{nM} & 0\,\text{s} \leq t < 40000\,\text{s} \\ 1\,\text{nM} & 40000\,\text{s} \leq t < 70000\,\text{s} \\ 0\,\text{nM} & 70000\,\text{s} \leq t \end{cases} . \tag{5.7b}$$

In Figure 5.4a we have the positive dynamics in the natural coordinates $x_j^\pm$ from (5.3). In Figure 5.4b, the I/O linear dynamics are recovered from the MAK with $p_j = x_j^+ - x_j^-$, and the linear control system's output $y = p_5$ successfully tracks the reference r.

In the same manner as in previous chapters, the CRN in (5.2) can be systematically translated to DSD reactions. The equivalences between each elementary reaction in (2.24) and the sets of DSD reactions for Example 5.1 are detailed in Section 5.5.

5.1 Dynamics of the chemical reaction network

We now define the deterministic dynamics for the general class of systems analysed in this chapter. The presented results are applicable not only to Example 5.1 and the examples in the other chapters, but also to any linear negative feedback system that follows the dual-rail construction method in Section 2.3.1.

The representation relies on mapping ODE's to deterministic MAK (constraining the representation to the assumptions of the latter), and allows the chemical representation of negative gains and negative feedback present in the I/O dynamics. However, we retain the natural non-negative coordinates, where states are the concentrations $x_j^\pm$, and apply the definitions in Section 2.2.2 for positive systems.

Definition 5.1. *Defining the input vector with both positive and negative components for the reference* $\mathbf{r} = [r^+, r^-]^T$, $r^\pm \in \mathbb{R}_0^+$, *and the state* $\mathbf{x} \in \mathbb{R}_0^+$ *as the vector of species concentrations with*

$$\mathbf{x} = \left[\begin{array}{c} \mathbf{x}^+ \\ \hdashline \mathbf{x}^- \end{array}\right] = \left[\begin{array}{ccc|ccc} x_1^+ & \dots & x_N^+ & x_1^- & \dots & x_N^- \end{array}\right]^T \tag{5.8}$$

we have that for the CRN of a dual-rail representation constructed from the elementary reactions in (2.24), the MAK result

$$\Rightarrow \dot{\mathbf{x}} \;=\; \left(\mathbf{A}^{\boxtimes} - \mathbf{D}\left\{|\mathbf{a}|\right\}\right)\mathbf{x} + \mathbf{B}\mathbf{r} - \eta\left(\mathbf{P}\mathbf{x}\right) \circ \mathbf{x}, \quad \mathbf{x}(0) \geq 0 \; \textit{given} \tag{5.9}$$

where

$$\left(\mathbf{P}\mathbf{x}\right) \circ \mathbf{x} \;=\; \begin{bmatrix} \mathbf{x}^{+} \circ \mathbf{x}^{-} \\ \mathbf{x}^{+} \circ \mathbf{x}^{-} \end{bmatrix} \Rightarrow \mathbf{P} = \begin{bmatrix} \mathbf{0} & \mathbf{I} \\ \mathbf{I} & \mathbf{0} \end{bmatrix} . \tag{5.10}$$

The construction method results in several structural properties of the dynamics:

- The dynamics of the unimolecular reactions depend linearly on the state with $\mathbf{A}\mathbf{x}$, where $\mathbf{A} = \mathbf{A}^{\boxtimes} - \mathbf{D}\left\{|\mathbf{a}|\right\}$.
- By construction, we have a Metzler matrix $\mathbf{A} \in \mathcal{M}$, since the catalysis rates are on the off-diagonal elements $\mathbf{A}^{\boxtimes} \geq 0$
- The degradation rates result in non-positive elements in the diagonal of $\mathbf{D}\left\{\mathbf{a}\right\}$ with $\mathbf{a} \leq 0$.
- The contributions from the annihilation reactions are in the terms $-\eta\mathbf{x}^{+} \circ \mathbf{x}^{-}$.

Furthermore, we can decompose the dynamics into non-negative and non-positive contributions where

$$\mathbf{D}\left\{\mathbf{a}\right\} - \eta\left(\mathbf{P}\mathbf{x}\right) \circ \mathbf{x} \;\leq\; 0 \tag{5.11a}$$

$$\mathbf{A}^{\boxtimes}\mathbf{x} + \mathbf{B}\mathbf{r} \;\geq\; 0\,. \tag{5.11b}$$

Finally, decomposing the dynamics (5.9) according to the partition in (5.8) yields

$$\begin{cases} \dot{\mathbf{x}}^{+} = \mathbf{A}_1^{+}\mathbf{x}^{+} + \mathbf{A}_2^{-}\mathbf{x}^{-} + \mathbf{B}_1^{+}r^{+} - \eta\mathbf{x}^{+} \circ \mathbf{x}^{-} \\ \dot{\mathbf{x}}^{-} = \mathbf{A}_2^{+}\mathbf{x}^{+} + \mathbf{A}_1^{-}\mathbf{x}^{-} + \mathbf{B}_1^{-}r^{-} - \eta\mathbf{x}^{+} \circ \mathbf{x}^{-} \end{cases} \tag{5.12a}$$

$$\Leftrightarrow \dot{\mathbf{x}}^{\pm} = \mathbf{A}_1^{\pm}\mathbf{x}^{\pm} + \mathbf{A}_2^{\mp}\mathbf{x}^{\mp} + \mathbf{B}_1^{\pm}r^{\pm} - \eta\mathbf{x}^{+} \circ \mathbf{x}^{-}, \quad \mathbf{x}^{\pm}(0) \geq 0 \; \textit{given} \tag{5.12b}$$

and we have matrices $\mathbf{A}$ and $\mathbf{B}$ structured into the following forms:

$$\mathbf{A} = \begin{bmatrix} \mathbf{A}_1^+ & \mathbf{A}_2^- \\ \mathbf{A}_2^+ & \mathbf{A}_1^- \end{bmatrix} \tag{5.13a}$$

$$\mathbf{B} = \begin{bmatrix} \mathbf{B}_1^+ & \mathbf{0} \\ \mathbf{0} & \mathbf{B}_1^- \end{bmatrix} \tag{5.13b}$$

$$\mathbf{A}_1^\pm = \left(\mathbf{A}_1^\pm\right)^{\boxtimes} + \mathbf{D}\left\{\mathbf{a}_1^\pm\right\} \tag{5.13c}$$

$$\mathbf{a}_1^\pm \leq 0 \tag{5.13d}$$

$$\mathbf{A}_2^\pm = \left(\mathbf{A}_2^\pm\right)^{\boxtimes} . \tag{5.13e}$$

From Definition 5.1 we have that $\mathbf{A} \in \mathcal{M} \Rightarrow \mathbf{A}_j^\pm \in \mathcal{M}$ and the degradation rates are in the diagonal of $\mathbf{A}_1^\pm$. For the catalysis reaction rates, we have the rates as off-diagonal elements of $\left(\mathbf{A}_1^\pm\right)^{\boxtimes}$ with

$$\gamma : X_i^\pm \xrightarrow{\gamma} X_i^\pm + X_j^\pm, j \neq i \Rightarrow \gamma = \left[\left(\mathbf{A}_1^\pm\right)^{\boxtimes}\right]_{ji} \tag{5.14}$$

except for the crossed catalysis representing negative signs. In that case, the reaction rates are elements of $\left(\mathbf{A}_2^\pm\right)^{\boxtimes}$, with

$$\gamma : X_i^\pm \xrightarrow{\gamma} X_i^\pm + X_j^\mp, j \neq i \Rightarrow \gamma = \left[\mathbf{A}_2^\pm\right]_{ji} . \tag{5.15}$$

Remark 5.2. *Because the catalysis and degradation reactions are duplicated, both matrices $\mathbf{A}_i^\pm$ retain the same structure, but not necessarily the same parameterisation (similarly for the pair $\mathbf{B}_1^\pm$). Matrices $\mathbf{A}_i^+$ and $\mathbf{B}_1^+$ are populated with the reaction rates γ_j^+, and their counterparts $\mathbf{A}_i^-$ and $\mathbf{B}_1^-$ with γ_i^-.*

5.1.1 The dynamics in the natural coordinates are positive and nonlinear

The structure of the dynamics in (5.9) emerges for any network built according to Section 2.3.1, and several structural properties can be derived for the class of systems in Definition 5.1 and Equations (5.11-5.13).

The positivity of the dynamics depend on the basis of the coordinates, and positivity occurs usually in the natural coordinates of the system (in this case concentrations) [122]. With $\mathbf{v} = \mathbf{B}\mathbf{r} \geq 0$, and $\mathbf{g}\{\mathbf{x}\} = -\eta(\mathbf{P}\mathbf{x})$, the following Lemma 5.1 shows that the nonlinear dynamics in their natural coordinates in (5.9) are indeed non-negative.

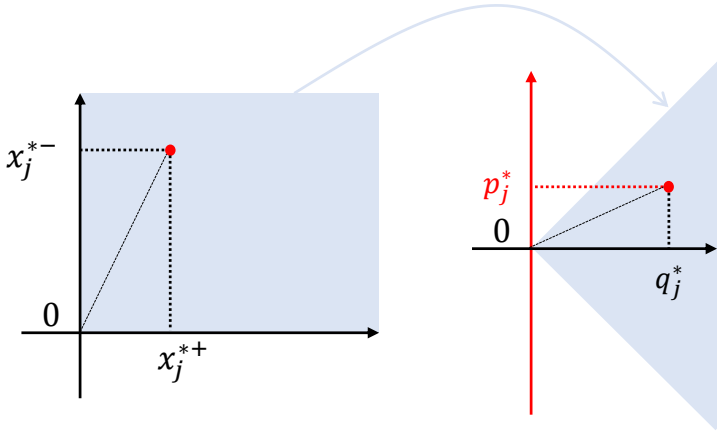

Figure 5.5: The transformation in (5.18) rotates the domain of the non-negative natural coordinates $x_j^{\pm}$ on the left, to the cone on the right with $p_j = x_j^+ - x_j^-$ and $q_j = x_j^+ + x_j^-$. Although $x_j^{\pm} \geq 0$, we have that $p_j \in \mathbb{R}$ is not restricted to positivity. The *orthogonal* coordinates q_j remain positive coordinates, and if a positive equilibrium $\mathbf{x}^*$ exists, then we also have positive equilibria q_j^*.

Lemma 5.1. *For a vector function* $\mathbf{g}\{\mathbf{x}\} \in \mathbb{R}$, *if* $\mathbf{M} \in \mathcal{M}$, $\mathbf{v} \geq 0$, *and* $\mathbf{x}(0) > 0$, *the dynamics* $\dot{\mathbf{x}} = \mathbf{M}\mathbf{x} + \mathbf{x} \circ \mathbf{g}\{\mathbf{x}\} + \mathbf{v}$ *are non-negative.*

Proof. For each component of the state vector we have

$$\dot{x}_j = [\mathbf{M}\mathbf{x}]_j + x_j [\mathbf{g}\{\mathbf{x}\}]_j + v_j \tag{5.16a}$$

$$= m_{jj}x_j + \sum_{i \neq j} m_{ji}x_i + x_j [\mathbf{g}\{\mathbf{x}\}]_j + v_j \ . \tag{5.16b}$$

Recall that $\mathbf{M} \in \mathcal{M}$, hence, for $j \neq i$, we have $m_{ji} \geq 0$. If $x_j = 0$ and $\exists_{i \neq j} : x_i > 0$, then

$$\dot{x}_j = [\mathbf{M}\mathbf{x}]_j + \mathbf{v} = \sum_{i \neq j} m_{ji}x_i + v_j \geq 0 \tag{5.17}$$

and the trajectory remains in $\mathbb{R}_0^+$. □

5.1.2 The positive nonlinear dynamics are unobservable in the I/O dynamics of the linear representation

The construction of the CRN for the dual-rail representation in Section 2.3.1 relies on Assumption 2.1 of symmetrical nominal reaction rates to have an equivalency between the resulting I/O system of Definition 2.17 and a linear control system

that we wish to represent. The consequences of Assumption 2.1 on the nonlinear dynamics constructed in (5.9) become clearer in new rotated coordinates. The system can be positive or not depending on the basis of coordinates [122], and we can see the dual-rail I/O system and the differences of concentrations as a coordinate transformation which turns parts of the state into real numbers, as illustrated in Figure 5.5.

Definition 5.2. *The rotated coordinates* $p_j = x_j^+ - x_j^- \in \mathbb{R}$ *and* $q_j = x_j^+ + x_j^- \in \mathbb{R}_0^+$ *result from the similarity transformation* $\mathbf{W}$*, where*

$$\left[\begin{array}{c} \mathbf{p} \\ \mathbf{q} \end{array}\right] = \left[\begin{array}{cc} \mathbf{I} & -\mathbf{I} \\ \mathbf{I} & \mathbf{I} \end{array}\right] \mathbf{x} = \left[\begin{array}{c} \mathbf{W}_p \\ \mathbf{W}_q \end{array}\right] \mathbf{x} = \mathbf{W}\mathbf{x} \ . \tag{5.18}$$

The transformation is a global diffeomorphism [88], it is continuously differentiable, its Jacobian is non-singular $\forall \mathbf{x} \in \mathbb{R}^{2N}$*, and* $\lim_{\|\mathbf{x}\|\to\infty} \|\mathbf{W}\mathbf{x}\| = \infty$*. For the inverse transformation we have* $\mathbf{W}^{-1} = \frac{1}{2}\mathbf{W}^T$ *and*

$$\mathbf{x} = \mathbf{W}^{-1} \left[\begin{array}{c} \mathbf{p} \\ \mathbf{q} \end{array}\right] = \frac{1}{2}\mathbf{W}^T \left[\begin{array}{c} \mathbf{p} \\ \mathbf{q} \end{array}\right] \Rightarrow \mathbf{x} = \frac{1}{2} \left[\begin{array}{cc} +\mathbf{I} & +\mathbf{I} \\ -\mathbf{I} & +\mathbf{I} \end{array}\right] \left[\begin{array}{c} \mathbf{p} \\ \mathbf{q} \end{array}\right] \ . \tag{5.19}$$

The transformation of coordinates is applied to (5.9) to determine the rotated dynamics.

Proposition 5.1. *The dynamics in the rotated coordinates are given by*

$$\left[\begin{array}{c} \dot{\mathbf{p}} \\ \dot{\mathbf{q}} \end{array}\right] = \left[\begin{array}{cc} \mathbf{R}_{11} & \mathbf{R}_{12} \\ \mathbf{R}_{21} & \mathbf{R}_{22} \end{array}\right] \left[\begin{array}{c} \mathbf{p} \\ \mathbf{q} \end{array}\right] + \left[\begin{array}{c} \mathbf{W}_p \\ \mathbf{W}_q \end{array}\right] \mathbf{B}\mathbf{r} - \frac{\eta}{2} \left[\begin{array}{c} \mathbf{0} \\ \mathbf{q} \circ \mathbf{q} - \mathbf{p} \circ \mathbf{p} \end{array}\right] \tag{5.20a}$$

$$\text{given } \mathbf{x}^{\pm}(0) \geq 0 \Rightarrow \mathbf{p}(0) = \mathbf{x}^+(0) - \mathbf{x}^-(0), \ \mathbf{q}(0) = \mathbf{x}^+(0) + \mathbf{x}^-(0) \ . \tag{5.20b}$$

Proof. Applying the mapping in Definition 5.2 and its inverse to the dynamics in the natural coordinates (5.1) yields

$$\mathbf{W}\dot{\mathbf{x}} = \mathbf{W}\mathbf{A}\mathbf{x} - \eta\mathbf{W}\left(\mathbf{x} \circ \mathbf{P}\mathbf{x}\right) + \mathbf{W}\mathbf{B}\mathbf{r} \tag{5.21a}$$

$$\Rightarrow \left[\begin{array}{c} \dot{\mathbf{p}} \\ \dot{\mathbf{q}} \end{array}\right] = \frac{1}{2}\mathbf{W}\mathbf{A}\mathbf{W}^T \left[\begin{array}{c} \mathbf{p} \\ \mathbf{q} \end{array}\right] - \eta\mathbf{W}\left(\mathbf{x} \circ \mathbf{P}\mathbf{x}\right) + \left[\begin{array}{c} \mathbf{W}_p \\ \mathbf{W}_q \end{array}\right] \mathbf{B}\mathbf{r} \ . \tag{5.21b}$$

From (5.10) we have

$$\mathbf{W}\left(\mathbf{x} \circ \mathbf{P}\mathbf{x}\right) = = \left[\begin{array}{cc} \mathbf{I} & -\mathbf{I} \\ \mathbf{I} & \mathbf{I} \end{array}\right] \left[\begin{array}{c} \mathbf{x}^+ \circ \mathbf{x}^- \\ \mathbf{x}^+ \circ \mathbf{x}^- \end{array}\right] = 2 \left[\begin{array}{c} \mathbf{0} \\ \mathbf{x}^+ \circ \mathbf{x}^- \end{array}\right] \tag{5.22}$$

and since $\mathbf{x}^{\pm} = \frac{1}{2}(\mathbf{q} \pm \mathbf{p})$ then

$$\mathbf{W}(\mathbf{x} \circ \mathbf{P}\mathbf{x}) = 2 \begin{bmatrix} \mathbf{0} \\ \frac{1}{2}(\mathbf{q}+\mathbf{p}) \circ \frac{1}{2}(\mathbf{q}-\mathbf{p}) \end{bmatrix} = \frac{1}{2} \begin{bmatrix} \mathbf{0} \\ \mathbf{q} \circ \mathbf{q} - \mathbf{p} \circ \mathbf{p} \end{bmatrix} . \tag{5.23}$$

From the structure of $\mathbf{A}$ in (5.13) and defining

$$\begin{aligned} \mathbf{R} &= \begin{bmatrix} \mathbf{R}_{11} & \mathbf{R}_{12} \\ \mathbf{R}_{21} & \mathbf{R}_{22} \end{bmatrix} = \mathbf{W}\mathbf{A}\mathbf{W}^{-1} = \frac{1}{2}\mathbf{W}\mathbf{A}\mathbf{W}^{T} && \text{(5.24a)} \\ &= \frac{1}{2} \begin{bmatrix} +\mathbf{I} & -\mathbf{I} \\ +\mathbf{I} & +\mathbf{I} \end{bmatrix} \begin{bmatrix} \mathbf{A}_1^{+} & \mathbf{A}_2^{-} \\ \mathbf{A}_2^{+} & \mathbf{A}_1^{-} \end{bmatrix} \begin{bmatrix} +\mathbf{I} & +\mathbf{I} \\ -\mathbf{I} & +\mathbf{I} \end{bmatrix} && \text{(5.24b)} \\ &= \frac{1}{2} \begin{bmatrix} \left(\mathbf{A}_1^{+} + \mathbf{A}_1^{-} - \mathbf{A}_2^{+} - \mathbf{A}_2^{-}\right) & \left(\mathbf{A}_1^{+} - \mathbf{A}_1^{-} + \mathbf{A}_2^{-} - \mathbf{A}_2^{+}\right) \\ \left(\mathbf{A}_1^{+} - \mathbf{A}_1^{-} + \mathbf{A}_2^{+} - \mathbf{A}_2^{-}\right) & \left(\mathbf{A}_1^{+} + \mathbf{A}_1^{-} + \mathbf{A}_2^{+} + \mathbf{A}_2^{-}\right) \end{bmatrix} && \text{(5.24c)} \end{aligned}$$

we finally have the structure in (5.20). □

Remark 5.3. *Recalling that by construction* $\mathbf{a}_1^{\pm} \leq 0$*, from the structures in Definition 5.1 and* (5.13)*, we can write*

$$\begin{aligned} \mathbf{R_{22}} &= \tfrac{1}{2}\left(\mathbf{A_1^{+}} + \mathbf{A_1^{-}} + \mathbf{A_2^{+}} + \mathbf{A_2^{-}}\right)^{\boxtimes} - \tfrac{1}{2}\mathbf{D}\left\{\left|\mathbf{a_1^{+}}\right| + \left|\mathbf{a_1^{-}}\right|\right\} && \text{(5.25a)} \\ \mathbf{R_{11}} &= \tfrac{1}{2}\left(\mathbf{A_1^{+}} + \mathbf{A_1^{-}} - \mathbf{A_2^{+}} - \mathbf{A_2^{-}}\right)^{\boxtimes} - \tfrac{1}{2}\mathbf{D}\left\{\left|\mathbf{a_1^{+}}\right| + \left|\mathbf{a_1^{-}}\right|\right\} && \text{(5.25b)} \\ \mathbf{R_{12}} &= \tfrac{1}{2}\left(\mathbf{A_1^{+}} - \mathbf{A_1^{-}} - \mathbf{A_2^{+}} + \mathbf{A_2^{-}}\right)^{\boxtimes} - \tfrac{1}{2}\mathbf{D}\left\{\left|\mathbf{a_1^{+}}\right| - \left|\mathbf{a_1^{-}}\right|\right\} && \text{(5.25c)} \\ \mathbf{R_{21}} &= \tfrac{1}{2}\left(\mathbf{A_1^{+}} - \mathbf{A_1^{-}} + \mathbf{A_2^{+}} - \mathbf{A_2^{-}}\right)^{\boxtimes} - \tfrac{1}{2}\mathbf{D}\left\{\left|\mathbf{a_1^{+}}\right| - \left|\mathbf{a_1^{-}}\right|\right\} . && \text{(5.25d)} \end{aligned}$$

Additionally, we have some structural properties of $\mathbf{R}_{22}$ *where*

- *The diagonal of* $\mathbf{R}_{22}$ *is non-positive and the average of the diagonals of* $\mathbf{A}_1^{\pm}$*.*
- $\mathbf{A}_j^{\pm} \in \mathcal{M} \Rightarrow \mathbf{R}_{22} \in \mathcal{M}$*.*

Definition 5.3. *Consider the condition of perfectly identical reaction rates of a symmetrical parameterisation in Assumption 2.1. In this case, we can define the nominal matrices (represented with an upper bar) as* $\mathbf{A}_1^{\pm} = \bar{\mathbf{A}}_1$ *(and therefore* $\mathbf{a}_1^{\pm} = \bar{\mathbf{a}}_1$*),* $\mathbf{A}_2^{\pm} = \bar{\mathbf{A}}_2$*,* $\mathbf{B}_1^{\pm} = \bar{\mathbf{B}}_1$*.*

Proposition 5.2. *For the nominal symmetrical parameterisation in Definition 5.3, the nonlinear dynamics are unobservable in the I/O system, due to the serial structure of the nominal rotated dynamics given by*

$$\begin{aligned} \dot{\mathbf{p}} &= \bar{\mathbf{R}}_{11}\mathbf{p} + \mathbf{W}_p\bar{\mathbf{B}}\mathbf{r}, \quad \mathbf{p}(0) = 0 && \text{(5.26a)} \\ \dot{\mathbf{q}} &= \bar{\mathbf{R}}_{22}\mathbf{q} + \mathbf{W}_q\bar{\mathbf{B}}\mathbf{r} + \frac{\eta}{2}\mathbf{p} \circ \mathbf{p} - \frac{\eta}{2}\mathbf{q} \circ \mathbf{q}, \quad \mathbf{q}(0) \geq 0 . && \text{(5.26b)} \end{aligned}$$

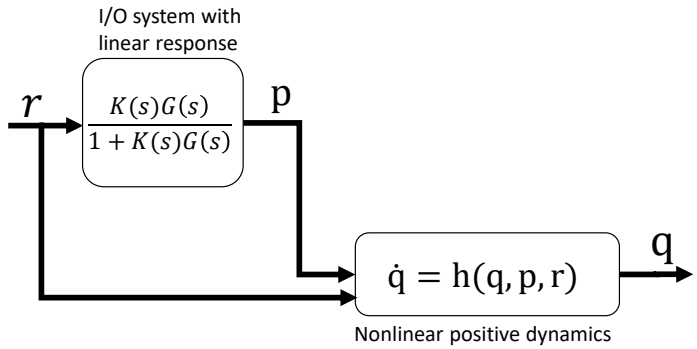

Figure 5.6: Cascaded interconnection between the I/O dynamics and the underlying positive dynamics in the rotated coordinates, for the nominal symmetrical parameterisation in Definition 5.3.

Proof. Applying Definition 5.3 to the matrices in Remark 5.3, it follows immediately that $\bar{\mathbf{R}}_{12} = \bar{\mathbf{R}}_{21} = 0$, $\bar{\mathbf{R}}_{11} = \bar{\mathbf{A}}_1 - \bar{\mathbf{A}}_2$, $\bar{\mathbf{R}}_{22} = \bar{\mathbf{A}}_1 + \bar{\mathbf{A}}_2$. Thus, the serial structure of (5.26) (illustrated in Figure 5.6) has $\mathbf{p}$ evolving independently of $\mathbf{q}$, making $\mathbf{q}$ unobservable in any output of the I/O dynamics. □

Noting that (5.26a) corresponds to the dynamics of the I/O system from Definition 2.17, we can use $\mathbf{W}$ and the new coordinates to analyse the interactions between the linear I/O dynamics $\dot{\mathbf{p}}$ and the remaining internal dynamics $\dot{\mathbf{q}}$. Besides nonlinear we have that Equation (5.26b) is non-negative, since by Definition 5.2, $x_j^{\pm} \geq 0 \Rightarrow q_j \geq 0$.

Assumption 5.1. *Assume hereafter that the dynamics we wish to represent result in stable I/O dynamics, and therefore* $\bar{\mathbf{R}}_{11} \in \mathcal{H}$ *and* $\bar{\mathbf{R}}_{11}^{-1}$ *exists. Such an assumption is expected for the design of feedback systems, where nominal stability is a requirement.*

5.2 Equilibria of the chemical reaction network

We now compare the equilibria of the CRN with and without feedback, to analyse how representing negative feedback changes the fundamental properties of the CRN.

Definition 5.4. *A cascaded system is a set of DSD reactions without feedback, where the catalysis reactions do not depend directly or indirectly on the chemical species downstream.*

Cascaded strand displacement reactions are well suited to systematically build large computational and logic gate circuitry [31, 71]. The cascaded structure of the represented linear system results in a state matrix that can be permuted

such that $\bar{\mathbf{R}}_{11} \in \mathcal{L}$. Under Assumptions 2.1 and 5.1 (nominal parameters with stable I/O system), and from Remark 5.3, we have that

$$\bar{\mathbf{R}}_{11} \in \mathcal{L} \Rightarrow \bar{\mathbf{A}}_1, \bar{\mathbf{A}}_2 \in \mathcal{L} \tag{5.27a}$$

$$\bar{\mathbf{R}}_{11} \in \mathcal{L}, \mathcal{H} \Rightarrow \bar{\mathbf{R}}_{22} \in \mathcal{L}, \mathcal{H} \ . \tag{5.27b}$$

For example, representing the open loop of Figure 5.2 without feedback (removing $X_5^{\pm} \to X_5^{\pm} + X_1^{\mp}$ in Figure 5.3) results in a cascade of serial and parallel unimolecular reactions. The feedback reactions $X_5^{\pm} \to X_5^{\pm} + X_1^{\mp}$ connect the output to the input of the cascade, and mass is transferred back into the input of the cascade. Including feedback in the I/O dynamics leads to feedback within the network, and the cascaded structure is lost.

Remark 5.4. *In this particular case, removing the feedback also results in* $\bar{\mathbf{A}}_2 = 0$*, but in general, we can have* $\bar{\mathbf{A}}_2 \geq 0$ *if there are subtractions in the cascaded I/O dynamics.*

Due to the cascaded structure, the equilibrium of the unforced dynamics can be computed sequentially for each coordinate to show that it is unique.

Lemma 5.2. *For the unforced response (*$\mathbf{r} = 0$*) of a cascaded system with nominal and symmetrical parameterisation (Definition 5.3), the dynamics of* (5.26) *have a single equilibrium for* $\mathbf{p}^* = \mathbf{q}^* = 0$*.*

Proof. For $\mathbf{r} = 0$, we have directly from (5.26) that

$$\mathbf{r} = 0 \Rightarrow \mathbf{p}^* = 0 \Rightarrow 0 = \bar{\mathbf{R}}_{22}\mathbf{q}^* - \frac{\eta}{2}\mathbf{q}^* \circ \mathbf{q}^* \ . \tag{5.28}$$

If the CRN is a unidirectional cascade of reactions, we can order the states so that $\bar{\mathbf{R}}_{11}$ is a lower triangular matrix, and $\bar{\mathbf{A}}_1, \bar{\mathbf{A}}_2 \in \mathcal{L} \Rightarrow \bar{\mathbf{R}}_{22} \in \mathcal{L}$. For the diagonal elements we have from Remark 5.3 and Definition 5.3 that $\left[\bar{\mathbf{R}}_{22}\right]_{jj} = -\left|\bar{a}_j\right|$. Solving sequentially for each coordinate q_j yields

$$\begin{aligned}
\bar{\mathbf{R}}_{22} \in \mathcal{L} \Rightarrow \forall_{i>1}, \left[\bar{\mathbf{R}}_{22}\right]_{1i} = 0 \Rightarrow \left(-\left|\bar{a}_1\right| - \frac{\eta}{2}q_1^*\right) q_1^* = 0 \Rightarrow q_1^* = 0 \\
q_1^* = 0 \wedge \forall_{i>2}, \left[\bar{\mathbf{R}}_{22}\right]_{2i} = 0 \Rightarrow \left(-\left|\bar{a}_2\right| - \frac{\eta}{2}q_2^*\right) q_2^* = 0 \Rightarrow q_2^* = 0 \\
\vdots \\
\forall_{i<j}, q_i^* = 0 \wedge \forall_{i>j}, \left[\bar{\mathbf{R}}_{22}\right]_{ji} = 0 \Rightarrow \left(-\left|\bar{a}_j\right| - \frac{\eta}{2}q_j^*\right) q_j^* = 0 \Rightarrow q_j^* = 0
\end{aligned}$$

where the negative solutions $q_j^* = -\frac{2|\bar{a}_1|}{\eta} < 0$ are discarded. Hence, $\mathbf{p}^* = \mathbf{q}^* = 0$. □

In the presence of feedback the cascaded structure is lost, since the states will depend on the output. All the states involved in the represented closed loop become interdependent, and $\bar{\mathbf{R}}_{11}$ cannot be a lower triangular matrix. The interdependent evolution of all the states is reflected in the irreducibility [122] of the state matrix $\bar{\mathbf{R}}_{11}$, and recalling Definition 2.15 we have $\bar{\mathbf{R}}_{11} \in \mathcal{I}$.

Remark 5.5. *It follows that for each coordinate j we have $\exists_{i>j} : \left[\bar{\mathbf{R}}_{11}\right]_{ji} > 0$, either due to $\bar{\mathbf{A}}_1$ (from catalysis representing positive feedback) or due to $\bar{\mathbf{A}}_2$ (from catalysis representing negative feedback). Since $\bar{\mathbf{R}}_{22} = \bar{\mathbf{A}}_1 + \bar{\mathbf{A}}_2$ we have also that $\bar{\mathbf{R}}_{22} \in \mathcal{I}, \mathcal{M}$, and for each coordinate j we have that $\exists_{i\neq j} : \left[\bar{\mathbf{R}}_{22}\right]_{ji} > 0$ where the trajectory of q_j will always depend on another coordinate q_i.*

The representation of feedback in the I/O dynamics ($\bar{\mathbf{R}}_{11} \in \mathcal{I}$) leads to an irreducible network ($\bar{\mathbf{A}} \in \mathcal{I}$) and a fundamental change in the possible number and nature of the equilibria for the positive internal dynamics $\mathbf{q}^*$.

Proposition 5.3. *Consider $\mathbf{M} \in \mathcal{I}, \mathcal{M}$ such that $\mathbf{M} = \mathbf{M}^{\boxtimes} + \mathbf{D}\{\mathbf{m}\}$, $\mathbf{m} \leq 0$, a scalar $k > 0$, and the dynamics $\dot{\mathbf{q}} = \mathbf{M}\mathbf{q} - k\mathbf{q} \circ \mathbf{q}$, $\mathbf{q}(0) \geq 0$, with equilibrium $\mathbf{q}^*$. Then we have the following:*

i) either all states are at equilibrium at the origin or none are. That is, if $\exists_j q_j^* = 0$ then $\forall_{i\neq j}, q_i^* = 0$;

ii) the unforced dynamics may admit a second positive equilibrium $\mathbf{q}^* > 0$, proportional to k^{-1}.

Proof. For each coordinate q_j, we have

$$\dot{\mathbf{q}} = \mathbf{M}\mathbf{q} - k\mathbf{q} \circ \mathbf{q} \quad \Rightarrow \quad \dot{q}_j = m_{jj}q_j + \sum_{i\neq j} m_{ji}q_i - kq_j^2 \tag{5.29}$$

$$\mathbf{m} \leq 0 \quad \Rightarrow \quad \dot{q}_j = -|m_{jj}|q_j + \sum_{i\neq j} m_{ji}q_i - kq_j^2 \ . \tag{5.30}$$

From the equilibrium condition for q_j we have the system of equations

$$0 \quad = \quad kq_j^2 + |m_{jj}|q_j - \sum_{i\neq j} m_{ji}q_i \tag{5.31a}$$

$$\Rightarrow q_j \quad = \quad \frac{1}{2k}\left(-|m_{jj}| \pm \sqrt{m_{jj}^2 + 4k\sum_{i\neq j} m_{ji}q_i}\right) \ . \tag{5.31b}$$

From $\mathbf{M} \in \mathcal{M}$ and positivity constraint $q_i \geq 0$, we have $4k\sum_{i\neq j} m_{ji}q_i \geq 0$ and the

non-negative root is given by

$$\Rightarrow q_j \;=\; \frac{1}{2k}\left(-|m_{jj}| + \sqrt{m_{jj}^2 + 4k\sum_{i\neq j} m_{ji}q_i}\right) \geq 0\ . \tag{5.32}$$

i) The equilibrium $\mathbf{q}^* = 0$ is the trivial solution of the equilibrium condition. However, we can state more.

If $\mathbf{M} \in \mathcal{I}$ then $\forall_j, \exists_{i\neq j} : m_{ji} > 0$, that is, the dynamics of each coordinate $\dot{q}_j$ will depend on at least one other state q_i, and at the same time, each coordinate q_i will contribute to the dynamics of at least one other state $\dot{q}_j$.

From the root solution for each coordinate, this results in the condition that $q_j^* = 0 \Rightarrow \sum_{i\neq j} m_{ji}q_i^* = 0$. Hence, for $q_j^* = 0$ it is necessary that all other states $q_{i\neq j}$ on which $\dot{q}_j$ depends to have $q_i^* = 0$, that is, $\forall_{i\neq j} : m_{ji} > 0$ we have $q_j^* = 0 \Rightarrow q_i^* = 0$.

Due to $\mathbf{M} \in \mathcal{I}$, each and every state q_j is a dependency on another state, and therefore, $\forall_j, q_j^* = 0 \Rightarrow q_{i\neq j}^* = 0$. We then conclude that an irreducible $\mathbf{M}$ (and the interdependence of all states) implicates that we cannot have an equilibrium where only some of the states are at zero.

ii) If $\exists_{i\neq j} : m_{ji} > 0$ and the coordinate i is at a positive equilibrium $q_{i\neq j}^* > 0$, then $\sum_{i\neq j} m_{ji}q_i^* > 0$ and $q_j^* > 0$. In turn, the irreducibility of $\mathbf{M}$ ensures that $\exists_{j\neq i} : m_{ij} > 0$ and $q_i^* > 0$. The non-negative roots for each coordinate j result from solving the system of equations in (5.32) and note that even if $m_{jj} = 0$, then $q_j^* > 0$ with

$$q_j^* = \frac{1}{\sqrt{k}}\sqrt{\sum_{i\neq j} m_{ji}q_i^*} > 0\ . \tag{5.33}$$

Combining **i)** and **ii)**, if $\mathbf{M} \in \mathcal{I}$, the system may have a positive equilibrium $\mathbf{q}^* > 0$, which can be scaled inversely to k, since in (5.32) we have $\lim_{k\to\infty} q_j^* = 0$. □

Example 5.2. *Consider the CRN representation of a linear system with a single input u and negative feedback between its states x and y ($d_1, d_2, c_1, c_2 > 0$)*

$$\dot{x} = -d_1 x - \boldsymbol{c_2 y} + u \tag{5.34a}$$

$$\dot{y} = -d_2 y + c_1 x \tag{5.34b}$$

where the feedback parameter c_2 has a direct impact on the characteristic polynomial of the closed loop transfer function

$$Y(s) = \frac{c_1}{s^2 + s\,(d_1 + d_2) + d_1 d_2 + c_1\boldsymbol{c_2}}U(s)\ . \tag{5.35}$$

Using the dual-rail representation with $u = u^+ - u^-$, $x = x^+ - x^-$ *and* $y = y^+ - y^-$, *we construct the CRN given by*

$$U^{\pm} \xrightarrow{1} U^{\pm} + X^{\pm},\ X^{\pm} \xrightarrow{d_1} \emptyset,\ X^+ + X^- \xrightarrow{k} \emptyset \tag{5.36a}$$

$$X^{\pm} \xrightarrow{c_1} X^{\pm} + Y^{\pm},\ Y^{\pm} \xrightarrow{d_2} \emptyset,\ Y^+ + Y^- \xrightarrow{k} \emptyset \tag{5.36b}$$

$$Y^{\pm} \xrightarrow{c_2} Y^{\pm} + X^{\mp} \tag{5.36c}$$

where (5.36c) *represents the negative feedback. Writing the MAK we get*

$$\dot{x}^+ = -d_1 x^+ + c_2 y^- + u^+ - k x^+ x^- \tag{5.37a}$$

$$\dot{y}^+ = -d_2 y^+ + c_1 x^+ - k y^+ y^- \tag{5.37b}$$

$$\dot{x}^- = -d_1 x^- + c_2 y^+ + u^- - k x^+ x^- \tag{5.37c}$$

$$\dot{y}^- = -d_2 y^- + c_1 x^- - k y^+ y^- \tag{5.37d}$$

$$x^{\pm}(0) = y^{\pm}(0) = 0\ . \tag{5.37e}$$

Writing the dynamics according to Definition 5.1, considering that in this case we have $\mathbf{A}_1^+ = \mathbf{A}_1^-$ *and* $\mathbf{A}_2^+ = \mathbf{A}_2^-$, *yields*

$$\begin{bmatrix} \dot{x}^+ \\ \dot{y}^+ \\ \dot{x}^- \\ \dot{y}^- \end{bmatrix} = \begin{bmatrix} \bar{\mathbf{A}}_1 & \bar{\mathbf{A}}_2 \\ \bar{\mathbf{A}}_2 & \bar{\mathbf{A}}_1 \end{bmatrix} \begin{bmatrix} x^+ \\ y^+ \\ x^- \\ y^- \end{bmatrix} + \begin{bmatrix} 1 & 0 \\ 0 & 0 \\ 0 & 1 \\ 0 & 0 \end{bmatrix} \begin{bmatrix} u^+ \\ u^- \end{bmatrix} - k \begin{bmatrix} x^+x^- \\ y^+y^- \\ x^+x^- \\ y^+y^- \end{bmatrix} \tag{5.38}$$

with

$$\bar{\mathbf{A}}_1 = \begin{bmatrix} -d_1 & 0 \\ c_1 & -d_2 \end{bmatrix}, \bar{\mathbf{A}}_2 = \begin{bmatrix} 0 & c_2 \\ 0 & 0 \end{bmatrix}\ . \tag{5.39}$$

The state space matrix for the I/O dynamics $\bar{\mathbf{R}}_{11}$ *and the linear term of the internal positive nonlinear dynamics* $\bar{\mathbf{R}}_{22}$ *are given by*

$$\bar{\mathbf{R}}_{11} = \bar{\mathbf{A}}_1 - \bar{\mathbf{A}}_2 = \begin{bmatrix} -d_1 & -c_2 \\ c_1 & -d_2 \end{bmatrix} \tag{5.40a}$$

$$\bar{\mathbf{R}}_{22} = \bar{\mathbf{A}}_1 + \bar{\mathbf{A}}_2 = \begin{bmatrix} -d_1 & c_2 \\ c_1 & -d_2 \end{bmatrix}\ . \tag{5.40b}$$

Looking at the unforced dynamics

$$\dot{\mathbf{q}} = \bar{\mathbf{R}}_{22}\mathbf{q} - k\mathbf{q} \circ \mathbf{q} \Leftrightarrow \begin{cases} \dot{q}_1 = & -d_1 q_1 + c_2 q_2 - k q_1^2 \\ \dot{q}_2 = & -d_2 q_2 + c_1 q_1 - k q_2^2 \end{cases} \tag{5.41}$$

we have that without feedback ($c_2 = 0$) the system simplifies to a reducible serial cascade where $\bar{\mathbf{R}}_{11} = \bar{\mathbf{R}}_{22} = \bar{\mathbf{A}}_1 \in \mathcal{L}$, with a single non-negative equilibrium at $\mathbf{q} = 0$:

$$k q_1^2 + d_1 q_1 = 0 \Rightarrow q_1 = 0 \Rightarrow k q_2^2 + d_2 q_2 - c_1 q_1 = 0 \Rightarrow q_2 = 0 \ . \tag{5.42}$$

With feedback ($c_2 > 0$) we solve $q_2 = c_2^{-1} q_1 (k q_1 + d_1)$ in the equilibrium condition for q_1, and replace it in the equilibrium condition for q_2 to obtain

$$\begin{aligned} 0 &= k q_2^2 + d_2 q_2 - c_1 q_1 && \text{(5.43a)} \\ \Rightarrow 0 &= c_2^{-2} k q_1^2 (k q_1 + d_1)^2 + c_2^{-1} d_2 k q_1^2 + c_2^{-1} d_2 d_1 q_1 - c_1 q_1 && \text{(5.43b)} \\ \Rightarrow 0 &= k q_1^2 \left(k^2 q_1^2 + 2 d_1 k q_1 + d_1^2\right) + c_2 d_2 k q_1^2 + c_2 d_2 d_1 q_1 - c_2^2 c_1 q_1 && \text{(5.43c)} \\ &= k^3 q_1^4 + k^2 2 d_1 q_1^3 + \left(k d_1^2 + d_2 c_2 k\right) q_1^2 + c_2 (d_2 d_1 - c_2 c_1) q_1 \ . && \text{(5.43d)} \end{aligned}$$

The parameters in the polynomial coefficients are all positive, resulting in negative polynomial coefficients only if $c_2 > d_2 d_1 c_1^{-1}$. If that is the case, there is a change of sign in the coefficients, and Descartes' rule of signs tells us that there exists exactly one positive root, and therefore a positive equilibrium $q_1^* > 0$ exists.

Remark 5.6. *Note that the use of $\bar{\mathbf{A}}_2 \geq 0$ to represent negative feedback in the I/O dynamics in (5.26a) with $\bar{\mathbf{R}}_{11} = \bar{\mathbf{A}}_1 - \bar{\mathbf{A}}_2$, results in positive feedback in the nonlinear dynamics in (5.26b) with $\bar{\mathbf{R}}_{22} = \bar{\mathbf{A}}_1 + \bar{\mathbf{A}}_2$. This difference captures a fundamental property of the dual-rail representation, where the representation of negative feedback is in fact introducing positive feedback within the CRN.*

In (5.40) of Example 5.2, c_2 impacts on the spectral radius of $\bar{\mathbf{R}}_{11}$ and $\bar{\mathbf{R}}_{22}$ differently. From the characteristic polynomial,

$$\begin{aligned} \lambda \in \rho\left\{\bar{\mathbf{R}}_{11}\right\} \ &\Rightarrow \ \lambda^2 + \lambda (d_1 + d_2) + d_1 d_2 + c_1 c_2 = 0 && \text{(5.44a)} \\ &\Rightarrow \ \lambda = -\frac{(d_1 + d_2)}{2} \pm \frac{1}{2}\sqrt{(d_1 + d_2)^2 - 4 (d_1 d_2 + c_1 c_2)} && \text{(5.44b)} \\ \Rightarrow c_2 > 0 \ &\Rightarrow \ \alpha\left\{\bar{\mathbf{R}}_{11}\right\} < 0 && \text{(5.44c)} \end{aligned}$$

we have stable I/O dynamics ($\bar{\mathbf{R}}_{11} \in \mathcal{H}$) for any $c_2 > 0$. But in the case of $\bar{\mathbf{R}}_{22}$,

where

$$\lambda \in \rho\left\{\bar{\mathbf{R}}_{22}\right\} \quad \Rightarrow \quad \lambda^2 + \lambda\left(d_1 + d_2\right) + d_1 d_2 - c_1 c_2 = 0 \tag{5.45a}$$

$$\Rightarrow \quad \lambda = -\frac{\left(d_1 + d_2\right)}{2} \pm \frac{1}{2}\sqrt{\left(d_1 + d_2\right)^2 - 4\left(d_1 d_2 - c_1 c_2\right)} \tag{5.45b}$$

$$\Rightarrow c_2 > \frac{d_1 d_2}{c_1} \quad \Rightarrow \quad \alpha\left\{\bar{\mathbf{R}}_{22}\right\} > 0 \tag{5.45c}$$

for a sufficiently high gain $c_2 > d_2 d_1 c_1^{-1}$ we get $\alpha\left\{\bar{\mathbf{R}}_{22}\right\} > 0$ and therefore $\bar{\mathbf{R}}_{22} \notin \mathcal{H}$. Not coincidentally, it is the same domain for which $\mathbf{q}^* > 0$ exists.

Remark 5.7. *The existence of positive equilibrium conditions for linear feedback systems has direct consequences for the experimental construction of these circuits. Operating at an equilibrium corresponding to high concentrations aggravates leaky reactions, where undesired triggering of strand displacement leads to unwanted outputs in the absence of inputs. Furthermore, if* $\mathbf{q}^* \geq 0$ *with input* $\mathbf{r} = 0$*, then the reactions persist even if the I/O dynamics are at rest* $\mathbf{p} = 0$*, leading to unnecessary, irreversible, and costly consumption of fuel species. This is in direct contrast to cascaded systems, where without input to the I/O dynamics, the CRN is at equilibrium at* $\mathbf{x} = 0$*, and no reactions occur.*

5.3 Stability

We postulated the stability of the represented I/O system with Assumption 5.1. We now investigate the stability of the internal positive dynamics and the MAK of the complete CRN.

We begin by proving the following lemma, which is applicable to the unforced dynamics of (5.9) and (5.26b).

Lemma 5.3. *If* $\mathbf{M} \in \mathcal{M}, \mathcal{H}$*, and* $\mathbf{g}\{\mathbf{x}\} < 0$ *for* $\mathbf{x} > 0$*, then the system with dynamics* $\dot{\mathbf{x}} = \mathbf{M}\mathbf{x} + \mathbf{x} \circ \mathbf{g}\{\mathbf{x}\}$ *is GAS at* $\mathbf{x} = 0$*.*

Proof. From Theorem 2.2 [122], if $\mathbf{M} \in \mathcal{M}, \mathcal{H}$ then $\exists_{\mathbf{d}>0} : \mathbf{M}^T\mathbf{D}\{\mathbf{d}\} + \mathbf{D}\{\mathbf{d}\}\mathbf{M} = -\mathbf{I}$. We take the Lyapunov function $V_d\{\mathbf{x}\} = \mathbf{x}^T\mathbf{D}\{\mathbf{d}\}\mathbf{x} > 0$, yielding

$$\begin{aligned}
\dot{V}_d(\mathbf{x}) &= \left(\mathbf{x}^T\mathbf{M}^T + \mathbf{g}\{\mathbf{x}\}^T\mathbf{D}\{\mathbf{x}\}\right)\mathbf{D}\{\mathbf{d}\}\mathbf{x} \\
&\quad + \mathbf{x}^T\mathbf{D}\{\mathbf{d}\}\left(\mathbf{M}\mathbf{x} + \mathbf{D}\{\mathbf{x}\}\mathbf{g}\{\mathbf{x}\}\right) && (5.46a) \\
&= \mathbf{x}^T\left(\mathbf{M}^T\mathbf{D}\{\mathbf{d}\} + \mathbf{D}\{\mathbf{d}\}\mathbf{M}\right)\mathbf{x} \\
&\quad + \mathbf{g}\{\mathbf{x}\}^T\left(\mathbf{x} \circ \mathbf{d} \circ \mathbf{x}\right) + \mathbf{x}^T\left(\mathbf{d} \circ \mathbf{x} \circ \mathbf{g}\{\mathbf{x}\}\right) && (5.46b) \\
&= -\mathbf{x}^T\mathbf{x} + 2\mathbf{g}\{\mathbf{x}\}^T\left(\mathbf{d} \circ \mathbf{x} \circ \mathbf{x}\right) < 0\ . && (5.46c)
\end{aligned}$$

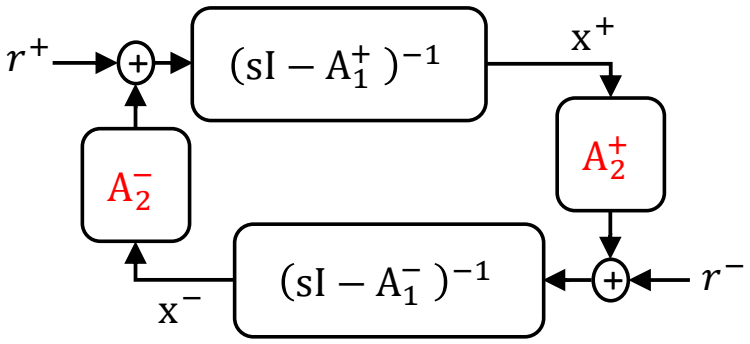

Figure 5.7: Representing negative feedback with $\mathbf{A}_2^{\pm} \geq 0$, introduces positive feedback between positive dynamics $\mathbf{A}_1^{\pm} \in \mathcal{M}$.

Since $\mathbf{d} > 0$ exists, this guarantees that $\mathbf{d} \circ \mathbf{x} \circ \mathbf{x} > 0$. With $\mathbf{g}\{\mathbf{x}\} < 0$ for $\mathbf{x} > 0$, we obtain $\dot{V}_d(\mathbf{x}) < 0$ and global asymptotic convergence to $\mathbf{x} = 0$. □

With $\mathbf{g}\{\mathbf{x}\} = -\mathbf{P}\mathbf{x}$, Lemma 5.3 ensures that if the network of catalysis and degradation reactions is stable, $\mathbf{A} \in \mathcal{H}$, the bimolecular reactions cannot destabilise (5.9). A stable CRN with $\mathbf{A} \in \mathcal{H}$ can occur if the degradation of each species is faster than their overall production, and $\mathbf{A}$ has a dominant diagonal.

However, this is not the general case. The dynamics without the bimolecular reactions result in the positive feedback loop between two positive systems (see Figure 5.7). Since we cannot stabilise the non-negative dynamics $\mathbf{A}_1^{\pm} \in \mathcal{M}$ with non-negative matrices $\mathbf{A}_2^{\pm} \geq 0$ [128, 129], it is sufficient to have $\mathbf{A}_1^{\pm} \notin \mathcal{H}$ to give $\mathbf{A} \notin \mathcal{H}$.

Even for the nominal symmetrical parameterisation, the representation has modes that are not present in the represented linear I/O system since $\rho\{\bar{\mathbf{R}}\} = \rho\{\bar{\mathbf{R}}_{11}\} \cup \rho\{\bar{\mathbf{R}}_{22}\}$. For Example 5.2, the spectral radii in (5.44) and (5.45) show that for $c_2 > d_2 d_1 c_1^{-1}$, $\bar{\mathbf{R}}$ (and consequently $\bar{\mathbf{A}}$) will have unstable modes even if $\bar{\mathbf{R}}_{11} \in \mathcal{H}$.

5.3.1 The I/O dynamics determine the stability for the nominal symmetrical case

While having $\bar{\mathbf{R}}_{22} \notin \mathcal{H}$ is a problem for IPR with linear positive systems [142] and at first glance it seems precarious to have unobservable nonlinear dynamics, we will now see how the presence of the bimolecular reactions are sometimes sufficient for stabilisation. In fact, for the designed *nominal symmetrical* case in Definition 5.3, it is possible to provide guarantees for stability and boundedness.

Proposition 5.4. *The* cascaded *systems from Definition 5.4 representing stable I/O dynamics, have GAS unforced nonlinear dynamics, for* $\mathbf{x} > 0$.

Proof. From Remark 5.3, in cascaded systems $\bar{\mathbf{R}}_{11}, \bar{\mathbf{R}}_{22} \in \mathcal{L}$, and $\rho\left\{\bar{\mathbf{R}}_{11}\right\} = \rho\left\{\bar{\mathbf{R}}_{22}\right\}$. If the I/O system is stable, then $\alpha\left\{\bar{\mathbf{R}}_{11}\right\} = \alpha\left\{\bar{\mathbf{R}}_{22}\right\} < 0$ and Lemma 5.3 ensures $\dot{\mathbf{q}} = \bar{\mathbf{R}}_{22}\mathbf{q} - \frac{\eta}{2}\mathbf{q} \circ \mathbf{q}$ is GAS at $\mathbf{q} = 0$. □

Remark 5.8. *We can apply Proposition 5.4 to the representation of individual linear operations, which by themselves are cascaded reactions. It results directly that the CRNs for summation, gain, and subtraction by themselves, have GAS unforced dynamics, and are bounded for bounded inputs. More importantly, applying it to CRNs assembled from cascading those linear operations, results in a single stable equilibrium for the complete circuit.*

With the introduction of feedback, even for the representation of stable I/O linear dynamics ($\bar{\mathbf{R}}_{11} \in \mathcal{H}$), we lose the cascaded structure and create an irreducible system, impacting the stability at the origin.

Lemma 5.4. *For the dynamics* $\dot{\mathbf{q}} = \mathbf{M}\mathbf{q} - k\mathbf{q} \circ \mathbf{q}$, $\mathbf{q}(0) \geq 0$, *with a scalar* $k > 0$, *and* $\mathbf{M} \in \mathcal{M}, \mathcal{I}$ *but* $\mathbf{M} \notin \mathcal{H}$, *the equilibrium at the origin* $\mathbf{q} = 0$ *is unstable.*

Proof. Applying Theorem 2.4 [122] for the Frobenius eigenvalue and eigenvector of an irreducible Metzler matrix $\mathbf{M} \in \mathcal{M}, \mathcal{I}$, we have that $\exists_{\mathbf{w}_F > 0} : \mathbf{w}_F^T\mathbf{M} = \lambda_F\mathbf{w}_F^T$ and $\lambda_F = \alpha\{\mathbf{M}\}$. Defining the Lyapunov function $V_F(\mathbf{q}) = \mathbf{w}_F^T\mathbf{q}$, we have that $\mathbf{q} > 0 \Rightarrow V_F(\mathbf{q}) > 0$ and

$$\begin{aligned}
\dot{V}_F(\mathbf{q}) &= \mathbf{w}_F^T\dot{\mathbf{q}} && \text{(5.47a)}\\
&= \mathbf{w}_F^T\mathbf{M}\mathbf{q} - k\mathbf{w}_F^T\mathbf{q} \circ \mathbf{q} && \text{(5.47b)}\\
&= \lambda_F\mathbf{w}_F^T\mathbf{q} - k\mathbf{w}_F^T\mathbf{q} \circ \mathbf{q} && \text{(5.47c)}\\
&= \mathbf{w}_F^T\left(\mathbf{q} \circ \left(\lambda_F\mathbf{1} - k\mathbf{q}\right)\right) . && \text{(5.47d)}
\end{aligned}$$

Since $\mathbf{M} \notin \mathcal{H} \Rightarrow \lambda_F > 0$, and for the domain where $\forall_j, q_j < \frac{\lambda_F}{k}$ we have that $\dot{V}_F\{\mathbf{q}\} > 0$. Hence, the system is divergent close to the origin, and the equilibrium at $\mathbf{q} = 0$ is therefore unstable. □

If feedback leads to $\bar{\mathbf{R}}_{22} \notin \mathcal{H}$, then Lemma 5.4 states that unforced trajectories diverge away from the origin due to a diverging mode of $\bar{\mathbf{R}}_{22}$, as illustrated in Figure 5.8. The IPR of a stable system using only linear positive systems is therefore not guaranteed to be stable [142]. However, for the nonlinear positive dynamics (5.26b) in Proposition 5.2, we can still ensure boundedness with the following result.

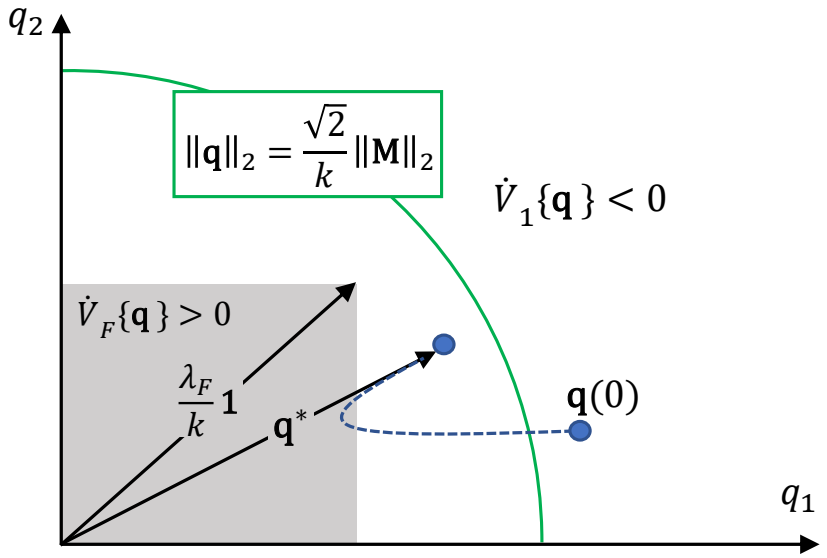

Figure 5.8: Illustration of the exclusion area from Lemma 5.4 (gray), and the upper bound from Lemma 5.5 (green), for the trajectories of the unforced nominal nonlinear dynamics of a 2 dimensional system, considering $\mathbf{M} \in \mathcal{I}, \mathcal{M}$ and $\mathbf{M} \notin \mathcal{H}$. The trajectories close to the origin will diverge and the dashed curve is an illustration of convergence to a positive equilibrium $\mathbf{q}^*$.

Lemma 5.5. *For $\mathbf{M} \in \mathcal{M}$, $\mathbf{q}(0) > 0$, and a bounded input $\mathbf{v} \geq 0$, if $\mathbf{g}\{\mathbf{q}\} \leq -k\mathbf{q}$ (scalar $k > 0$) then the trajectories of $\dot{\mathbf{q}} = \mathbf{M}\mathbf{q} + \mathbf{q} \circ \mathbf{g}\{\mathbf{q}\} + \mathbf{v}$ are non-negative ($\mathbf{q} \in \mathbb{R}_0^{N+}$) and bounded by $\|\mathbf{q}\|_2 < k^{-1}\left(\sqrt{N}\|\mathbf{M}\|_2 + \|\mathbf{v}\|_1\|\mathbf{q}\|_2^{-1}\right)$.*

Proof. For $\mathbf{M} \in \mathcal{M}$, Lemma 5.1 guarantees that the trajectories are non-negative for $\mathbf{q}(0) > 0$. If $\mathbf{M} \in \mathcal{H}$, Lemma 5.3 guarantees that the system is asymptotically stable in $\mathbb{R}_0^+$ with an equilibrium at $\mathbf{q} = 0$. If $\mathbf{M} \notin \mathcal{H}$, we can still show boundedness, using the linear Lyapunov function $V_1\{\mathbf{q}\} = \mathbf{1}^T\mathbf{q} = \sum_j q_j > 0$, in the domain $\mathbf{q} > 0$. We then have

$$\begin{aligned}
\dot{V}_1\{\mathbf{q}\} &= \mathbf{1}^T\mathbf{M}\mathbf{q} + \mathbf{1}^T\mathbf{v} + \mathbf{1}^T\mathbf{D}\{\mathbf{q}\}\mathbf{g}\{\mathbf{q}\} && \text{(5.48a)}\\
&= \mathbf{1}^T\mathbf{M}\mathbf{q} + \|\mathbf{v}\|_1 + \mathbf{q}^T\mathbf{g}\{\mathbf{q}\} && \text{(5.48b)}\\
&\leq \|\mathbf{M}\mathbf{q}\|_1 + \|\mathbf{v}\|_1 - k\mathbf{q}^T\mathbf{q} && \text{(5.48c)}\\
&\leq \sqrt{N}\|\mathbf{M}\|_2\|\mathbf{q}\|_2 + \|\mathbf{v}\|_1 - k\|\mathbf{q}\|_2^2 \,. && \text{(5.48d)}
\end{aligned}$$

We can always find large enough values of $\mathbf{q}$ such that $\|\mathbf{q}\|_2 > \frac{\sqrt{N}}{k}\|\mathbf{M}\|_2 + \frac{1}{k}\frac{\|\mathbf{v}\|_1}{\|\mathbf{q}\|_2}$ where we have $\dot{V}_1\{\mathbf{q}\} < 0$. □

Applying Lemma 5.5 with $\mathbf{g}\{\mathbf{q}\} = -\frac{\eta}{2}\mathbf{q}$ to the unforced dynamics in (5.26b) we have $\|\mathbf{q}\|_2 < 2\eta^{-1}\sqrt{N}\|\bar{\mathbf{R}}_{22}\|_2$. In general, Lemma 5.5 is not applicable to the

nonlinear dynamics (5.9), due to the matrix $\mathbf{P}$.

Proposition 5.5. *Consider the nominal dynamics in (5.26a-5.26b), with the symmetrical parameterisation from Definition 5.3. Under Assumption 5.1, the I/O dynamics (5.26a) are stable, and the concentrations in the complete CRN are bounded and can be scaled down with a faster annihilation reaction rate η.*

Proof. Assumption 5.1 ensures the trajectories of $\mathbf{p}$ are bounded. We can treat $\mathbf{p}$ as an additional input to the system (5.26b) and apply Lemma 5.5 with a positive input $\mathbf{v} = \mathbf{W}_q\bar{\mathbf{B}}\mathbf{r} + \frac{\eta}{2}\mathbf{p}\circ\mathbf{p}$. The unobserved dynamics are then bounded for bounded inputs $\mathbf{r}, \mathbf{p} > 0$, and are scaled down by increasing η. □

The same feedback responsible for stable I/O linear dynamics can result in $\bar{\mathbf{R}}_{22} \notin \mathcal{H}$ (see Remark 5.6). Designing feedback to ensure that $\bar{\mathbf{R}}_{11}, \bar{\mathbf{R}}_{22} \in \mathcal{H}$ is impractical since it would put constraints on which I/O systems could be represented. It is one of the challenges of representing stable linear systems relying only on linear positive systems [142], where we would need $\bar{\mathbf{A}} \in \mathcal{H}$ for the IPR to be stable. Lemma 5.5 and Proposition 5.5 lift this constraint, albeit at the cost of a positive equilibrium.

Remark 5.9. *With $\bar{\mathbf{A}}_1 \in \mathcal{M}$ but $\bar{\mathbf{A}}_1 \notin \mathcal{H}$, there is no $\bar{\mathbf{A}}_2 \geq 0$ such that $\bar{\mathbf{R}}_{22} = \bar{\mathbf{A}}_1 + \bar{\mathbf{A}}_2 \in \mathcal{H}$ [128, 129]. Starting from a marginally stable state matrix $\alpha\left\{\bar{\mathbf{A}}_1\right\} = 0$, the introduction of feedback leads to $\alpha\left\{\bar{\mathbf{R}}_{22}\right\} \geq 0$. This raises an interesting trade-off, where the controllers that introduce integrators in the loop transfer function (for example, PI controller) lead to a positive equilibrium, which is inconvenient for implementation.*

Remark 5.10. *With the introduction of feedback, the concentrations involved in the irreducible parts of the CRN will have positive equilibria, and $\exists_j\ q_j(t) > 0$ even if $\mathbf{r} = 0$ and the I/O dynamics are stable $\alpha\left\{\bar{\mathbf{R}}_{11}\right\} < 0$. In practice, Proposition 5.5 motivates the designed CRN to include the annihilation reactions since the bound in Lemma 5.5 tells us that, as long as the represented I/O system is stable, the annihilation reactions in the constructed CRN will result in bounded concentrations. Furthermore, the bounding limit in Lemma 5.5 is in agreement with the experimental practice of maximising the annihilation rate η as high as feasibly possible to minimise the concentrations during operation or at equilibrium.*

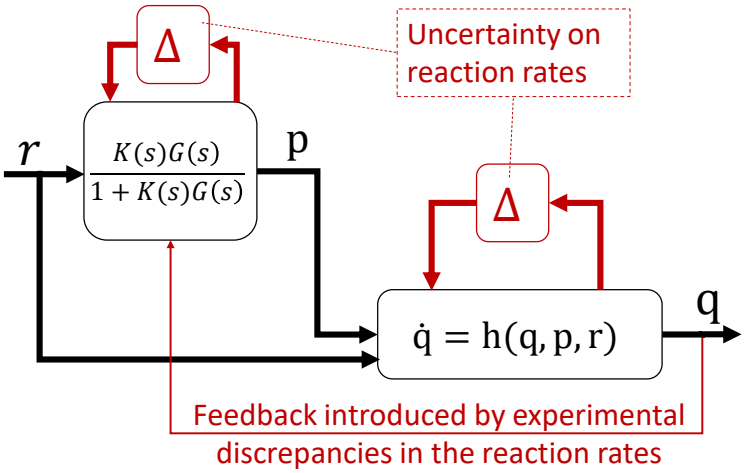

Figure 5.9: Interconnection between the I/O dynamics and the underlying positive dynamics in the rotated coordinates, in the presence of uncertainty leading to an asymmetrical parameterisation. The red feedback connection is absent with the nominal symmetric parameterisation from Definition 5.3.

5.4 Stability with asymmetrical parameterisation resulting from experimental variability

The construction of the I/O dynamics in (5.26a) assumes the symmetrical parameterisation in Definition 5.3, and we have shown some of the properties intrinsic to the design methods, like positive equilibria and internal stability conditions.

When analysing for parametric scattering of the $\bar{\mathbf{R}}_{11}$ in (5.26a) we must be aware that we are still within Assumption 2.1 of perfect symmetric parameterisation, and as long as the I/O linear dynamics are stable $\bar{\mathbf{R}}_{11} \in \mathcal{H}$, Proposition 5.5 guarantees that the nonlinear dynamics are bounded.

However, besides the stochastic nature of DSD reactions and inherent noise (especially in applications with low number of copies), the experimental implementation of DNA systems also suffers from several spurious processes that alter the effective hybridisation rates. The granular and imperfect design of toehold hybridisation rates [74], initial and gradual leakage due to undesired reactions that release output species without input, and synthesis errors which result in unproductive species can alter the stoichiometry of the reactions. Additionally, crosstalk between different DSD strands with common toeholds also affects the dynamics, with temporary unproductive interactions slowing down the triggering of strand displacements [29].

Even if we can approximately avoid the stochasticity of the system (with the assumption of well mixed and and large number of molecules), there are still uncertain and uncharacterised processes affecting the parameterisation of the hybridisation rates in a deterministic model. Hence, when verifying the implementation of the CRN, we must account for such experimental error and analyse robustness to parameteric variability in all the reaction rates outside Assumption 2.1, and realistically allow the reaction rates in the CRN to vary independently.

Definition 5.5. *We define the* asymmetric parameterisation *as the case when Assumption 2.1 is not applicable, resulting in* $\mathbf{A}_1^+ \neq \mathbf{A}_1^-$, $\mathbf{A}_2^+ \neq \mathbf{A}_2^-$, *and* $\mathbf{B}_1^+ \neq \mathbf{B}_1^-$. *This will be the non-nominal case when considering independent uncertainty in the reaction rates due to experimental variability.*

The consequences of this asymmetry are clarified in the rotated coordinates: although the I/O dynamics $\dot{\mathbf{p}}$ are still linear in (5.20) ($\mathbf{W}_p(\mathbf{P}\mathbf{x} \circ \mathbf{x}) = 0$), they depend on the nonlinear dynamics through the term $\mathbf{R}_{12}\mathbf{q}$ (absent in (5.26a)), with

$$\dot{\mathbf{p}} \;\; = \;\; \mathbf{R}_{11}\mathbf{p} + \mathbf{W}_p\mathbf{B}\mathbf{r} + \mathbf{R}_{12}\mathbf{q} \; . \tag{5.49}$$

Remark 5.11. *With experimental variability, we lose the serial structure from (5.26). A stable I/O dynamics* $\mathbf{R}_{11} \in \mathcal{H}$ *no longer provides guarantee of boundedness, since it ignores the feedback between the I/O linear dynamics and the underlying nonlinear dynamics (feedback connection in Figure 5.9). Therefore, we need to analyse the stability of the complete nonlinear dynamics of (5.9).*

We investigate the stability of the nonlinear system using Lyapunov's indirect method, and the eigenvalues of the linearisation at the equilibrium of the system [88].

Definition 5.6. *Given an equilibrium of the system* $\mathbf{x}^*$ *for a steady state input* $\mathbf{r}^*$, *we define the perturbation input* $\mathbf{r}_e = \mathbf{r} - \mathbf{r}^*$ *and resulting perturbed trajectories around the equilibrium as* $\mathbf{x}_e = \mathbf{x} - \mathbf{x}^*$.

Proposition 5.6. *The linearised dynamics of the system in Definition 5.1, around the trim point* $\mathbf{x} = \mathbf{x}^* + \mathbf{x}_e$, $\mathbf{r} = \mathbf{r}^* + \mathbf{r}_e$, *yield*

$$\dot{\mathbf{s}} \;\; = (\mathbf{A} + \eta\mathbf{J}\{\mathbf{x}^*\})\,\mathbf{s} + \mathbf{B}\mathbf{r}_e = \mathbf{A}_s\mathbf{s} + \mathbf{B}\mathbf{r}_e, \quad \mathbf{s}(0) = 0 \tag{5.50}$$

where locally around the trim point $\mathbf{x} \approx \mathbf{x}^* + \mathbf{s}$, *with*

$$\mathbf{A}_s \;\; = \mathbf{A} + \eta\mathbf{J}\{\mathbf{x}^*\} \tag{5.51}$$

and

$$\mathbf{J}\{\mathbf{x}^*\} = -\mathbf{D}\{\mathbf{P}\mathbf{x}^*\} - \mathbf{D}\{\mathbf{x}^*\}\mathbf{P} = -\begin{bmatrix} \mathbf{D}\{\mathbf{x}^{*-}\} & \mathbf{D}\{\mathbf{x}^{*+}\} \\ \mathbf{D}\{\mathbf{x}^{*-}\} & \mathbf{D}\{\mathbf{x}^{*+}\} \end{bmatrix} . \quad (5.52)$$

Proof. Writing the dynamics for the perturbed system $\mathbf{x} = \mathbf{x}^* + \mathbf{x}_e$ we have

$$\begin{aligned} \frac{d}{dt}(\mathbf{x}^* + \mathbf{x}_e) &= \mathbf{A}(\mathbf{x}^* + \mathbf{x}_e) + \mathbf{B}(\mathbf{r}^* + \mathbf{r}_e) \\ &\quad -\eta(\mathbf{P}\mathbf{x}^* + \mathbf{P}\mathbf{x}_e) \circ (\mathbf{x}^* + \mathbf{x}_e) \quad (5.53a) \\ \Leftrightarrow \frac{d\mathbf{x}^*}{dt} + \frac{d\mathbf{x}_e}{dt} &= (\mathbf{A}\mathbf{x}^* + \mathbf{B}\mathbf{r}^* - \eta\mathbf{P}\mathbf{x}^* \circ \mathbf{x}^*) + \mathbf{A}\mathbf{x}_e + \mathbf{B}\mathbf{r}_e \\ &\quad -\eta(\mathbf{P}\mathbf{x}^* \circ \mathbf{x}_e + \mathbf{P}\mathbf{x}_e \circ \mathbf{x}^* + \mathbf{P}\mathbf{x}_e \circ \mathbf{x}_e) . \quad (5.53b) \end{aligned}$$

Since at equilibrium we have $\frac{d\mathbf{x}^*}{dt} = 0 = \mathbf{A}\mathbf{x}^* + \mathbf{B}\mathbf{r}^* - \eta\mathbf{P}\mathbf{x}^* \circ \mathbf{x}^*$ yields

$$\begin{aligned} \dot{\mathbf{x}}_e &= \mathbf{A}\mathbf{x}_e - \eta(\mathbf{P}\mathbf{x}^* \circ \mathbf{x}_e + \mathbf{P}\mathbf{x}_e \circ \mathbf{x}^*) + \mathbf{B}\mathbf{r}_e - \eta\mathbf{P}\mathbf{x}_e \circ \mathbf{x}_e \quad (5.54a) \\ &= (\mathbf{A} - \eta\mathbf{D}\{\mathbf{P}\mathbf{x}^*\} - \eta\mathbf{D}\{\mathbf{x}^*\}\mathbf{P})\mathbf{x}_e + \mathbf{B}\mathbf{r}_e - \eta\mathbf{P}\mathbf{x}_e \circ \mathbf{x}_e \quad (5.54b) \\ &= (\mathbf{A} + \eta\mathbf{J}\{\mathbf{x}^*\})\mathbf{x}_e + \mathbf{B}\mathbf{r}_e - \eta\mathbf{P}\mathbf{x}_e \circ \mathbf{x}_e . \quad (5.54c) \end{aligned}$$

The linear system in (5.50) results from the linearisation of the perturbation model in (5.54c), $\mathbf{x}_e = \mathbf{x}_e^* + \mathbf{s}$, around the equilibrium at the origin $\mathbf{x}_e^* = 0$. □

From Theorem 2.1, if $\alpha\{\mathbf{A}_s\} < 0$ in (5.50), then the nonlinear system in Definition 5.1 is locally exponentially stable around the equilibrium [88], and the equilibrium $\mathbf{x}^* = 0$ is stable if and only if $\mathbf{A} \in \mathcal{H}$ (which is in agreement with Lemma 5.3). Even if $\mathbf{A} \notin \mathcal{H}$, the linearisation can still be stable around the equilibrium $\mathbf{x}^* > 0$, with the participation of $\mathbf{J}\{\mathbf{x}^*\}$ showing the stabilising role of the bimolecular reactions. It is also noteworthy that

$$\mathbf{W}_p\mathbf{J}\{\mathbf{x}^*\} = \begin{bmatrix} \mathbf{I} & -\mathbf{I} \end{bmatrix}\mathbf{J}\{\mathbf{x}^*\} = 0 \quad (5.55)$$

hence $\alpha\{\mathbf{R}_{11}\}$ and the stability of the linear I/O dynamics does not depend on the equilibrium of the CRN.

5.4.1 Stability analysis of an example with feedback under parametric variability

We now illustrate the above results for the simplest feedback control system configuration in Example 5.1. With the nominal parameter values in Table 5.1, we have in Table 5.2 that $\bar{\mathbf{R}}_{22} \notin \mathcal{H}$, and the origin is unstable (Lemma 5.4). This is

Table 5.2: Poles with maximum real part, for the I/O and linearised dynamics, for the nominal and asymmetrical parameterisations.

Matrix $\mathbf{M}$	Poles corresponding to $\alpha\{\mathbf{M}\}$	Stability
$\bar{\mathbf{R}}_{11}$	$(-6.3741 \pm i8.0364) \times 10^{-4}$	$\bar{\mathbf{R}}_{11} \in \mathcal{H}$
$\bar{\mathbf{R}}_{22}$	$+5.2991 \times 10^{-4}$	$\bar{\mathbf{R}}_{22} \notin \mathcal{H}$
$\bar{\mathbf{A}}_s$	-5.1614×10^{-4}	$\bar{\mathbf{A}}_s \in \mathcal{H}$
$\mathbf{R}_{11}$	$(-0.21874 \pm i15.031) \times 10^{-4}$	$\mathbf{R}_{11} \in \mathcal{H}$
$\mathbf{A}_s$	$(+0.27197 \pm i15.325) \times 10^{-4}$	$\mathbf{A}_s \notin \mathcal{H}$

Table 5.3: An asymmetrical parameterisation of Example 5.1 which results in unstable dynamics of the CRN.

Plant	$k_1^{\pm} = 0.001064$/s, $k_2^{\pm} = 0.00067$/s
Integrator	$k_0^{\pm} = 0.00133$/s
Steady state computations	$\gamma_4^{\pm} = 0.001675$/s, $\gamma_5^{\pm} = 0.00665$/s ($k_P^{\pm} = 0.25188$)
	$\gamma_1^{\pm} = \gamma_2^{\pm} = \gamma_3^{-} = 0.00665$/s, $\gamma_3^{+} = 0.00335$/s
	$\gamma_6^{-} = \gamma_7^{\pm} = \gamma_8^{-} = 0.00665$/s, $\gamma_6^{+} = \gamma_8^{+} = 0.00335$/s
Annihilation rate	$\eta = 5 \times 10^5$/M/s

confirmed in Figure 5.4a, where for $t > 7 \times 10^4$ s the reference returns to $r^{\pm} = 0$ and the state converges to a positive equilibrium $\bar{\mathbf{x}}^{+*} = \bar{\mathbf{x}}^{-*} > 0$. Table 5.2 shows that the nominal I/O dynamics $\bar{\mathbf{R}}_{11} \in \mathcal{H}$ and the linearisation around the nominal equilibrium $\bar{\mathbf{A}}_s \in \mathcal{H}$, despite $\bar{\mathbf{R}}_{22} \notin \mathcal{H}$.

Considering experimental variability in the reaction rates leads to asymmetric parameterisations, and the stability of I/O dynamics does not guarantee stability of the CRN. To account for realistic levels of experimental variability, we introduce an uncertainty of ±33% in the reaction rates. This level of variability reflects what should be achievable experimentally, since models based on a toehold sequence can predict hybridisation rates within factors of 2 and 3, and the uncertainty can be further reduced with experimental parameter fitting and iterative designs of toeholds and auxiliary species concentrations [29, 74]. For this system and this level of variability, it is possible to find unstable parameterisations through Monte Carlo search, including the asymmetrical parameterisation from Table 5.3.

Perturbing the unforced nonlinear dynamics for this case around its equilibrium ($\mathbf{x}^* > 0$, $\mathbf{r} = 0$), results in the unstable response of Figure 5.10. The system's response is consistent with the poles in Table 5.2 for the asymmetrical parameterisation, where the linearisation captures the increasing oscillations with a pair of conjugated poles in the right-half plane ($\alpha\{\mathbf{A}_s\} > 0$). Although the observed response has increased amplitudes consistent with the eigenvalues for the linearisation, the stability result is only local for a region around the equilibrium. It is undeter-

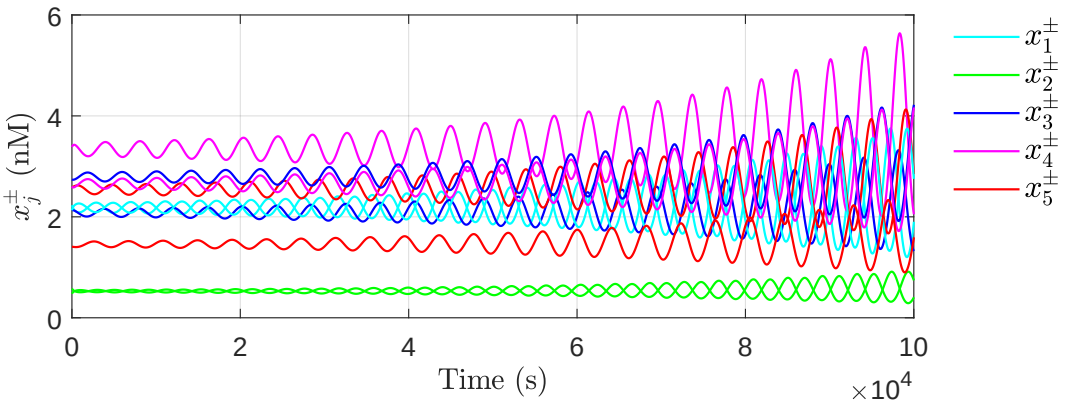

Figure 5.10: Unstable unforced trajectories of the concentrations $x_j^{\pm}$ for the MAK parameterised with the rates from Table 5.3 ($\mathbf{r} = 0$).

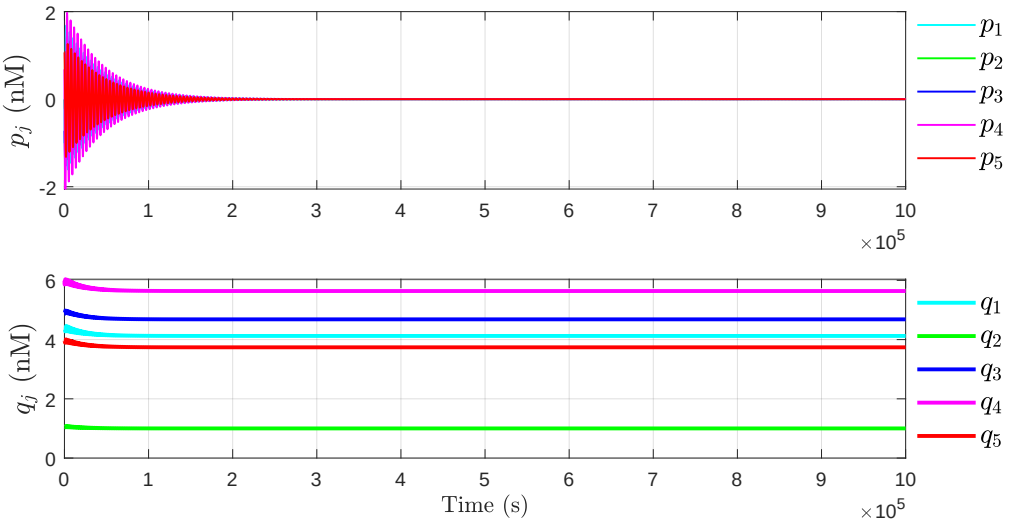

Figure 5.11: Simulation of the rotated dynamics of $\dot{\mathbf{p}}$ and $\dot{\mathbf{q}}$ with decoupled matrix $\mathbf{R}$ where $\mathbf{R}_{21} = \mathbf{R}_{12} = 0$, for the parameters in Table 5.3.

mined if the amplitudes increase in an unbounded manner or if the dynamics allow for limit cycles.

The CRN results in an unstable system despite the stability of the I/O linear system $\mathbf{R}_{11} \in \mathcal{H}$, which suggests, as discussed in Remark 5.11, that the source of the instability is the additional feedback in Figure 5.9 introduced by the asymmetry in the parameterisation. Indeed, integrating the rotated dynamics with a decoupled matrix $\mathbf{R}$, where we force $\mathbf{R}_{21} = \mathbf{R}_{12} = 0$, we obtain the response of Figure 5.11, where both $\mathbf{p}$ and $\mathbf{q}$ have bounded trajectories. This shows that the source of the instability of the complete nonlinear system is neither $\dot{\mathbf{p}}$ nor $\dot{\mathbf{q}}$ individually, and stability must be analysed for the complete interconnected dynamics.

5.4.2 Stability of the CRN representation for a cascaded system, under parametric variability

For the particular case of cascaded systems, as long as all species degrade at some non-zero rate, we can show that the CRN is stable, even if experimental variability results in an asymmetrical parameterisation.

Proposition 5.7. *Take the representation of a stable cascaded system* $\dot{\mathbf{p}} = \bar{\mathbf{R}}_{11}\mathbf{p}$*, with* $\bar{\mathbf{R}}_{11} \in \mathcal{L}, \mathcal{H}$*. For an asymmetrical parameterisation (without Assumption 2.1), if* $\mathbf{a}_1^{\pm} < 0$*, the unforced dynamics* $\dot{\mathbf{x}} = \mathbf{A}\mathbf{x} - \eta\mathbf{x} \circ (\mathbf{P}\mathbf{x})$*,* $\mathbf{x} \geq 0$*, are GAS for* $\mathbf{x} = 0$*.*

Proof. Given a cascaded linear system, we can permute the state $\mathbf{p}$ so that $\bar{\mathbf{R}}_{11} \in \mathcal{L}$, resulting also in $\bar{\mathbf{A}}_1, \bar{\mathbf{A}}_2 \in \mathcal{L}$. In the presence of variability, $\mathbf{A}_\mathbf{1}^{\pm}$ have the same structure as $\bar{\mathbf{A}}_1$ but with different parameterisations, still resulting in $\mathbf{A}_\mathbf{1}^{\pm} \in \mathcal{L}$. In the same way, $\mathbf{A}_2^{\pm} \in \mathcal{L}$.

Now take the permutation matrix $\mathbf{Q}$

$$\mathbf{Q} = \left[\begin{array}{cccc|cccc} 1 & 0 & \dots & 0 & 0 & 0 & \dots & 0 \\ 0 & 0 & \dots & 0 & 1 & 0 & \dots & 0 \\ \hline 0 & 1 & \dots & 0 & 0 & 0 & \dots & 0 \\ 0 & 0 & \dots & 0 & 0 & 1 & \dots & 0 \\ \hline \vdots & \vdots & \ddots & \vdots & \vdots & \vdots & \ddots & \vdots \\ \hline 0 & 0 & \dots & 1 & 0 & 0 & \dots & 0 \\ 0 & 0 & \dots & 0 & 0 & 0 & \dots & 1 \end{array}\right] \tag{5.56}$$

such that

$$\mathbf{z} = \mathbf{Q}\mathbf{x} = \mathbf{Q}\left[\begin{array}{c} \mathbf{x}^+ \\ \mathbf{x}^- \end{array}\right] = \left[\begin{array}{cc|cc|c|cc} x_1^+ & x_1^- & x_2^+ & x_2^- & \dots & x_N^+ & x_N^- \end{array}\right]^T \tag{5.57}$$

$$\mathbf{Q}\mathbf{P}\mathbf{x} = \mathbf{Q}\left[\begin{array}{c} \mathbf{x}^- \\ \mathbf{x}^+ \end{array}\right] = \left[\begin{array}{cc|cc|c|cc} x_1^- & x_1^+ & x_2^- & x_2^+ & \dots & x_N^- & x_N^+ \end{array}\right]^T . \tag{5.58}$$

The dynamics of the permuted state yield

$$\dot{\mathbf{z}} = \mathbf{L}\mathbf{z} + \eta\mathbf{z} \circ \mathbf{g}\left\{\mathbf{z}\right\}, \mathbf{z}(0) \geq 0 \tag{5.59}$$

where $\mathbf{z} > 0$, $\mathbf{g}\{\mathbf{z}\} = -\left[\begin{array}{cccccc} x_1^- & x_1^+ & x_2^- & x_2^+ & \dots & x_N^- & x_N^+ \end{array}\right]^T < 0$. Moreover, from the cascaded structure and ordering the states such that $\bar{\mathbf{R}}_{11} \in \mathcal{L}$, we have that $x_j^{\pm}$

Table 5.4: Assuming the I/O system is stable, we can state properties about the stability of the CRN representation and its respective unforced equilibria $\mathbf{x}^*$.

Parameterisation	Cascaded	With negative feedback
Nominal with $\bar{\mathbf{R}}_{11} \in \mathcal{H}$	$\mathbf{x}^* = 0$ Unforced dynamics are GAS	Possible $\mathbf{x}^* > 0$ Bounded unforced dynamics
Asymmetrical with $\mathbf{R}_{11} \in \mathcal{H}$	$\mathbf{x}^* = 0$ Unforced dynamics are GAS if additionally $\mathbf{a}_1^{\pm} < 0$	Possible $\mathbf{x}^* > 0$ CRN may be unstable

do not depend on $x_i^{\pm}$ for any $i > j$, resulting

$$\mathbf{L} = \begin{bmatrix} \mathbf{L}_{11} & \mathbf{0} \\ \mathbf{L}_{21} & \mathbf{L}_{22} \end{bmatrix} . \tag{5.60}$$

The structures of $\mathbf{L}_{jj}$ are determined by the structure of $\mathbf{A}_1^{\pm}$, and $\mathbf{L}_{21} \geq 0$ contains the cross terms which result in subtractions in the I/O dynamics (elements in $\mathbf{A}_2^{\pm}$). We have that $\mathbf{A_1}^{\pm}, \mathbf{A_2}^{\pm} \in \mathcal{L} \Rightarrow \mathbf{L} \in \mathcal{L}$. Moreover, $\mathbf{L} = \mathbf{L}^{\boxtimes} + \mathbf{D}\{\mathbf{l}\}$ where

$$\mathbf{l} = \mathbf{Q} \begin{bmatrix} \mathbf{a_1}^+ \\ \mathbf{a_1}^- \end{bmatrix} = \left[\begin{array}{cc|cc|c|cc} a_1^+ & a_1^- & a_2^+ & a_2^- & \dots & a_N^+ & a_N^- \end{array} \right]^T . \tag{5.61}$$

It thus results directly that $\rho\{\mathbf{L}\} = \rho\left\{\mathbf{A}_1^+\right\} \cup \rho\left\{\mathbf{A}_1^-\right\}$ and $\mathbf{a}_1^{\pm} < 0 \Leftrightarrow \mathbf{L} \in \mathcal{H}$.

If the represented cascaded linear dynamics are stable, then $\mathbf{L} \in \mathcal{H}$. Moreover, even with uncertainty, as long as the degradation rates remain strictly positive, we have $\mathbf{L} \in \mathcal{H}$, and we can invoke Lemma 5.3 to establish $\dot{\mathbf{z}} = \mathbf{L}\mathbf{z} + \eta\mathbf{z} \circ \mathbf{g}\{\mathbf{z}\}$ is GAS around $\mathbf{z} = 0$. Then the implication of GAS for $\dot{\mathbf{x}}$ at $\mathbf{x} = 0$ is straightforward. □

The implication of Proposition 5.7 is that in the presence of variability and mismatching rates, as long as all species degrade for some non-zero rate, the unforced dynamics of the cascaded system will have a single stable non-negative equilibrium, and without input the concentrations will converge to $\mathbf{x} = 0$. Table 5.4 summarises the derived properties, depending on the structure of the DSD network (cascaded *versus* with feedback).

Example 5.3 (Cascaded system with subtraction)**.** *Take the linear system with the transfer function*

$$Y(s) \;=\; \left(1 - \frac{1}{s+a}\right) U(s) \Leftrightarrow Y(s) = U(s) - X(s) \tag{5.62}$$

with $X(s) = \frac{1}{s+a}U(s)$*. Due to the presence of subtraction, we use a dual-rail repre-*

sentation of the system with the CRN

$$U^{\pm} \xrightarrow{1} U^{\pm} + X^{\pm}, \quad X^{\pm} \xrightarrow{a} \emptyset \tag{5.63a}$$

$$U^{\pm} \xrightarrow{c} U^{\pm} + Y^{\pm}, \quad X^{\pm} \xrightarrow{c} X^{\pm} + Y^{\mp},\ Y^{\pm} \xrightarrow{c} \emptyset \tag{5.63b}$$

$$X^{+} + X^{-} \xrightarrow{\eta} \emptyset, \quad Y^{+} + Y^{-} \xrightarrow{\eta} \emptyset\ . \tag{5.63c}$$

From the MAK

$$\dot{x}^{\pm} = -a^{\pm}x^{\pm} + c^{\pm}u^{\pm} - \eta x^{+}x^{-} \tag{5.64a}$$

$$\dot{y}^{\pm} = -c^{\pm}y^{\pm} + c^{\mp}x^{\mp} + c^{\pm}u^{\pm} - \eta y^{+}y^{-} \tag{5.64b}$$

$$x^{\pm}(0) = 0,\ y^{\pm}(0) = 0 \tag{5.64c}$$

and assuming the nominal parameterisation under Assumption 2.1 ($a^{+} = a^{-} = a$, $c^{+} = c^{-} = c$) and timescale separation ($c \gg a$), we recover the linear I/O system

$$\dot{x} = -ax + u, \quad x(0) = 0 \tag{5.65a}$$

$$y \approx -x + u\ . \tag{5.65b}$$

The representation is a cascaded system from $U^{\pm}$ to $Y^{\pm}$, which is reflected in the structure of the I/O dynamics and the reducibility of the CRN. Reordering the state vector $\mathbf{z} = \mathbf{Q}\mathbf{x} = [x^{+}, x^{-}, y^{+}, y^{-}]^{T}$ results in a lower diagonal state matrix where

$$\mathbf{Q} = \left[\begin{array}{cc|cc} 1 & 0 & 0 & 0 \\ 0 & 0 & 1 & 0 \\ \hline 0 & 1 & 0 & 0 \\ 0 & 0 & 0 & 1 \end{array}\right] \tag{5.66a}$$

$$\mathbf{L} = \left[\begin{array}{cc|cc} -a^{+} & 0 & 0 & 0 \\ 0 & -a^{-} & 0 & 0 \\ \hline 0 & c^{-} & -c^{+} & 0 \\ c^{+} & 0 & 0 & -c^{-} \end{array}\right] \in \mathcal{M}, \mathcal{L}\ . \tag{5.66b}$$

Then $\rho\{\mathbf{L}\} = \{-a^{+}, -a^{-}, -c^{+}, -c^{-}\}$, and $\mathbf{L} \in \mathcal{H}$ if and only if all degradation rates are positive. If $a^{\pm}, c^{\pm} > 0 \Rightarrow \mathbf{L} \in \mathcal{H}$ and Lemma 5.3 ensures that $\dot{\mathbf{z}} = \mathbf{L}\mathbf{z} + \eta\mathbf{z} \circ \mathbf{g}\{\mathbf{z}\}$ is GAS for its single non-negative equilibrium $\mathbf{z} = 0$.

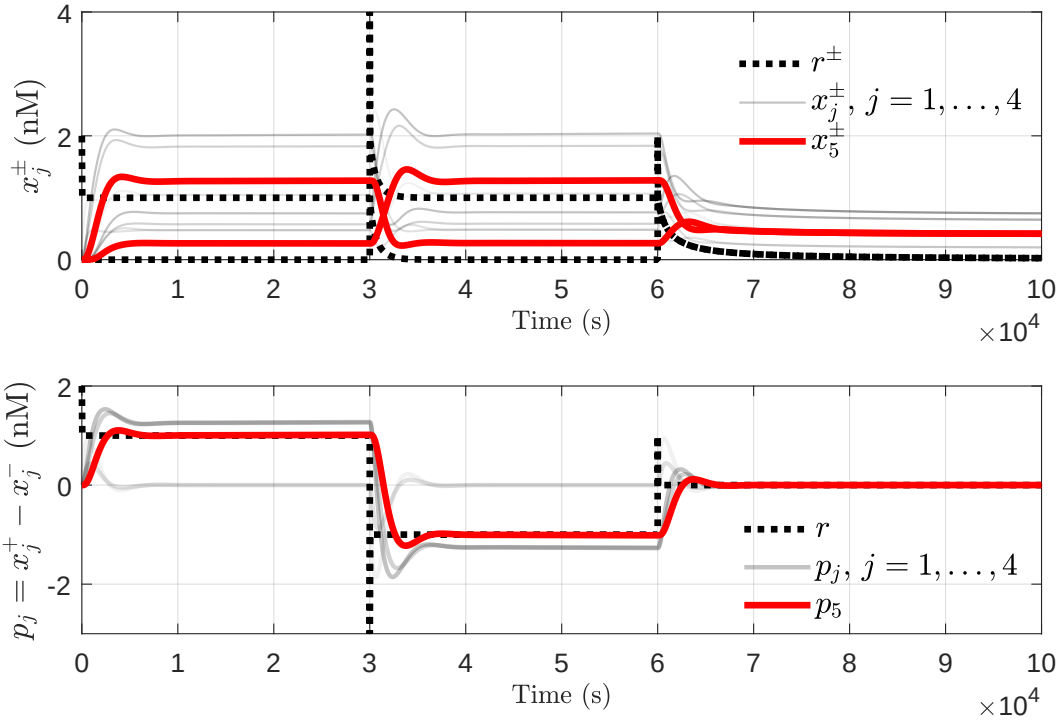

Figure 5.12: Simulation in Visual DSD of the DSD reactions for the symmetrical nominal system, with $\mathbf{x}(0) = 0$ nM and a sequence of steps for the input $\mathbf{r}$.

5.5 Stability of the controller implementation with DSD reactions

It remains to verify whether the stability properties predicted in Table 5.2 from analysing the system's CRNs are observed when the closed-loop system is implemented with nucleic acids. The DSD circuitry is verified in Visual DSD [80], a rapid prototyping tool for precise analysis of reactions with nucleic acids, via both deterministic and stochastic simulations.

For the control system of Example 5.1, each of the elementary reactions in (2.24) is translated to the DSD networks with the same architecture and considerations Section 3.5, and the hybridisation reactions are depicted in Figures 3.9, 3.10 and 3.11.

The auxiliary species are initialised at a large concentration C_{max}, to prevent their consumption from impacting the dynamics significantly (see Assumption 4.1 in Section 4.2.3). Considering the large C_{max} approximation and buffering cancellation discussed in [21, 79], the unimolecular reaction rates in Example 5.1 are translated

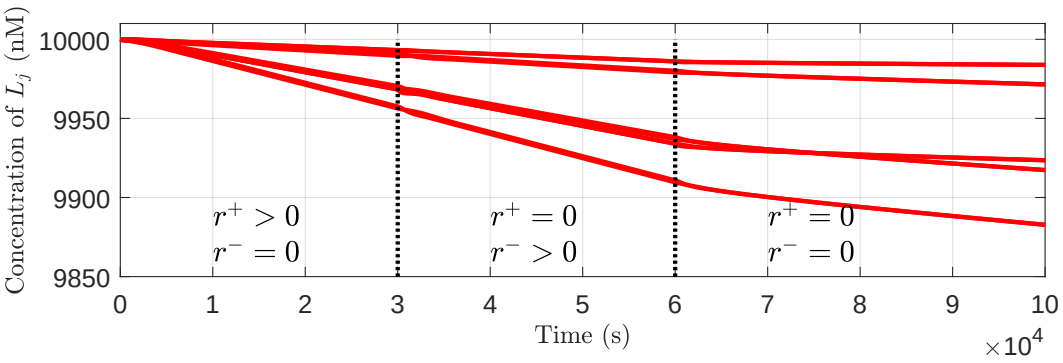

Figure 5.13: Concentrations of the auxiliary strands L_j used for the annihilation reactions (according to (5.68)) for the simulation in Figure 5.12. The positive equilibrium of the CRN results in persistent and irreversible consumption, even if the I/O dynamics are at rest for $t > 7 \times 10^4$ s.

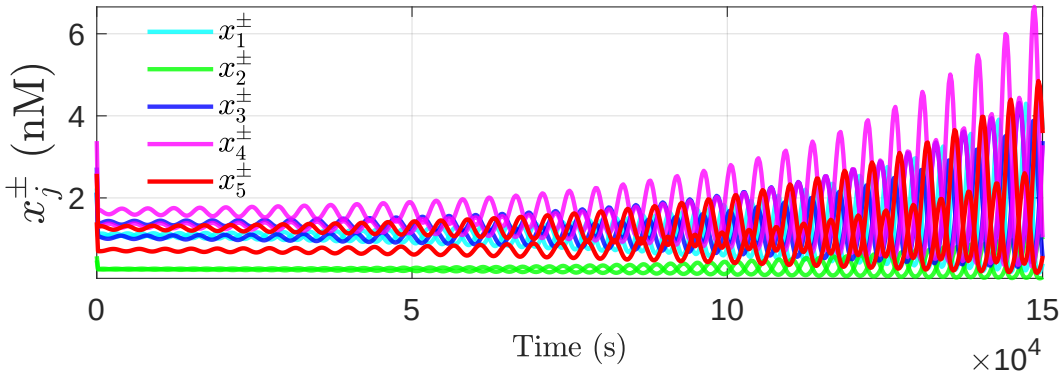

Figure 5.14: Simulation in Visual DSD of the DSD network, for the asymmetrical destabilising parameterisation, with $\mathbf{r} = 0$.

into toehold affinities with

$$q_{ki}^{\pm} = \frac{2k_i^{\pm}}{C_{max}}, i \in \{0, 1, 2\} \tag{5.67a}$$

$$q_{\gamma j}^{\pm} = \frac{2\gamma_j^{\pm}}{C_{max}}, j \in \{1, 2, 3, 4, 5, 6, 7, 8\} \ . \tag{5.67b}$$

We set $C_{max} = 10^4$ nM, and with $c_M = 2\eta$ we get the maximum hybridisation rate for full toehold binding of $k_s = 10^6 (\text{Ms})^{-1}$ [74].

With the nominal symmetrical parameterisation, we have in Figure 5.12 that $y = p_5$ tracks the step inputs of r, and that for $t > 6 \times 10^4$ s, when $r^{\pm} = 0$, the concentrations converge to an unforced positive equilibrium $x_j^{\pm}(t) > 0$.

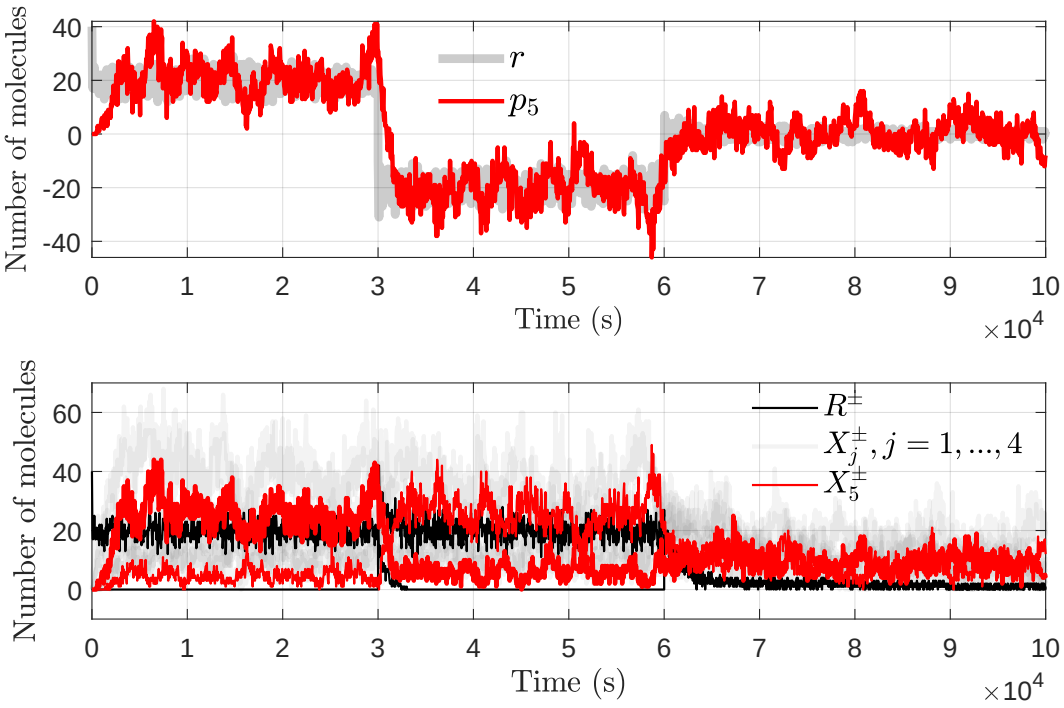

Figure 5.15: Stochastic simulations of the DSD network for the nominal parameterisation. With low number of molecules and inherent noise, the I/O dynamics still track the reference.

Recalling the network of DSD reactions to implement the annihilation reaction $X_i + X_j \xrightarrow{\emptyset}$, where

$$X_i + L_i \underset{k_s}{\overset{k_s}{\rightleftharpoons}} H_i + B_i \tag{5.68a}$$

$$X_j + H_i \xrightarrow{k_s} \emptyset \tag{5.68b}$$

$$X_j + L_j \underset{k_s}{\overset{k_s}{\rightleftharpoons}} H_j + B_j \tag{5.68c}$$

$$X_i + H_j \xrightarrow{k_s} \emptyset \tag{5.68d}$$

the impact of the positive equilibrium is seen in Figure 5.13, where the auxiliary strands L_j in (5.68) remain around $C_{max} = 10^4$ nM but are still depleted even if $r^{\pm} = p_j = 0$. With the destabilising parameterisation from Table 5.3, the time histories in Figure 5.14 show that the equivalent DSD reactions are also unstable around its equilibrium, emphasising the practical relevance of the stability results.

For a low copy number of molecules, we move away from the assumption of MAK used to represent ODEs with CRNs. More work is needed to generalise our results to a stochastic interpretation of the CRN programs, e.g. through analysis

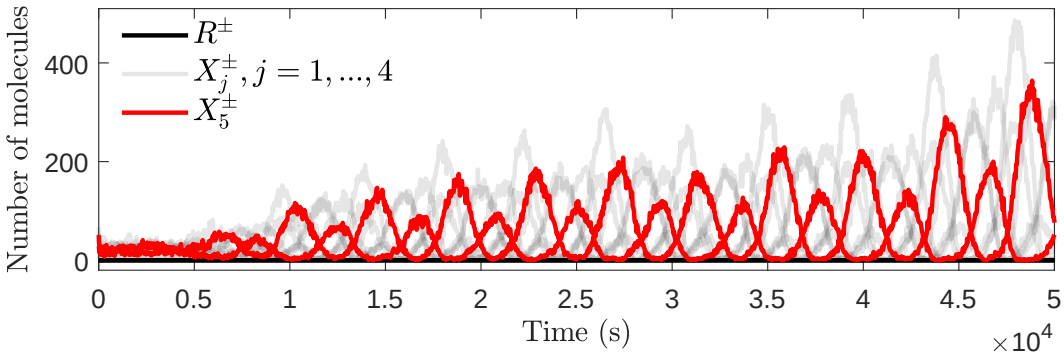

Figure 5.16: Stochastic simulations with the destabilising parameterisation result in divergent trajectories for the DSD network.

using the Linear Noise Approximation of the chemical master equation [114]. Here, we verify stochastically the results through simulation of the DSD network with Gillespie's algorithm [149] in Visual DSD, where we see in Figure 5.15 the reference tracking behaviour of the nominal system, and in Figure 5.16 the unstable departure from equilibrium with the asymmetrical parameterisation of Table 5.3.

5.6 Conclusions

Several recent works have applied the dual-rail representation of CRNs to obtain linear I/O models of synthetic feedback control systems, but have not explicitly considered the potential impact of the underlying nonlinear annihilation reactions in their analysis.

This chapter framed the dynamics of dual-rail representation as a new class of IPR which relies on internally nonlinear positive dynamics, and were analysed with results from positive systems theory. The dynamics of the CRNs involved in a typical linear controller design are decomposed to highlight the effects of the non-observable and nonlinear dynamics.

In particular, it is shown that under parametric variability (which is inevitable from experimental implementation), the stability of the represented linear model does not imply the stability of the underlying chemical network. Variability in the reaction rates breaks the symmetrical parameterisation assumed by the dual-rail representation, and introduces feedback between the linear I/O dynamics and the internal nonlinear dynamics of the IPR. The additional looped interconnection between the internal and the I/O dynamics can lead to unstable behaviour, and the stability of the dual-rail representation must be checked with the MAK of the CRN representation.

The presented example illustrates this phenomenon, where the I/O linear system does not capture the instability of the full nonlinear system. The results confirm that the stability of nucleic acid-based controllers must be analysed using the linearisation of the complete nonlinear system, and provide a rigorous theoretical approach for conducting such an analysis.

Chapter 6

Robustness analysis of a nucleic acid controller using the structured singular value

The available mapping between transfer functions, CRNs and DSD reactions enables the use of classical control theory in the *synthesis* of biomolecular control systems, [76, 79, 154]. However, the implementation using DSD reaction networks is limited by the experimental accuracy of the affinities in the biomolecular network [74], which leads to variability in the reaction rates and uncertainty in the parameterisation of the network. The previous chapter exemplified why such variability must be accounted in the *analysis* of the CRN implementation, and this chapter shows how a rigorous analysis of the robust stability properties of the CRN representation of linear negative feedback can be carried out using the SSV framework.

For stability analysis, the nonlinear dynamics are linearised around a fixed point, the equilibrium of the system, to represent the uncertain system with a LFT [99]. Since the equilibria can change with parametric variations, the dependency of the equilibrium on uncertainty is included in the LFT, to capture the *movement of the equilibrium* [165]. In our case, we do not have an analytical solution for this dependency, and the equilibrium variation is approximated by a function which can be represented as an LFT.

The SSV framework (or μ-analysis) [82, 98] can then be applied to the LFT representation of the uncertain system, to provide quantifiable margins. For example, the work in [166] applies the SSV with the LFT description to assess how far the system is from bifurcation, and to compute boundaries for the eigenvalues of

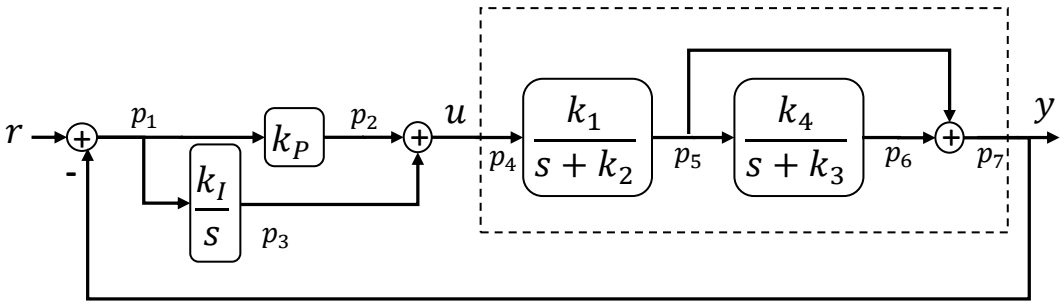

Figure 6.1: Closed loop system with a second order plant, for reference tracking with a PI controller.

the uncertain system. In this chapter, we use the SSV to obtain a stability margin, which tells us how much the uncertain parameters can vary before losing closed-loop stability, and it allows us to identify the smallest level of uncertainty (and corresponding parameterisation) which destabilises the controller. Our approach is similar to [167], where the nonlinear dynamics in the presence of real parametric uncertainties are analysed locally, and a stability margin is defined and numerically computed for the linearisation around an equilibrium of the system. The value of developing a rigorous theoretical framework for this analysis is demonstrated by the failure of a standard Monte Carlo simulation campaign to find the worst-case uncertainty combination for a particular example.

Finally, we discuss the applicability of our results to implementations using DSD reactions. CRN-based representations of feedback systems can be unfeasible when mapped into DNA chemistry, since large species concentrations deplete auxiliary DNA fuel species, and even assuming as in [62] that these are replenished, there are physical limits on the rates and concentrations that are achievable. This is addressed in [21] by scaling the magnitude of the concentrations and the response time of the network to ensure a feasible DNA implementation. We show here that the robustness results for a CRN representation also hold when such scaling is applied for implementation with nucleic acid-based chemistry.

6.1 Chemical representation of linear negative feedback

In this section, we build the chemical network used to represent the plant, controller and linear negative feedback in Figure 6.1. We have a reference tracking control problem with reference input r and output y, and PI control actuation u. We need to represent negative and positive control errors p_1, although the concentrations of species are limited to non-negative values. We resort once again to the *dual-*

rail representation from Definition 2.16 to express the Single Input Single Output (SISO) transfer function as the I/O dynamics of a dual-rail CRN. Each signal is split into two contributions $p_j = x_j^+ - x_j^-$, where x_j^+ and x_j^- are chemical species concentrations. The MAK and dynamics for $x_j^\pm$ as then used to define an I/O linear system $G(s)$ such that for Figure 6.1 we have

$$\left(y^+ - y^-\right) = G(s)\left(r^+ - r^-\right) \ . \tag{6.1}$$

6.1.1 Representing the linear plant

Take the plant as the second order system with a zero, decomposed into first order systems according to Figure 6.1, where

$$Y(s) = \frac{k_1}{s+k_2}\left(1 + \frac{k_4}{s+k_3}\right)U(s) = \frac{k_1}{s+k_2}\left(\frac{s+k_4+k_3}{s+k_3}\right)U(s) \tag{6.2}$$

and we define the two states of the plant such that $y = p_5 + p_6$ and

$$\dot{p}_5 = -k_2 p_5 + k_1 p_4 \quad \Rightarrow \quad P_5(s) = \frac{k_1}{s+k_2}P_4(s) \tag{6.3}$$

$$\dot{p}_6 = -k_3 p_6 + k_4 p_5 \quad \Rightarrow \quad P_6(s) = \frac{k_4}{s+k_3}P_5(s) \ . \tag{6.4}$$

For the plant, we define the dual sets of elementary reactions as

$$x_4^\pm \xrightarrow{k_1} x_4^\pm + x_5^\pm \quad , \quad x_5^\pm \xrightarrow{k_2} \emptyset \tag{6.5a}$$

$$x_5^\pm \xrightarrow{k_4} x_5^\pm + x_6^\pm \quad , \quad x_6^\pm \xrightarrow{k_3} \emptyset \tag{6.5b}$$

$$x_5^\pm \xrightarrow{\gamma} x_5^\pm + x_7^\pm \quad , \quad x_6^\pm \xrightarrow{\gamma} x_6^\pm + x_7^\pm, \quad x_7^\pm \xrightarrow{\gamma} \emptyset \tag{6.5c}$$

$$x_5^+ + x_5^- \xrightarrow{\eta} \emptyset \quad , \quad x_6^+ + x_6^- \xrightarrow{\eta} \emptyset, \quad x_7^+ + x_7^- \xrightarrow{\eta} \emptyset \ . \tag{6.5d}$$

The parameters γ and η are the rates for the auxiliary reactions of catalysis, degradation, and annihilation as defined in Section 2.3.1. Assuming timescale separation (as in the analysis of $\gamma \to \infty$ in [79]), the species p_7 is considered to be at quasi-steady state [109] and

$$\gamma^{-1}\dot{p}_7 = p_5 + p_6 - p_7 \approx 0 \Rightarrow p_7 \approx p_5 + p_6 \tag{6.6}$$

setting $P_7(s)$ as the sum of the previous transfer functions with

$$P_7(s) \ = P_5(s) + P_6(s) = \left(1 + \tfrac{k_4}{s+k_3}\right)P_5(s) = \tfrac{s+k_4+k_3}{s+k_3}\tfrac{k_1}{s+k_2}P_4(s) \ . \tag{6.7}$$

From the CRN in (6.5) we recover the SISO transfer function where the zero depends on the reaction rates k_3 and k_4, and the poles result from the two degradation reaction rates k_2 and k_3.

6.1.2 Dual-rail representation of linear negative feedback

The remaining linear operations in the feedback loop can be found in literature (see e.g., [76, 79]) and previous chapters. For the integration $\dot{p}_3 = k_I p_1$ we have

$$x_1^{\pm} \xrightarrow{k_I} x_1^{\pm} + x_3^{\pm} \quad , \quad x_3^{+} + x_3^{-} \xrightarrow{\eta} \emptyset \; . \tag{6.8}$$

The algebraic operations are represented by dual-rail CRNs, assuming quasi steady state of the output signals. The signal $p_1^* = r^* - y^* = r^* - p_7^*$ for the two-sided subtraction is computed with

$$r^{\pm} \xrightarrow{\gamma} r^{\pm} + x_1^{\pm} \quad , \quad x_7^{\pm} \xrightarrow{\gamma} x_7^{\pm} + x_1^{\mp} \tag{6.9a}$$

$$x_1^{\pm} \xrightarrow{\gamma} \emptyset \quad , \quad x_1^{+} + x_1^{-} \xrightarrow{\eta} \emptyset \; . \tag{6.9b}$$

The CRN for the gain $p_2^* = k_P p_1^*$ is

$$x_1^{\pm} \xrightarrow{\gamma k_P} x_1^{\pm} + x_2^{\pm},\; x_2^{\pm} \xrightarrow{\gamma} \emptyset,\; x_2^{+} + x_2^{-} \xrightarrow{\eta} \emptyset \tag{6.10}$$

and finally the summation $p_4^* = p_2^* + p_3^*$ is set with

$$x_2^{\pm} \xrightarrow{\gamma} x_2^{\pm} + x_4^{\pm} \quad , \quad x_3^{\pm} \xrightarrow{\gamma} x_3^{\pm} + x_4^{\pm} \tag{6.11a}$$

$$x_4^{\pm} \xrightarrow{\gamma} \emptyset \quad , \quad x_4^{+} + x_4^{-} \xrightarrow{\eta} \emptyset \; . \tag{6.11b}$$

Using the law of mass action in (2.16), the complete set of ODEs is given by

$$\dot{x}_1^{\pm} = -\gamma x_1^{\pm} + \gamma x_7^{\mp} + \gamma r^{\pm} - \eta x_1^{+} x_1^{-} \tag{6.12a}$$

$$\dot{x}_2^{\pm} = \gamma k_P x_1^{\pm} - \gamma x_2^{\pm} - \eta x_2^{+} x_2^{-} \tag{6.12b}$$

$$\dot{x}_3^{\pm} = k_I x_1^{\pm} - \eta x_3^{+} x_3^{-} \tag{6.12c}$$

$$\dot{x}_4^{\pm} = \gamma x_2^{\pm} + \gamma x_3^{\pm} - \gamma x_4^{\pm} - \eta x_4^{+} x_4^{-} \tag{6.12d}$$

$$\dot{x}_5^{\pm} = k_1 x_4^{\pm} - k_2 x_5^{\pm} - \eta x_5^{+} x_5^{-} \tag{6.12e}$$

$$\dot{x}_6^{\pm} = k_4 x_5^{\pm} - k_3 x_6^{\pm} - \eta x_6^{+} x_6^{-} \tag{6.12f}$$

$$\dot{x}_7^{\pm} = \gamma x_5^{\pm} + \gamma x_6^{\pm} - \gamma x_7^{\pm} - \eta x_7^{+} x_7^{-} \tag{6.12g}$$

$$x_i^{\pm}(0) = 0, \quad i = 1, \ldots, 7 \; . \tag{6.12h}$$

Finally, applying the transformation from Definition 5.2 where $p_j = x_j^+ - x_j^-$ and $r = r^+ - r^-$, we get the I/O linear dynamics $\dot{p}_j = \dot{x}_j^+ - \dot{x}_j^-$

$$\dot{\mathbf{p}} = \mathbf{A}_p\mathbf{p} + \mathbf{B}_p r, \quad \mathbf{p}(0) = 0 \tag{6.13}$$

with $\mathbf{p} = \begin{bmatrix} p_1 & \dots & p_7 \end{bmatrix}^T \in \mathbb{R}^{7\times 1}$, $r \in \mathbb{R}$, and

$$\mathbf{A}_p = \begin{bmatrix} -\gamma & 0 & 0 & 0 & 0 & 0 & -\gamma \\ \gamma k_P & -\gamma & 0 & 0 & 0 & 0 & 0 \\ k_I & 0 & 0 & 0 & 0 & 0 & 0 \\ 0 & \gamma & \gamma & -\gamma & 0 & 0 & 0 \\ 0 & 0 & 0 & k_1 & -k_2 & 0 & 0 \\ 0 & 0 & 0 & 0 & k_4 & -k_3 & 0 \\ 0 & 0 & 0 & 0 & \gamma & \gamma & -\gamma \end{bmatrix}, \; \mathbf{B}_p = \begin{bmatrix} \gamma \\ 0_{6\times 1} \end{bmatrix} . \tag{6.14}$$

The rate of the catalysis reaction from the output into the error species in (6.9a) (in the representation of the subtraction), ends up as an element of $\mathbf{A}_2$, resulting in the off-diagonal element $-\gamma$ of $\mathbf{A}_p$.

The linear state space (6.13) represents the I/O linear response from r to the outputs p_j, and it contains additional dynamics besides the controller and the plant, introduced by the CRN representations of the algebraic operations. However, the approximation to the feedback loop transfer function improves with the assumption of timescale separation of the dynamics for the linear operators. Expressing the dynamics of the auxiliary dynamics as a singular perturbation model [109], we have

$$\gamma^{-1}\dot{p}_1 = -p_1 + r - p_7 \tag{6.15a}$$
$$\gamma^{-1}\dot{p}_2 = -p_2 + k_P p_1 \tag{6.15b}$$
$$\gamma^{-1}\dot{p}_4 = -p_4 + p_2 + p_3 \tag{6.15c}$$
$$\gamma^{-1}\dot{p}_7 = -p_7 + p_5 + p_6 \; . \tag{6.15d}$$

If the auxiliary reaction rates $\gamma \to \infty$, we get $\lim_{\gamma\to\infty} \frac{1}{\gamma}\dot{p}_j = 0$, $(j = 1, 2, 4, 7)$, and

with the QSS approximation we recover the algebraic relations

$$p_1 \approx r - p_7 \tag{6.16a}$$
$$p_2 \approx k_P p_1 \tag{6.16b}$$
$$p_4 \approx p_2 + p_3 \tag{6.16c}$$
$$p_7 \approx p_5 + p_6 \ . \tag{6.16d}$$

The remaining dynamics correspond to the transfer functions in Figure 6.1, where

$$\dot{p_3} = k_I p_1 \tag{6.17a}$$
$$\dot{p_5} = k_1 p_4 - k_2 p_5 \tag{6.17b}$$
$$\dot{p_6} = k_4 p_5 - k_3 p_6 \tag{6.17c}$$
$$p_3(0) = 0,\ p_5(0) = 0,\ p_6(0) = 0 \ . \tag{6.17d}$$

6.2 Nonlinear model of the CRN

The linear system in (6.13) represents only the dynamics between the input signal r and the signals p_j, and the contribution from the nonlinear terms are removed when we compute $\dot{p}_j = \dot{x}_j^+ - \dot{x}_j^-$. Hence, as seen in Chapter 5, the impact of the annihilation reactions in the dynamics is not observable in the I/O linear system.

To analyse the complete dynamics of the concentrations in the CRN, we define instead define the input vector $\mathbf{r} = [r^+ \, r^-]^T$ and recall the order of the state vector $\mathbf{x} \geq 0$ from Definition 5.1, such that

$$\mathbf{x} = \left[\begin{array}{ccc|ccc} x_1^+ & \dots & x_N^+ & x_1^- & \dots & x_N^- \end{array} \right]^T = \left[\begin{array}{c} \mathbf{x}^+ \\ \hline \mathbf{x}^- \end{array} \right] \ . \tag{6.18}$$

We can use the Hadamard element-wise product $\circ$ and the permutation matrix

$$\mathbf{P} = \begin{bmatrix} 0 & \mathbf{I} \\ \mathbf{I} & 0 \end{bmatrix} \tag{6.19}$$

to express the bimolecular terms, and compact the ODEs into the form of Definition 5.1, resulting in:

$$\dot{\mathbf{x}} = \mathbf{A}\mathbf{x} + \mathbf{B}\mathbf{r} - \eta\,(\mathbf{P}\mathbf{x}) \circ \mathbf{x}, \quad \textit{given } \mathbf{x}(0) \geq 0 \ . \tag{6.20}$$

In its natural coordinates $x_j^\pm$ the dynamics result in a positive system [122], and

contain nonlinearities. Furthermore, the I/O dynamics assume that the representation of the signals p_j depends either on x_j^+ or x_j^- at each instant, as a result of very fast annihilation reactions $x_j^+ + x_j^- \xrightarrow{\eta} \emptyset$. However, as pointed out in Section 5.2, the system can have a positive equilibrium in which both dual species x_j^+ and x_j^- coexist. Moreover, the designed dynamics (6.17) also assume that $k_j^+ = k_j^-$ and $\gamma_j^+ = \gamma_j^-$ (the Assumption 2.1).

Let us instead move away from Definition 5.3 and a symmetrical parameterisation, and take the nonlinear model (6.20) considering possible mismatches between the dual rates and consider independent rates for each reaction. Decomposing the dynamics matrix $\mathbf{A}$ according to

$$\mathbf{A} = \begin{bmatrix} \mathbf{A}_1^+ & \mathbf{A}_2^- \\ \mathbf{A}_2^+ & \mathbf{A}_1^- \end{bmatrix}, \ \mathbf{B} = \begin{bmatrix} \mathbf{B}_1^+ & 0 \\ 0 & \mathbf{B}_1^- \end{bmatrix} \tag{6.21}$$

we get the sub-matrices

$$\mathbf{A}_1^{\pm} = \begin{bmatrix} -\gamma_3^{\pm} & 0 & 0 & 0 & 0 & 0 & 0 \\ (\gamma_4 k_P)^{\pm} & -\gamma_5^{\pm} & 0 & 0 & 0 & 0 & 0 \\ k_I^{\pm} & 0 & 0 & 0 & 0 & 0 & 0 \\ 0 & \gamma_6^{\pm} & \gamma_7^{\pm} & -\gamma_8^{\pm} & 0 & 0 & 0 \\ 0 & 0 & 0 & k_1^{\pm} & -k_2^{\pm} & 0 & 0 \\ 0 & 0 & 0 & 0 & k_4^{\pm} & -k_3^{\pm} & 0 \\ 0 & 0 & 0 & 0 & \gamma_9^{\pm} & \gamma_{10}^{\pm} & -\gamma_{11}^{\pm} \end{bmatrix} \tag{6.22a}$$

$$\mathbf{A}_2^{\pm} = \begin{bmatrix} 0_{1\times 6} & \gamma_2^{\pm} \\ 0_{6\times 6} & 0_{6\times 1} \end{bmatrix} \tag{6.22b}$$

$$\mathbf{B}_1^{\pm} = \begin{bmatrix} \gamma_1^{\pm} \\ 0_{6\times 1} \end{bmatrix}. \tag{6.22c}$$

6.2.1 I/O system and nominal nonlinear dynamics

The connections between the I/O linear system and the nonlinear dynamics can be seen more clearly with the change of coordinates from Definition 5.2 where

$$\begin{bmatrix} \mathbf{p} \\ \mathbf{q} \end{bmatrix} = \left[\begin{array}{c} \mathbf{W}_p \\ \hdashline \mathbf{W}_q \end{array}\right] \mathbf{x} = \left[\begin{array}{cc} \mathbf{I} & -\mathbf{I} \\ \hdashline \mathbf{I} & \mathbf{I} \end{array}\right] \mathbf{x} = \mathbf{W}\mathbf{x} \tag{6.23}$$

and $\mathbf{p} = \mathbf{x}^+ - \mathbf{x}^-$ and $\mathbf{q} = \mathbf{x}^+ + \mathbf{x}^-$. The coordinates $\mathbf{p}$ correspond to the states of the I/O dynamics, and the change of coordinates reveals the underlying dynamics $\dot{\mathbf{q}}$, which are not observed in (6.13).

The dynamics in these *rotated coordinates* are given in Proposition 5.1 by

$$\begin{bmatrix} \dot{\mathbf{p}} \\ \dot{\mathbf{q}} \end{bmatrix} = \begin{bmatrix} \mathbf{R}_{11} & \mathbf{R}_{12} \\ \mathbf{R}_{21} & \mathbf{R}_{22} \end{bmatrix} \begin{bmatrix} \mathbf{p} \\ \mathbf{q} \end{bmatrix} + \begin{bmatrix} \mathbf{W}_p \\ \mathbf{W}_q \end{bmatrix} \mathbf{B}\mathbf{r} - \frac{\eta}{2} \begin{bmatrix} \mathbf{0} \\ \mathbf{q} \circ \mathbf{q} - \mathbf{p} \circ \mathbf{p} \end{bmatrix} \tag{6.24a}$$

$$\textit{given } \mathbf{x}^{\pm}(0) \geq 0 \Rightarrow \mathbf{p}(0) = \mathbf{x}^{+}(0) - \mathbf{x}^{-}(0),\ \mathbf{q}(0) = \mathbf{x}^{+}(0) + \mathbf{x}^{-}(0)\ . \tag{6.24b}$$

Recall from (5.24) that

$$\mathbf{R}_{11} = \tfrac{1}{2}\left(\mathbf{A}_1^{+} + \mathbf{A}_1^{-}\right) - \tfrac{1}{2}\left(\mathbf{A}_2^{+} + \mathbf{A}_2^{-}\right) \tag{6.25a}$$

$$\mathbf{R}_{22} = \tfrac{1}{2}\left(\mathbf{A}_1^{+} + \mathbf{A}_1^{-}\right) + \tfrac{1}{2}\left(\mathbf{A}_2^{+} + \mathbf{A}_2^{-}\right) \tag{6.25b}$$

$$\mathbf{R}_{12} = \tfrac{1}{2}\left(\mathbf{A}_1^{+} - \mathbf{A}_1^{-}\right) - \tfrac{1}{2}\left(\mathbf{A}_2^{+} - \mathbf{A}_2^{-}\right) \tag{6.25c}$$

$$\mathbf{R}_{21} = \tfrac{1}{2}\left(\mathbf{A}_1^{+} - \mathbf{A}_1^{-}\right) + \tfrac{1}{2}\left(\mathbf{A}_2^{+} - \mathbf{A}_2^{-}\right)\ . \tag{6.25d}$$

Let us first consider the nominal case from Definition 5.3, when $\mathbf{A}_j^{+} = \mathbf{A}_j^{-} = \bar{\mathbf{A}}_j$ and $\mathbf{B}_1^{+} = \mathbf{B}_1^{-} = \bar{\mathbf{B}}_1$. In this case we recover the linear system (6.13) with $\mathbf{A}_p = \bar{\mathbf{R}}_{11} = \frac{1}{2}\mathbf{W}_p\bar{\mathbf{A}}\mathbf{W}_p^T$ and $\mathbf{B}_p r = \mathbf{W}_p\bar{\mathbf{B}}\mathbf{r}$. We have also that $\bar{\mathbf{R}}_{12} = \bar{\mathbf{R}}_{21} = 0$, the I/O dynamics are independent of $\mathbf{q}$ (Proposition 5.2), and the nominal nonlinear dynamics result as:

$$\dot{\mathbf{q}} = \bar{\mathbf{R}}_{22}\mathbf{q} + \bar{\mathbf{B}}_1\left(r^{+} + r^{-}\right) + \frac{\eta}{2}\left(\mathbf{p} \circ \mathbf{p} - \mathbf{q} \circ \mathbf{q}\right), \quad \textit{given } \mathbf{q}(0) \geq 0\ . \tag{6.26}$$

Since $\mathbf{x} \geq 0$, $\mathbf{r} \geq 0$, $\bar{\mathbf{B}} \geq 0$, and $\bar{\mathbf{A}}$ is Metzler, Lemma 5.1 tells us the system is non-negative in the natural coordinates. Moreover, since $\bar{\mathbf{A}} \in \mathcal{M}$ then $\bar{\mathbf{A}}_1$, $\bar{\mathbf{A}}_2$ and $\bar{\mathbf{R}}_{22} = \bar{\mathbf{A}}_1 + \bar{\mathbf{A}}_2$ are also Metzler. The same lemma shows that (6.26) is non-negative.

Using Lemma 5.5 we show that the trajectories of (6.26) are bounded. Considering the Lyapunov function $V = \sum q_j$ ($\forall_{\mathbf{q}>0} : V > 0$), the lemma shows that given the input vector $\mathbf{v} = \bar{\mathbf{B}}_1\left(r^{+} + r^{-}\right) + \frac{\eta}{2}\left(\mathbf{p} \circ \mathbf{p}\right) > 0$, the trajectories converge for a domain where

$$\|\mathbf{q}\|_2 < \frac{2}{\eta}\sqrt{N}\|\bar{\mathbf{R}}_{22}\|_2 + \frac{2}{\eta}\frac{\|\mathbf{v}\|_1}{\|\mathbf{q}\|_2}\ . \tag{6.27}$$

For the unforced response, $\mathbf{v} = 0$, the bound simplifies to $\|\mathbf{q}\|_2 < \frac{2}{\eta}\sqrt{N}\|\mathbf{R}_{22}\|_2$.

As discussed in Proposition 5.5, the trajectories $\mathbf{q}$ are bounded for bounded inputs $\mathbf{r}$ and $\mathbf{p}$, and can be limited by increasing the reaction rate η. Hence, with the nominal parameterisation the unobserved nonlinear dynamics do not pose a problem for the CRN representation of the I/O linear dynamics.

However, in general, the parameterisation of the CRN will be affected by variability in the reaction rates, causing mismatches between the sub-matrices of $\mathbf{A}$

and $\mathbf{B}$. The crossed terms become $\mathbf{R}_{12} \neq 0$, $\mathbf{R}_{21} \neq 0$, and create a feedback loop between the linear and nonlinear dynamics (see Remark 5.11). The discussion and demonstration in Section 5.4 with a destabilising parameterisation motivates the inclusion of the nonlinear dynamics in the stability analysis, since a stable $\mathbf{R}_{11}$ does not guarantee the stability of the coupled nonlinear dynamics in (6.24).

6.2.2 Linearisation and local stability

Both Lyapunov's indirect method and robustness stability analysis provide a local result around the trim point (or equilibrium point) where the system is in a steady state.

Definition 6.1. *Define the positive vector*

$$\mathbf{x}^0 \quad = \quad \begin{bmatrix} \mathbf{x}^{0+} \\ \mathbf{x}^{0-} \end{bmatrix} \tag{6.28}$$

as the unforced equilibrium of the nonlinear dynamics (6.20). Then, for a null trim input $\mathbf{r}^0 = 0$, we have the equilibrium condition for $\dot{\mathbf{x}} = 0$ as

$$\mathbf{A}\mathbf{x}^0 - \eta \mathbf{P}\mathbf{x}^0 \circ \mathbf{x}^0 = 0 \Leftrightarrow \mathbf{A}\mathbf{x}^0 = \eta \mathbf{P}\mathbf{x}^0 \circ \mathbf{x}^0 \ . \tag{6.29}$$

For a steady state perturbation input $\mathbf{r}_e$ around the unforced response $\mathbf{r} = \mathbf{r}^0 + \mathbf{r}_e = \mathbf{r}_e$, the perturbation trajectories around the equilibrium $\mathbf{x}^0$ are defined as $\mathbf{x}_e = \mathbf{x} - \mathbf{x}^0$. From Proposition 5.6 we also have that the linearised dynamics around $\mathbf{x}^0$, $\mathbf{r}^0 = 0$ are given by

$$\dot{\mathbf{s}} = \left(\mathbf{A} + \eta \mathbf{J}\left\{\mathbf{x}^0\right\}\right)\mathbf{s} + \mathbf{B}\mathbf{r}_e, \quad \mathbf{s}(0) = 0 \tag{6.30}$$

and even if $\mathbf{A} \notin \mathcal{H}$, the linearisation can still be stable if $\mathbf{x}^0 > 0$ exists, resulting in

$$\mathbf{J}\left\{\mathbf{x}^0\right\} = -\begin{bmatrix} \mathbf{D}\left\{\mathbf{x}^{0-}\right\} & \mathbf{D}\left\{\mathbf{x}^{0+}\right\} \\ \mathbf{D}\left\{\mathbf{x}^{0-}\right\} & \mathbf{D}\left\{\mathbf{x}^{0+}\right\} \end{bmatrix} \leq 0 \ . \tag{6.31}$$

Remark 6.1. *We do not have a closed form solution for the equilibrium. However, it is noteworthy that, from* (6.29)*, we have at equilibrium*

$$\begin{cases} \mathbf{A}_1^+\mathbf{x}^{0+} + \mathbf{A}_2^-\mathbf{x}^{0-} - \eta \mathbf{x}^{0+} \circ \mathbf{x}^{0-} = 0 \\ \mathbf{A}_2^+\mathbf{x}^{0+} + \mathbf{A}_1^-\mathbf{x}^{0-} - \eta \mathbf{x}^{0+} \circ \mathbf{x}^{0-} = 0 \end{cases} \tag{6.32a}$$

$$\Rightarrow \quad \mathbf{A}_1^+\mathbf{x}^{0+} + \mathbf{A}_2^-\mathbf{x}^{0-} - \left(\mathbf{A}_2^+\mathbf{x}^{0+} + \mathbf{A}_1^-\mathbf{x}^{0-}\right) = 0 \tag{6.32b}$$

$$\Rightarrow \quad \left(\mathbf{A}_1^- - \mathbf{A}_2^-\right)\mathbf{x}^{0-} = \left(\mathbf{A}_1^+ - \mathbf{A}_2^+\right)\mathbf{x}^{0+} \tag{6.32c}$$

and half of the equilibrium vector is constrained by

$$\mathbf{x}^{0-} = \left(\mathbf{A}_1^- - \mathbf{A}_2^-\right)^{-1}\left(\mathbf{A}_1^+ - \mathbf{A}_2^+\right)\mathbf{x}^{0+} \ . \tag{6.33}$$

6.2.3 Solving for the positive equilibrium

The linearisation relies on the solution to the equilibrium condition (6.29) subject to the constraint (6.33) for which we do not have a closed-form expression. Using (6.33) to replace $\mathbf{x}^{0-}$ in (6.29) and applying numerical solvers for $\mathbf{x}^{0+}$ proved unreliable and very dependent on the initial guess. Fortunately, in this case, it is straightforward to integrate (6.20) with $\mathbf{r} = 0$ and $\mathbf{x}(0) > 0$, as long as the equilibrium is stable.

For stability analysis we need to compute at least the equilibrium for the nominal parameterisation.

Definition 6.2. *The* nominal *equilibrium* $\bar{\mathbf{x}}^0$ *is the solution to*

$$\bar{\mathbf{A}}\bar{\mathbf{x}}^0 - \eta\mathbf{P}\bar{\mathbf{x}}^0 \circ \bar{\mathbf{x}}^0 = 0 \tag{6.34}$$

where $\bar{\mathbf{A}}$ *is the* nominal *matrix, without uncertainty or mismatch between the reaction rates, such that* $\mathbf{A}_1^+ = \mathbf{A}_1^- = \bar{\mathbf{A}}_1$, $\mathbf{A}_2^+ = \mathbf{A}_2^- = \bar{\mathbf{A}}_2$, *and* $\mathbf{B}_1^+ = \mathbf{B}_1^- = \bar{\mathbf{B}}_1$.

In the nominal case, we only need to ensure that by design the nominal I/O dynamics are stable (see Assumption 5.1 and details in Section 5.3.1), and we can then find $\bar{\mathbf{x}}^0$ by integrating the nominal dynamics with $\mathbf{r} = 0$ and $\mathbf{x}(0) > 0$.

Since we wish to verify the robustness results by checking the local stability with Lyapunov's indirect method, we may need to linearise the dynamics around unstable equilibria, which cannot be found by integrating the dynamics (6.20). We are able to circumvent this difficulty by defining new dynamics based on rotated coordinates.

Definition 6.3. *Take the reduced model with unforced dynamics given by*

$$\dot{\mathbf{c}} = \left(\mathbf{R}_{22} - \mathbf{R}_{21}\mathbf{R}_{11}^{-1}\mathbf{R}_{12}\right)\mathbf{c} + \frac{\eta}{2}\left(\mathbf{R}_{11}^{-1}\mathbf{R}_{12}\mathbf{c}\right) \circ \left(\mathbf{R}_{11}^{-1}\mathbf{R}_{12}\mathbf{c}\right) - \frac{\eta}{2}\mathbf{c} \circ \mathbf{c} \tag{6.35a}$$

$$\mathbf{c}(0) = 2\bar{\mathbf{x}}^{0+} \ . \tag{6.35b}$$

This system is built from (6.24)*, where the feedback interconnection with the I/O dynamics is replaced with the static gain matrix* $-\mathbf{R}_{11}^{-1}\mathbf{R}_{12}$*, coming from the equilibrium solution* $\mathbf{p}^0$ *as a function of* $\mathbf{q}$ *with* $\mathbf{p}^0 = -\mathbf{R}_{11}^{-1}\mathbf{R}_{12}\mathbf{q}^0$*. Forcing* $\mathbf{p} = \mathbf{p}^0$ *and*

$\dot{\mathbf{p}} = 0$ *in* (6.24)*, and defining a new state variable* $\mathbf{c}$ *with the dynamics*

$$\begin{bmatrix} 0 \\ \dot{\mathbf{c}} \end{bmatrix} = \begin{bmatrix} \mathbf{R}_{11} & \mathbf{R}_{12} \\ \mathbf{R}_{21} & \mathbf{R}_{22} \end{bmatrix} \begin{bmatrix} \mathbf{p}^0 \\ \mathbf{c} \end{bmatrix} - \frac{\eta}{2} \begin{bmatrix} \mathbf{0} \\ \mathbf{c} \circ \mathbf{c} - \mathbf{p}^0 \circ \mathbf{p}^0 \end{bmatrix} \tag{6.36}$$

then

$$\begin{aligned} 0 &= \bar{\mathbf{R}}_{11}\mathbf{p}^0 + \bar{\mathbf{R}}_{12}\mathbf{c} \Rightarrow && \text{(6.37a)} \\ \mathbf{p}^0 &= -\bar{\mathbf{R}}_{11}^{-1}\bar{\mathbf{R}}_{12}\mathbf{c} \Rightarrow && \text{(6.37b)} \\ \dot{\mathbf{c}} &= \mathbf{R}_{21}\mathbf{p}^0 + \mathbf{R}_{22}\mathbf{c} - \frac{\eta}{2}\mathbf{c} \circ \mathbf{c} + \frac{\eta}{2}\mathbf{p}^0 \circ \mathbf{p}^0 && \text{(6.37c)} \\ &= \left(\mathbf{R}_{22} - \mathbf{R}_{21}\bar{\mathbf{R}}_{11}^{-1}\bar{\mathbf{R}}_{12}\right)\mathbf{c} - \frac{\eta}{2}\mathbf{c} \circ \mathbf{c} + \frac{\eta}{2}\left(\bar{\mathbf{R}}_{11}^{-1}\bar{\mathbf{R}}_{12}\mathbf{c}\right) \circ \left(\bar{\mathbf{R}}_{11}^{-1}\bar{\mathbf{R}}_{12}\mathbf{c}\right) \ . && \text{(6.37d)} \end{aligned}$$

The constrained dynamics in (6.35) are of interest because they share the same equilibrium as the rotated dynamics $\mathbf{c}^0 = \mathbf{q}^0$, but display better stability properties. It then results in that even if the interconnection CRN has unstable dynamics (and the equilibrium is unstable), the reduced model still converges to the equilibrium $\mathbf{c}^0$.

Although we do not prove here if (6.35) is always stable around $\mathbf{c}_0$, it was always possible to integrate (6.35) for initial conditions $\mathbf{c}(0) = 2\bar{\mathbf{x}}^{0+}$. The value of $\bar{\mathbf{x}}^0$ was always retrievable for a stable nominal I/O dynamics, and the constraint (6.33) is fulfilled with $\bar{\mathbf{x}}^{0+} = \bar{\mathbf{x}}^{0-}$.

The reduced model in Definition 6.3 provides us with a system to find the equilibrium $\mathbf{c}_0$ independently of the stability of (6.20), and the rotated equilibrium is obtained directly with $\mathbf{q}^0 = \mathbf{c}^0$ and $\mathbf{p}^0 = -\mathbf{R}_{11}^{-1}\mathbf{R}_{12}\mathbf{c}^0$. The equilibrium in natural coordinates is finally recovered with $\mathbf{x}^{0\pm} = \frac{1}{2}\left(\mathbf{q}^0 \pm \mathbf{p}^0\right)$ (from the transformation in Definition 5.2).

6.2.4 Uncertainty and equilibrium model

The implementation of the CRNs is limited by the predictability of the affinities in the biomolecular network [74]. This leads to uncertain variability in the reaction rates and uncertainty in the implemented network. Moreover, in the case of the nonlinear system, the equilibrium in (6.29) moves depending on the parameterisation [165].

Since we do not have an analytical solution for the equilibrium of (6.20) we cannot explicitly express this dependency in the linearised system (except for the trivial equilibrium solution for $\mathbf{r} = 0$, $\mathbf{x} = 0$). A first approach is to fix the linearisation around the unforced equilibrium of the nominal system.

Definition 6.4. *Define the linearisation around a Fixed Equilibrium (FE) given by the solution* $\bar{\mathbf{x}}^0$ *of (6.34) where the uncertainty affects only the matrix* $\mathbf{A}$ *in*

$$\dot{\mathbf{s}} = \left(\mathbf{A} + \eta\mathbf{J}\left\{\bar{\mathbf{x}}^0\right\}\right)\mathbf{s}, \quad \mathbf{s}(0) = 0 \ . \tag{6.38}$$

However, the linearisation should also depend on the uncertainty through the equilibrium of the non-nominal system in $\mathbf{J}\left\{\mathbf{x}^0\right\}$. To express this dependency, the equilibrium variation is modelled as an approximate function of the uncertain state matrix and the nominal conditions.

Lemma 6.1. *If the variation in the equilibrium* $\mathbf{e} = \mathbf{x}^0 - \bar{\mathbf{x}}^0$ *is small with* $|\bar{x}_j^0| > |e_j|$*, then the moving unforced equilibrium* $\mathbf{x}^0$ *can be approximated by the estimator* $\hat{\mathbf{x}}^0$ *defined as*

$$\hat{\mathbf{x}}^0 := -\left(\mathbf{A} + \eta\mathbf{J}\left\{\bar{\mathbf{x}}^0\right\}\right)^{-1}\bar{\mathbf{A}}\bar{\mathbf{x}}^0 \ . \tag{6.39}$$

Proof. From the equilibrium condition $\mathbf{x}^0 = \bar{\mathbf{x}}^0 + \mathbf{e}$ we have

$$0 = \mathbf{A}\mathbf{x}^0 - \eta\mathbf{P}\left(\bar{\mathbf{x}}^0 + \mathbf{e}\right) \circ \left(\bar{\mathbf{x}}^0 + \mathbf{e}\right) \ . \tag{6.40}$$

We extend the nonlinear product into

$$\begin{aligned} 0 &= \mathbf{A}\mathbf{x}^0 - \eta\mathbf{P}\bar{\mathbf{x}}^0 \circ \bar{\mathbf{x}}^0 - \eta\mathbf{P}\mathbf{e} \circ \mathbf{e} - \eta\left(\mathbf{P}\bar{\mathbf{x}}^0 \circ \mathbf{e} + \bar{\mathbf{x}}^0 \circ \mathbf{P}\mathbf{e}\right) && \text{(6.41a)} \\ &= \mathbf{A}\mathbf{x}^0 - \eta\mathbf{P}\bar{\mathbf{x}}^0 \circ \bar{\mathbf{x}}^0 - \eta\mathbf{P}\mathbf{e} \circ \mathbf{e} + \eta\mathbf{J}\left\{\bar{\mathbf{x}}^0\right\}\mathbf{e} \ . && \text{(6.41b)} \end{aligned}$$

With small relative variations in the equilibrium $|\bar{x}_j^0| > |e_j|$, then for the quadratic terms we have $|\mathbf{P}\bar{\mathbf{x}}^0 \circ \bar{\mathbf{x}}^0| \gg |\mathbf{P}\mathbf{e} \circ \mathbf{e}|$ and

$$0 \approx \mathbf{A}\mathbf{x}^0 + \eta\mathbf{J}\left\{\bar{\mathbf{x}}^0\right\}\mathbf{e} - \eta\mathbf{P}\bar{\mathbf{x}}^0 \circ \bar{\mathbf{x}}^0 \ . \tag{6.42}$$

Substituting $\mathbf{e} = \mathbf{x}^0 - \bar{\mathbf{x}}^0$ we have

$$\begin{aligned} 0 \approx \ & \mathbf{A}\mathbf{x}^0 + \eta\mathbf{J}\left\{\bar{\mathbf{x}}^0\right\}\mathbf{x}^0 - \eta\mathbf{J}\left\{\bar{\mathbf{x}}^0\right\}\bar{\mathbf{x}}^0 - \eta\mathbf{P}\bar{\mathbf{x}}^0 \circ \bar{\mathbf{x}}^0 && \text{(6.43a)} \\ \Rightarrow \quad & \left(\mathbf{A} + \eta\mathbf{J}\left\{\bar{\mathbf{x}}^0\right\}\right)\mathbf{x}^0 \approx \eta\mathbf{J}\left\{\bar{\mathbf{x}}^0\right\}\bar{\mathbf{x}}^0 + \eta\mathbf{P}\bar{\mathbf{x}}^0 \circ \bar{\mathbf{x}}^0 \ . && \text{(6.43b)} \end{aligned}$$

Furthermore, from

$$\mathbf{J}\left\{\bar{\mathbf{x}}^0\right\}\bar{\mathbf{x}}^0 = -\left(\mathbf{P}\bar{\mathbf{x}}^0 \circ \bar{\mathbf{x}}^0 + \bar{\mathbf{x}}^0 \circ \mathbf{P}\bar{\mathbf{x}}^0\right) = -2\left(\mathbf{P}\bar{\mathbf{x}}^0 \circ \bar{\mathbf{x}}^0\right) \tag{6.44}$$

we have that

$$\begin{aligned}
\eta\mathbf{J}\left\{\bar{\mathbf{x}}^0\right\}\bar{\mathbf{x}}^0 + \eta\mathbf{P}\bar{\mathbf{x}}^0 \circ \bar{\mathbf{x}}^0 &= -2\eta\mathbf{P}\bar{\mathbf{x}}^0 \circ \bar{\mathbf{x}}^0 + \eta\mathbf{P}\bar{\mathbf{x}}^0 \circ \bar{\mathbf{x}}^0 && \text{(6.45a)}\\
&= -\eta\mathbf{P}\bar{\mathbf{x}}^0 \circ \bar{\mathbf{x}}^0 && \text{(6.45b)}\\
&= -\bar{\mathbf{A}}\bar{\mathbf{x}}^0 && \text{(6.45c)}\\
\Rightarrow \left(\mathbf{A} + \eta\mathbf{J}\left\{\bar{\mathbf{x}}^0\right\}\right)\mathbf{x}^0 &\approx -\bar{\mathbf{A}}\bar{\mathbf{x}}^0\ . && \text{(6.45d)}
\end{aligned}$$

Since $\mathbf{A} + \eta\mathbf{J}\left\{\bar{\mathbf{x}}^0\right\}$ is always invertible, we arrive at the defined estimator $\hat{\mathbf{x}}^0$. □

Proposition 6.1. *The solution in* (6.39) *satisfies the constraint*

$$\hat{\mathbf{x}}^{0-} = \left(\mathbf{A}_1^- - \mathbf{A}_2^-\right)^{-1}\left(\mathbf{A}_1^+ - \mathbf{A}_2^+\right)\hat{\mathbf{x}}^{0+} \tag{6.46}$$

given in (6.33)*.*

Proof. From $\left(\mathbf{A} + \eta\mathbf{J}\left\{\bar{\mathbf{x}}^0\right\}\right)\hat{\mathbf{x}}^0 = -\bar{\mathbf{A}}\bar{\mathbf{x}}^0$ we have

$$\begin{cases}
\mathbf{A}_1^+\hat{\mathbf{x}}^{0+} + \mathbf{A}_2^-\hat{\mathbf{x}}^{0-} - \eta\left(\bar{\mathbf{x}}^{0-} \circ \mathbf{x}^{0+} + \bar{\mathbf{x}}^{0+} \circ \mathbf{x}^{0-}\right) = -\bar{\mathbf{A}}_1\bar{\mathbf{x}}^{0+} - \bar{\mathbf{A}}_2\bar{\mathbf{x}}^{0-}\\
\mathbf{A}_2^+\hat{\mathbf{x}}^{0+} + \mathbf{A}_1^-\hat{\mathbf{x}}^{0-} - \eta\left(\bar{\mathbf{x}}^{0-} \circ \mathbf{x}^{0+} + \bar{\mathbf{x}}^{0+} \circ \mathbf{x}^{0-}\right) = -\bar{\mathbf{A}}_2\bar{\mathbf{x}}^{0+} - \bar{\mathbf{A}}_1\bar{\mathbf{x}}^{0-}
\end{cases} \tag{6.47}$$

and subtracting the two equations, we have

$$\begin{aligned}
&\mathbf{A}_1^+\hat{\mathbf{x}}^{0+} + \mathbf{A}_2^-\hat{\mathbf{x}}^{0-} - \left(\mathbf{A}_2^+\hat{\mathbf{x}}^{0+} + \mathbf{A}_1^-\hat{\mathbf{x}}^{0-}\right) = 0 && \text{(6.48a)}\\
&\Rightarrow \left(\mathbf{A}_1^+ - \mathbf{A}_2^+\right)\hat{\mathbf{x}}^{0+} - \left(\mathbf{A}_1^- - \mathbf{A}_2^-\right)\hat{\mathbf{x}}^{0-} = 0 && \text{(6.48b)}
\end{aligned}$$

and we recover the constraint in (6.46). □

We now use the estimator defined in (6.39) to enrich the linearisation model.

Definition 6.5. *The linearisation model including the Moving Equilibrium (ME) is performed around the estimator, resulting in*

$$\dot{\mathbf{s}} = \left(\mathbf{A} + \eta\mathbf{J}\left\{\hat{\mathbf{x}}^0\right\}\right)\mathbf{s} + \mathbf{B}\mathbf{r}_e, \quad \mathbf{s}(0) = 0 \tag{6.49}$$

where, in turn, $\hat{\mathbf{x}}^0$ *is a function of the uncertain dynamics matrix* $\mathbf{A}$ *and the nominal system and equilibrium, as defined in Lemma 6.1.*

Remark 6.2. *Performing the linearisation around the estimator provides the stability analysis with the impact of the uncertainty on the movement of the equilibrium [165]. However, the use of this model is limited by the assumption of "small" variations in the equilibrium with respect to nominal.*

How "small" this is will vary for each individual application, and the sensitivity of the equilibrium value to parameter variation. The fitting error should be checked with the system parameterised with samples from the considered uncertainty interval, to asses the validity of the assumption and if (6.39) *does provide an approximation of the moving equilibrium.*

6.3 Robust Stability Analysis

To demonstrate how robustness analysis can be applied, we create a nominal parameterisation for the example built in Section 6.1. We chose the nominal parameters as $k_1 = k_2 = 0.01\,\mathrm{s}^{-1}$, $k_3 = 0.0163\,\mathrm{s}^{-1}$, $k_4 = 0.185\,\mathrm{s}^{-1}$ for the plant, and $k_I = 0.01\,\mathrm{s}^{-1}$, $k_P = 0.53$ for the controller. The parameterisation ensures we have a prescribed nominal system which is stable and tracks a reference composed of step inputs.

Concerning the CRN and dual rail representation, we set the auxiliary rate $\gamma = 10 \times k_4 = 1.85\,\mathrm{s}^{-1}$, to be faster with respect to k_i, $i = 1, \ldots, 4$ and k_I. The annihilation rate at $\eta = 5 \times 10^5\ (\mathrm{Ms})^{-1}$ comes from the maximum toehold hybridisation rates observed experimentally [74]. Although we apply timescale separation to the reactions with auxiliary rates γ and η, no QSS approximation or model reduction is applied to the MAK. The simulations use the nonlinear model from (6.20) with the matrices defined in (6.22).

To simulate the response of the I/O system, we define the piecewise reference input r given by

$$r(t) = \begin{cases} 0\,\mathrm{nM} & 0\,\mathrm{s} \leq t < 1000\,\mathrm{s} \\ 1\,\mathrm{nM} & 1000\,\mathrm{s} \leq t < 4000\,\mathrm{s} \\ -1\,\mathrm{nM} & 4000\,\mathrm{s} \leq t < 7000\,\mathrm{s} \\ 0\,\mathrm{nM} & 7000\,\mathrm{s} \leq t \end{cases} . \tag{6.50}$$

Since the CRN is a dual rail representation with two inputs, the reference input is split into two components $r = r^+ - r^-$, given by

$$r^+(t) = \begin{cases} 0\,\mathrm{nM} & 0\,\mathrm{s} \leq t < 1000\,\mathrm{s} \\ 1\,\mathrm{nM} & 1000\,\mathrm{s} \leq t < 4000\,\mathrm{s} \\ 0\,\mathrm{nM} & 4000\,\mathrm{s} \leq t \end{cases}, \; r^-(t) = \begin{cases} 0\,\mathrm{nM} & 0\,\mathrm{s} \leq t < 4000\,\mathrm{s} \\ 1\,\mathrm{nM} & 4000\,\mathrm{s} \leq t < 7000\,\mathrm{s} \\ 0\,\mathrm{nM} & 7000\,\mathrm{s} \leq t \end{cases} . \tag{6.51}$$

The time response of the nominal system in Figure 6.2 shows the I/O system signal y tracking the input steps in r. A positive $x_j(0) > 0$ causes the concentrations

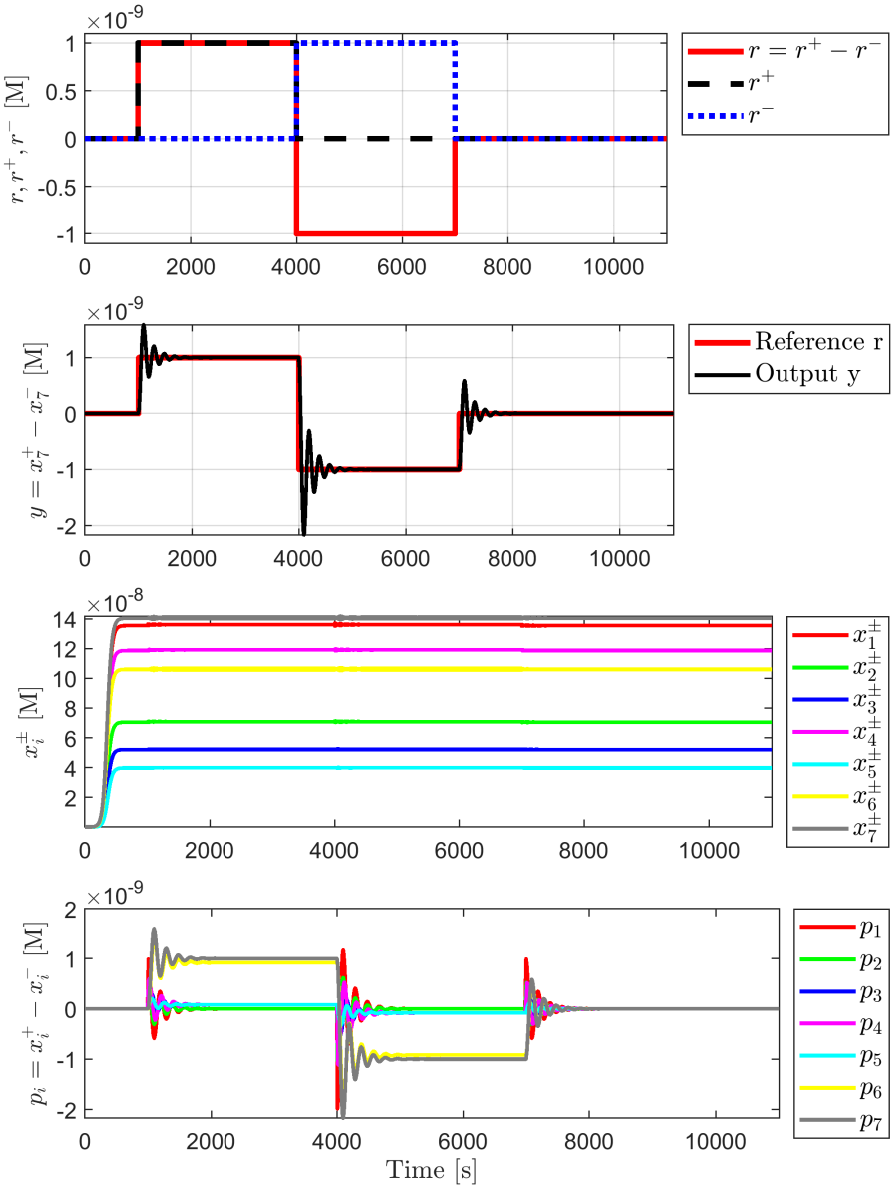

Figure 6.2: Nominal time response of the reference input r and the tracking output y. The reference signal $r = r^+ - r^-$ is such that only one of the $r^\pm$ components exist at each given time at steady state, resulting in the ideal sequence of reference steps. The concentrations $x_i^\pm$ converge to a positive equilibrium even if $r^\pm = 0$, and the differences between the dual concentrations represent the state of the I/O linear dynamics p_i.

to converge and remain in the nominal operating equilibrium even if $r^\pm = 0$ after $t \geq 7000$ s.

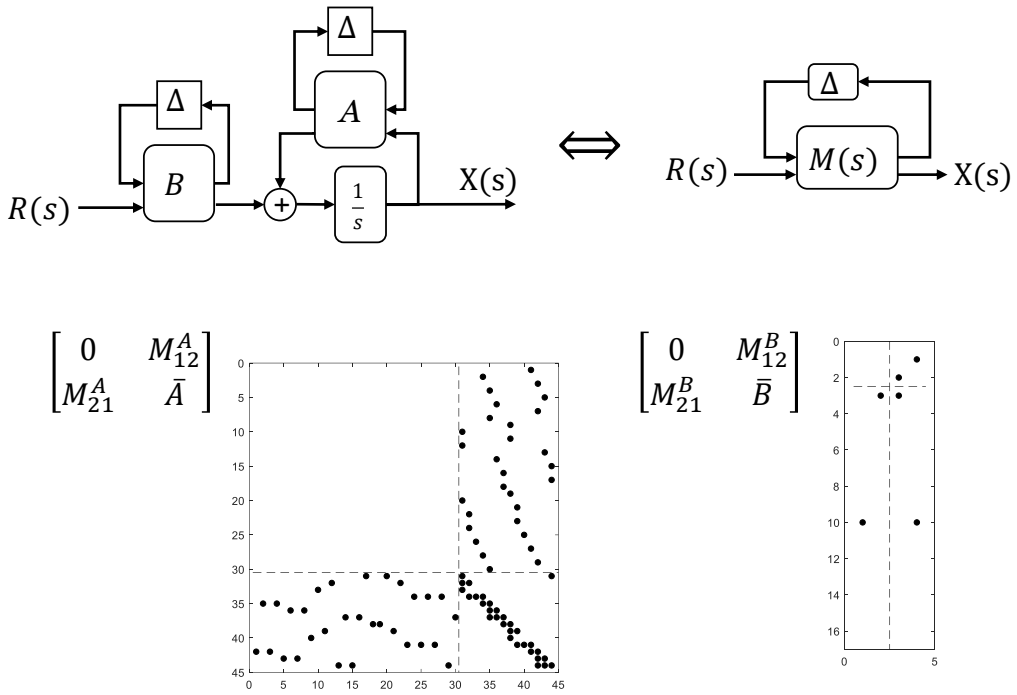

Figure 6.3: Above: the uncertainties in the matrices of the CRN dynamics **A** and **B** are aggregated into the SSV **M**-Δ structure. Below: sparsity of the M structure of the matrices **A** (with 30 uncertainties) and **B** (with 2 uncertainties).

Remark 6.3. *At this point in the analysis we are not concerned with the feasibility of the reaction rates in the CRN, and assume that scaling the system is possible to ensure a realisation with DSD [21]. The consequences of such scaling are discussed below in Section 6.4.*

6.3.1 Analysis with the structured singular value

The structured singular value framework, or μ-analysis, is an established validation method for uncertain LTI systems [82]. An uncertain plant $G(s, \Delta)$ represents the infinite family of transfer functions that depends on an uncertain system Δ, which can assume any value in a continuous interval. The structure of Δ is typically a block diagonal of real and normalised uncertainties such that $|\Delta| \leq 1$, and μ is defined as the inverse of the minimum possible value of Δ that destabilises the system [98, 99]. As discussed in Section 2.1.2, the value of μ is approximated by upper and lower bounds, and $G(s, \Delta)$ is robust to all possible parameterisations in the uncertainty intervals if $1/\mu < 1$ for all frequencies.

The uncertainty models are built and manipulated within Matlab™ and the Robust Control Toolbox™ [148], and the μ bounds are computed with the function

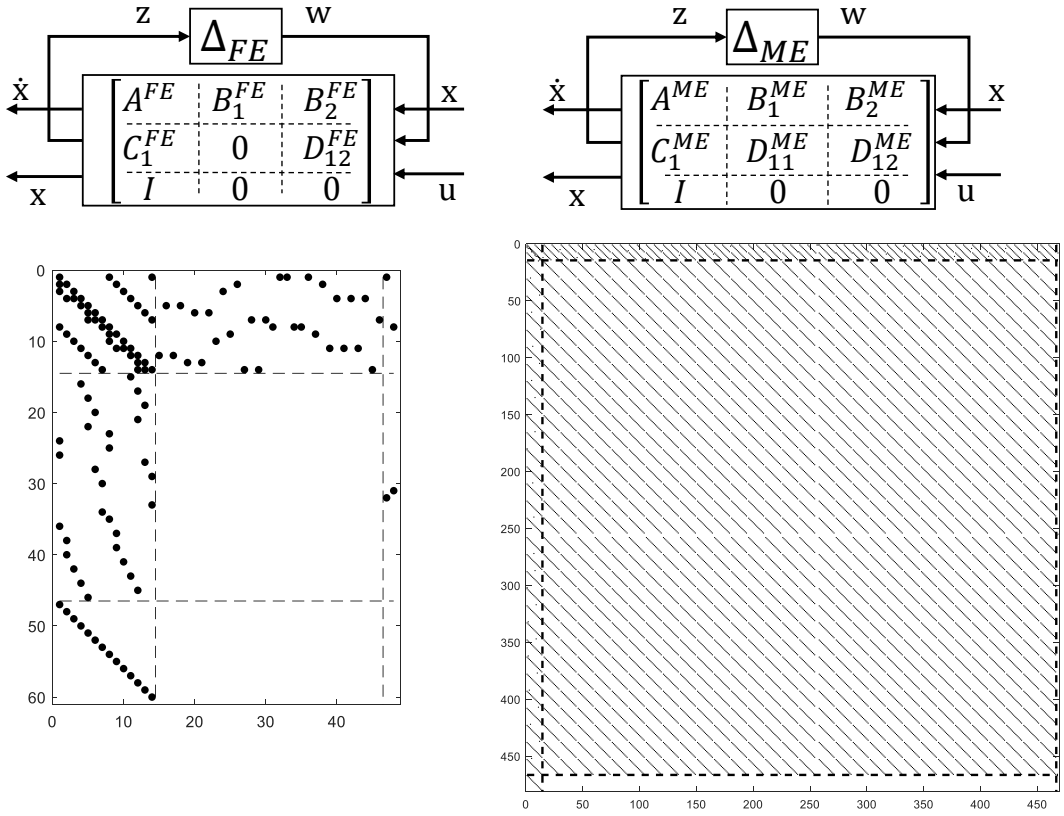

Figure 6.4: Structure of the matrix $\mathbf{M}$ in the $\mathbf{M}$-Δ decomposition for both of the analysed cases FE (left) and ME (right). The LFT for ME is much larger, and the uncertainties are coupled through D_{11}^{ME}.

`robstab` and its default options. To build the uncertain systems, each reaction rate is set as an `ureal` object with a multiplicative real variation $\delta \in \mathbb{R}$. For example, $\delta_{\gamma_1^+} \in \mathbb{R} : \gamma_1^+ = \bar{\gamma}_1^+ \left(1 + \delta_{\gamma_1^+}\right)$. This results in a total of 32 uncertain rates, which are set as the elements of the uncertain matrices $\mathbf{A}$ and $\mathbf{B}$ used in (6.20), to build the uncertain state space (`uss` object), Figure 6.3.

The robustness analysis is carried for $|\Delta| \leq 7\%$, for both of the linearisations around the FE in (6.38) and using the ME in (6.49). The linearisation around a FE results in a Δ_{FE} matrix 32×32, with diagonal real uncertainties, where each uncertainty occurs only once. In the linearisation with a ME, the estimation function of the equilibrium $\hat{\mathbf{x}}^0$ is taken from (6.39) and used to build $\mathbf{J}\left\{\hat{\mathbf{x}}^0\right\}$. The matrix Δ_{ME} is also real and diagonal, but becomes 452×452, where each uncertainty occurs 15 times (except for $\gamma_1^{\pm}$ which are not used in $\hat{\mathbf{x}}^0$, and therefore occurs only once).

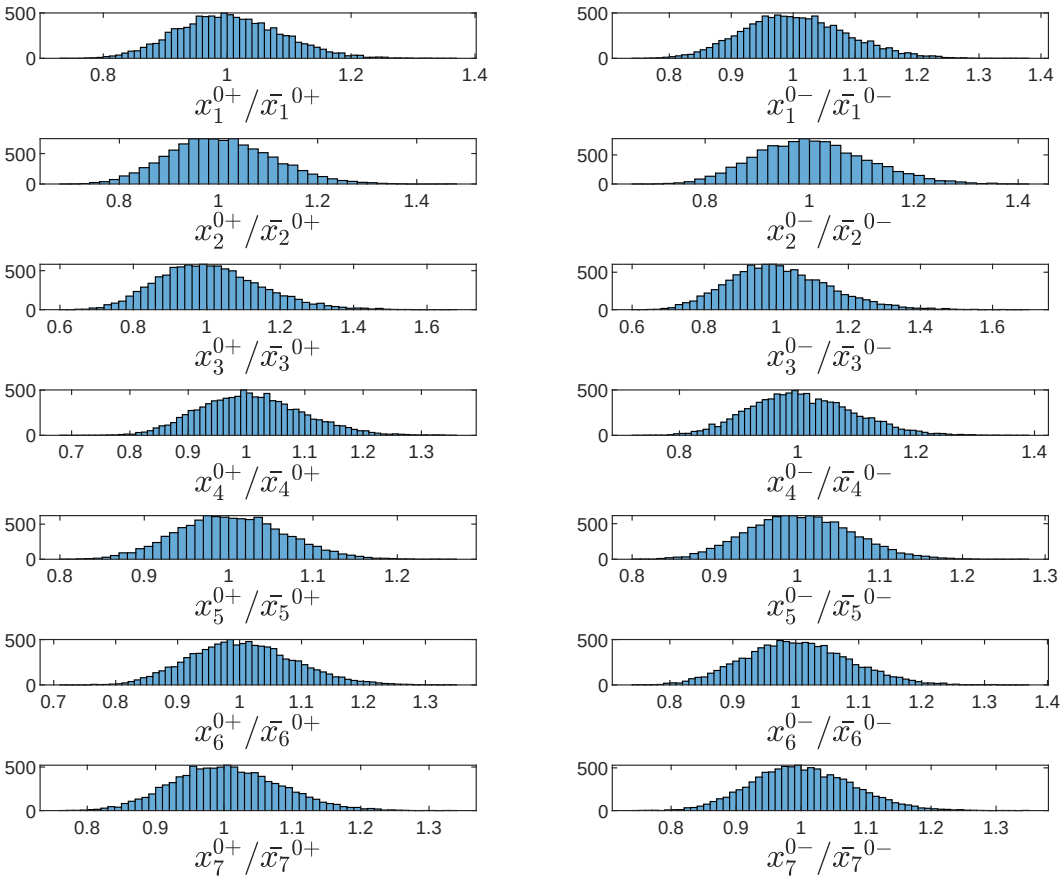

Figure 6.5: Distribution of the relative variation of elements of the moving equilibrium x_j^0 with respect to the nominal equilibrium value $\bar{x}_j^0$, for the 10000 uncertainty samples (for $|\Delta| < 7\%$). The deviations with respect to the nominal equilibrium values $\bar{x}_j^0$ are $\pm 20\%$ to $\pm 50\%$.

The structures can be represented by:

$$\Delta_{FE} = \{\mathbf{D}\,\{[\delta_1, \delta_2, \ldots, \delta_{32}]\} : \delta_i \in \mathbb{R}\} \tag{6.52a}$$

$$\Delta_{ME} = \{\mathbf{D}\,\{[\delta_1, \delta_2, \delta_3\mathbf{I}_{15}, \ldots, \delta_{32}\mathbf{I}_{15}]\} : \delta_i \in \mathbb{R}\} \tag{6.52b}$$

where $\mathbf{I}_{15}$ is the 15×15 identity matrix. The structures of the matrix $\mathbf{M}(s)$ for the LFTs in both cases are detailed in Figure 6.4. They show clearly the increase in size and complexity of the LFT in the case with ME, where D_{11}^{ME} is composed of diagonals coupling all uncertainties.

Figure 6.5 shows the normalised distributions of the equilibrium for 10000 sampled systems and confirms a movement of 20% to 50% due to uncertainty. For each sample, the true equilibrium $\mathbf{x}^0$ is compared with its estimation $\hat{\mathbf{x}}^0$ in Figure 6.6.

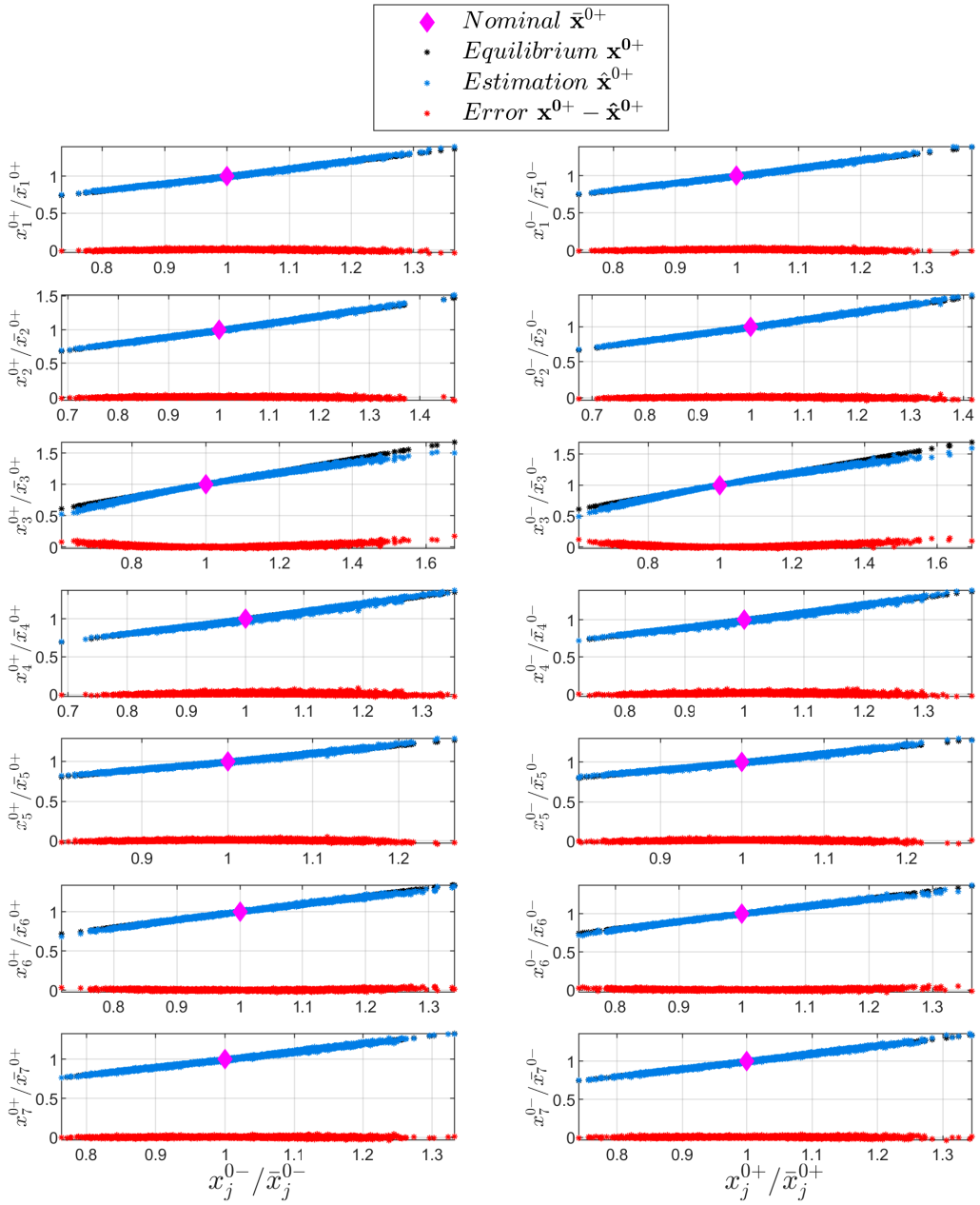

Figure 6.6: Comparison between the approximation and the numerically determined element j of the equilibrium, for each of 10000 samples. In black are the true equilibria $\mathbf{x}^0$, in blue are the approximated equilibria $\hat{\mathbf{x}}^0$, and in red are the approximation errors. The axes are normalised by the nominal equilibrium values, hence the nominal value of each element $\bar{x}_j^0$ is mapped into the coordinates $(1, 1)$.

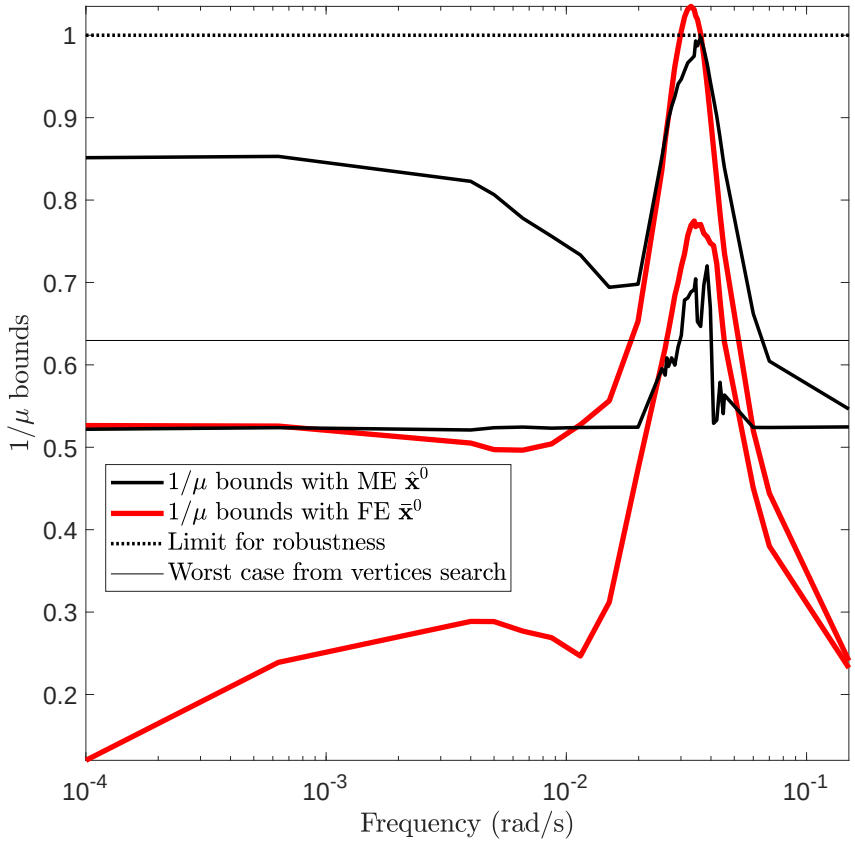

Figure 6.7: Comparison of μ bounds for linearisation around a fixed and moving equilibrium. The bounds are lower for the latter, which includes the equilibrium variation with uncertainty.

Following Remark 6.2, it is necessary to check if we have a small relative difference to the nominal equilibrium for the considered uncertainty level, which is an assumption necessary for Lemma 6.1.

The bounds for μ indicate that the linearisation around the FE is marginally stable, with stability assured only up to $|\Delta| = 6.763\%$. The identified worst-case uncertainty combination at $|\Delta_{FE}| = 9.037\%$ results in a conjugate pair of complex poles $-9.7 \times 10^{-14} \pm 0.034064i$. The bounds are lower for the μ-analysis with the moving equilibrium model (6.49), Figure 6.7, and the linearisation is robust up to $|\Delta| = 7.016\%$. The minimum destabilising $|\Delta_{ME}| = 9.720\%$ is also higher than with a FE, and results in the conjugate pair of complex poles $7.102 \times 10^{-15} \pm 0.038551i$. In this case, the inclusion of the moving equilibrium model results in a linearisation which is more robust than just linearising around the FE.

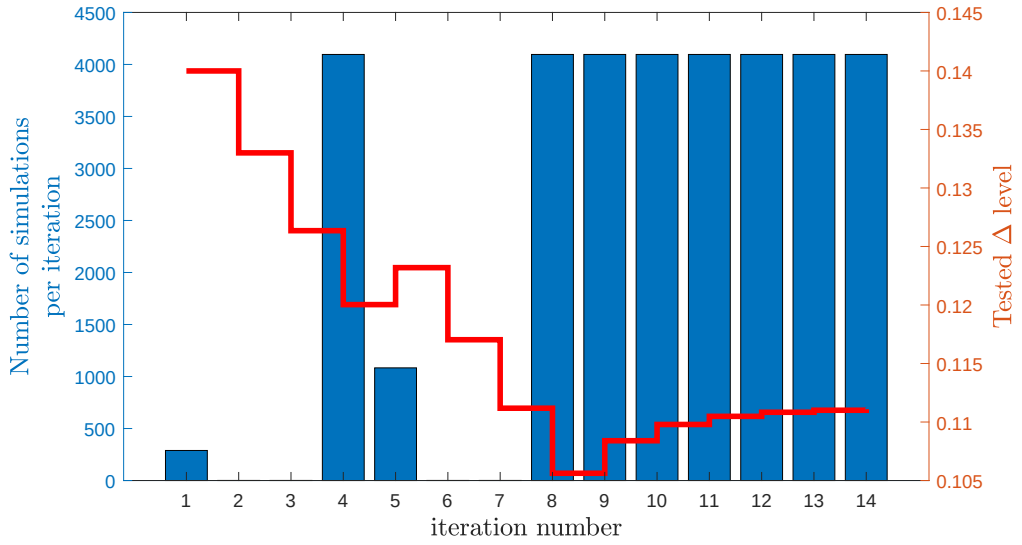

Figure 6.8: History of simulations per iteration in the search of a minimum destabilising bound, and the history of tested levels of Δ.

6.3.2 Sample based analysis with exact equilibrium movement calculation

For purposes of assessing the efficacy of the analysis based on the SSV, we carry out two sample based searches using the nonlinear system.

The first search carries out a Monte Carlo campaign for a variability in the reaction rates of $|\Delta_{MC}| = 10\%$, where all elements of $\mathbf{A}$ and $\mathbf{B}$ were scattered 10000 times. For each parameter vector, the equilibrium is solved using (6.35) and the local stability is checked using the linearised system (6.30). All the sampled parameterisations in this Monte Carlo campaign resulted in stable closed-loop systems, with the eigenvalues closest to the imaginary axis at $-0.00237686 \pm 0.0325045i$. Based on the high number of samples, the Monte Carlo test indicates that the system should be robust for $|\Delta| < 10\%$.

The alternative method is an iterative search for a destabilising parameterisation, where for each level of $|\Delta|$, 2^{12} out of 2^{32} possible vertices of the parameter space are randomly selected and evaluated for stability.

The magnitude of the uncertainty $|\Delta|$ is updated heuristically, where in the applied example, the search evaluated a total of 34 144 cases. The history of the tested magnitudes $|\Delta|$ and the number of simulations for each value of $|\Delta|$ is presented in Figure 6.8. The minimum destabilising amplitude was found for an uncertainty level of $|\Delta_{IT}| = 11.118\%$, which is consistent with the Monte Carlo results, but still above the results from the μ-analysis.

Table 6.1: Verification with the nonlinear system of the destabilising parameterisations identified with μ and sample based analysis: eigenvalues of the linearisation around the true equilibrium for each identified worst case parameterisation.

RS with $\bar{\mathbf{x}}^0(\mathbf{k})$ $\lvert\Delta_{FE}\rvert = 9.037\%$	RS with $\hat{\mathbf{x}}^0(\mathbf{k})$ $\lvert\Delta_{ME}\rvert = 9.720\%$	Vertices search $\lvert\Delta_{IT}\rvert = 11.118\%$
$\mathbf{-0.001073 \pm 0.03361i}$	$\mathbf{+1.916 \times 10^{-6} \pm 0.03855i}$	$\mathbf{+3.399 \times 10^{-5} \pm 0.03242i}$
$-2.296 \pm 0.2353i$	$-2.224 \pm 0.2435i$	$-2.261 \pm 0.2204i$
-2.268	-2.196	-2.265
$-1.92 \pm 0.3411i$	$-1.795 \pm 0.3598i$	$-1.866 \pm 0.3149i$
$-1.718 \pm 0.2867i$	$-1.652 \pm 0.2821i$	$-1.66 \pm 0.253i$
-1.44	-1.344	-1.4
-0.1403	-0.1486	-0.1311
-0.07358	-0.08013	-0.07016
-0.03283	-0.03356	-0.02978
-0.02103	-0.02551	-0.02375

6.3.3 Verification with the nonlinear system

The introduction of the additional effect of the uncertainty in the linearisation with the ME should capture more of the system in the analysis, and the μ bounds suggest that the linearisation with a FE is conservative with respect to using the ME. Moreover, both Monte Carlo simulation and a brute-force vertices search suggest the system is robust for uncertainty levels up to 10% contradicting the destabilising levels of uncertainty identified with the μ bounds.

To assess the validity of the different methods, the identified worst case parameterisations are now verified directly with the nonlinear system. For each set of destabilising parameters, the dynamics are linearised around their true equilibrium, and the respective poles are compared in Table 6.1.

The unstable parameterisation found with the FE actually results in a stable system. Instead of poles on the imaginary axis, the critical poles around the true equilibrium are stable at $-0.001073 \pm 0.03361i$, indicating conservatism when analysing the linearisation around the nominal equilibrium.

On the other hand, the unstable linearisation with the ME does correspond to an unstable nonlinear system with poles close to the imaginary axis at $+1.916 \times 10^{-6} \pm 0.03855i$, again confirming that use of the ME more accurately captures the impact of the uncertainties on the system, including loss of stability.

Furthermore, the unstable parameterisation identified with the ME model is inside the parameter space covered in the Monte Carlo campaign, showing that analysis based on sampling methods can be unreliable since there is no guarantee of complete coverage of the uncertainty space.

6.4 Independence of robustness levels from scaling for feasibility of DNA implementation

So far we have focused on the analysis of the CRN representation of the biomolecular control system, without addressing the implementation using DSD reactions, which has its own challenges. In particular, there is a physical limit for the bimolecular rate η, which is usually set close to the maximum hybridisation rate around $10^6\,(\mathrm{Ms})^{-1}$ [74, 168]. This, together with limits in concentrations, can impose constraints incompatible with the parameterisation of the CRN.

6.4.1 Scaling for feasibility with DNA chemistry

For the cases where the parameterisation of the CRN are not feasible for an implementation with DSD reactions, the procedure in [21] scales down the parameters to obtain feasible reaction rates and an accurate representation of the CRN.

Definition 6.6 (Scaling of reaction rates from [21])**.** *If $\mathbf{z}(t)$ is a solution to the ODEs of the CRN, then given two scalars $a, b > 0$, the function $b\mathbf{z}(\frac{1}{a}t)$ is also a solution to the ODEs, where the unimolecular rates γ_i are scaled by a^{-1}, the bimolecular rate η by $a^{-1}b^{-1}$, and the concentrations are scaled by b.*

We now investigate the impact of such scaling on dynamics and robustness.

Definition 6.7. *Let us define the basis dynamics by*

$$\dot{\mathbf{z}} = \frac{d\mathbf{z}}{dt} = \mathbf{A}_z\mathbf{z} + \mathbf{B}_z\mathbf{r}_z - \eta_z\mathbf{P}\mathbf{z}\circ\mathbf{z},\ \textit{given}\ \mathbf{z}(0) \geq 0 \tag{6.53}$$

with a bimolecular reaction η_z, and the unimolecular reaction rates in the network are the elements of $\mathbf{A}_z$. Define $\mathbf{z}^0$ as the equilibrium solution of $\mathbf{A}_z\mathbf{z}^0 = \eta_z\mathbf{P}\mathbf{z}^0\circ\mathbf{z}^0$, where $\mathbf{z}^0$ depends only on the parameterisation of ${\eta_z}^{-1}\mathbf{A}_z$.

Proposition 6.2. *Defining a scaled system $\mathbf{x}(t) = b\mathbf{z}(\tau)$ where $\tau = \frac{1}{a}t$ (scalars $a > 0$, $b > 0$), the scaled dynamics to a scaled input $b\mathbf{r}$ result in*

$$\dot{\mathbf{x}} \;=\; \mathbf{A}\mathbf{x} + \mathbf{B}\mathbf{r} - \eta\mathbf{P}\mathbf{x}\circ\mathbf{x},\ \textit{given}\ \mathbf{x}(0) \geq 0 \tag{6.54}$$

where $\mathbf{r} = b\mathbf{r}_z$, $\mathbf{A} = a^{-1}\mathbf{A}_z$, $\mathbf{B} = a^{-1}\mathbf{B}_z$, $\eta = \frac{1}{ab}\eta_z$.

Proof. The dynamics of the scaled system can be expressed as a scaling of the basis dynamics with

$$\dot{\mathbf{x}} \;=\; \frac{d\mathbf{x}}{dt} = b\frac{d\mathbf{z}}{d\tau}\frac{d\tau}{dt} = a^{-1}b\dot{\mathbf{z}}\ . \tag{6.55}$$

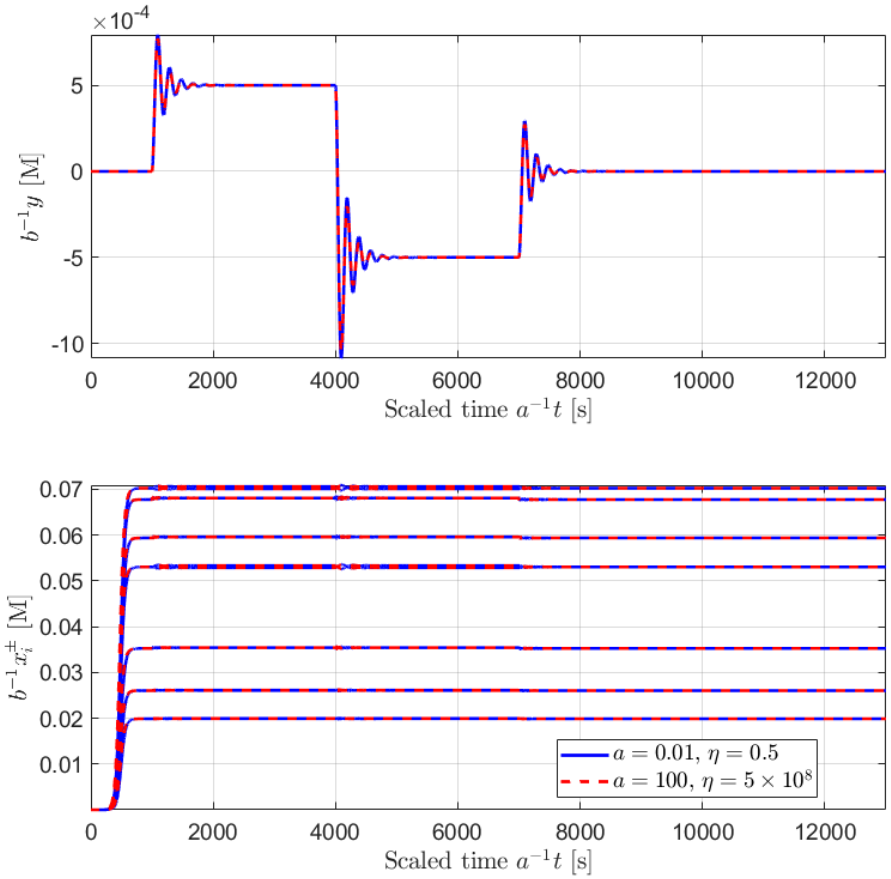

Figure 6.9: Time histories of the scaled output and concentrations for two examples with opposite values of $b = (a\eta)^{-1} = 200$ and $b = (a\eta)^{-1} = 2 \times 10^{-11}$. The time is scaled by a^{-1} to adjust for the change in dynamics' speed. The concentrations are scaled by b^{-1}, and the reference input is scaled by $b^{-1}r = 5 \times 10^{-4}$ [M].

Writing the scaled dynamics in terms of the new state, using the scaled gains $\mathbf{A}$, $\mathbf{B}$ and η, we have

$$
\begin{aligned}
a^{-1}b\dot{\mathbf{z}} &= a^{-1}b\mathbf{A}_z\mathbf{z} + a^{-1}b\mathbf{B}_z\mathbf{r} - a^{-1}b\eta_z\mathbf{P}\mathbf{z}\circ\mathbf{z} && \text{(6.56a)}\\
\Rightarrow \dot{\mathbf{x}} &= a^{-1}\mathbf{A}_z b\mathbf{z} + a^{-1}\mathbf{B}_z b\mathbf{r} - a^{-1}b\eta_z\mathbf{P}\mathbf{z}\circ\mathbf{z} && \text{(6.56b)}\\
&= a^{-1}\mathbf{A}_z\mathbf{x} + a^{-1}\mathbf{B}_z b\mathbf{r} - a^{-1}b^{-1}\eta_z\mathbf{P}\mathbf{x}\circ\mathbf{x} && \text{(6.56c)}\\
&= \mathbf{A}\mathbf{x} + \mathbf{B}b\mathbf{r} - \eta\mathbf{P}\mathbf{x}\circ\mathbf{x} && \text{(6.56d)}
\end{aligned}
$$

and we recover the nonlinear dynamics in (6.54). □

The scaling factors impact differently on the dynamics. If the unimolecular rates are not scaled ($a = 1$) then b only scales the concentrations of the system, without changing the poles and response time of the system.

Proposition 6.3. *When scaling the dynamics* $\mathbf{A} = a^{-1}\mathbf{A}_z$*, the equilibrium solutions are scaled by* $\mathbf{x}^0 = b\mathbf{z}^0$*.*

Proof. Replacing the dynamics matrix $\mathbf{A}$, η, and the scaled equilibrium $\mathbf{x}^0 = b\mathbf{z}^0$ in the equation for the unforced equilibrium of the basis system,

$$\begin{aligned} \mathbf{A}_z\mathbf{z}^0 &= \eta_z\mathbf{P}\mathbf{z}^0 \circ \mathbf{z}^0 && \text{(6.57a)} \\ \Rightarrow a\mathbf{A}b^{-1}\mathbf{x}^0 &= \eta_z\left(\mathbf{P}b^{-1}\mathbf{x}^0\right) \circ \left(b^{-1}\mathbf{x}^0\right) && \text{(6.57b)} \\ \Rightarrow ab^{-1}\mathbf{A}\mathbf{x}^0 &= b^{-2}\eta_z\mathbf{P}\mathbf{x}^0 \circ \mathbf{x}^0 && \text{(6.57c)} \\ \Rightarrow \mathbf{A}\mathbf{x}^0 &= \frac{\eta_z}{ab}\mathbf{P}\mathbf{x}^0 \circ \mathbf{x}^0 = \eta\mathbf{P}\mathbf{x}^0 \circ \mathbf{x}^0 && \text{(6.57d)} \end{aligned}$$

we arrive at the equation of the unforced equilibrium for the scaled system. □

Figure 6.9 compares the time response of the system in Section 6.1 for scalings that result in very large concentrations ($a = 0.01, \eta = 0.5$), and in very low concentrations ($a = 100, \eta = 5 \times 10^8$). If we reverse the scaling in the axes of time and concentrations, the time histories are identical.

6.4.2 Robustness of scaled parameterisations

If the nonlinear dynamics (6.53) are locally robustly stable, is the scaled system (6.54) also robustly stable? We now show how the scaling procedure does not affect the robustness of the stability, and the robustness of the original CRN is preserved in the scaling in Definition 6.6.

We start by looking at the properties of the linearisation of the scaled system. Applying the same derivation as in Proposition 5.6, we can define the perturbation state $\mathbf{z}_e = \mathbf{z} - \mathbf{z}^0$ for the basis system, and derive perturbation dynamics given by

$$\dot{\mathbf{z}}_e = \left(\mathbf{A}_z + \eta_z\mathbf{J}\left\{\mathbf{z}^0\right\}\right)\mathbf{z}_e + \mathbf{B}\mathbf{r}_e - \eta_z\mathbf{P}\mathbf{z}_e \circ \mathbf{z}_e, \quad \mathbf{z}_e(0) = 0\ . \tag{6.58}$$

In turn, the linearisation around the equilibrium $\mathbf{z} = \mathbf{z}^0 + \mathbf{h}$ is given by

$$\begin{aligned} \dot{\mathbf{h}} &= \left(\mathbf{A}_z - \eta_z\mathbf{D}\left\{\mathbf{P}\mathbf{z}^0\right\} - \eta_z\mathbf{D}\left\{\mathbf{z}^0\right\}\mathbf{P}\right)\mathbf{h} + \mathbf{B}_z\mathbf{r}_e && \text{(6.59a)} \\ &= \left(\mathbf{A}_z + \eta_z\mathbf{J}\left\{\mathbf{z}^0\right\}\right)\mathbf{h} + \mathbf{B}_z\mathbf{r}_e, \quad \mathbf{h}(0) = 0\ . && \text{(6.59b)} \end{aligned}$$

Proposition 6.4. *Scaling the perturbation and linearisation states according to* $\mathbf{x}_e = b\mathbf{z}_e = b\left(\mathbf{z} - \mathbf{z}^0\right)$ *and* $\mathbf{s} = b\mathbf{h}$*, the linearisation dynamics are scaled in the same manner as in Proposition 6.2, where*

$$\dot{\mathbf{s}} = \left(\mathbf{A} + \eta\mathbf{J}\left\{\mathbf{x}^0\right\}\right)\mathbf{s} + \mathbf{B}b\mathbf{r}_e, \quad \mathbf{s}(0) = 0 \tag{6.60}$$

with $\mathbf{A} = a^{-1}\mathbf{A}_z$, $\mathbf{B} = a^{-1}\mathbf{B}_z$, $\eta = \frac{1}{ab}\eta_z$.

Proof. As in Proposition 6.2, it results that $\dot{\mathbf{s}} = a^{-1}b\dot{\mathbf{h}}$ and

$$\begin{aligned}
a^{-1}b\dot{\mathbf{h}} &= a^{-1}b\left(\mathbf{A}_z + \eta_z\mathbf{J}\left\{\mathbf{z}^0\right\}\right)\mathbf{h} + a^{-1}b\mathbf{B}_z\mathbf{r}_e && \text{(6.61a)}\\
\Rightarrow \dot{\mathbf{s}} &= a^{-1}\left(\mathbf{A}_z + \eta_z\mathbf{J}\left\{\mathbf{z}^0\right\}\right)\mathbf{s} + a^{-1}\mathbf{B}_z b\mathbf{r}_e && \text{(6.61b)}\\
&= a^{-1}\left(a\mathbf{A} + \eta_z\mathbf{J}\left\{b^{-1}\mathbf{x}^0\right\}\right)\mathbf{s} + \mathbf{B}b\mathbf{r}_e && \text{(6.61c)}\\
&= \left(\mathbf{A} + a^{-1}b^{-1}\eta_z\mathbf{J}\left\{\mathbf{x}^0\right\}\right)\mathbf{s} + \mathbf{B}b\mathbf{r}_e && \text{(6.61d)}\\
&= \left(\mathbf{A} + \eta\mathbf{J}\left\{\mathbf{x}^0\right\}\right)\mathbf{s} + \mathbf{B}b\mathbf{r}_e\ . && \text{(6.61e)}
\end{aligned}$$

□

While the concentrations of the input are scaled by b, the state matrix is directly scaled in the matrix $\mathbf{A}$ and the equilibrium $\mathbf{x}^0$. For a fixed b, the poles of the linearisation are scaled by a^{-1} changing the timescale of the system dynamics without scaling the concentrations.

Theorem 6.1. *The scaled dynamics* $\dot{\mathbf{x}}$ *in (6.54) are locally robustly stable around* $\mathbf{x}^0$ *if and only if the original dynamics* $\dot{\mathbf{z}}$ *in (6.53) are locally robustly stable around* $\mathbf{z}^0$*.*

Proof. We can relate the spectral abscissae of the basis and scaled systems with

$$\begin{aligned}
\frac{1}{a}\left(\mathbf{A}_z + \eta_z\mathbf{J}\left\{\mathbf{z}^0\right\}\right) &= \mathbf{A} + \eta\mathbf{J}\left\{\mathbf{x}^0\right\} && \text{(6.62a)}\\
\Rightarrow \frac{1}{a}\alpha\left\{\mathbf{A}_z + \eta_z\mathbf{J}\left\{\mathbf{z}^0\right\}\right\} &= \alpha\left\{\mathbf{A} + \eta\mathbf{J}\left\{\mathbf{x}^0\right\}\right\}\ . && \text{(6.62b)}
\end{aligned}$$

In terms of stability, given that $a > 0$, we have the equivalences

$$\begin{aligned}
&i) \quad \frac{1}{a}\alpha\left\{\mathbf{A}_z + \eta_z\mathbf{J}\left\{\mathbf{z}^0\right\}\right\} < 0 \Leftrightarrow \alpha\left\{\mathbf{A} + \eta\mathbf{J}\left\{\mathbf{x}^0\right\}\right\} < 0 && \text{(6.63a)}\\
&ii) \quad \frac{1}{a}\left(\mathbf{A}_z + \eta_z\mathbf{J}\left\{\mathbf{z}^0\right\}\right) \in \mathcal{H} \Leftrightarrow \left(\mathbf{A} + \eta\mathbf{J}\left\{\mathbf{x}^0\right\}\right) \in \mathcal{H}\ . && \text{(6.63b)}
\end{aligned}$$

This means that if the basis system is locally stable at $\mathbf{z}^0$ then the scaled system is

locally stable at $\mathbf{x}^0$. Furthermore, if an uncertain $\dot{\mathbf{h}}$ is stable for any $|\Delta| < 1$, then

$$\left(\mathbf{A}_z + \eta_z \mathbf{J}\left\{\mathbf{z}^0\right\}\right) \in \mathcal{H},\ \forall_{|\Delta|<1} \Leftrightarrow \left(\mathbf{A} + \eta \mathbf{J}\left\{\mathbf{x}^0\right\}\right) \in \mathcal{H},\ \forall_{|\Delta|<1}\ . \tag{6.64}$$

Hence, if the linearisation of the original system is robust then the scaled linearisation is also robust, independent of the scaling used. □

When rescaling the concentrations and timescale of the system, Theorem 6.1 frees us from rechecking the robustness of the scaled system.

We saw how the example in Section 6.3 illustrates that accounting for the movement of the equilibrium with the uncertainty can provide a less conservative analysis. We now consider the impact of the scaling from Definition 6.2 in the estimator of the equilibrium proposed in Lemma 6.1.

Proposition 6.5. *Consider $\bar{\mathbf{A}}_z$ as the nominal dynamics of the original system, with the nominal equilibrium solution $\bar{\mathbf{z}}^0$. Applying the scaling of Proposition 6.2, results in a scaling of the estimator proposed in Lemma 6.1 with $\hat{\mathbf{x}}^0 = b\hat{\mathbf{z}}^0$.*

Proof. Applying the scaling to the estimator of the basis system, we have

$$\begin{aligned}
b\hat{\mathbf{z}}^0 &= -b\left(\mathbf{A}_z + \eta_z \mathbf{J}\left\{\bar{\mathbf{z}}^0\right\}\right)^{-1} \bar{\mathbf{A}}_z \bar{\mathbf{z}}^0 && \text{(6.65a)}\\
&= -\left(\mathbf{A}_z + \eta_z \mathbf{J}\left\{\bar{\mathbf{z}}^0\right\}\right)^{-1} \bar{\mathbf{A}}_z \bar{\mathbf{x}}^0 && \text{(6.65b)}\\
&= -\left(a\mathbf{A} + b^{-1}\eta_z \mathbf{J}\left\{\bar{\mathbf{x}}^0\right\}\right)^{-1} a\bar{\mathbf{A}} \bar{\mathbf{x}}^0 && \text{(6.65c)}\\
&= -\left(\mathbf{A} + a^{-1}b^{-1}\eta_z \mathbf{J}\left\{\bar{\mathbf{x}}^0\right\}\right)^{-1} \bar{\mathbf{A}} \bar{\mathbf{x}}^0 && \text{(6.65d)}\\
&= -\left(\mathbf{A} + \eta \mathbf{J}\left\{\bar{\mathbf{x}}^0\right\}\right)^{-1} \bar{\mathbf{A}} \bar{\mathbf{x}}^0 && \text{(6.65e)}\\
&= \hat{\mathbf{x}}^0 && \text{(6.65f)}
\end{aligned}$$

and we recover the definition of the estimator for the scaled system. □

We can then generalise the properties of the scaled system to the use of Lemma 6.1, by scaling the estimator of the moving equilibrium. Furthermore, the stability and invariance results still apply if we replace the equilibria $\mathbf{x}^0$ and $\mathbf{z}^0$ with their estimations $\hat{\mathbf{x}}^0$ and $\hat{\mathbf{z}}^0$.

In Figure 6.10, the robust stability was investigated for the same system as in Section 6.3, but scaling the dynamics by a and the equilibrium by η. The bounds for both ME and FE are in general very similar, apart from the shift in frequency due to a. With ME, for very small $b = 1/(a\eta) \leq 5 \times 10^{-8}$, the upper bound does change.

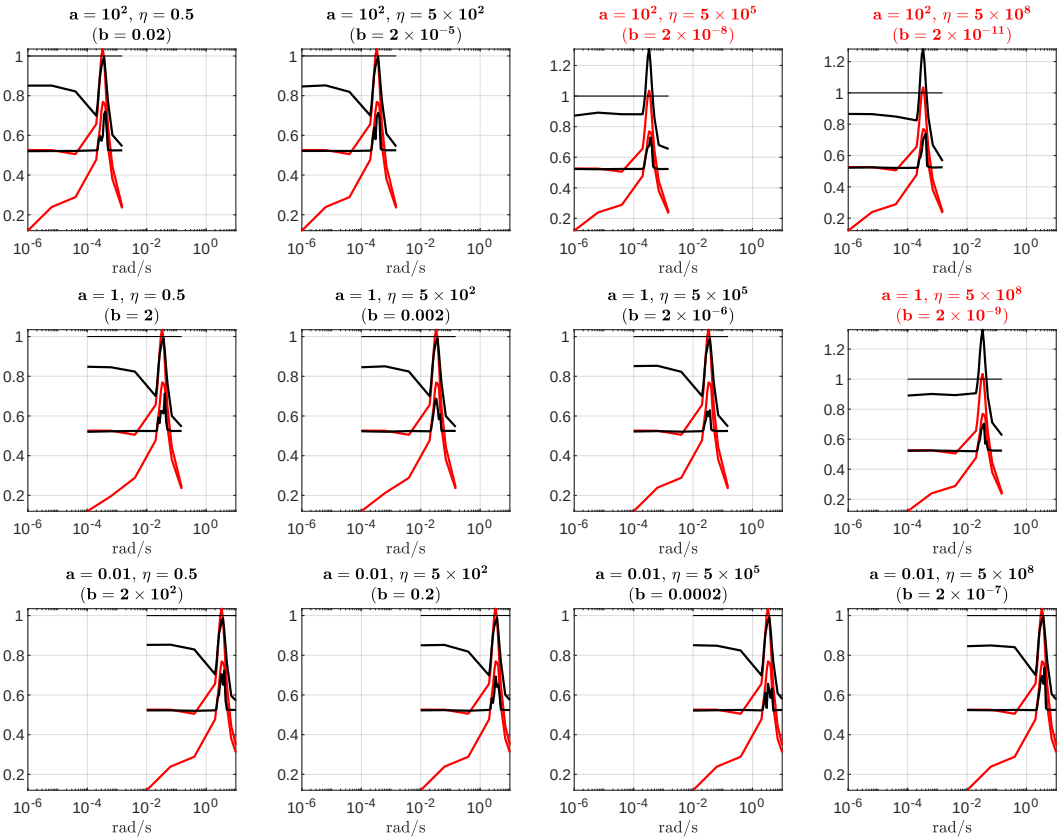

Figure 6.10: Robustness analysis for variations on scaling parameters $a^{-1}\gamma_j$, $a^{-1}k_j$ and η. The bounds with ME, in black, are invariant for the changes in scale, except for cases where $b \leq 10^{-7}$. With FE (in red) the results are independent of the parameterisation. The variation in a shifts the response in frequency, but the bounds remain very similar.

However, this may be due to numerical issues in the computation of $\mathbf{J}\{\bar{\mathbf{x}}^0\}$, with the very small values of $\bar{\mathbf{x}}^0$ in Figure 6.11. Any numerical discrepancies are then amplified by a large η value and the computation of the inversion $\left(\mathbf{A} + \eta \mathbf{J}\left\{\bar{\mathbf{x}}^0\right\}\right)^{-1}$ in the estimator $\hat{\mathbf{x}}^0$.

Nevertheless, the destabilising $|\Delta_{IT}|$ in Figure 6.12, found by testing the vertices of the parameter space, are comparable for all combinations of the scaling. This suggests there are no changes to the upper bounds, including the numerically difficult ones.

Remark 6.4. *Such invariance to scaling means that the robustness results for $\dot{\mathbf{z}}$ are applicable for any scaled system $\dot{\mathbf{x}}$, and decouple the design and analysis of the CRN from the scaled parameters used for implementation.*

In fact, scaling can be used to avoid numerical issues, by carrying out the

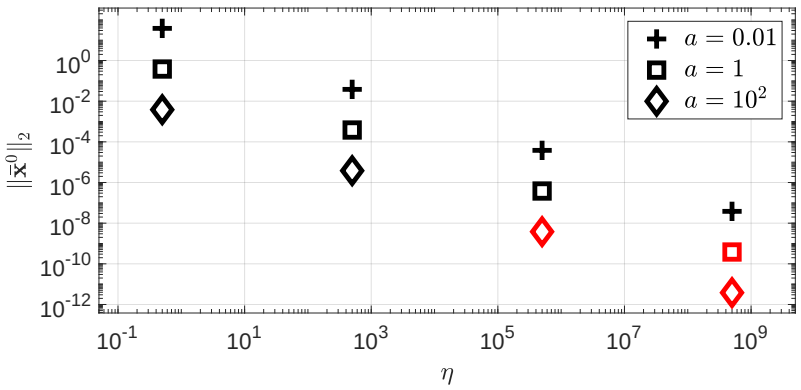

Figure 6.11: Norm of the nominal equilibrium $\bar{\mathbf{x}}^0$ of the system in Section 6.1 for variations in the scaling parameters $a^{-1}\gamma_j$, $a^{-1}k_j$ and η. The cases $(a\eta)^{-1} = b < 10^{-7}$ are in red.

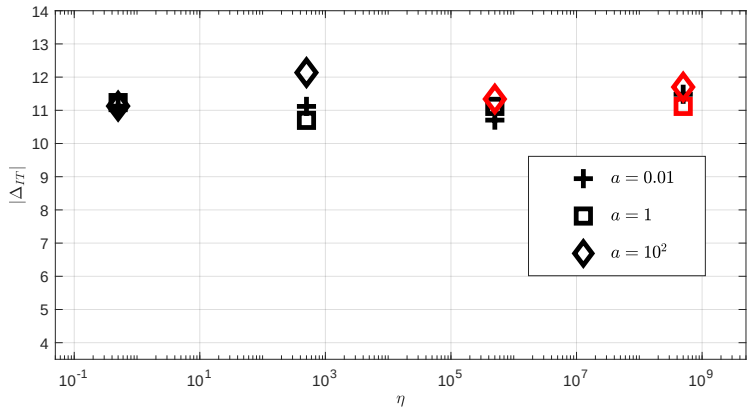

Figure 6.12: Destabilising $|\Delta_{IT}|$ found for variations in the scaling parameters $a^{-1}\gamma_j$, $a^{-1}k_j$ and η. They are close for every variation of the parameters, including the cases $(a\eta)^{-1} = b < 10^{-7}$ (in red).

controller design and performing the robustness analysis with possibly unfeasible but numerically balanced parameterisations, before finally scaling the systems appropriately for DSD implementation.

6.5 Conclusions

This chapter presents how robust stability analysis based on the structured singular value technique can be applied to the CRN representation of a linear negative feedback system. It is critical to address the nonlinearities resulting from the use of chemical reactions, and to operate within the natural coordinates of the CRN

accounting for the positivity of the system and the dependency of its equilibrium on the uncertainty.

The results indicate that it is possible to provide highly accurate guarantees on robustness for such systems by applying μ-analysis to the linearisation of the nonlinear dynamics.

Although the use of μ-analysis around a fixed equilibrium is computationally cheaper, it provides a conservative uncertainty bound, thus underestimating the level of uncertainty for which the closed-loop system remains stable.

Improving the linearisation model with a moving equilibrium produced robustness results that showed better agreement with the behaviour of the nonlinear system. Use of formal robustness analysis methods based on μ provided more reliable outcomes than sampling-based methods such as Monte Carlo campaigns and testing vertices of the parameter space.

Finally, it was shown how the analysis of the CRN can be decoupled from a scaled parameterisation that ensures a feasible implementation with nucleic acid-based chemistry, since existing scaling procedures preserve the robustness of the original parameterisation of the CRN representation.

Chapter 7

Conclusions and future works

Chemical reaction networks provide a powerful intermediate abstract layer to conceptualise computations with biomolecular circuits, which can be readily mapped into equivalent reactions using nucleic acids. In turn, frameworks based on DSD reactions, which use the sequences of DNA strands to program biochemical computers, have the capability to operate *in vivo* and interface with endogenous cellular machinery. This potential has been demonstrated in mammalian cells, making circuits based on nucleic acids strong potential candidates for many computing and control applications in synthetic biology.

There is a current effort in synthetic biology to bring control engineering concepts into biological implementations, calling for theoretical frameworks for design and analysis of stable feedback regulation of concentrations of biomolecules. The use of the dual-rail representation to overcome positivity enables the application of linear control theory to biochemistry, by providing a framework to systematically represent linear negative feedback systems with elementary reactions and nucleic acids. The work presented here has built on current research and the literature to expand the theoretical tools for the design and analysis of such class of systems, and aims to provide stepping-stones for the use linear control theory in a synthetic biological context.

In particular, the thesis starts by proposing representations for PID and state feedback controllers, expanding the control architectures available in the literature. The novel representations of delay and differentiation with chemical reactions provide a derivative term for the PID controller, maturing this architecture and tuning rules in a biochemical environment. Despite its heritage, it still results in a cumbersome number of reactions, and suffers from a filtered approximation of the derivative, with a fundamental trade-off between the accuracy of differentiation and the fea-

sibility of chemical reaction binding rates. The simpler structure relying on state feedback and integral control can regulate the same system with zero steady-states, but resulting in CRNs with fewer chemical reactions and species.

The readiness level of this technology has not followed the theoretical developments, and we are lacking experimental validation of such systems. This work proposes two control problems, which can be represented with very few CRN and DSD reactions, as minimally complex candidates for future experimental validation of feedback circuits using strand displacement reaction networks. The reduced number of reactions puts these DSD networks within the current capabilities for experimental investigation, while still capturing important features of general linear feedback control systems. Although simple, the circuits are interesting for immediate experimental investigation of the dependence of closed-loop dynamics on toehold design, and integration of the annihilation reactions.

The proposed architectures rely in the dual-rail representation of the signals, which has become common in biochemical applications to overcome the positivity inherent in chemical networks. However, the positivity and nonlinearity of such schemes are seldom addressed in the literature. This work presents explicitly the potential impact of the underlying nonlinear annihilation reactions, highlighting some of the dynamical and steady state characteristics of this class of systems. Unavoidable variability in the implemented binding rates leads to uncertainty in the parameterisation of the kinetics of the CRN. Consequently, stability can be affected by the looped interconnection between the nonlinear dynamics arising from biochemical implementation and the linear I/O dynamics resulting from the controller designs. The provided analysis details how the representation of feedback generally introduces a positive equilibrium, and in terms of stability, it shows that even if the designed linear I/O dynamics is robust, the robustness of the experimental CRN is not guaranteed.

The presented results confirm that the stability of nucleic acid-based controllers must be analysed using the linearisation of the complete nonlinear system, and this work provides a rigorous theoretical approach for conducting such an analysis. The structured singular value framework is successfully applied to the CRN representation of the biomolecular linear feedback system operating within the positive natural coordinates of the CRN, addressing the nonlinearities in the kinetics, and accounting for the equilibrium dependency on the uncertainty. With the equilibrium dependency in the linearisation the model captured better the behaviour of the nonlinear system, and uncovered worst case parameterisations missed by exhaustive brute force methods like Monte Carlo campaigns and sampling vertices of

the parameter space. Moreover, the robustness results are not affected by existing scaling methods of the reaction rates to represent the CRN with feasible DNA binding rates between. Such decoupling between the scaling of the CRN and the experimental implementation, introduces flexibility in the design and analysis of the circuits.

The proposed constructions, DSD realisations, theoretical results and analysis contributed to the the main goals of this thesis: the narrowing of the gap between engineering and biochemistry and to provide a bridge between linear control theory and synthetic biology.

Overall, the work statement from Section 1.3 was accomplished. The proposed designs fulfilled the purpose of expanding the available linear controllers realisable with nucleic acids. The analysis carried out managed to bring consolidated and rigorous tools from linear robust control to this new class of systems. Furthermore, this work provided theoretical understanding to the behaviour of the resulting CRNs, and successfully informed the experimentalists with new insights about the requirements and limitations of the implemented DSD networks.

The objective of exploiting dual rail representation and DSD reactions was achieved, with the proposal of novel constructions, where the dual-rail representation of I/O systems simplified and allowed the realisation of linear operators that were missing in literature. The constructions were tested and analysed with the most current specialised software, at different levels of detail.

The objective of interacting with biochemists was also very fruitful. A successful collaboration was established with world class experts in DSD networks, to move towards the implementation for the first time of representations of linear negative feedback systems with DSD reactions. The collaboration was crucial to understand the experimental challenges impact the constructions of the feedback system, and derive realistic realisations. An experimental implementation was not achieved, but from that synergy resulted constructions and DSD circuits which are feasible with the current capabilities for implementations using nucleic acids. The results were presented to the community, and hopefully it will contribute to the first tests of these types of systems.

Another objective was a rigorous characterisation and analysis of the dual-rail representation of negative feedback systems and resulting CRN. The theoretical analysis uncovered unexpected properties that were never addressed in the literature, with some very relevant for the DSD realisation. The role of the annihilation reactions, particularly in the dual-rail representation of linear negative feedback systems, is now completely justified in terms of stability conditions.

Variability and mismatching of the reaction rates is known to be an issue in the dual-rail representation. The problem of mismatching reaction rates had been raised in literature, but the presented work managed to address it formally and rigorously with established analysis tools. Robust control techniques were successfully adapted to address uncertainty, positivity and nonlinearities, and able to provide a representative and quantified robustness margin for stability of the CRN.

Due to time constraints, one objective that fell short was the development of refined models of the DSD mechanisms and realisation, to refine the dependency of the reaction rates of the CRN on effects and physical parameters from the DSD implementation. Such modelling effort is discussed in future works, and should be one of the first tasks in any follow up work.

7.1 Future works

For analysis, future work must develop representative and non-conservative uncertainty models for the DNA controllers, using detailed data from experimentation to characterise the different sources of uncertainty and map them to the MAK of the designed CRN. Effects to be modelled include initial and gradual leakage due to interactions between DNA strands present at high concentrations, truncated species, domain occlusion, and unproductive toehold binding events. Distinguishing the different effects would allow the construction of mechanistic and sharper uncertainty models to reliably evaluate and compare the limits of performance and robustness properties of different candidate controller designs. Such models would allow the comparison of different potential DSD architectures to identify best practices and correlate strategies to mitigate the different sources of uncertainty. For example, the use of clamps [160] mitigates directly spurious reactions and leakage, compartmentalisation of species avoids undesired hybridisation between toehold domains [163], and distance between tethering of species influences the accuracy of hybridisation rates [162, 169].

Moreover, the minimal size and uniqueness of the CRN representation for a given I/O dynamics is an open topic. For example, the complexity of the constructions in Chapter 4 was reduced manually by combining the computation of the subtraction and integration in the same set of reactions. It is not an automatic process and the minimum CRN size to represent any given I/O dynamics will depend on the dynamics and algebraic operations we wish to represent. Moreover, even for the small example of state feedback, there was a choice between using degradation reactions or catalytic degradation reactions [76] to represent the same I/O dynam-

ics. Better and more refined models of the DSD realisation could also improve the choice and optimisation of the set of reactions in the CRN representation.

Minimising the number of species and reactions that represent a given I/O dynamics may not be enough. Even if the goal is to chemically represent a given I/O dynamics, we should ensure the identifiability of the CRN including the internal dynamics of the I/O system. The different physical processes that influence the DSD realisation should also be identifiable, since the coexistence of the realisations for different reactions with common species lead to loss of modularity. The strand release rates depend not only on the toehold design but also on buffering and the multiplicity of the pathways of the input species. For example, buffering of a species in the realisation of the annihilation influences the effective release rates in the realisation of catalysis.

Not only do the characteristics and parameter identification of the realisation of an individual reaction not necessarily hold after integration in the system, but there are also different effects influencing the effective reaction rate. The CRN and its realisation should be identifiable, with the possibility to characterise not only the reaction rates, but also the different spurious and crosstalk effects. Finer detailed models of the DSD realisations will be necessary to inform the parameterisation of the CRN, since minimising and optimising the chemical representation, while keeping some degree of modularity, insulation, and identifiability will be an increasing challenge as the complexity of these type of systems increase.

Another direction of interest is the integration of feedback controllers with spatial strategies that are expected to allow faster, more accurate and more robust DNA based circuitry. New experimental developments include DNA walker circuits [161], tethered reactants in a DNA tile [162], or functional modules compartmentalised in proto-cells and droplets [163]. Such strategies allow for spatial programming of reaction pathways and population based distributed control like consensus/consortium and multi-agent systems [72, 163]. Tethering DNA gates to a substrate relaxes some of the current constraints on speed and accuracy of hybridisation rates [170], where co-localising reactions can result in faster reaction rates decreasing computation times from hours to minutes [162]. The implementation of distributed DSD architectures in proto-cell populations with diffusive molecular communication, with segregation of reactants of spurious reactions in different compartments, decreases crosstalk and avoids unproductive toehold occlusions [163].

Clusters of reactions associated with a function can provide modules for a higher-level synthesis and scalable arrangement of complex DNA systems. Analysis of the topological and geometric constraints in DNA circuits can be carried

out with additional use of Partial Differential Equation (PDE) to account for diffusion models [163, 171], some already available for simulations in tools like Visual DSD [172, 173]. Topological schemes can be exploited to optimise the chemical pathways and provide orthogonality, to allow the reuse of toehold sequences. This is crucial for the case of dual-rail controllers, which are expensive in their use of both species and reactions. On the other hand, spatial distribution plays a role in the efficiency and robustness of tethered strand displacement cascades [174] and it is a source of distributed delays as species diffuse between compartments [175], all critical issues for the design feedback control.

Despite the use of bimolecular reactions, dual-rail controllers can chemically represent linear dynamic output-feedback controllers avoiding the positive realisation problem [176]. Nevertheless, framing the class of circuits presented in this thesis as internally positive systems [142] provided some useful insights, and such analysis should be continued with further use of tools from positive [129, 177] and bilinear control theory [178], or from circuits with common features. For example, with its use of annihilation reactions for feedback control of positive processes, the proposed controllers and systems can be related to approaches based on sequestration reactions [179, 180] and the antithetic controller [59, 180], subjects of current intense investigation.

The results in this work are under the assumptions of MAK that provide the ODEs to map linear dynamics to circuits based on a CRN. Although the proposed circuits can be verified with stochastic simulations for a low number of molecules, it is absent from any stochastic interpretation of the theoretical results. Stochastic control theory can be applied to develop feedback control of downstream biomolecular processes with low copy-numbers [114,115,149], and under some assumptions we can derive stochastic differential equations [112,113] for modelling and analysis [114]. Such research is fundamental to understand the application of the presented circuits *in vivo* with low copy of molecules.

Finally, it would be of interest to investigate the combination of dual-rail systems with positive systems. If one can devise aptamers for local sensing and actuation on a biological process, like a genetic network, the information processing and control law could be implemented using a dual-rail representation based on nucleic-acids. The combination of linear negative feedback control with a positive plant would be a natural next step to get linear control theory closer to biological applications.

Appendix A

Code in Visual DSD for the simulation of the PID and state feedback integral control

This chapter lists the code for the simulation in Visual DSD of the examples in Chapter 3, for the simulations presented in Figure 3.12 and Figure 3.13.

The coding of the systems follows the approach of the examples found in [76], with the declaration of reusable primitives for

- `Degradation(tin,c,(x,x'))` - realisation of the dual rail degradation reactions
- `Annihilation(tin, (x,x'))` - realisation of the annihilation reaction
- `Catalysis(tin,c,(x,x'),(y,y'))` - realisation of the dual rail catalysis reactions
- `Subtracting(tin,c,(x,x'),(y,y'))` - realisation of the dual rail catalysis reactions with crossed contributions that lead to subtraction between two signals

The system is then assembled by calling the primitives with the signal species as arguments.

After the definition of the signals and respective species, the primitives are reused to assemble the complete system. The auxiliary species and their initialisation are automatically defined by Visual DSD.

A.1 Visual DSD code for PID controller with FOTD

This section lists the code regarding the PID controller.

```
directive declare
directive simulation deterministicstiff
(* directive simulation stochastic *)
directive scale 100.0 (* for stochastic simulation *)
directive tolerance 1e-9

directive parameters
  [ x0 = 1.0 (* nM *)
  ; scalet = 100000.0
    (* complementarity degree ratios qi/qmax *)
   ; c0 = 5e-05 (* - *)
   ; c1 = 1.9e-06 (* - *)
   ; c3 = 1.6e-05 (* - *)
   ; c4 = 8e-06 (* - *)
   ; c5 = 1e-06 (* - *)
   ; c6 = 1e-06 (* - *)
   ; c7 = 4e-06 (* - *)
   ; c8 = 8e-06 (* - *)
   ; Cmax = 10000.0 (* nM *)
   ; k2 = 4.0(* - *)
   ; bind = 0.001 (* 1/nM/s *)
    ; unbind =  0.1 (* 1/s *)
   ]


directive duration scalet*30.0 points 2000
directive event R() 1.0*x0 @  scalet*0.0
directive event R'() 2.0*x0 @  scalet*10.0
directive event R() 1.0*x0 @ scalet*20.0

directive plot
 R();R'();
 X1();X1'();
 X2();X2'();
 X3();X3'();
 X4();X4'();
 U();U'();
 X6();X6'();
 X7();X7'();
 Y();Y'();
sub (R(); R'());
sub (X1(); X1'());
```

```
sub (X2(); X2'());
sub (X3(); X3'());
sub (X4(); X4'());
sub (U(); U'());
sub (X6(); X6'());
sub (X7(); X7'());
sub (Y(); Y'())

(*------------------ CRN ------------------*)
directive compilation infinite
new tt@bind,unbind
new tu@bind,unbind

new y new y' new r new r' new x1 new x1' (* Feedback *)
new x2 new x2' new x3 new x3' new x4 new x4' new u new u' (* PID
    controller *)
new x6 new x6' new x7 new x7' (* Plant *)
new i

(* create signal with toehold *)
def Signal(tin,(x,x')) = <tin^ x>
def Signal'(tin,(x,x')) = Signal(tin,(x',x))

def sr = (r,r')
def sy = (y,y')
def sx1 = (x1,x1')
def sx2 = (x2,x2')
def sx3 = (x3,x3')
def sx4 = (x4,x4')
def su = (u,u')
def sx6 = (x6,x6')
def sx7 = (x7,x7')

def R()  = Signal(tt,sr)
def R'() = Signal'(tt,sr)
def Y()  = Signal(tt,sy)
def Y'() = Signal'(tt,sy)
def X1()  = Signal(tt,sx1)
def X1'() = Signal'(tt,sx1)
def X2()  = Signal(tt,sx2)
def X2'() = Signal'(tt,sx2)
def X3()  = Signal(tt,sx3)
def X3'() = Signal'(tt,sx3)
def X4()  = Signal(tt,sx4)
def X4'() = Signal'(tt,sx4)
def U()  = Signal(tt,su)
```

```
def U'() = Signal'(tt,su)
def X6()  = Signal(tt,sx6)
def X6'() = Signal'(tt,sx6)
def X7()  = Signal(tt,sx7)
def X7'() = Signal'(tt,sx7)

(*------------------ Primitives ----------------------------------*)

 (* def Degradation(deg,x) = rxn Signal(x) ->{deg}  *)
  def Degradation(tin,c,(x,x')) = Cmax * {tin^(c)*}[x]

def Annihilation(tin, (x,x')) =
( Cmax * {tin^*}[x tin^]:[x']
| Cmax * {tin^*}[x' tin^]:[x]
| Cmax * <x tin^>
| Cmax * <x' tin^>
)
  (* def Annihilation(x) =  rxn Signal(x) + Signal'(x) ->{ann}  *)

  def Catalysis(tin,c,(x,x'),(y,y')) =
( Cmax * {tin^(c)*}[x tu^]:[y tu^]:[i]
| Cmax * [i]:[tin^ x]{tu^*}
| Cmax * [i]:[tin^ y]{tu^*}
| Cmax * <tu^ y>
| Cmax * <tu^ i>
| Cmax * <i tin^>
)
(* def Catalysis(cat,x,y) = rxn Signal(x) ->{cat} Signal(x) + Signal(y
    )  *)

def Catalysis'(tin,c,(x,x'),(y,y')) = Catalysis(tin,c,(x',x),(y',y))
def Subtracting(tin,c,(x,x'),(y,y')) = Catalysis(tin,c,(x',x),(y,y'))
def Subtracting'(tin,c,(x,x'),(y,y')) = Subtracting(tin,c,(x',x),(y',y
    ))
def Degradation'(tin,c,(x,x')) =  Degradation(tin,c,(x',x))

(*------------------ system ----------------------------------*)

def System() =
(
 0 * R() |   0 * R'() |
  0 * Y() |   0 * Y'() |
  0 * U() |   0 * U'() |
  0 * X1() |   0 * X1'()|
  0 * X2() |   0 * X2'()|
  0 * X3() |   0 * X3'()|
```

```
  0 * X4() |   0 * X4'()|
  0 * X6() |   0 * X6'()|
  0 * X7() |   0 * X7'()
  (* Subtraction *)
| Catalysis(tt,c0,sr,sx1)
| Catalysis'(tt,c0,sr,sx1)
| Degradation(tt,c0,sx1)
| Degradation'(tt,c0,sx1)
| Annihilation(tt,sr)
| Annihilation(tt,sx1)
(* To close the loop *)
 | Subtracting(tt,c0,sy,sx1)
| Subtracting'(tt,c0,sy,sx1)
(* Controller *)
| Catalysis(tt,c3,sx1,sx4) (* filtered D *)
| Catalysis'(tt,c3,sx1,sx4)
| Degradation(tt,c4,sx4)
| Degradation'(tt,c4,sx4)
| Catalysis(tt,c0*k2,sx1,sx2) (* P *)
| Catalysis'(tt,c0*k2,sx1,sx2)
| Degradation(tt,c0,sx2)
| Degradation'(tt,c0,sx2)
| Catalysis(tt,c1,sx1,sx3) (* I *)
| Catalysis'(tt,c1,sx1,sx3)
| Annihilation(tt,sx2)
| Annihilation(tt,sx3)
| Annihilation(tt,sx4)
(* sum junction to comput U *)
| Catalysis(tt,c0,sx2,su)
| Catalysis'(tt,c0,sx2,su)
| Catalysis(tt,c0,sx3,su)
| Catalysis'(tt,c0,sx3,su)
| Subtracting(tt,c0,sx4,su)
| Subtracting'(tt,c0,sx4,su)
| Degradation(tt,c0,su)
| Degradation'(tt,c0,su)
| Annihilation(tt,su)
(* Plant *)
| Catalysis(tt,c5,su,sx6)
| Catalysis'(tt,c5,su,sx6)
| Degradation(tt,c6,sx6)
| Degradation'(tt,c6,sx6)
| Catalysis(tt,c8,sx6,sx7)
| Catalysis'(tt,c8,sx6,sx7)
| Degradation(tt,c7,sx7)
| Degradation'(tt,c7,sx7)
```

```
| Catalysis(tt,c0,sx7,sy)(* summation *)
| Catalysis'(tt,c0,sx7,sy)
| Subtracting(tt,c0,sx6,sy)
| Subtracting'(tt,c0,sx6,sy)
| Degradation(tt,c0,sy)
| Degradation'(tt,c0,sy)
| Annihilation(tt,sx6)
| Annihilation(tt,sx7)
| Annihilation(tt,sy)
)

(*------------------ Run ------------------------------------*)
System()
```

A.2 Visual DSD code for SFI controller with FOTD

This section lists the code regarding the SFI control.

```
directive declare
directive simulation deterministicstiff
(*  directive simulation stochastic *)
directive scale 100.0 (* for stochastic simulation *)
directive tolerance 1e-9

directive parameters
  [ x0 = 1.0 (* nM *)
  ; scalet = 100000.0 (* scalet = 50000.0 *)
    (* complementarity degree ratios qi/qmax *)
   ; cu = 5e-05 (* - *)
   ; cy = 5e-05 (* - *)
   ; cu6 = 0.00018632 (* - *)
   ; cuy = 2.032e-05 (* - *)
   ; cur = 0.00020664 (* - *)
   ; c1y = 1.3312e-06 (* - *)
   ; c5 = 1e-06 (* - *)
   ; c6 = 1e-06 (* - *)
   ; c7 = 4e-06 (* - *)
   ; c8 = 8e-06 (* - *)
   ; Cmax = 10000.0 (* nM *)
   ; bind = 0.001 (* 1/nM/s *)
    ; unbind =  0.1 (* 1/s *)
   ]

directive duration scalet*30.0 points 500
directive event R() 1.0*x0 @  scalet*0.0
```

```
directive event R'() 2.0*x0 @  scalet*10.0
directive event R() 1.0*x0 @ scalet*20.0

directive plot
 R();R'();
 U();U'();
 X1();X1'();
 X6();X6'();
 X7();X7'();
 Y();Y'();
sub (R(); R'());
sub (U(); U'());
sub (X1(); X1'());
sub (X6(); X6'());
sub (X7(); X7'());
sub (Y(); Y'())

(*------------------ CRN ------------------*)
directive compilation infinite
new tt@bind,unbind
new tu@bind,unbind

new y new y' new r new r' new u new u' (* closed loop  *)
new x1 new x1' new x6 new x6' new x7 new x7' (* Plant *)
new i

(* create signal with toehold *)
def Signal(tin,(x,x')) = <tin^ x>
def Signal'(tin,(x,x')) = Signal(tin,(x',x))

def sr = (r,r')
def sy = (y,y')
def su = (u,u')
def sx6 = (x6,x6')
def sx7 = (x7,x7')
def sx1 = (x1,x1')

def R()  = Signal(tt,sr)
def R'() = Signal'(tt,sr)
def Y()  = Signal(tt,sy)
def Y'() = Signal'(tt,sy)
def U()  = Signal(tt,su)
def U'() = Signal'(tt,su)
def X6()  = Signal(tt,sx6)
def X6'() = Signal'(tt,sx6)
def X7()  = Signal(tt,sx7)
```

```
def X7'() = Signal'(tt,sx7)
def X1()  = Signal(tt,sx1)
def X1'() = Signal'(tt,sx1)

(*------------------ Primitives -----------------------------------*)

(* def Degradation(deg,x) = rxn Signal(x) ->{deg}  *)
def Degradation(tin,c,(x,x')) = Cmax * {tin^(c)*}[x]

def Annihilation(tin, (x,x')) =
( Cmax * {tin^*}[x tin^]:[x']
| Cmax * {tin^*}[x' tin^]:[x]
| Cmax * <x tin^>
| Cmax * <x' tin^>
)
(* def Annihilation(x) =  rxn Signal(x) + Signal'(x) ->{ann}  *)

def Catalysis(tin,c,(x,x'),(y,y')) =
( Cmax * {tin^(c)*}[x tu^]:[y tu^]:[i]
| Cmax * [i]:[tin^ x]{tu^*}
| Cmax * [i]:[tin^ y]{tu^*}
| Cmax * <tu^ y>
| Cmax * <tu^ i>
| Cmax * <i tin^>
)
(* def Catalysis(cat,x,y) = rxn Signal(x) ->{cat} Signal(x) + Signal(y
   )  *)

def Catalysis'(tin,c,(x,x'),(y,y')) = Catalysis(tin,c,(x',x),(y',y))
def Subtracting(tin,c,(x,x'),(y,y')) = Catalysis(tin,c,(x',x),(y,y'))
def Subtracting'(tin,c,(x,x'),(y,y')) = Subtracting(tin,c,(x',x),(y',y
   ))
def Degradation'(tin,c,(x,x')) =  Degradation(tin,c,(x',x))

(*------------------ system -----------------------------------*)
def System() =
(
 0 * R() |   0 * R'() |
  0 * Y() |   0 * Y'() |
  0 * U() |   0 * U'() |
  0 * X6() |   0 * X6'()|
  0 * X7() |   0 * X7'() |
  0 * X1() |   0 * X1'()
(*          Summing Junction          *)
(* Reference *)
| Catalysis(tt,cur,sr,su)
```

```
| Catalysis'(tt,cur,sr,su)
(* Feedback Y *)
| Subtracting(tt,cuy,sy,su)
| Subtracting'(tt,cuy,sy,su)
(* Feedback X6 *)
| Subtracting(tt,cu6,sx6,su)
| Subtracting'(tt,cu6,sx6,su)
(* Adding x1 *)
| Catalysis(tt,cu,sx1,su)
| Catalysis'(tt,cu,sx1,su)
(* Degradation U *)
| Degradation(tt,cu,su)
| Degradation'(tt,cu,su)
(*        Error integration        *)
(* R-Y *)
 | Catalysis(tt,c1y,sr,sx1)
| Catalysis'(tt,c1y,sr,sx1)
| Subtracting(tt,c1y,sy,sx1)
| Subtracting'(tt,c1y,sy,sx1)
(*          Plant                 *)
| Catalysis(tt,c5,su,sx6)
| Catalysis'(tt,c5,su,sx6)
| Degradation(tt,c6,sx6)
| Degradation'(tt,c6,sx6)
| Catalysis(tt,c8,sx6,sx7)
| Catalysis'(tt,c8,sx6,sx7)
| Degradation(tt,c7,sx7)
| Degradation'(tt,c7,sx7)
(* Junction to compute Y *)
| Catalysis(tt,cy,sx7,sy)
| Catalysis'(tt,cy,sx7,sy)
| Subtracting(tt,cy,sx6,sy)
| Subtracting'(tt,cy,sx6,sy)
| Degradation(tt,cy,sy)
| Degradation'(tt,cy,sy)
(* Annihilation of dual species *)
| Annihilation(tt,sx6)
| Annihilation(tt,sx7)
| Annihilation(tt,sy)
| Annihilation(tt,sr)
| Annihilation(tt,su)
| Annihilation(tt,sx1)
)
(*------------------ Run -----------------------------------*)
System()
```

Appendix B

Example with detailed derivation and code for simulation of the DSD system

In Chapter 4, one of the proposed systems is a reference tracking with integral control of a first order system. The ODEs of the closed loop system are given by

$$\dot{y} = bv - ay, \quad y(0) = 0 \tag{B.1a}$$
$$\dot{v} = k_i (r - y), \quad v(0) = 0 \tag{B.1b}$$

where y is the controlled output, v is the control actuation, and r is a constant reference signal to be tracked ($\dot{r} = 0$).

B.1 Representation with a CRN

In the defined closed loop system we have $y^{\pm}, v^{\pm}, r^{\pm} \in \mathbb{R}$. For an implementation based on positive concentrations of chemical species, we employ a dual-rail representation with positive quantities, where we split the real signals $y, v, r \in \mathbb{R}$ into contributions of pairs of positive signals $y^{\pm}, v^{\pm}, r^{\pm} \in \mathbb{R}_0^+$. With the transformations $y = y^+ - y^-$, $v = v^+ - v^-$, and $r = r^+ - r^-$, we replace the signals in (B.1) with

$$\dot{y}^+ - \dot{y}^- = b\left(v^+ - v^-\right) - a\left(y^+ - y^-\right) \tag{B.2a}$$
$$= \left(bv^+ + ay^+\right) - \left(bv^- + ay^-\right) \tag{B.2b}$$
$$\dot{v}^+ - \dot{v}^- = k_i\left(r^+ - r^-\right) - k_i\left(y^+ - y^-\right) \tag{B.2c}$$
$$= k_i\left(r^+ + y^-\right) - k_i\left(r^- + y^+\right) \ . \tag{B.2d}$$

To ensure that the dynamics are positive, the ODEs from (B.1) are now defined as the I/O dynamics of the positive system

$$\dot{y}^+ = bv^+ - ay^+, \quad y^+(0) = 0 \tag{B.3a}$$
$$\dot{y}^- = bv^- - ay^-, \quad y^-(0) = 0 \tag{B.3b}$$
$$\dot{v}^+ = k_i\left(r^+ + y^-\right), \quad v^+(0) = 0 \tag{B.3c}$$
$$\dot{v}^- = k_i\left(r^- + y^+\right), \quad v^-(0) = 0\ . \tag{B.3d}$$

The reference input r is transformed into a pair of concentrations such that $r = r^+ - r^-$, and the states of the I/O dynamics are given by the differences $y = y^+ - y^-$ and $v = v^+ - v^-$. With this method, the subtraction $r - y$ results from crossing the contributions from y^- to v^+ and y^+ to v^-, and allows to introduce a subtraction in the I/O dynamics while maintaining the positivity of the dual-rail dynamics.

Looking at (B.3) as the MAK of a CRN, the representation can now be programmed using only degradation and catalysis reactions. The representation is not unique, and one possibility is given by:

$$V^+ \xrightarrow{b} V^+ + Y^+ \tag{B.4a}$$
$$Y^+ \xrightarrow{a} \emptyset \tag{B.4b}$$
$$V^- \xrightarrow{b} V^- + Y^- \tag{B.4c}$$
$$Y^- \xrightarrow{a} \emptyset \tag{B.4d}$$
$$R^+ \xrightarrow{k_i} R^+ + V^+ \tag{B.4e}$$
$$R^- \xrightarrow{k_i} R^- + V^- \tag{B.4f}$$
$$Y^+ \xrightarrow{k_i} Y^+ + V^- \tag{B.4g}$$
$$Y^- \xrightarrow{k_i} Y^- + V^+ \tag{B.4h}$$

where $y^+ = [Y^+]$, $y^- = [Y^-]$, $v^+ = [V^+]$, $v^- = [V^-]$, $r^+ = [R^+]$, and $r^- = [R^-]$.

As discussed through out the main text and in [62, 79], what is left is to add annihilation reactions to limit the simultaneous existence of the species in each of the pairs representing the signals. Therefore, the final chemical program also includes:

$$V^+ + V^- \xrightarrow{\eta} \emptyset \tag{B.5a}$$
$$Y^+ + Y^- \xrightarrow{\eta} \emptyset\ . \tag{B.5b}$$

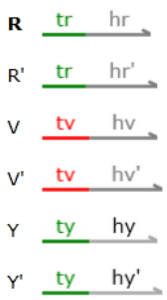

Figure B.1: Definition of the strands used to represent the signals in the DSD reactions.

The final positive dynamics are then is given by

$$\dot{y}^+ = bv^+ - ay^+ - \eta y^+ y^-, \quad y^+(0) = 0 \tag{B.6a}$$
$$\dot{y}^- = bv^- - ay^- - \eta y^+ y^-, \quad y^-(0) = 0 \tag{B.6b}$$
$$\dot{v}^+ = k_i \left(r^+ + y^-\right) - \eta v^+ v^-, \quad v^+(0) = 0 \tag{B.6c}$$
$$\dot{v}^- = k_i \left(r^- + y^+\right) - \eta v^+ v^-, \quad v^-(0) = 0 \tag{B.6d}$$

which results in the same I/O system, since the nonlinear terms cancel out when applying the input and output transformations.

B.2 Construction of the CRN with DSD reactions

At this point, we have our closed loop system represented by the I/O dynamics of the MAK of a set of chemical reactions. The constructions described in Section 4.2.3 provide a mapping to implement each of the reactions in (B.4) and (B.5) with sets of DSD reactions.

Let us first define the signal strands, used to represent the signals as differences in concentrations. The abstract chemical species in the chemical program in (B.4) are replaced with the strands defined in Figure B.1, such that the I/O dynamics have the states given by the difference of pairs of concentrations, given by

$$r = [R] - \left[R'\right] \tag{B.7a}$$
$$y = [Y] - \left[Y'\right] \tag{B.7b}$$
$$v = [V] - \left[V'\right] \ . \tag{B.7c}$$

Using the terminology from VisualDSD, we have that each strand has a unique binding domain ($< hr >$, $< hr' >$, $< hy >$, $< hy' >$, $< hv >$, $< hv' >$), and a toehold domain that will be used to initiate strand displacement reactions. The toehold domains ($< tr >$, $< ty >$ and $< tv >$) are not unique, and determine which strands interact and their affinity for interaction.

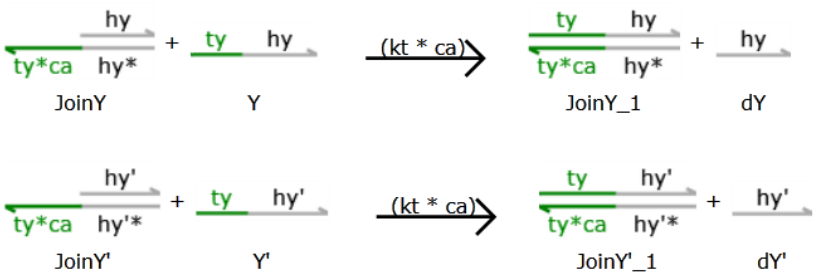

Figure B.2: DSD reactions for the implementation of $Y \to \emptyset$ and $Y' \to \emptyset$.

The implementation of the degradation reaction is the most straightforward, using only additional auxiliary templates $JoinY$ and $JoinY'$. For $Y^+ \to \emptyset$ and $Y^- \to \emptyset$, we use the construction with DSD reactions in Figure B.2, where

$$Y + JoinY \xrightarrow{c_a \times k_t} JoinY_1 + dY \tag{B.8a}$$

$$Y' + JoinY' \xrightarrow{c_a \times k_t} JoinY'_1 + dY' \ . \tag{B.8b}$$

Therefore, the implementation of the degradation reactions needs only the presence of two auxiliary templates initialised with

$$[JoinY](0) = \left[JoinY'\right](0) = C_{max} \tag{B.9}$$

where, under Assumption 4.1, C_{max} is high enough for the consumption of the templates to have a negligible effect on the dynamics. The construction also assumes the capacity to refine the complementarity degree $0 < ca < 1$ between the toeholds $< ty >$ and $< ty* >$, resulting in a reaction rate below the maximum binding toehold rate kt.

For the annihilation reaction, the cooperative hybridisation scheme [144,145] employs a single auxiliary template, where the reaction is irreversible only in the presence of both signal strands. The annihilation reaction $V^+ + V^- \xrightarrow{\eta} \emptyset$ can then

be mapped into DSD sets of reactions with

$$Ann_{VV} + V \underset{k_{ubnd}}{\overset{c_{VV} \times k_t}{\rightleftharpoons}} I_V \tag{B.10a}$$

$$I_V + V' \xrightarrow{c_{VV} \times k_t} W_V + W_{V'} \tag{B.10b}$$

$$Ann_{VV} + V \underset{k_{ubnd}}{\overset{c_{VV} \times k_t}{\rightleftharpoons}} I_{V'} \tag{B.10c}$$

$$I_{V'} + V \xrightarrow{c_{VV} \times k_t} W_V + W_{V'} \tag{B.10d}$$

as illustrated in Figure 4.4. For the annihilation reaction $Y^+ + Y^- \xrightarrow{\eta} \emptyset$ we have

$$Ann_{YY} + Y \underset{k_{ubnd}}{\overset{c_{YY} \times k_t}{\rightleftharpoons}} I_Y \tag{B.11a}$$

$$I_Y + Y' \xrightarrow{c_{YY} \times k_t} W_Y + W_{Y'} \tag{B.11b}$$

$$Ann_{YY} + Y \underset{k_{ubnd}}{\overset{c_{YY} \times k_t}{\rightleftharpoons}} I_{Y'} \tag{B.11c}$$

$$I_{Y'} + Y \xrightarrow{c_{YY} \times k_t} W_Y + W_{Y'} \ . \tag{B.11d}$$

The construction is implemented by including in the system the auxiliary templates at very large concentrations, for example with

$$[AnnYY](0) = [AnnVV](0) = C_{max} \ . \tag{B.12}$$

The construction of the catalysis reaction relies in more auxiliary templates. As depicted in Figure 4.3, besides the Fork and Join templates, there are additional strands and toeholds along the cascade of reactions. For example, the catalysis reaction $R^+ \xrightarrow{ci \times kt} R^+ + V^+$, is mapped into the set of reactions given by

$$R + Join_{VR} \underset{k_{bnd}}{\overset{c_i \times k_t}{\rightleftharpoons}} Join_{VR}^{-1} + aux_{hrtp} \tag{B.13a}$$

$$Join_{VR}^{-1} + aux_{tphpr} \underset{k_{bnd}}{\overset{k_{bnd}}{\rightleftharpoons}} Join_{VR}^{-2} + sig_{hprtq} \tag{B.13b}$$

$$sig_{hprtq} + Fork_{VR} \underset{k_{bnd}}{\overset{k_{bnd}}{\rightleftharpoons}} Fork_{VR}^{-1} + aux_{tphpr} \tag{B.13c}$$

$$Fork_{VR}^{-1} + aux_{hrtp} \underset{k_t}{\overset{k_{bnd}}{\rightleftharpoons}} Fork_{VR}^{-2} + R \tag{B.13d}$$

$$Fork_{VR}^{-2} + aux_{hvtr} \underset{k_t}{\overset{k_t}{\rightleftharpoons}} Fork_{VR}^{-3} + V \tag{B.13e}$$

$$Fork_{VR}^{-3} + aux_{hitv} \xrightarrow{k_t} \emptyset \ . \tag{B.13f}$$

The maximum toehold binding rate k_{bnd} for the toeholds $< tp >$ and $< tq >$ (Figure 4.3) is set $k_{bnd} > k_t$ to ensure the intermediary reactions do not limit the reaction, and the auxiliary strands have binding domains specific to the Fork and Join templates they interact with (for example, the domain $< hpr >$ in aux_{tphpr} to bind to $< hpr* >$ in the produced strand $Join^{-1}_{VR}$ (Figure 4.3).

The cascade of DSD reactions is implemented by initialising the the auxiliary strands at high concentrations, with

$$[Join_{VR}](0) = [aux_{hrtp}](0) = [aux_{tphpr}](0) = C_{max} \tag{B.14a}$$
$$[Fork_{VR}](0) = [aux_{hvtr}](0) = [aux_{hitv}](0) = C_{max}\ . \tag{B.14b}$$

For the other component $R^- \xrightarrow{ci \times kt} R^- + V^-$, we have the set of reactions given by

$$R' + Join_{V'R'} \underset{k_{bnd}}{\overset{c_i \times k_t}{\rightleftharpoons}} Join^{-1}_{V'R'} + aux_{hr'tp} \tag{B.15a}$$
$$Join^{-1}_{V'R'} + aux_{tphpr'} \underset{k_{bnd}}{\overset{k_{bnd}}{\rightleftharpoons}} Join^{-2}_{V'R'} + sig_{hpr'tq} \tag{B.15b}$$
$$sig_{hpr'tq} + Fork_{V'R'} \underset{k_{bnd}}{\overset{k_{bnd}}{\rightleftharpoons}} Fork^{-1}_{V'R'} + aux_{tphpr'} \tag{B.15c}$$
$$Fork^{-1}_{V'R'} + aux_{hr'tp} \underset{k_t}{\overset{k_{bnd}}{\rightleftharpoons}} Fork^{-2}_{V'R'} + R' \tag{B.15d}$$
$$Fork^{-2}_{V'R'} + aux_{hv'tr} \underset{k_t}{\overset{k_t}{\rightleftharpoons}} Fork^{-3}_{V'R'} + V' \tag{B.15e}$$
$$Fork^{-3}_{V'R'} + aux_{hitv} \xrightarrow{k_t} \emptyset \tag{B.15f}$$
$$\tag{B.15g}$$

with the initialisation

$$[Join_{V'R'}](0) = \left[aux_{hr'tp}\right](0) = \left[aux_{tphpr'}\right](0) = C_{max} \tag{B.16a}$$
$$[Fork_{V'R'}](0) = [aux_{hv'tr}](0) = C_{max}\ . \tag{B.16b}$$

When accounting for all the necessary six catalysis reactions, the initial con-

ditions for the auxiliary strands are

$$[Join_{VY'}](0) = [aux_{hytp}](0) = [aux_{tphp}](0) = C_{max} \tag{B.17a}$$
$$[Fork_{VY'}](0) = [aux_{hvty}](0) = C_{max} \tag{B.17b}$$
$$[Join_{V'Y}](0) = \left[aux_{hy'tp}\right](0) = \left[aux_{tphp'}\right](0) = C_{max} \tag{B.17c}$$
$$[Fork_{V'Y}](0) = \left[aux_{hv'ty}\right](0) = C_{max} \tag{B.17d}$$
$$[Join_{VR}](0) = [aux_{hrtp}](0) = [aux_{tphpr}](0) = C_{max} \tag{B.17e}$$
$$[Fork_{VR}](0) = [aux_{hvtr}](0) = [aux_{hitv}](0) = C_{max} \tag{B.17f}$$
$$[Join_{V'R'}](0) = \left[aux_{hr'tp}\right](0) = \left[aux_{tphpr'}\right](0) = C_{max} \tag{B.17g}$$
$$[Fork_{V'R'}](0) = [aux_{hv'tr}](0) = C_{max} \tag{B.17h}$$
$$[Join_{YV}](0) = [aux_{hvtp}](0) = [aux_{tphpv}](0) = C_{max} \tag{B.17i}$$
$$[Fork_{YV}](0) = [aux_{hytv}](0) = [aux_{hity}](0) = C_{max} \tag{B.17j}$$
$$[Join_{Y'V'}](0) = \left[aux_{hv'tp}\right](0) = \left[aux_{tphpv'}\right](0) = C_{max} \tag{B.17k}$$
$$[Fork_{Y'V'}](0) = \left[aux_{hy'tv}\right](0) = C_{max}\ . \tag{B.17l}$$

The presence of the auxiliary strands results in that in the presence of the input species, the cascades are triggered, and the equivalency between the bimolecular reactions in the cascade and the unimolecular reactions of the CRN result from Assumption 4.1, where in the design the concentrations of the auxiliary reactions are considered to be constant.

B.3 Parameterising the reaction rates

When parameterising the toehold binding rates (for example through the complementary degree coefficients) there are several effects that may affect the mapping of the reaction rates in the CRN to the affinities in the DSD reaction rates.

B.3.1 Approximating unimolecular reactions with bimolecular reactions using the approximation of large concentrations

For example the example of the degradation reaction rate, for $Y \to \emptyset$ we have the implementation with bimolecular DSD reactions where

$$Y + JoinY \xrightarrow{c_a \times k_t} JoinY_1 + dY\ . \tag{B.18a}$$

Considering the products $JoinY_1$ and $dY$are waste species which do not have exposed toeholds, we assume an irreversible reaction of inert products. Applying

Assumption 4.1 we can map the unimolecular degradation reaction

$$Y^+ \xrightarrow{a} \emptyset \Rightarrow \dot{y^+} = -ay^+ \tag{B.19}$$

using the DSD network from (B.8a), by parameterising the reaction rate with $a = c_a C_{max} k_t$ s^{-1}, and initialising the strands with $[Y](0) = y^+(0)$, $[JoinY](0) = C_{max} \gg y^+$.

This can be seen from the MAK of the DSD implementation given by

$$\frac{d}{dt}[Y] = -c_a k_t [JoinY][Y] \tag{B.20a}$$

$$\frac{d}{dt}[JoinY] = -c_a k_t [JoinY][Y] \tag{B.20b}$$

where the concentration of the auxiliary species $[JoinY]$ follows the same dynamics as $[Y]$. By design $[JoinY](0) = C_{max} \gg [Y](0)$, $[JoinY](t) \gg [Y](t)$, and $[JoinY](t) > 0$, resulting that

$$\frac{d}{dt}[Y] = -c_a k_t [JoinY][Y] < 0, \forall_t \tag{B.21}$$

and therefore steady state is $[Y]^* = 0$. Given the assumption of large concentrations, we have

$$C_{max} \gg [Y] \Rightarrow [JoinY]^* = C_{max} - [Y](0) \approx C_{max} \Rightarrow \frac{d}{dt}[JoinY] \approx 0\ . \tag{B.22}$$

Then, for large concentrations of C_{max} we have $\frac{d}{dt}[JoinY](t) \approx 0$, and we can approximate the bimolecular reaction with the unimolecular reaction

$$Y^+ \xrightarrow{C_{max} c_a k_t} \emptyset \tag{B.23}$$

and the equivalent reaction rate $a = C_{max} c_a k_t$ of the elementary CRN.

Furthermore, the initial conditions of this approximating unimolecular reaction rate are the same as in the implementation with bimolecular reactions $[Y^+](0) = [Y](0)$. This may not be the case, if there is buffering of one of the input strands in the cascaded reactions.

B.3.2 The impact of initial buffering of strands in reversible and unproductive bindings

Take the example of the implementation of the annihilation reactions where the simultaneous sequestration of V and V' is mediated by a template species $AnnVV$

supplied at a high concentration C_{max}. The species $AnnVV$ has two exposed toeholds and complementary domains to hybridise simultaneously with V and V' to irreversibly produce two waste species without toeholds, and there are two possible pathways for $AnnVV$ to sequester simultaneously V and V' where

$$AnnVV + V \underset{k_{ubnd}}{\overset{c_{VV}\times k_t}{\rightleftharpoons}} Vseq \tag{B.24a}$$

$$Vseq + V' \xrightarrow{c_{VV}\times k_t} W_V + W_{V'} \tag{B.24b}$$

$$AnnVV + V' \underset{k_{ubnd}}{\overset{c_{VV}\times k_t}{\rightleftharpoons}} V'seq \tag{B.24c}$$

$$V'seq + V \xrightarrow{c_{VV}\times k_t} W_V + W_{V'} \ . \tag{B.24d}$$

Within Assumption 4.1, we consider $[AnnVV](t) \approx C_{max}$, to approximate the MAK with the network

$$V \underset{k_{ubnd}}{\overset{C_{max}\times c_{VV}\times k_t}{\rightleftharpoons}} Vseq \tag{B.25a}$$

$$Vseq + V' \xrightarrow{c_{VV}\times k_t} W_V + W_{V'} \tag{B.25b}$$

$$V' \underset{k_{ubnd}}{\overset{C_{max}\times c_{VV}\times k_t}{\rightleftharpoons}} V'seq \tag{B.25c}$$

$$V'seq + V \xrightarrow{c_{VV}\times k_t} W_V + W_{V'} \tag{B.25d}$$

and the respective ODEs given by

$$\frac{d}{dt}[V] = -c_{VV}k_tC_{max}[V] + k_{ubnd}[V_{seq}] - c_{VV}k_t[V]\left[V'_{seq}\right] \tag{B.26a}$$

$$\frac{d}{dt}[V_{seq}] = +c_{VV}k_tC_{max}[V] - k_{ubnd}[V_{seq}] - c_{VV}k_t\left[V'\right][V_{seq}] \tag{B.26b}$$

$$\frac{d}{dt}\left[V'\right] = -c_{VV}k_tC_{max}\left[V'\right] + k_{ubnd}\left[V'_{seq}\right] - c_{VV}k_t\left[V'\right][V_{seq}] \tag{B.26c}$$

$$\frac{d}{dt}\left[V'_{seq}\right] = +c_{VV}k_tC_{max}\left[V'\right] - k_{ubnd}\left[V'_{seq}\right] - c_{VV}k_t[V]\left[V'_{seq}\right] \ . \tag{B.26d}$$

The cascade is irreversible only if species V and V' are present simultaneously, so that the second step can occur. For example, in the absence of V', the strands V that hybridised to $AnnVV$ are released again at a rate k_{ubnd}. However, this reversible reaction will cause a fraction of V to be temporarily sequestered to $AnnVV$.

Example B.1 (Sequestration of signal species in implementation of annihilation)**.** *Consider that for the reactions in* (B.25) *the signal species is absent* $[V'] = 0$*. In that case, it results that* $[V'seq] = 0$ *and the steady state is given by the equilibrium*

between $[V]^*$ *and* $[V_{seq}]^*$*, with*

$$\begin{aligned} 0 &= -c_{VV}k_tC_{max}[V]^* + k_{ubnd}[V_{seq}]^* && \text{(B.27a)} \\ \Rightarrow [V_{seq}]^* &= \frac{c_{VV}k_tC_{max}}{k_{ubnd}}[V]^* \ . && \text{(B.27b)} \end{aligned}$$

In the absence of $[V_{seq}]$*, the intial total amount of the strand* V *is either free or sequestered, with a total amount of strands* $[V_{total}](0) = [V](t) + [V_{seq}](t)$*, and at equilibrium*

$$\begin{aligned} [V]^* &= [V_{total}](0) - [V_{seq}]^* && \text{(B.28a)} \\ &= [V_{total}](0) - \frac{c_{VV}k_tC_{max}}{k_{ubnd}}[V]^* && \text{(B.28b)} \\ \Rightarrow k_{ubnd}[V]^* &= k_{ubnd}[V_{total}](0) - c_{VV}k_tC_{max}[V]^* && \text{(B.28c)} \\ \Rightarrow [V]^* &= \frac{k_{ubnd}}{c_{VV}C_{max}k_t + k_{ubnd}}[V_{total}](0) && \text{(B.28d)} \\ \Rightarrow [V_{seq}]^* &= \frac{c_{VV}C_{max}k_t}{c_{VV}C_{max}k_t + k_{ubnd}}[V_{total}](0) \ . && \text{(B.28e)} \end{aligned}$$

For every quantity of V *introduced, a* fraction *will remain free, and a fraction will be temporarily bound in* $AnnVV$*.*

Definition B.1. *Define the annihilation* buffering coefficient $0 < \gamma_{VV} < 1$ *as*

$$\gamma_{VV} = \frac{k_{ubnd}}{c_{VV}C_{max}k_t + k_{ubnd}}[V_{total}](0) \tag{B.29}$$

resulting that $[V]^* = \gamma_{VV}[V_{total}](0)$ *and* $[V_{seq}]^* = (1-\gamma_{VV})[V_{total}](0)$*.*

We can then show that under Assumption 4.1 the elementary CRN for annihilation

$$V^+ + V^- \xrightarrow{\eta} \emptyset \tag{B.30}$$

can be implemented with the network of DSD reactions from (B.24), with the equivalence

$$\eta = 2c_{VV}k_t\frac{c_{VV}C_{max}k_t}{c_{VV}C_{max}k_t + k_{ubnd}} \tag{B.31}$$

and initial conditions $v^+(0) = \gamma_{VV}[V](0)$, $v^-(0) = \gamma_{VV}[V'](0)$.

Recalling the assumption of signal concentrations much lower that C_{max}, we have that $C_{max} \gg [V]$,$C_{max} \gg [V_{seq}]$, and also $k_{ubnd} \gg c_{VV}k_t[V]$. The result is that the dynamics have fast and a slow components. The fast dynamics result from

$$\frac{d}{dt}[V] \approx -c_{VV}k_tC_{max}[V] + k_{ubnd}[V_{seq}] \quad \text{(B.32a)}$$

$$\frac{d}{dt}[V_{seq}] \approx +c_{VV}k_tC_{max}[V] - k_{ubnd}[V_{seq}] \quad \text{(B.32b)}$$

$$\frac{d}{dt}[V'] \approx -c_{VV}k_tC_{max}[V'] + k_{ubnd}[V'_{seq}] \quad \text{(B.32c)}$$

$$\frac{d}{dt}[V'_{seq}] \approx +c_{VV}k_tC_{max}[V'] - k_{ubnd}[V'_{seq}] \quad \text{(B.32d)}$$

since the bimolecular reactions depend on slower reaction rates and signal rates much lower than C_{max}. At every instant of time where $[V]$ is added or consumed, the fast dynamis keep $[V]$ and $[V_{seq}]$ at equilibrium, and we can use (B.27b), (B.28d) and (B.28e) as constraints approximatively kept during the slower dynamics.

Writing the MAK for the total amount of the strain V, with $[V_{total}] = [V] + [V_{seq}]$, we have that

$$\frac{d}{dt}[V_{total}] = \frac{d}{dt}[V] + \frac{d}{dt}[V_{seq}] \quad \text{(B.33a)}$$

$$= -c_{VV}k_t\left([V]\left[V'_{seq}\right] + \left[V'\right][V_{seq}]\right) . \quad \text{(B.33b)}$$

Using the constraint from the equilibrium of the fast dynamics $[V_{seq}] = \frac{c_{VV}C_{max}k_t}{k_{ubnd}}[V]$ (and $\left[V'_{seq}\right] = \frac{c_{VV}C_{max}k_t}{k_{ubnd}}[V']$) we have

$$\frac{d}{dt}[V_{total}] = -c_{VV}k_t\left([V]\left[V'_{seq}\right] + \left[V'\right][V_{seq}]\right) \quad \text{(B.34a)}$$

$$\approx -c_{VV}k_t\left([V]\frac{c_{VV}C_{max}k_t}{k_{ubnd}}\left[V'\right] + \left[V'\right]\frac{c_{VV}C_{max}k_t}{k_{ubnd}}[V]\right) \quad \text{(B.34b)}$$

$$= -2c_{VV}k_t\frac{c_{VV}C_{max}k_t}{k_{ubnd}}[V]\left[V'\right] . \quad \text{(B.34c)}$$

Writing the dynamics for the fraction of available strands $\frac{d}{dt}[V]$ from the total left free from the fast dynamics we have

$$\frac{d}{dt}[V] = \gamma_{VV}\frac{d}{dt}[V_{total}] = \frac{k_{ubnd}}{c_{VV}C_{max}k_t + k_{ubnd}}\frac{d}{dt}[V_{total}] \quad \text{(B.35a)}$$

$$= -2c_{VV}k_t\frac{c_{VV}C_{max}k_t}{k_{ubnd}}\left(\frac{k_{ubnd}}{c_{VV}C_{max}k_t + k_{ubnd}}\right)[V]\left[V'\right] \quad \text{(B.35b)}$$

$$\Rightarrow \frac{d}{dt}[V] = -2c_{VV}k_t\frac{c_{VV}C_{max}k_t}{c_{VV}C_{max}k_t + k_{ubnd}}[V]\left[V'\right] . \quad \text{(B.35c)}$$

Doing the same for $[V']$ we get the final reduced dynamics

$$\frac{d}{dt}[V] = \frac{-2c_{VV}^2 k_t^2 C_{max}}{c_{VV} C_{max} k_t + k_{ubnd}} [V]\left[V'\right] = -2c_{VV} k_t (1-\gamma_{VV})[V]\left[V'\right] \quad \text{(B.36a)}$$

$$\frac{d}{dt}\left[V'\right] = \frac{-2c_{VV}^2 k_t^2 C_{max}}{c_{VV} C_{max} k_t + k_{ubnd}} [V]\left[V'\right] = -2c_{VV} k_t (1-\gamma_{VV})[V]\left[V'\right] \quad \text{(B.36b)}$$

with the equivalent $\eta = 2c_{VV} k_t \frac{c_{VV} C_{max} k_t}{c_{VV} C_{max} k_t + k_{ubnd}}$.

Interestingly, the gain 2 is a structural consequence, resulting from two possible annihilation pathways. Furthermore, the net annihilation rate depends not only on the reaction rate of the slower reaction ($c_{VV} k_t$) but also on the other parameters that define the fractions of available free and sequestered strands.

The design of the toehold affinities need some care, since

$$c_{VV} C_{max} k_t \gg k_{ubnd} \quad \Rightarrow \quad \eta \approx 2c_{VV} k_t, [V] \ll [V_{total}] \quad \text{(B.37a)}$$

$$c_{VV} C_{max} k_t \ll k_{ubnd} \quad \Rightarrow \quad \eta \approx 2c_{VV} k_t \frac{c_{VV} C_{max} k_t}{k_{ubnd}}, [V] \approx [V_{total}] \ . \quad \text{(B.37b)}$$

The unbinding rate k_{ubnd} is limited by the biophysics of the reaction, and reducing c_{VV} results in a very slow reaction and large concentrations in the operations of the circuits [79]. In practice, the parameterisation $c_{VV} C_{max} k_t$ is kept as large as possible to ensure a very fast reaction and keep low levels of concentrations. However, a faster toehold binding rate $c_{VV} k_t$ leads to the removal of free signal strands, and reduces the availability to trigger other reactions. For $c_{VV} C_{max} k_t = k_{ubnd}$ we get the special case

$$c_{VV} C_{max} k_t = k_{ubnd} \quad \Rightarrow \eta \approx c_{VV} k_t, [V] \approx \tfrac{1}{2}[V_{total}] \quad \text{(B.38)}$$

where η does match the reaction rate of the removal dynamics, but we still need to account for the buffering of half of the signal strands.

This design ensures that the reaction is irreversible only if both species are simultaneously present. However, a fraction of the available signal species will be quickly buffered in the reversible binding for the implementation of the annihilation reaction at the start of the reaction, leading to a very fast consumption of the strand when it is added to the system. The effect of such initial buffering has been also illustrated in [76].

B.3.3 Modelling with finite unbinding reaction

If the simulation accounts for a finite unbinding rate, then the coefficients in the catalysis need to reflect buffering effects of the input strand in the cascade of strands displacements. Considering a finite unbinding rate k_{ubnd} entails that hybridised complementary toeholds can unbind before triggering the strand displacement. The temporarily bound toeholds introduce intermediary species for such unproductive events, increasing the number of species and reactions. The reactions go now through a reversible middle step, where the binding event can either reverse back or trigger the DSD reaction. For example, the network for the catalysis in (4.7) expands to

$$V + JoinYV \underset{k_{ubnd}}{\overset{c_b \times k_t}{\rightleftharpoons}} T_V \underset{k_{bnd}}{\overset{k_{ubnd}}{\rightleftharpoons}} JoinYV_1 + aux\_hvtp \tag{B.39a}$$

$$JoinYV_1 + aux\_tphpv \underset{k_{ubnd}}{\overset{k_{bnd}}{\rightleftharpoons}} T_J \underset{k_{bnd}}{\overset{k_{ubnd}}{\rightleftharpoons}} JoinYV_2 + sig\_hpvtq \tag{B.39b}$$

$$sig\_hpvtq + ForkYV \underset{k_{ubnd}}{\overset{k_{bnd}}{\rightleftharpoons}} T_{sig} \underset{k_{bnd}}{\overset{k_{ubnd}}{\rightleftharpoons}} ForkYV_1 + aux\_tphpv \tag{B.39c}$$

$$ForkYV_1 + aux\_hvtp \underset{k_{ubnd}}{\overset{k_{bnd}}{\rightleftharpoons}} T_{FV} \underset{k_t}{\overset{k_{ubnd}}{\rightleftharpoons}} ForkYV_2 + V \tag{B.39d}$$

$$ForkYV_2 + aux\_hytv \underset{k_{ubnd}}{\overset{k_t}{\rightleftharpoons}} T_{FY} \underset{k_t}{\overset{k_{ubnd}}{\rightleftharpoons}} ForkYV_3 + Y \tag{B.39e}$$

$$ForkYV_3 + aux\_hity \xrightarrow{k_t} \emptyset \tag{B.39f}$$

to include the temporary intermediary and reversible bounded strands.

Assumption B.1. *Assume that the concentrations for intermediary and signal species remain well below than C_{max}, and that $c_b \ll 1$ such that we can consider timescale separation where $c_b k_t \ll k_{bnd}$ and $c_b k_t \ll k_t$.*

Under this assumption, most of the dynamics of the cascade is much faster than the limiting reaction rate $cb \times kt$, and we can employ time scale separation and assumptions of QSS [109].

Applying the approximation of large concentrations from Assumption 4.1,

we can simplify many of the bimolecular reactions to unimolecular reactions, with

$$V \underset{k_{ubnd}}{\overset{C_{max}c_b k_t}{\rightleftharpoons}} T_V \quad \underset{k_{bnd}C_{max}}{\overset{k_{ubnd}}{\rightleftharpoons}} JoinYV_1 \tag{B.40a}$$

$$JoinYV_1 \underset{k_{ubnd}}{\overset{C_{max}k_{bnd}}{\rightleftharpoons}} T_J \quad \underset{k_{bnd}}{\overset{k_{ubnd}}{\rightleftharpoons}} JoinYV_2 + sig\_hpvtq \tag{B.40b}$$

$$sig\_hpvtq \underset{k_{ubnd}}{\overset{C_{max}k_{bnd}}{\rightleftharpoons}} T_{sig} \quad \underset{C_{max}k_{bnd}}{\overset{k_{ubnd}}{\rightleftharpoons}} ForkYV_1 \tag{B.40c}$$

$$ForkYV_1 \underset{k_{ubnd}}{\overset{C_{max}k_{bnd}}{\rightleftharpoons}} T_{FV} \quad \underset{k_t}{\overset{k_{ubnd}}{\rightleftharpoons}} ForkYV_2 + V \tag{B.40d}$$

$$ForkYV_2 \underset{k_{ubnd}}{\overset{C_{max}k_t}{\rightleftharpoons}} T_{FY} \quad \underset{k_t}{\overset{k_{ubnd}}{\rightleftharpoons}} ForkYV_3 + Y \tag{B.40e}$$

$$ForkYV_3 \xrightarrow{C_{max}k_t} \emptyset \ . \tag{B.40f}$$

The respective MAK results

$$\begin{aligned}
\frac{d}{dt}[V] &= -C_{max}c_b k_t [V] - k_t [ForkYV_2][V] + k_{ubnd}[T_V] \\
&\quad + k_{ubnd}[T_{FV}] && \text{(B.41a)} \\
\frac{d}{dt}[T_V] &= -2k_{ubnd}[T_V] + C_{max}c_b k_t [V] \\
&\quad + C_{max}k_{bnd}[JoinYV_1] && \text{(B.41b)} \\
\frac{d}{dt}[JoinYV_1] &= -C_{max}k_{bnd}[JoinYV_1] - C_{max}k_{bnd}[JoinYV_1] \\
&\quad + k_{ubnd}([T_V] + [T_J]) && \text{(B.41c)} \\
\frac{d}{dt}[T_J] &= -2k_{ubnd}[T_J] + C_{max}k_{bnd}[JoinYV_1] \\
&\quad + k_{bnd}[JoinYV_2][sig_hpvtq] && \text{(B.41d)} \\
\frac{d}{dt}[sig_hpvtq] &= -C_{max}k_{bnd}[sig_hpvtq] - k_{bnd}[JoinYV_2][sig_hpvtq] \\
&\quad + k_{ubnd}([T_J] + [T_{sig}]) && \text{(B.41e)} \\
\frac{d}{dt}[T_{sig}] &= -2k_{ubnd}[T_{sig}] + C_{max}k_{bnd}[sig_hpvtq] \\
&\quad + C_{max}k_{bnd}[ForkYV_1] && \text{(B.41f)} \\
\frac{d}{dt}[ForkYV_1] &= -2C_{max}k_{bnd}[ForkYV_1] + k_{ubnd}([T_{sig}] + [T_{FV}]) && \text{(B.41g)} \\
\frac{d}{dt}[T_{FV}] &= -2k_{ubnd}[T_{FV}] + C_{max}k_{bnd}[ForkYV_1] \\
&\quad + k_t [ForkYV_2][V] && \text{(B.41h)} \\
\frac{d}{dt}[ForkYV_2] &= -C_{max}k_t [ForkYV_2] - k_t [ForkYV_2][V] \\
&\quad + k_{ubnd}([T_{FV}] + [T_{FY}]) && \text{(B.41i)} \\
\frac{d}{dt}[T_{FY}] &= -2k_{ubnd}[T_{FY}] + C_{max}k_t [ForkYV_2] \\
&\quad + k_t [ForkYV_3][Y] && \text{(B.41j)} \\
\frac{d}{dt}[ForkYV_3] &= -C_{max}k_t [ForkYV_3] - k_t [ForkYV_3][Y] \\
&\quad + k_{ubnd}[T_{FY}] && \text{(B.41k)} \\
\frac{d}{dt}[Y] &= -k_t [ForkYV_3][Y] + k_{ubnd}[T_{FY}] \ . && \text{(B.41l)}
\end{aligned}$$

To resolve the steady state overall gain, we apply again Assumption 4.1, so that $C_{max} \gg [Y]$, $C_{max} \gg [V]$, and $C_{max} \gg [JoinYV_2]$. We then have at steady

state that

$$0 = -C_{max}k_t\left[ForkYV_3\right]^* - k_t\left[ForkYV_3\right]^*\left[Y\right] + k_{ubnd}\left[T_{FY}\right]^* \quad \text{(B.42a)}$$

$$\Rightarrow \left[ForkYV_3\right]^* = \frac{k_{ubnd}}{k_t\left(C_{max} + \left[Y\right]\right)}\left[T_{FY}\right]^* \quad \text{(B.42b)}$$

$$C_{max} \gg \left[Y\right] \Rightarrow \left[ForkYV_3\right]^* \approx \frac{k_{ubnd}}{C_{max}k_t}\left[T_{FY}\right]^* \ . \quad \text{(B.42c)}$$

Then, we have

$$\begin{aligned} 0 &= -2k_{ubnd}\left[T_{FY}\right]^* + C_{max}k_t\left[ForkYV_2\right]^* + k_t\left[ForkYV_3\right]^*\left[Y\right] && \text{(B.43a)} \\ &\approx -2k_{ubnd}\left[T_{FY}\right]^* + C_{max}k_t\left[ForkYV_2\right]^* + \frac{k_{ubnd}}{C_{max}}\left[T_{FY}\right]^*\left[Y\right] && \text{(B.43b)} \\ \Rightarrow \left[T_{FY}\right]^* &\approx \frac{C_{max}k_t\left[ForkYV_2\right]^*}{2k_{ubnd} - \frac{k_{ubnd}}{C_{max}}\left[Y\right]} = \frac{C_{max}k_t\left[ForkYV_2\right]^*}{k_{ubnd}\left(2 - \frac{\left[Y\right]}{C_{max}}\right)} && \text{(B.43c)} \\ &\approx \frac{C_{max}k_t}{2k_{ubnd}}\left[ForkYV_2\right]^* \ . && \text{(B.43d)} \end{aligned}$$

Carrying on with the steady state conditions for all strands in the cascade, we have

$$\begin{aligned} 0 &= -C_{max}k_t\left[ForkYV_2\right]^* - k_t\left[ForkYV_2\right]^*\left[V\right] \\ &\quad + k_{ubnd}\left(\left[T_{FV}\right]^* + \left[T_{FY}\right]^*\right) && \text{(B.44a)} \\ &\approx -\left(C_{max}k_t + k_t\left[V\right]^*\right)\left[ForkYV_2\right]^* + k_{ubnd}\left[T_{FV}\right]^* \\ &\quad + \frac{1}{2}C_{max}k_t\left[ForkYV_2\right]^* && \text{(B.44b)} \\ \Rightarrow \left[ForkYV_2\right]^* &\approx \frac{k_{ubnd}}{k_t\left(C_{max} - \frac{1}{2}C_{max} + \left[V\right]^*\right)}\left[T_{FV}\right]^* \\ &\approx \frac{2k_{ubnd}}{C_{max}k_t}\left[T_{FV}\right]^* && \text{(B.44c)} \end{aligned}$$

$$
\begin{aligned}
0 &= -2k_{ubnd}\left[T_{FV}\right]^* + C_{max}k_{bnd}\left[ForkYV_1\right]^* \\
&\quad +k_t\left[ForkYV_2\right]^*\left[V\right]^* && \text{(B.45a)} \\
&\approx -2k_{ubnd}\left[T_{FV}\right]^* + C_{max}k_{bnd}\left[ForkYV_1\right]^* \\
&\quad +k_t\frac{2k_{ubnd}}{C_{max}k_t}\left[T_{FV}\right]^*\left[V\right]^* && \text{(B.45b)} \\
\Rightarrow \left[T_{FV}\right]^* &\approx \frac{C_{max}k_{bnd}\left[ForkYV_1\right]^*}{\left(2k_{ubnd}-\frac{2k_{ubnd}}{C_{max}}\left[V\right]^*\right)} \approx \frac{C_{max}k_{bnd}\left[ForkYV_1\right]^*}{2k_{ubnd}\left(1-\frac{\left[V\right]^*}{C_{max}}\right)} \\
&\approx \frac{C_{max}k_{bnd}}{2k_{ubnd}}\left[ForkYV_1\right]^* && \text{(B.45c)}
\end{aligned}
$$

$$
\begin{aligned}
0 &= -2C_{max}k_{bnd}\left[ForkYV_1\right]^* + k_{ubnd}\left[T_{sig}\right]^* \\
&\quad +k_{ubnd}\left[T_{FV}\right]^* && \text{(B.46a)} \\
0 &\approx -2C_{max}k_{bnd}\left[ForkYV_1\right]^* + k_{ubnd}\left[T_{sig}\right]^* \\
&\quad +k_{ubnd}\frac{C_{max}k_{bnd}}{2k_{ubnd}}\left[ForkYV_1\right]^* && \text{(B.46b)} \\
\Rightarrow \left[ForkYV_1\right]^* &\approx \frac{k_{ubnd}\left[T_{sig}\right]^*}{2C_{max}k_{bnd}-\frac{C_{max}k_{bnd}}{2}} \approx \frac{k_{ubnd}\left[T_{sig}\right]^*}{2C_{max}k_{bnd}-\frac{1}{2}C_{max}k_{bnd}} \\
&= \frac{2}{3}\frac{k_{ubnd}}{k_{bnd}C_{max}}\left[T_{sig}\right]^* && \text{(B.46c)}
\end{aligned}
$$

$$
\begin{aligned}
0 &= -2k_{ubnd}\left[T_{sig}\right]^* + C_{max}k_{bnd}\left[sig\_hpvtq\right]^* \\
&\quad +C_{max}k_{bnd}\left[ForkYV_1\right]^* && \text{(B.47a)} \\
0 &\approx -2k_{ubnd}\left[T_{sig}\right]^* + C_{max}k_{bnd}\left[sig\_hpvtq\right]^* \\
&\quad +C_{max}k_{bnd}\frac{2}{3}\frac{k_{ubnd}}{k_{bnd}C_{max}}\left[T_{sig}\right]^* && \text{(B.47b)} \\
\Rightarrow \left[T_{sig}\right]^* &\approx \frac{C_{max}k_{bnd}\left[sig\_hpvtq\right]^*}{2k_{ubnd}-\frac{2}{3}k_{ubnd}} \\
&\approx \frac{3}{4}\frac{C_{max}k_{bnd}}{k_{ubnd}}\left[sig\_hpvtq\right]^* && \text{(B.47c)}
\end{aligned}
$$

$$
\begin{aligned}
0 &= -C_{max}k_{bnd}\left[sig\_hpvtq\right]^* - k_{bnd}\left[JoinYV_2\right]^*\left[sig\_hpvtq\right]^* \\
&\quad +k_{ubnd}\left(\left[T_J\right]^* + \left[T_{sig}\right]^*\right) && \text{(B.48a)} \\
&\approx -\left(C_{max}k_{bnd} + k_{bnd}\left[JoinYV_2\right]^* - k_{ubnd}\frac{3}{4}\frac{C_{max}k_{bnd}}{k_{ubnd}}\right)\left[sig\_hpvtq\right]^* \\
&\quad +k_{ubnd}\left[T_J\right]^* && \text{(B.48b)} \\
\Rightarrow \left[sig\_hpvtq\right]^* &\approx \frac{k_{ubnd}\left[T_J\right]^*}{C_{max}k_{bnd} + k_{bnd}\left[JoinYV_2\right]^* - \frac{3}{4}C_{max}k_{bnd}} \\
&\approx \frac{4k_{ubnd}}{C_{max}k_{bnd}}\left[T_J\right]^* && \text{(B.48c)}
\end{aligned}
$$

$$
\begin{aligned}
0 &= -2k_{ubnd}\left[T_J\right]^* + C_{max}k_{bnd}\left[JoinYV_1\right]^* \\
&\quad +k_{bnd}\left[JoinYV_2\right]^*\left[sig\_hpvtq\right]^* && \text{(B.49a)} \\
&\approx -2k_{ubnd}\left[T_J\right]^* + C_{max}k_{bnd}\left[JoinYV_1\right]^* \\
&\quad +k_{bnd}\left[JoinYV_2\right]^*\frac{4k_{ubnd}}{C_{max}k_{bnd}}\left[T_J\right]^* && \text{(B.49b)} \\
\Rightarrow \left[T_J\right]^* &\approx \frac{C_{max}k_{bnd}\left[JoinYV_1\right]^*}{k_{ubnd}\left(2 - 4\frac{\left[JoinYV_2\right]}{C_{max}}\right)} \\
&\approx \frac{1}{2}\frac{C_{max}k_{bnd}}{k_{ubnd}}\left[JoinYV_1\right]^* && \text{(B.49c)}
\end{aligned}
$$

$$
\begin{aligned}
0 &= -C_{max}k_{bnd}\left[JoinYV_1\right]^* - C_{max}k_{bnd}\left[JoinYV_1\right]^* + k_{ubnd}\left[T_J\right]^* \\
&\quad +k_{ubnd}\left[T_V\right]^* && \text{(B.50a)} \\
&\approx -2C_{max}k_{bnd}\left[JoinYV_1\right]^* + k_{ubnd}\frac{1}{2}\frac{C_{max}k_{bnd}}{k_{ubnd}}\left[JoinYV_1\right]^* \\
&\quad +k_{ubnd}\left[T_V\right]^* && \text{(B.50b)} \\
\Rightarrow \left[JoinYV_1\right]^* &\approx \frac{k_{ubnd}\left[T_V\right]^*}{2C_{max}k_{bnd} - \frac{1}{2}C_{max}k_{bnd}} \\
&= \frac{2}{3}\frac{k_{ubnd}}{C_{max}k_{bnd}}\left[T_V\right]^* && \text{(B.50c)}
\end{aligned}
$$

$$
\begin{aligned}
0 &= -2k_{ubnd}\,[T_V]^* + C_{max}c_b k_t\,[V]^* + C_{max}k_{bnd}\,[JoinYV_1]^* && \text{(B.51a)}\\
&\approx -2k_{ubnd}\,[T_V]^* + C_{max}c_b k_t\,[V]^* \\
&\quad + C_{max}k_{bnd}\frac{2}{3}\frac{k_{ubnd}}{C_{max}k_{bnd}}\,[T_V]^* && \text{(B.51b)}\\
\Rightarrow [T_V]^* &\approx \frac{C_{max}c_b k_t\,[V]^*}{2k_{ubnd} - \frac{2}{3}k_{ubnd}} = \frac{C_{max}c_b k_t}{\frac{4}{3}k_{ubnd}}\,[V]^* \\
&\approx \frac{3}{4}\frac{C_{max}c_b k_t}{k_{ubnd}}\,[V]^*\ . && \text{(B.51c)}
\end{aligned}
$$

We can now write the intermediate steady states as function of $[V]^*$ with

$$
\begin{aligned}
[JoinYV_1]^* &\approx \frac{2}{3}\frac{k_{ubnd}}{C_{max}k_{bnd}}\,[T_V]^* = \frac{2}{3}\frac{k_{ubnd}}{C_{max}k_{bnd}}\frac{3}{4}\frac{C_{max}c_b k_t}{k_{ubnd}}\,[V]^* \\
&= \frac{1}{2}\frac{c_b k_t}{k_{bnd}}\,[V]^* && \text{(B.52a)}\\
[sig\_hpvtq]^* &\approx \frac{4k_{ubnd}}{C_{max}k_{bnd}}\,[T_J]^* \approx \frac{4k_{ubnd}}{C_{max}k_{bnd}}\frac{1}{2}\frac{C_{max}k_{bnd}}{k_{ubnd}}\frac{1}{2}\frac{c_b k_t}{k_{bnd}}\,[V]^* \\
&= \frac{c_b k_t}{k_{bnd}}\,[V]^* && \text{(B.52b)}\\
[ForkYV_1]^* &\approx \frac{2}{3}\frac{k_{ubnd}}{k_{bnd}C_{max}}\,[T_{sig}]^* \approx \frac{2}{3}\frac{k_{ubnd}}{k_{bnd}C_{max}}\frac{3}{4}\frac{C_{max}k_{bnd}}{k_{ubnd}}\,[sig\_hpvtq]^* && \text{(B.52c)}\\
&\approx \frac{2}{3}\frac{k_{ubnd}}{k_{bnd}C_{max}}\frac{3}{4}\frac{C_{max}k_{bnd}}{k_{ubnd}}\frac{c_b k_t}{k_{bnd}}\,[V]^* \\
&= \frac{1}{2}\frac{c_b k_t}{k_{bnd}}\,[V]^* && \text{(B.52d)}\\
[ForkYV_2]^* &\approx \frac{2k_{ubnd}}{C_{max}k_t}\,[T_{FV}]^* \approx \frac{2k_{ubnd}}{C_{max}k_t}\frac{C_{max}k_{bnd}}{2k_{ubnd}}\,[ForkYV_1]^* && \text{(B.52e)}\\
&\approx \frac{2k_{ubnd}}{C_{max}k_t}\frac{C_{max}k_{bnd}}{2k_{ubnd}}\frac{1}{2}\frac{c_b k_t}{k_{bnd}}\,[V]^* = \frac{1}{2}c_b\,[V]^* && \text{(B.52f)}\\
[ForkYV_3]^* &\approx \frac{k_{ubnd}}{C_{max}k_t}\,[T_{FY}]^* \approx \frac{k_{ubnd}}{C_{max}k_t}\frac{C_{max}k_t}{2k_{ubnd}}\,[ForkYV_2]^* \\
&\approx \frac{1}{4}c_b\,[V]^*\ . && \text{(B.52g)}
\end{aligned}
$$

Due to the pathway structure of the cascade, the steady states are not defined only by the parameters, but also by fractional gains due to the fact that the same strand is consumed as an input to different DSD reactions.

Remark B.1. *Only the intermediary structures involved in the unbinding reactions depend on k_{ubnd} (T_V, T_J, T_{sig}, T_{FV}, T_{FY}). For faster unbinding rates, the steady*

state of the temporary bindings get smaller, where

$$[T_V]^* \approx \frac{3}{4}\frac{C_{max}c_b k_t}{k_{ubnd}}[V]^* \Rightarrow \lim_{k_{ubnd}\to\infty}[T_V]^* = 0 \tag{B.53a}$$

$$[T_J]^* \approx \frac{1}{2}\frac{C_{max}k_{bnd}}{k_{ubnd}}[JoinYV_1]^* \Rightarrow \lim_{k_{ubnd}\to\infty}[T_J]^* = 0 \tag{B.53b}$$

$$[T_{sig}]^* \approx \frac{3}{4}\frac{C_{max}k_{bnd}}{k_{ubnd}}[sig\_hpvtq]^* \Rightarrow \lim_{k_{ubnd}\to\infty}[T_{sig}]^* = 0 \tag{B.53c}$$

$$[T_{FV}]^* \approx \frac{C_{max}k_{bnd}}{2k_{ubnd}}[ForkYV_1]^* \Rightarrow \lim_{k_{ubnd}\to\infty}[T_{FV}]^* = 0 \tag{B.53d}$$

$$[T_{FY}]^* \approx \frac{C_{max}k_t}{2k_{ubnd}}[ForkYV_2]^* \Rightarrow \lim_{k_{ubnd}\to\infty}[T_{FY}]^* = 0\ . \tag{B.53e}$$

Definition B.2. *Define the catalysis* buffering coefficient $\gamma_b \leq 1$ *such that*

$$\gamma_b = \frac{1}{1 + 2\frac{C_{max}c_b k_t}{k_{ubnd}} + 2\frac{c_b k_t}{k_{bnd}}}\ . \tag{B.54}$$

Assumption B.2. *Assume that in the design* $c_b k_t \ll k_{bnd}$ *and* $c_b C_{max} k_t \ll k_{ubnd}$*, resulting* $\gamma_b \approx 1$*.*

With such assumption, the biophysics of binding and unbinding reactions limit k_{bnd} and k_{ubnd} and the speed of the circuit. However, it allows us to state an equivalency between the implementation with DSD reactions (considering a finite k_{ubnd}) and the elementary catalysis reaction.

Given the elementary catalysis reaction $V^+ \xrightarrow{b} V^+ + Y^+$ and respective MAK

$$\dot{y}^+ = bv^+ \tag{B.55}$$

under Assumption B.1, we can approximate the parameterisation of the CRN with the parameterisation of the DSD reactions using

$$b = \frac{1}{4} \times c_b \times C_{max} \times k_t\ . \tag{B.56}$$

Furthermore, if Assumption B.2 is valid, we can neglect the buffering of the inputs, and set the initial conditions for the input in the DSD implementation with $\gamma_b \approx 1$, and

$$[V](0) \approx v^+(0)\ . \tag{B.57}$$

To see why, assume QSS for $[ForkYV_3]$, so that we have from the equilibrium

condition of $[ForkYV_3]$ that

$$\frac{d}{dt}[ForkYV_3] = 0 \tag{B.58a}$$
$$\Rightarrow -C_{max}k_t[ForkYV_3] - k_t[ForkYV_3][Y] + k_{ubnd}[T_{FY}] = 0 \tag{B.58b}$$
$$\Rightarrow -k_t[ForkYV_3]^*[Y] = C_{max}k_t[ForkYV_3]^* - k_{ubnd}[T_{FY}]^* \ . \tag{B.58c}$$

and we can express the output dynamics as function of the steady state concentrations with

$$\begin{aligned}
\frac{d}{dt}[Y] &= -k_t[ForkYV_3][Y] + k_{ubnd}[T_{FY}] && \text{(B.59a)}\\
&\approx C_{max}k_t[ForkYV_3]^* - k_{ubnd}[T_{FY}]^* + k_{ubnd}[T_{FY}]^* && \text{(B.59b)}\\
&= C_{max}k_t\frac{1}{4}c_b[V]^* && \text{(B.59c)}\\
\Rightarrow \frac{d}{dt}[Y] &\approx \frac{1}{4}C_{max}k_tc_b[V]^* = b[V]^* \ . && \text{(B.59d)}
\end{aligned}$$

The net reaction rate of the elementary catalisys does not depend on the k_{ubnd}, and the gain from $[V]^*$ to the auxiliary and intermediary strands do not depdend on k_{ubnd} at steady state. The gain $\frac{1}{4}$ and results from additional reactions in the network, and it is a structural property.

The other consequence is that the finite rate k_{ubnd} affects the steady state of the input signal $[V]^* \neq [V](0)$. During the fast dynamics when the intermediary species converge to steady state, a fraction of the input strands is sequestered so that the reversible reactions reach equilibrium. From the MAK in (B.41), we have the conservation law

$$\begin{aligned}
&\frac{d}{dt}[V] + \frac{d}{dt}[T_V] + \frac{d}{dt}[JoinYV_1] + \frac{d}{dt}[T_J] + \frac{d}{dt}[sig_hpvtq]\\
&+\frac{d}{dt}[T_{sig}] + \frac{d}{dt}[ForkYV_1] + \frac{d}{dt}[T_{FV}] = 0 \ .
\end{aligned} \tag{B.60}$$

Comparing the initial conditions with the steady state solutions we have

$$\begin{aligned}
&[V](0) + [T_V](0) + [JoinYV_1](0) + [T_J](0)\\
&+ [sig_hpvtq](0) + [T_{sig}](0) + [ForkYV_1](0) + [T_{FV}](0)\\
&= [V]^* + [T_V]^* + [JoinYV_1]^* + [T_J]^* + [sig_hpvtq]^*\\
&+ [T_{sig}]^* + [ForkYV_1]^* + [T_{FV}]^* && \text{(B.61)}\\
\Rightarrow [V](0) &= [V]^* + [T_V]^* + [JoinYV_1]^* + [T_J]^* + [sig_hpvtq]^* + [T_{sig}]^*\\
&+ [ForkYV_1]^* + [T_{FV}]^* \ . && \text{(B.62)}
\end{aligned}$$

Writing the steady states as function of $[V]^*$ we have

$$\begin{aligned}\frac{[V](0)}{[V]^*} &= 1+\frac{3C_{max}c_bk_t}{4k_{ubnd}}+\frac{c_bk_t}{2k_{bnd}}+\frac{C_{max}c_bk_t}{4k_{ubnd}}+\frac{c_bk_t}{k_{bnd}} \\ &\quad +\frac{3}{4}\frac{C_{max}c_bk_t}{k_{ubnd}}+\frac{c_bk_t}{2k_{bnd}}+\frac{C_{max}c_bk_t}{4k_{ubnd}} \qquad \text{(B.63a)} \\ \Rightarrow \frac{1}{\gamma_b} &= \frac{[V](0)}{[V]^*} = 1+2\frac{C_{max}c_bk_t}{k_{ubnd}}+2\frac{c_bk_t}{k_{bnd}}\ . \qquad \text{(B.63b)}\end{aligned}$$

The value of γ_b quantifies the buffering of the input strand in triggering the cascade, where a fraction of the input strand V is sequestered in the reversible reactions of the DSD cascade. The impact of this buffering effect can be seen in Figure 4.12, and most noticeably in Figure 4.7b, where fractions instantly removed when R^+ or R^- are introduced into the system.

Remark B.2. *We can apply Assumption B.2 to set $\gamma_b \approx 1$, but this entails to slow down the dynamics of the circuit. The faster the gain in the catalysis, the more relevant becomes the buffering of the input, since we are limited by the physics and the unbinding rate k_{ubnd}.*

In this case, the reversibility introduced by a finite unbinding rate introduces an additional mismatch between the input concentrations, and the steady state of the input concentration during the operation of the reaction. If we do not model the unbinding reactions (corresponding to the 'Infinite' mode in Visual DSD) we consider the limit where $k_{ubnd} \to \infty$. In this case we recover a simpler result for an infinite unbinding rate where given the elementary catalysis reaction $V^+ \xrightarrow{b_\infty} V^+ + Y^+$ and respective MAK

$$\dot{y}^+ = b_\infty v^+ \qquad \text{(B.64)}$$

under Assumption B.1, we can approximate the parameterisation of the CRN with the parameterisation of the DSD reactions using

$$b_\infty = \frac{1}{2} \times c_b \times C_{max} \times k_t\ . \qquad \text{(B.65)}$$

This is the equivalency found in some literature [79]. Disregarding the intermediary bounded strands, we remove the number of reactions where the strands are inputs, and the structure of the network introduces a gain of only 1/2.

Assuming an infinite unbinding rate also simplifies the buffering of the input, and how the input concentrations need to be adjusted to compensate for the removed fraction. Assuming $c_bk_t \ll k_{bnd}$, the removal of input strand V due to buffering is

negligible with

$$\frac{[V](0)}{v^{+}(0)} = \left(1 + 2\frac{c_b k_t}{k_{bnd}}\right) \approx 1 \ . \tag{B.66}$$

B.4 DSD program for simulation with VisualDSD

The final program of the DSD system for the system in Section 4.2.3 is provided in this section.

The configuration of the simulation itself is set with directives supplied by Visual DSD. For example, concentrations are set in nM, the number of points is set to 1000, and the directive for compilation is set to 'default' to consider a finite unbinding rate k_{ubnd}. Regarding the solver, it is set for 'deterministicsiff' (since we have timescale separation), with directives to set the tolerances. For a stochastic simulation, the directive 'simulation' should be changed to 'stochastic'.

The parameterisation is set with the directive 'parameters', where we define the reaction rates, initial concentration for the auxiliary species, and the degrees of complementarity of the toeholds with

```
(*              Parameters                    *)
directive parameters [
kbnd = 0.001 (* 1/nM/s *) (* toehold maximum binding rate *)
; kt=0.0001 (* 1/nM/s *) (* toeholds binding rate *)
; kubnd =  0.1 (* 1/s *)  (* unbind rate *)
; simtime = 24000.0 (* simulation time *)
; Cmax = 10000.0  (* nM *)(* initial concentration for auxiliary
  strands *)
(* complementarity degree ratios *)
; ca= 2.5e-03
; cb=  1e-03
; ci= 0.05
; cVV = 0.25
]
```

The strands are programmed using Visual DSD syntax, to define the toehold and specific domains, such that the cascade progresses as expected. We start by defining the toehold and specific domains, where we set maximum toehold binding rates, and unbinding rate with

```
new tr={colour = "green";bind = kt; unbind=kubnd} (* reference *)
new ty={colour = "green";bind = kt; unbind=kubnd} (* feedback input *)
new tv={colour = "red";bind = kt; unbind=kubnd}   (* control action *)
new tp={colour = "blue";bind = kbnd; unbind=kubnd} (* aux *)
new tq={colour = "blue";bind = kbnd; unbind=kubnd} (* aux *)
```

The toeholds that interact with the signal strands are set with a maximum toehold binding rate k_t, while $< tp >$ and $< tq >$ are set with a maximum toehold binding rate k_{bnd}.

The specific domains are defined with

```
(* specific domains for binding domains *)
new dr = {colour = "gray"}
new dr' = {colour = "gray"}
new dy = {colour = "gray"}
new dy' = {colour = "gray"}
new dv = {colour = "gray"}
new dv' = {colour = "gray"}
(* remaining auxiliary domains *)
new hr = {colour = "gray"}
new hv = {colour = "gray"}
new hp = {colour = "blue"}
new hi = {colour = "blue"}
new hr' = {colour = "gray"}
new hv' = {colour = "gray"}
new hp' = {colour = "blue"}
```

Then we can start constructing the signal and auxiliary strands. For example, the definition of the strand Y is given by

```
  def Y()= <ty^ hy>
```

The definition of the auxiliary strand $JoinY$, and the complementary domains for the toehold and specific domains are set with

```
def JoinY() ={ty^(ca)*}:[hy]
```

where ca is the complementary degree of the toehold in $JoinY$.

More complex strands are the ones used in catalysis. For example, the templates for $R \rightarrow R + V$ are defined with

```
def JoinVR() ={tr^(ci)*}:[hr tp^]:[hpr tq^]
def ForkVR() =[hi]:[tv^ hv]:[tr^ hr]:[tp^ hpr]:{tq^*}
```

and involve multiple and different toeholds and specific domains.

Some intermediary and by-product strands like

```
def JoinVR_1() =[tr^(ci) hr]{tp^*}:[hpr tq^]
def JoinVR_2() =[tr^(ci) hr]:[tp^ hpr]:{tq^*}
```

are not present initially, but it can be useful to defined them so we can include their histories in the plot of Visual DSD. The directive 'plot' is followed by a list of concentrations to plot with

```
directive plot
(* dual rail signals *)
sub(R();R'()); sub(Y();Y'()); sub(V();V'())
(* signal strands *)
; R(); R'(); Y(); Y'(); V(); V'()
(* auxiliary strands to implement catalysis *)
;JoinVR()  ;JoinV'R'(); JoinV'Y()  ;JoinVY'()
;ForkVR()  ;ForkV'R'(); ForkV'Y()  ;ForkVY'()
; aux_hrtp() ; aux_hvtr() ; aux_tphpr(); aux_hitv();
JoinVR_1();JoinVR_2();ForkVR_1();ForkVR_2();ForkVR_3();ForkVR_4()
;sig_hprtq()
(* auxiliary strands to implement degradation *)
;JoinY()  ;JoinY'();
(* auxilairy strands to implement annihilation*)
AnnYY()  ; AnnVV()
```

The last section of the program, has the definition of the system to be simulated. In practice, it is an initialisation of the signal strands and all the auxiliary strands. It starts by defining the initial conditions of the signal strands with

```
def System()=(
(* initial conditions of the signal strands *)
0.0*V()
| 0.0*V'()
| 0.0*Y()
| 0.0*Y'()
| 0.0*R'()
| 0.2*R()
(* introduction of R' at half the running time *)
| 0.4*R'()@0.50*simtime
```

where the strands for the reference are introduced at $[R](0) = 0.2\,\text{nM}$ and $[R'](t_{final}/2) = 0.4$ nM, so that for a simulation of t_{final} seconds we have

$$[R](t) = 0.2\,\text{nM} \tag{B.67a}$$

$$[R'](t) = \begin{cases} 0\,\text{nM} & t < \frac{1}{2}t_{final} \\ 0.4\,\text{nM} & \frac{1}{2}t_{final} \leq t < t_{final} \end{cases} \tag{B.67b}$$

It then follows a list initialising all the auxiliary strands at C_{max}. For example,

```
| Cmax*JoinY'V'()
| Cmax*ForkY'V'()
| Cmax*aux_hv'tp()
| Cmax*aux_tphpv'()
| Cmax*aux_hy'tv()
| Cmax * JoinY()
```

```
| Cmax * JoinY'()
| Cmax*AnnVV()
```

The cascades are defined by the presence of these auxiliary templates. Apart from the signal strands R, R', V, V', Y, and Y', all the strands depicted in Figure 4.6 are initialised at a large concentration C_{max}.

B.4.1 Code to simulate in Visual DSD

The system can be run in Visual DSD at https://dsd.azurewebsites.net/beta/ using the final code file given below.

```
(*  Integral feedback circuit using Chen and Cherry reactions  *)

(*                configuration of the simulation             *)
directive concentration nM
directive duration simtime points 1000
directive compilation default
directive tolerance 1.0E-14
directive reltolerance 1.0E-14
directive scale 500.0
directive simulation deterministicstiff (* deterministicstiff *) (*
    stochastic *)

(*               Directive to plot concentrations            *)
directive plot
(* dual rail signals *)
sub(R();R'()); sub(Y();Y'()); sub(V();V'())
(* signal strands *)
; R(); R'(); Y(); Y'(); V(); V'()
(* auxiliary strands to implement catalysis *)
;JoinVR()  ;JoinV'R'(); JoinV'Y()  ;JoinVY'()
;ForkVR()  ;ForkV'R'(); ForkV'Y()  ;ForkVY'()
; aux_hrtp() ; aux_hvtr() ; aux_tphpr(); aux_hitv();
JoinVR_1();JoinVR_2();ForkVR_1();ForkVR_2();ForkVR_3();ForkVR_4()
;sig_hprtq()
(* auxiliary strands to implement degradation *)
;JoinY()  ;JoinY'();
(* auxilairy strands to implement annihilation*)
AnnYY()  ; AnnVV()

(*              Parameters                    *)
directive parameters [
 kbnd = 0.001 (* 1/nM/s *) (* toehold maximum binding rate *)
; kt=0.0001 (* 1/nM/s *) (* toeholds binding rate *)
; kubnd =  0.1 (* 1/s *)  (* unbind rate *)
```

```
; simtime = 24000.0 (* simulation time *)
; Cmax = 10000.0  (* nM *)(* initial concentration for auxiliary
    strands *)
 (* complementarity degree ratios *)
; ca= 2.5e-03
; cb=  1e-03
; ci= 0.05
; cVV = 0.25
]

(*              Definition of the domains             *)
(* toehold domains *)
new tr = {colour = "green";bind = kt; unbind=kubnd} (* reference *)
new ty = {colour = "green";bind = kt; unbind=kubnd} (* feedback input
    *)
new tv = {colour = "red";bind = kt; unbind=kubnd}   (* control action
    *)
new tp = {colour = "blue";bind = kbnd; unbind=kubnd} (* aux *)
new tq = {colour = "blue";bind = kbnd; unbind=kubnd} (* aux *)

(* specific domains for binding domains *)
new dr = {colour = "gray"}
new dr' = {colour = "gray"}
new dy = {colour = "gray"}
new dy' = {colour = "gray"}
new dv = {colour = "gray"}
new dv' = {colour = "gray"}

(* remaining auxiliary domains *)
new hr = {colour = "gray"}
new hv = {colour = "gray"}
new hp = {colour = "blue"}
new hi = {colour = "blue"}
new hr' = {colour = "gray"}
new hv' = {colour = "gray"}
new hp' = {colour = "blue"}


(* --------------------  Definition of the strands to implement the
    DSD reactions --------- *)

(* Signal strands to implement:
         reference input r = R - R';
     the output y = Y-Y' ;
     and the actuation input v = V- V' *)
def R()= <tr^ hr>
```

```
def R'()= <tr^ hr'>
def Y()= <ty^ hy>
def Y'()= <ty^ hy'>
def V()= <tv^ hv>
def V'()= <tv^ hv'>

(*                  DEGRADATION Y->0 and Y'->0           *)
(* templates*)
def JoinY() ={ty^(ca)*}:[hy]
def JoinY'() ={ty^(ca)*}:[hy']
(* by-products *)
def JoinY_1()= [ty^(ca ) hy]
def JoinY'_1()= [ty^(ca) hy']
def dY()=<hy>
def dY'()=<hy'>


(*                 ANNIHILATION  R+R'->0 ,  V+V'->0 , Y+Y'->0
    *)
(* templates *)
def AnnYY()= {ty^*}:[hy hy'*]<ty^*>
def AnnVV()= {tv^(cVV)*}:[hv hv'*]<tv^(cVV)*>
def AnnRR()= {tr^*}:[hr hr'*]<tr^*>

(* by-products *)
def Iv()=[tv^ hv]:<hv>[hv'*]<tv^*>
def Iv'()={tv^*}[hv]{hv'}:[hv'* tv^*]

(* waste species *)
def Wv()=<hv>[hv'* tv^*]
def Wv'()=[tv^ hv]{hv'}
def Wy()=<hy>[hy'* ty^*]
def Wy'()=[ty^ hy]{hy'}

(*                 CATALYSIS R   -> R +  V    *)
(* templates *)
def JoinVR() ={tr^(ci)*}:[hr tp^]:[hpr tq^]
def ForkVR() =[hi]:[tv^ hv]:[tr^ hr]:[tp^ hpr]:{tq^*}
(* auxiliary  *)
def aux_hrtp()= <hr tp^>
def aux_tphpr()= <tp^ hpr>
def aux_hvtr()= <hv tr^>
def aux_hitv()= <hi tv^>
def aux_tqhi() = <tq^ hi>

(*  intermediary and byproducts  *)
```

```
def JoinVR_1() =[tr^(ci) hr]{tp^*}:[hpr tq^]
def JoinVR_2() =[tr^(ci) hr]:[tp^ hpr]:{tq^*}
def ForkVR_1() =[hi]:[tv^ hv]:[tr^ hr]{tp^*}:[hpr tq^]
def ForkVR_2() =[hi]:[tv^ hv]:{tr^*}:[hr tp^]:[hpr tq^]
def ForkVR_3() =[hi]:{tv^*}:[hv tr^]:[hr tp^]:[hpr tq^]
def ForkVR_4() =[hi tv^]:[hv tr^]:[hr tp^]:[hpr tq^]
def sig_hprtq()= <hpr tq^>


(*                CATALYSIS R'   -> R' +  V'    *)
def JoinV'R'() ={tr^(ci)*}:[hr' tp^]:[hpr' tq^]
def ForkV'R'() =[hi]:[tv^ hv']:[tr^ hr']:[tp^ hpr']:{tq^*}
def aux_hr'tp()= <hr' tp^>
def aux_tphpr'()= <tp^ hpr'>
def aux_hv'tr()= <hv' tr^>

(*  intermediary and byproducts  *)
def JoinV'R'_1() =[tr^(ci) hr']{tp^*}:[hpr' tq^]
def JoinV'R'_2() =[tr^(ci) hr']:[tp^ hpr']:{tq^*}
def ForkV'R'_1() =[hi]:[tv^ hv']:[tr^ hr']{tp^*}:[hpr' tq^]
def ForkV'R'_2() =[hi]:[tv^ hv']:{tr^*}:[hr' tp^]:[hpr' tq^]
def ForkV'R'_3() =[hi]:{tv^*}:[hv' tr^]:[hr' tp^]:[hpr' tq^]
def ForkV'R'_4() =[hi tv^]:[hv' tr^]:[hr' tp^]:[hpr' tq^]
def sig_hpr'tq()= <hpr' tq^>


(*                CATALYSIS Y'   ->  Y'+ V    *)
(* templates *)
def JoinVY'() ={ty^(ci)*}:[hy' tp^]:[hp tq^]
def ForkVY'() =[hi]:[tv^ hv]:[ty^ hy']:[tp^ hp]:{tq^*}
(* auxiliary  *)
def aux_hy'tp()= <hy' tp^>
def aux_tphp()= <tp^ hp>
def aux_hvty()= <hv ty^>


(*                CATALYSIS  Y  -> Y +  V'     *)
(* templates *)
def JoinV'Y() ={ty^(ci)*}:[hy tp^]:[hp' tq^]
def ForkV'Y() =[hi]:[tv^ hv']:[ty^ hy]:[tp^ hp']:{tq^*}
(* auxiliary  *)
def aux_hytp()= <hy tp^>
def aux_tphp'()= <tp^ hp'>
def aux_hv'ty()= <hv' ty^>
```

```
(*                CATALYSIS V   ->  V + Y    *)
(* templates *)
def JoinYV() ={tv^(cb)*}:[hv tp^]:[hpv tq^]
def ForkYV() =[hi]:[ty^ hy]:[tv^ hv]:[tp^ hpv]:{tq^*}
(* auxiliary  *)
def aux_hvtp()= <hv tp^>
def aux_tphpv()= <tp^ hpv>
def aux_hytv()= <hy tv^>
def aux_hity()= <hi ty^>

(*                CATALYSIS  V'  ->  V' + Y'     *)
def JoinY'V'() ={tv^(cb)*}:[hv' tp^]:[hpv' tq^]
def ForkY'V'() =[hi]:[ty^ hy']:[tv^ hv']:[tp^ hpv']:{tq^*}
(* auxiliary  *)
def aux_hv'tp()= <hv' tp^>
def aux_tphpv'()= <tp^ hpv'>
def aux_hy'tv()= <hy' tv^>


(*  Definition of the System, with the initialisation of the auxliary
    strands, and the instants of introduction of the input strands R
    and R'  *)
def System()=(
  (* initial conditions of the signal strands *)
   0.0*V()
 | 0.0*V'()
 | 0.0*Y()
 | 0.0*Y'()
 | 0.0*R'()
 | 0.2*R()
 (* introduction of R' at half the running time *)
 | 0.4*R'()@0.50*simtime

(* Inital concentrations of strands for implementation of integral and
     subtractor *)
| Cmax * JoinVY'()
| Cmax * ForkVY'()
| Cmax * aux_hytp()
| Cmax * aux_hvty()
| Cmax * aux_tphp()

| Cmax * JoinV'Y()
| Cmax * ForkV'Y()
| Cmax * aux_hy'tp()
| Cmax * aux_hv'ty()
| Cmax * aux_tphp'()
```

```
| Cmax * JoinVR()
| Cmax * ForkVR()
| Cmax * aux_hrtp()
| Cmax * aux_hvtr()
| Cmax * aux_tphpr()

| Cmax * JoinV'R'()
| Cmax * ForkV'R'()
| Cmax * aux_hr'tp()
| Cmax * aux_hv'tr()
| Cmax * aux_tphpr'()

| Cmax * aux_hitv()

(* Inital concentrations of strands for implementation of the plant *)
| Cmax*JoinYV()
| Cmax*ForkYV()
| Cmax*aux_hvtp()
| Cmax*aux_tphpv()
| Cmax*aux_hytv()
| Cmax*aux_hity()

| Cmax*JoinY'V'()
| Cmax*ForkY'V'()
| Cmax*aux_hv'tp()
| Cmax*aux_tphpv'()
| Cmax*aux_hy'tv()

| Cmax * JoinY()
| Cmax * JoinY'()

(* Initialisation of the strand to implement the annihilation
    reactions *)
| Cmax*AnnVV()
(* | Cmax*AnnYY()*)  (* uncomment to introduce Y + Y'-> 0 *)
)

(* Run the system *)
System()

(*  EOF *)
```

References

[1] D. Endy, "Foundations for engineering biology," *Nature*, vol. 438, no. 7067, pp. 449–453, 2005.

[2] B. Canton, A. Labno, and D. Endy, "Refinement and standardization of synthetic biological parts and devices," *Nature Biotechnology*, vol. 26, no. 7, pp. 787–793, 2008.

[3] S. N. Semenov, A. S. Wong, R. M. Van Der Made, S. G. Postma, J. Groen, H. W. Van Roekel, T. F. De Greef, and W. T. Huck, "Rational design of functional and tunable oscillating enzymatic networks," *Nature Chemistry*, vol. 7, no. 2, pp. 160–165, 2015.

[4] T. S. Gardner, C. R. Cantor, and J. J. Collins, "Construction of a genetic toggle switch in Escherichia coli," *Nature*, vol. 403, no. 6767, pp. 339–342, 2000.

[5] A. A. Nielsen, B. S. Der, J. Shin, P. Vaidyanathan, V. Paralanov, E. A. Strychalski, D. Ross, D. Densmore, and C. A. Voigt, "Genetic circuit design automation," *Science*, vol. 352, no. 6281, 2016.

[6] M. B. Elowitz and S. Leibler, "A synthetic oscillatory network of transcriptional regulators," *Nature*, vol. 403, no. 6767, pp. 335–338, 2000.

[7] T. Sohka, R. A. Heins, R. M. Phelan, J. M. Greisler, C. A. Townsend, and M. Ostermeier, "An externally tunable bacterial band-pass filter," *Proceedings of the National Academy of Sciences*, vol. 106, no. 25, pp. 10135–10140, 2009.

[8] P. E. Purnick and R. Weiss, "The second wave of synthetic biology: from modules to systems," *Nature Reviews Molecular Cell Biology*, vol. 10, no. 6, pp. 410–422, 2009.

[9] D. Del Vecchio, A. J. Ninfa, and E. D. Sontag, "Modular cell biology: retroactivity and insulation," *Molecular Systems Biology*, vol. 4, no. 1, p. 161, 2008.

[10] S. Cardinale and A. P. Arkin, "Contextualizing context for synthetic biology–identifying causes of failure of synthetic biological systems," *Biotechnology Journal*, vol. 7, no. 7, pp. 856–866, 2012.

[11] D. Jeong, M. Klocke, S. Agarwal, J. Kim, S. Choi, E. Franco, and J. Kim, "Cell-free synthetic biology platform for engineering synthetic biological circuits and systems," *Methods and Protocols*, vol. 2, p. 39, may 2019.

[12] J. Garamella, R. Marshall, M. Rustad, and V. Noireaux, "The all E. coli TX-TL Toolbox 2.0: a platform for cell-free synthetic biology," *ACS Synthetic Biology*, vol. 5, no. 4, pp. 344–355, 2016.

[13] M. Yelleswarapu, A. J. Van Der Linden, B. Van Sluijs, P. A. Pieters, E. Dubuc, T. F. De Greef, and W. T. Huck, "Sigma factor-mediated tuning of bacterial cell-free synthetic genetic oscillators," *ACS Synthetic Biology*, vol. 7, no. 12, pp. 2879–2887, 2018.

[14] L. M. Adleman, "Computing with DNA," *Scientific American*, vol. 279, no. 2, pp. 54–61, 1998.

[15] D. Y. Zhang and G. Seelig, "Dynamic dna nanotechnology using strand-displacement reactions," *Nature Chemistry*, vol. 3, no. 2, pp. 103–113, 2011.

[16] A. Baccouche, K. Montagne, A. Padirac, T. Fujii, and Y. Rondelez, "Dynamic DNA-toolbox reaction circuits: A walkthrough," *Methods*, vol. 67, no. 2, pp. 234–249, 2014.

[17] N. Srinivas, T. E. Ouldridge, P. Šulc, J. M. Schaeffer, B. Yurke, A. A. Louis, J. P. Doye, and E. Winfree, "On the biophysics and kinetics of toehold-mediated DNA strand displacement," *Nucleic Acids Research*, vol. 41, no. 22, pp. 10641–10658, 2013.

[18] P. Irmisch, T. E. Ouldridge, and R. Seidel, "Modeling DNA-strand displacement reactions in the presence of base-pair mismatches," *Journal of the American Chemical Society*, vol. 142, no. 26, pp. 11451–11463, 2020.

[19] A. J. Turberfield, J. Mitchell, B. Yurke, A. P. Mills Jr, M. Blakey, and F. C. Simmel, "DNA fuel for free-running nanomachines," *Physical Review Letters*, vol. 90, no. 11, p. 118102, 2003.

[20] G. Seelig, D. Soloveichik, D. Y. Zhang, and E. Winfree, "Enzyme-free nucleic acid logic circuits," *Science*, vol. 314, no. 5805, pp. 1585–1588, 2006.

[21] D. Soloveichik, G. Seelig, and E. Winfree, "DNA as a universal substrate for chemical kinetics," *Proceedings of the National Academy of Sciences*, vol. 107, no. 12, pp. 5393–5398, 2010.

[22] M. You, G. Zhu, T. Chen, M. J. Donovan, and W. Tan, "Programmable and multiparameter dna-based logic platform for cancer recognition and targeted therapy," *Journal of the American Chemical Society*, vol. 137, no. 2, pp. 667–674, 2015.

[23] S. Bi, S. Yue, and S. Zhang, "Hybridization chain reaction: a versatile molecular tool for biosensing, bioimaging, and biomedicine," *Chemical Society Reviews*, vol. 46, no. 14, pp. 4281–4298, 2017.

[24] F. C. Simmel, B. Yurke, and H. R. Singh, "Principles and applications of nucleic acid strand displacement reactions," *Chemical Reviews*, vol. 119, no. 10, pp. 6326–6369, 2019.

[25] R. M. Dirks and N. A. Pierce, "Triggered amplification by hybridization chain reaction," *Proceedings of the National Academy of Sciences*, vol. 101, no. 43, pp. 15275–15278, 2004.

[26] L. Qian and E. Winfree, "A simple DNA gate motif for synthesizing large-scale circuits.," *Journal of the Royal Society Interface*, vol. 8, pp. 1281–1297, sep 2011.

[27] L. Qian, E. Winfree, and J. Bruck, "Neural network computation with DNA strand displacement cascades," *Nature*, vol. 475, no. 7356, pp. 368–372, 2011.

[28] C. Zechner, G. Seelig, M. Rullan, and M. Khammash, "Molecular circuits for dynamic noise filtering," *Proceedings of the National Academy of Sciences*, vol. 113, no. 17, pp. 4729–4734, 2016.

[29] N. Srinivas, J. Parkin, G. Seelig, E. Winfree, and D. Soloveichik, "Enzyme-free nucleic acid dynamical systems," *Science*, vol. 358, no. 6369, 2017.

[30] A. J. Genot, J. Bath, and A. J. Turberfield, "Combinatorial Displacement of DNA Strands: Application to Matrix Multiplication and Weighted Sums," *Angewandte Chemie*, vol. 125, no. 4, pp. 1227–1230, 2013.

[31] T. Song, S. Garg, R. Mokhtar, H. Bui, and J. Reif, "Analog computation by DNA strand displacement circuits," *ACS Synthetic Biology*, vol. 5, no. 8, pp. 898–912, 2016.

[32] C. Zou, X. Wei, Q. Zhang, C. Liu, and Y. Liu, "Solution of equations based on analog DNA strand displacement circuits," *IEEE Transactions on Nanobioscience*, vol. 18, no. 2, pp. 191–204, 2019.

[33] L. Oesinghaus and F. C. Simmel, "Nucleic acid-based computing in living cells using strand displacement processes," *DNA-and RNA-Based Computing Systems*, pp. 247–264, 2021.

[34] J. Hemphill and A. Deiters, "DNA computation in mammalian cells: MicroRNA logic operations," *Journal of the American Chemical Society*, vol. 135, no. 28, pp. 10512–10518, 2013.

[35] B. Groves, Y.-J. Chen, C. Zurla, S. Pochekailov, J. L. Kirschman, P. J. Santangelo, and G. Seelig, "Computing in mammalian cells with nucleic acid strand exchange," *Nature Nanotechnology*, vol. 11, no. 3, pp. 287–294, 2016.

[36] G. Chatterjee, Y.-J. Chen, and G. Seelig, "Nucleic acid strand displacement with synthetic mRNA inputs in living mammalian cells," *ACS Synthetic Biology*, vol. 7, no. 12, pp. 2737–2741, 2018.

[37] N. Dalchau, G. Szép, R. Hernansaiz-Ballesteros, C. P. Barnes, L. Cardelli, A. Phillips, and A. Csikász-Nagy, "Computing with biological switches and clocks," *Natural Computing*, vol. 17, no. 4, pp. 761–779, 2018.

[38] D. Del Vecchio, A. J. Dy, and Y. Qian, "Control theory meets synthetic biology.," *Journal of the Royal Society*, vol. 13, no. 120, pp. 3–43, 2016.

[39] D. Del Vecchio, Y. Qian, R. M. Murray, and E. D. Sontag, "Future systems and control research in synthetic biology," *Annual Reviews in Control*, vol. 45, pp. 5–17, 2018.

[40] F. Blanchini and G. Giordano, "Structural stability of biochemical networks: quadratic vs. polyhedral Lyapunov functions," *IFAC-PapersOnLine*, vol. 48, no. 14, pp. 278–283, 2015.

[41] M. Al-Radhawi and D. Angeli, "New Approach to the Stability of Chemical Reaction Networks: Piecewise Linear in Rates Lyapunov Functions," *IEEE Transactions on Automatic Control*, vol. 61, no. 1, pp. 76–89, 2016.

[42] R. Daniel, J. R. Rubens, R. Sarpeshkar, and T. K. Lu, "Synthetic analog computation in living cells," *Nature*, vol. 497, no. 7451, pp. 619–623, 2013.

[43] Y. Qian, C. McBride, and D. Del Vecchio, "Programming cells to work for us," *Annual Review of Control, Robotics, and Autonomous Systems*, vol. 1, no. 1, pp. 411–440, 2018.

[44] F. Blanchini, H. Ei-Samad, G. Giordano, and E. D. Sontag, "Control-theoretic methods for biological networks," in *Proceedings of the IEEE Conference on Decision and Control*, vol. 2018-Decem, pp. 466–483, 2019.

[45] E. J. Hancock and J. Ang, "Frequency domain properties and fundamental limits of buffer-feedback regulation in biochemical systems," *Automatica*, vol. 103, pp. 330–336, 2019.

[46] M. Siami, N. Motee, G. Buzi, B. Bamieh, M. Khammash, and J. C. Doyle, "Fundamental limits and tradeoffs in autocatalytic pathways," *IEEE Transactions on Automatic Control*, vol. 65, pp. 733–740, feb 2020.

[47] G. Ferreres, J. M. Biannic, Biannic, G. Ferreres, and J. M. Biannic, "Reliable computation of the robustness margin for a flexible aircraft," *Control Engineering Practice*, vol. 9, no. 12, pp. 1267–1278, 2001.

[48] D. G. Bates and I. Postlethwaite, "The structured singular value and mu-analysis," *Advanced Techniques for Clearance of Flight Control Laws*, pp. 37–55, 2002.

[49] L. Ma and P. A. Iglesias, "Quantifying robustness of biochemical network models.," *BMC Bioinformatics*, vol. 3, no. 1, p. 38, 2002.

[50] J. Kim, D. G. Bates, I. Postlethwaite, L. Ma, and P. A. Iglesias, "Robustness analysis of biochemical network models," *Systems Biology, IEE Proceedings*, vol. 153, no. 3, pp. 96–104, 2006.

[51] T. P. Prescott and A. Papachristodoulou, "Synthetic biology: A control engineering perspective," *2014 European Control Conference (ECC)*, pp. 1182–1186, 2014.

[52] F. He, E. Murabito, and H. V. Westerhoff, "Synthetic biology and regulatory networks: where metabolic systems biology meets control engineering," *Journal of The Royal Society Interface*, vol. 13, no. 117, p. 20151046, 2016.

[53] U. Alon, *An Introduction to Systems Biology Design Principles of Biological Circuits*. CRC Press, 2007.

[54] B. P. Ingalls, *Mathematical Modeling in Systems Biology: An Introduction*. Mathematical Modeling in Systems Biology, Cambridge, MA: The MIT Press, 2012.

[55] E. D. Sontag, "Molecular Systems Biology and Control," *European Journal of Control*, vol. 11, no. 4-5, pp. 396–435, 2005.

[56] D. Angeli and E. D. Sontag, "Monotone Control Systems," *IEEE TRANSACTIONS ON AUTOMATIC CONTROL*, vol. 48, no. 10, pp. 1684–1698, 2003.

[57] C. Cosentino and D. G. Bates, *Feedback control in systems biology*. CRC Press, 2012.

[58] J. E. Ferrell and S. H. Ha, "Ultrasensitivity part I: Michaelian responses and zero-order ultrasensitivity," *Trends in Biochemical Sciences*, vol. 39, no. 10, pp. 496–503, 2014.

[59] C. Briat, C. Zechner, and M. Khammash, "Design of a synthetic integral feedback circuit: dynamic analysis and DNA implementation," *ACS Synthetic Biology*, vol. 5, no. 10, pp. 1108–1116, 2016.

[60] C. Cuba Samaniego and E. Franco, "An ultrasensitive biomolecular network for robust feedback control," *IFAC-PapersOnLine*, vol. 50, no. 1, pp. 10950–10956, 2017.

[61] A. W. K. Harris, J. A. Dolan, C. L. Kelly, J. Anderson, and A. Papachristodoulou, "Designing genetic feedback controllers," *IEEE Transactions on Biomedical Circuits and Systems*, vol. 9, pp. 475–484, aug 2015.

[62] T. Y. Chiu, H. J. K. Chiang, R. Y. Huang, J. H. R. Jiang, and F. Fages, "Synthesizing configurable biochemical implementation of linear systems from their transfer function specifications," *PLoS ONE*, vol. 10, no. 9, p. e0137442, 2015.

[63] P. Tóth and J. Érdi, *Mathematical Models of Chemical Reactions: Theory and Applications of Deterministic and Stochastic Models*. Manchester University Press, 1989.

[64] M. Koch, J.-L. Faulon, and O. Borkowski, "Models for cell-free synthetic biology: make prototyping easier, better, and faster," *Frontiers in Bioengineering and Biotechnology*, vol. 6, pp. 1–6, nov 2018.

[65] O. Bournez, D. S. Graça, and A. Pouly, "Polynomial time corresponds to solutions of polynomial ordinary differential equations of polynomial length," *Journal of the ACM*, vol. 64, no. 6, pp. 1–76, 2017.

[66] F. Fages, G. Le Guludec, O. Bournez, and A. Pouly, "Strong Turing completeness of continuous chemical reaction networks and compilation of mixed analog-digital programs," in *Computational Methods in Systems Biology*, vol. 10545 LNBI, pp. 108–127, Springer, Cham, 2017.

[67] M. Vasić, D. Soloveichik, and S. Khurshid, "CRN++: Molecular programming language," *Natural Computing*, vol. 11145 LNCS, pp. 1–18, jan 2020.

[68] H. J. Buisman, H. M. M. ten Eikelder, P. A. J. Hilbers, and A. M. L. Liekens, "Computing Algebraic Functions with Biochemical Reaction Networks," *Artificial Life*, vol. 15, no. 1, pp. 5–19, 2008.

[69] S. A. Salehi, K. K. Parhi, and M. D. Riedel, "Chemical Reaction Networks for Computing Polynomials," *ACS Synthetic Biology*, vol. 6, no. 1, pp. 76–83, 2017.

[70] H.-L. Chen, D. Doty, and D. Soloveichik, "Rate-independent computation in continuous chemical reaction networks," in *Proceedings of the 5th Conference on Innovations in Theoretical Computer Science*, pp. 313–326, 2014.

[71] C. Zou, X. Wei, Q. Zhang, C. Liu, C. Zhou, and Y. Liu, "Four-analog computation based on DNA strand displacement," *ACS Omega*, vol. 2, no. 8, pp. 4143–4160, 2017.

[72] Y.-J. Chen, N. Dalchau, N. Srinivas, A. Phillips, L. Cardelli, D. Soloveichik, and G. Seelig, "Programmable chemical controllers made from DNA," *Nature Nanotechnology*, vol. 8, no. 10, pp. 755–762, 2013.

[73] L. Cardelli, "Two-domain DNA strand displacement," *Mathematical Structures in Computer Science*, vol. 23, pp. 247–271, apr 2013.

[74] J. X. Zhang, J. Z. Fang, W. Duan, L. R. Wu, A. W. Zhang, N. Dalchau, B. Yordanov, R. Petersen, A. Phillips, and D. Y. Zhang, "Predicting DNA hybridization kinetics from sequence," *Nature Chemistry*, vol. 10, no. 1, pp. 91–98, 2018.

[75] A. Phillips and L. Cardelli, "A programming language for composable DNA circuits," *Journal of The Royal Society Interface*, vol. 6, no. Suppl_4, pp. S419–S436, 2009.

[76] B. Yordanov, J. Kim, R. L. Petersen, A. Shudy, V. V. Kulkarni, and A. Phillips, "Computational Design of Nucleic Acid Feedback Control Circuits," *ACS Synthetic Biology*, vol. 3, no. 8, pp. 600–616, 2014.

[77] S. Badelt, S. W. Shin, R. F. Johnson, Q. Dong, C. Thachuk, and E. Winfree, "A general-purpose CRN-to-DSD compiler with formal verification, optimization, and simulation capabilities," in *DNA Computing and Molecular Programming*, pp. 232–248, Springer International Publishing, 2017.

[78] C. Cosentino, R. Ambrosino, M. Ariola, M. Bilotta, A. Pironti, and F. Amato, "On the realization of an embedded subtractor module for the control of chemical reaction networks," *IEEE Transactions on Automatic Control*, vol. 61, no. 11, pp. 3638–3643, 2016.

[79] K. Oishi and E. Klavins, "Biomolecular implementation of linear I/O systems.," *IET Systems Biology*, vol. 5, no. 4, pp. 252–260, 2011.

[80] M. R. Lakin, S. Youssef, F. Polo, S. Emmott, and A. Phillips, "Visual DSD: a design and analysis tool for DNA strand displacement systems," *Bioinformatics*, vol. 27, no. 22, pp. 3211–3213, 2011.

[81] J. M. Maciejowski, *Multivariable Feedback Design*. Addison-Wesley, 1989.

[82] S. Skogestad and I. Postlethwaite, *Multivariable Feedback Control: Analysis and Design*. John Wiley, 2005.

[83] J. C. Doyle, B. A. Francis, and A. R. Tannenbaum, *Feedback Control Theory*. Dover, 1992.

[84] K. Zhou, J. C. Doyle, and K. K. Glover, *Robust and Optimal Control*. Prentice Hall, 1996.

[85] D. Hinrichsen and A. J. Pritchard, *Mathematical Systems Theory I: Modelling, State Space Analysis, Stability and Robustness*, vol. 48 of *Texts in Applied Mathematics*. Springer Berlin Heidelberg, 2005.

[86] G. E. Dullerud and F. Paganini, *A Course in Robust Control Theory*, vol. 36 of *Texts in Applied Mathematics*. Springer New York, 2000.

[87] S. Boyd, L. El Ghaoui, E. Feron, and V. Balakrishnan, *Linear Matrix Inequalities in System and Control Theory*. Society for Industrial and Applied Mathematics, 1994.

[88] H. Khalil, *Nonlinear control, Global Edition*. Essex, England: Pearson Education Limited, 2015.

[89] J.-J. E. Slotine and W. Li, *Applied Nonlinear Control*. Prentice Hall, 1991.

[90] A. van der Schaft, *L2 - Gain and Passivity Techniques in Nonlinear Control*, vol. 218 of *Communications and Control Engineering*. Springer London, 2000.

[91] S. H. Strogatz, *Nonlinear Dynamics and Chaos : with applications to physics, biology, chemistry, and engineering*. Westview Press, 2nd ed., 2015.

[92] D. G. Luenberger, *Introduction to Dynamic Systems: Theory, Models, and Applications*. Wiley, 1979.

[93] O.-T. Chis, A. F. Villaverde, J. R. Banga, and E. Balsa-Canto, "On the relationship between sloppiness and identifiability," *Mathematical Biosciences*, vol. 282, pp. 147–161, dec 2016.

[94] M. Foo, R. Sawlekar, and D. G. Bates, "Exploiting the dynamic properties of covalent modification cycle for the design of synthetic analog biomolecular circuitry," *Journal of Biological Engineering*, vol. 10, no. 1, p. 15, 2016.

[95] R. Sawlekar, F. Montefusco, V. V. Kulkarni, and D. G. Bates, "Implementing Nonlinear Feedback Controllers Using DNA Strand Displacement Reactions," *IEEE Transactions on NanoBioscience*, vol. 15, no. 5, pp. 443–454, 2016.

[96] Camilla Trane and E. W. Jacobsen, "Structural robustness of biochemical networks: quantifying robustness and identifying fragilities," in *Control Theory and Systems Biology* (P. A. Iglesias and B. P. Ingalls, eds.), ch. 10, pp. 189–224, MIT Press, 2010.

[97] J. Kim and D. G. Bates, "Robustness of Oscillations in Biological Systems," in *Control Theory and Systems Biology* (P. Iglesias and B. Ingalls, eds.), pp. 225–242, MIT Press., 2010.

[98] J. Doyle, "Analysis of feedback systems with structured uncertainties," *IEE Proceedings D Control Theory and Applications*, vol. 129, no. 6, p. 242, 1982.

[99] J. Doyle, A. Packard, and K. Zhou, "Review of LFTs, LMIs, and mu," in *Proceedings of IEEE Conference on Decision and Control*, pp. 1227–1232, IEEE, 1991.

[100] R. Brijder, "Computing with chemical reaction networks: a tutorial," *Natural Computing*, vol. 9, no. 1, pp. 119–137, 2018.

[101] D. Angeli, "A tutorial on chemical reaction network dynamics," *European Journal of Control*, vol. 15, no. 3-4, pp. 398–406, 2009.

[102] A. David and E. D. Sontag, "Graphs and the dynamics of biochemical networks," in *Control Theory and Systems Biology*, pp. 125–143, MIT Press, 2010.

[103] M. Feinberg, "Chemical reaction network structure and the stability of complex isothermal reactors-I. The deficiency zero and deficiency one theorems," *Chemical Engineering Science*, vol. 42, no. 10, pp. 2229–2268, 1987.

[104] G. Craciun and M. Feinberg, "Multiple equilibria in complex chemical reaction networks: II. The species-reaction graph," *SIAM Journal on Applied Mathematics*, vol. 66, no. 4, pp. 1321–1338, 2006.

[105] G. Craciun and M. Feinberg, "Multiple equilibria in complex chemical reaction networks: I. The injectivity property," *SIAM Journal on Applied Mathematics*, vol. 65, no. 5, pp. 1526–1546, 2005.

[106] G. Shinar, U. Alon, and M. Feinberg, "Sensitivity and robustness in chemical reaction networks," *SIAM Journal on Applied Mathematics*, vol. 69, no. 4, pp. 977–998, 2009.

[107] I. Otero-Muras, G. Szederkényi, K. M. Hangos, and A. A. Alonso, "Dynamic analysis and control of biochemical reaction networks," *Mathematics and Computers in Simulation*, vol. 79, no. 4, pp. 999–1009, 2008.

[108] J. D. Murray, *Mathematical Biology*, vol. 17 of *Interdisciplinary Applied Mathematics*. Springer New York, 2004.

[109] P. Kokotovic, H. K. Khalil, and J. O'Reilly, *Singular Perturbation Methods in Control: Analysis and Design (vol 25)*. Siam, 1999.

[110] O. Radulescu, A. N. Gorban, A. Zinovyev, and V. Noel, "Reduction of dynamical biochemical reactions networks in computational biology," *Frontiers in Genetics*, vol. 3, p. 131, 2012.

[111] F. Blanchini and G. Giordano, "Piecewise-linear Lyapunov functions for structural stability of biochemical networks," *Automatica*, vol. 50, no. 10, pp. 2482–2493, 2014.

[112] D. T. Gillespie, "The chemical Langevin equation," *The Journal of Chemical Physics*, vol. 113, no. 1, pp. 297–306, 2000.

[113] N. G. Van Kampen, *Stochastic Processes in Physics and Chemistry*. Elsevier, 2007.

[114] L. Cardelli, M. Kwiatkowska, and L. Laurenti, "Stochastic analysis of chemical reaction networks using linear noise approximation," *BioSystems*, vol. 149, pp. 26–33, 2016.

[115] C. A. Gómez-Uribe and G. C. Verghese, "Mass fluctuation kinetics: capturing stochastic effects in systems of chemical reactions through coupled mean-variance computations," *Journal of Chemical Physics*, vol. 126, no. 2, 2007.

[116] D. T. Gillespie, "A rigorous derivation of the master chemical equation," *Physica*, vol. 188, pp. 404–425, 1992.

[117] D. T. D. Gillespie, "Stochastic simulation of chemical kinetics.," *Annual Review of Physical Chemistry*, vol. 58, pp. 35–55, 2007.

[118] G. Shinar and M. Feinberg, "Structural sources of robustness in biochemical reaction networks.," *Science*, vol. 327, no. 5971, pp. 1389–91, 2010.

[119] G. Shinar and M. Feinberg, "Design principles for robust biochemical reaction networks: what works, what cannot work, and what might almost work.," *Mathematical Biosciences*, vol. 231, no. 1, pp. 39–48, 2011.

[120] D. Hinrichsen and E. Plischke, "Robust stability and transient behaviour of positive linear systems," *Vietnam Journal of Mathematics*, vol. 35, no. 4, pp. 429–462, 2007.

[121] F. Knorn, O. Mason, and R. Shorten, "On linear co-positive Lyapunov functions for sets of linear positive systems," *Automatica*, vol. 45, no. 8, pp. 1943–1947, 2009.

[122] L. Farina and S. Rinaldi, *Positive Linear Systems: Theory and Applications*. Wiley, 2000.

[123] L. Farina, "Positive systems in the state space approach: main issues and recent results," in *Proceedings of the 15th International Symposium on Mathematical Theory of Networks and Systems*, p. 14900_1, 2002.

[124] N. K. Son and D. Hinrichsen, "Robust stability of positive continuous time systems," *Numerical Functional Analysis and Optimization*, vol. 17, no. 5-6, pp. 649–659, 1996.

[125] D. Hinrichsen, A. Fischer, and N. K. Son, "Stability radii of Metzler operators," *Vietnam Journal of Mathematics*, vol. 26, no. 1, pp. 147–163, 1998.

[126] K.-K. K. Kim and R. D. Braatz, "Computational complexity and related topics of robustness margin calculation using μ theory: A review of theoretical developments," *Computers & Chemical Engineering*, vol. 70, pp. 122–132, 2014.

[127] D. Hinrichsen and N. Son, "Mu-analysis and robust stability of positive linear systems," *International Journal of Applied Mathematics and Computer Science*, vol. 8, no. 2, pp. 253–268, 1998.

[128] B. Roszak and E. J. Davison, "Necessary and sufficient conditions for stabilizability of positive LTI systems," *Systems and Control Letters*, vol. 58, no. 7, pp. 474–481, 2009.

[129] P. De Leenheer and D. Aeyels, "Stabilization of positive linear systems," *Systems & Control Letters*, vol. 44, no. 4, pp. 259–271, 2001.

[130] M. A. Rami and F. Tadeo, "Controller synthesis for positive linear systems with bounded controls," *IEEE Transactions on Circuits and Systems II: Express Briefs*, vol. 54, no. 2, pp. 151–155, 2007.

[131] M. A. Rami, "Solvability of static output-feedback stabilization for LTI positive systems," *Systems and Control Letters*, vol. 60, no. 9, pp. 704–708, 2011.

[132] A. Rantzer, "Scalable control of positive systems," *European Journal of Control*, vol. 24, pp. 72–80, 2015.

[133] Y. Ebihara, D. Peaucelle, and D. Arzelier, "Optimal L1 -controller synthesis for positive systems and its robustness properties," *American Control Conference*, pp. 5992–5997, 2012.

[134] X. Chen, J. Lam, P. Li, and Z. Shu, "L1-induced norm and controller synthesis of positive systems," *Automatica*, vol. 49, no. 5, pp. 1377–1385, 2013.

[135] X. Chen, M. Chen, W. Qi, and J. Shen, "Dynamic output-feedback control for continuous-time interval positive systems under L1 performance," *Applied Mathematics and Computation*, vol. 289, pp. 48–59, 2016.

[136] J. Shen and J. Lam, "Static output-feedback stabilization with optimal," *Automatica*, vol. 63, pp. 248–253, 2016.

[137] C. Briat, "Robust stability and stabilization of uncertain linear positive systems via integral linear constraints: L_1 gain and L_∞-gain characterization," *International Journal of Robust and Nonlinear Control*, vol. 23, no. 17, pp. 1932–1954, 2013.

[138] Y. Ebihara, D. Peaucelle, and D. Arzelier, "LMI approach to linear positive system analysis and synthesis," *Systems & Control Letters*, vol. 63, pp. 50–56, 2014.

[139] T. Tanaka and C. Langbort, "The bounded real lemma for internally positive systems and H-infinity structured static state feedback," *IEEE Transactions on Automatic Control*, vol. 56, no. 9, pp. 2218–2223, 2011.

[140] G. S. Deaecto and J. C. Geromel, "H2 state feedback control design of positive switched linear systems," *IFAC-PapersOnLine*, vol. 50, no. 1, pp. 3081–3086, 2017.

[141] F. Cacace, A. Germani, and C. Manes, "Representation on a class of polynomial MIMO systems via positive realizations," in *2009 European Control Conference*, pp. 254–259, IEEE, 2009.

[142] F. Cacace, L. Farina, A. Germani, and C. Manes, "Internally positive representation of a class of continuous time systems," *IEEE Transactions on Automatic Control*, vol. 57, no. 12, pp. 3158–3163, 2012.

[143] R. Horton, L. Mauran, D. Rawn, G. Scrimgeour, and M. Perry, *Principles of Biochemistry, 5th Edition*. Pearson Education, 5 ed., 2011.

[144] D. Y. Zhang, "Cooperative hybridization of oligonucleotides," *Journal of the American Chemical Society*, vol. 133, no. 4, pp. 1077–1086, 2011.

[145] K. M. Cherry and L. Qian, "Scaling up molecular pattern recognition with DNA-based winner-take-all neural networks," *Nature*, vol. 559, no. 7714, pp. 370–376, 2018.

[146] J. N. Zadeh, C. D. Steenberg, J. S. Bois, B. R. Wolfe, M. B. Pierce, A. R. Khan, R. M. Dirks, and N. A. Pierce, "NUPACK: analysis and design of nucleic acid systems," *Journal of computational chemistry*, vol. 32, no. 1, pp. 170–173, 2011.

[147] M. R. Lakin, R. L. Petersen, and A. Phillips, *Visual DSD User Manual v0.14 beta*. Microsoft Corporation, 2017.

[148] G. Balas, R. Chiang, A. Packard, and M. Safonov, *Robust Control Toolbox, User's Guide*. The Math Works, Inc, Natick, Massachusetts, United States, r2018a ed., mar 2018.

[149] D. T. Gillespie, A. Hellander, and L. R. Petzold, "Perspective: Stochastic algorithms for chemical kinetics," *The Journal of Chemical Physics*, vol. 138, no. 17, p. 170901, 2013.

[150] N. Dalchau, G. Seelig, and A. Phillips, "Computational design of reaction-diffusion patterns using DNA-based chemical reaction networks," in *International Workshop on DNA-Based Computers*, pp. 84—-99, Springer, Cham, 2014.

[151] R. M. Dirks, J. S. Bois, J. M. Schaeffer, E. Winfree, and N. A. Pierce, "Thermodynamic analysis of interacting nucleic acid strands," *SIAM Review*, vol. 49, no. 1, pp. 65–88, 2007.

[152] C. Grun, K. Sarma, B. Wolfe, S. W. Shin, and E. Winfree, "A domain-level DNA strand displacement reaction enumerator allowing arbitrary non-pseudoknotted secondary structures," *arXiv*, p. arXiv:1505.03738, may 2015.

[153] L. Qian and E. Winfree, "Scaling up digital circuit computation with DNA strand displacement cascades," *Science*, vol. 332, no. 6034, pp. 1196–1201, 2011.

[154] M. Foo, J. Kim, R. Sawlekar, and D. G. Bates, "Design of an embedded inverse-feedforward biomolecular tracking controller for enzymatic reaction processes," *Computers & Chemical Engineering*, vol. 99, pp. 145–157, 2017.

[155] K. J. Aström and R. M. Murray, *Feedback Systems: An Introduction For Scientists And Engineers*. Princeton University Press, 2008.

[156] W. Halter, Z. A. Tuza, and F. Allgöwer, "Signal differentiation with genetic networks," *IFAC-PapersOnLine*, vol. 50, no. 1, pp. 10938–10943, 2017.

[157] M. Chevalier, M. Gómez-Schiavon, A. Ng, H. El-Samad, M. Gomez-Schiavon, A. Ng, and H. El-Samad, "Design and analysis of a Proportional-Integral-Derivative controller with biological molecules," *bioRxiv*, pp. 1–35, 2018.

[158] A. J. Thubagere, C. Thachuk, J. Berleant, R. F. Johnson, D. A. Ardelean, K. M. Cherry, and L. Qian, "Compiler-aided systematic construction of large-scale DNA strand displacement circuits using unpurified components," *Nature Communications*, vol. 8, 2017.

[159] C. Briat, A. Gupta, and M. Khammash, "Antithetic integral feedback ensures robust perfect adaptation in noisy biomolecular networks," *Cell systems*, vol. 2, no. 1, pp. 15–26, 2016.

[160] B. Wang, C. Thachuk, A. D. Ellington, and D. Soloveichik, "The Design Space of Strand Displacement Cascades with Toehold-Size Clamps," in *International Conference on DNA-Based Computers*, Lecture Notes in Computer Science, (Cham), pp. 64–81, Springer International Publishing, 2017.

[161] F. Dannenberg, M. Kwiatkowska, C. Thachuk, and A. J. Turberfield, "DNA walker circuits: computational potential, design, and verification," *Natural Computing*, vol. 14, no. 2, pp. 195–211, 2015.

[162] G. Chatterjee, N. Dalchau, R. A. Muscat, A. Phillips, and G. Seelig, "A spatially localized architecture for fast and modular DNA computing," *Nature Nanotechnology*, vol. 12, no. 9, pp. 920–927, 2017.

[163] A. Joesaar, S. Yang, B. Bögels, A. van der Linden, P. Pieters, B. V. Kumar, N. Dalchau, A. Phillips, S. Mann, and T. F. de Greef, "DNA-based communication in populations of synthetic protocells," *Nature Nanotechnology*, vol. 14, no. 4, pp. 369–378, 2019.

[164] B. Wang, C. Thachuk, A. D. Ellington, E. Winfree, and D. Soloveichik, "Effective design principles for leakless strand displacement systems," *Proceedings of the National Academy of Sciences*, vol. 115, no. 52, pp. E12182–E12191, 2018.

[165] L. Andersson and A. Rantzer, "Robustness of equilibria in nonlinear systems," *IFAC Proceedings Volumes*, vol. 32, no. 2, pp. 2256–2261, 1999.

[166] M. Kishida and R. D. Braatz, "On the analysis of the eigenvalues of uncertain Matrices by mu and v: applications to bifurcation avoidance and convergence rates," *IEEE Transactions on Automatic Control*, vol. 61, pp. 748–753, mar 2016.

[167] P. Psarris and C. A. Floudas, "Robust stability analysis of systems with real parametric uncertainty: a global optimization approach," *International Journal of Robust and Nonlinear Control*, vol. 5, no. 8, pp. 699–717, 1995.

[168] C. Zou, X. Wei, Q. Zhang, and Y. Liu, "Synchronization of chemical reaction networks based on DNA strand displacement circuits," *IEEE Access*, vol. 6, pp. 20584–20595, 2018.

[169] L. Qian and E. Winfree, "Parallel and scalable computation and spatial dynamics with DNA-based chemical reaction networks on a surface," *Lecture Notes in Computer Science*, vol. 8727, pp. 114–131, 2014.

[170] H. Bui, V. Miao, S. Garg, R. Mokhtar, T. Song, and J. Reif, "Design and analysis of localized DNA hybridization chain reactions," *Small*, vol. 13, no. 12, pp. 1–8, 2017.

[171] P. A. Iglesias and B. P. Ingalls, *Control theory and systems biology*. MIT Press, 2010.

[172] M. R. Lakin, A. Phillips, D. Stefanovic, M. A. Boemo, A. J. Turberfield, and L. Cardelli, *DNA Computing and Molecular Programming*, vol. 5877 of *Lecture Notes in Computer Science*. Springer Berlin Heidelberg, 2011.

[173] M. R. Lakin, R. Petersen, K. E. Gray, and A. Phillips, "Abstract modelling of tethered DNA circuits," *Lecture Notes in Computer Science*, vol. 8727, pp. 132–147, 2014.

[174] M. Teichmann, E. Kopperger, and F. C. Simmel, "Robustness of localized DNA strand displacement cascades," *ACS Nano*, vol. 8, no. 8, pp. 8487–8496, 2014.

[175] G. Lipták, M. Pituk, and K. M. Hangos, "Modelling and stability analysis of complex balanced kinetic systems with distributed time delays," *Journal of Process Control*, vol. 84, pp. 13–23, 2019.

[176] L. Farina, "On the existence of a positive realization," *Systems and Control Letters*, vol. 28, no. 4, pp. 219–226, 1996.

[177] A. Rantzer and M. E. Valcher, "A tutorial on positive systems and large scale control," in *Proceedings of IEEE Conference on Decision and Control*, pp. 3686–3697, IEEE, 2018.

[178] I. Zorzan and A. Rantzer, "L1 and H-infinity optimal control of positive bilinear systems," in *Proceedings of the IEEE 56th Annual Conference on Decision and Control*, pp. 727—-732, 2017.

[179] A.-A. Baetica, Y. P. Leong, N. Olsman, and R. M. Murray, "Design guidelines for sequestration feedback networks," *bioRxiv*, p. 455493, 2018.

[180] N. Olsman, A.-A. Baetica, F. Xiao, Y. P. Leong, R. M. Murray, and J. C. Doyle, "Hard Limits and performance tradeoffs in a class of antithetic integral feedback networks," *Cell Systems*, vol. 9, no. 1, pp. 49–63.e16, 2019.